The cell wall microstructures of syncytia induced by cyst nematodes

Li Zhang

Submitted in accordance with the requirements for
the degree of Doctor of Philosophy

The University of Leeds
School of Biology
Faculty of Biological Sciences

September 2016

The candidate confirms that the work submitted is his own and that appropriate credit has been given where reference has been made to the work of others.

Dedicated to my beloved parents.

Acknowledgements

Firstly, I would like to thank my supervisor Prof. Urwin for constant guidance and support in my PhD study.

I would also like to thank Dr Catherine J. Lilley for her patience, help and support throughout my experiment design and study; and thank Prof. Knox and Sue for providing all the antibodies and other technical support.

I take this opportunity to express my gratitude to all the people I met in this lab for creating a friendly environment to work in. I'm also grateful for the help I received from Fiona, Jennie and Bev in my experiments and the beautiful Christmas memories we shared in Jennie's home. I will also thank my friend Dr Chulin Sha for encouraging and helping me in my study and daily life.

My sincere thanks also goes to the doctors and nurses at St. James's University Hospital for keeping me healthy and happy in the past four years and providing the support when I needed the most.

Last but not the least, I would like to thank my family for supporting me spiritually throughout writing this thesis and my life in general.

Abstract

Plant parasitic cyst nematodes induce the formation of specialised feeding structures, termed syncytia, from which they feed within the host roots. The multinucleate syncytium initiates from a single host root cell and expands by the local cell wall dissolution of neighbouring cells.

In this study, a set of monoclonal antibodies were applied to reveal the microstructures of syncytial cell walls induced by four economically important cyst nematode species, *Globodera pallida*, *Heterodera glycines*, *Heterodera avenae* and *Heterodera filipjevi*, in their respective potato, soybean and wheat host roots. *In situ* fluorescence analysis revealed that cell walls of syncytia induced by *G. pallida* and *H. glycines* share high structural similarity. Both consisted of abundant xyloglucans, methyl-esterified homogalacturonan and pectic arabinans. In contrast, the walls of syncytia induced in wheat roots by *H. avenae* and *H. filipjevi* contain much less xyloglucan but are rich in feruloylated and substituted heteroxylans and arabinans, with variable levels of mixed-linkage glucans and galactans.

Further investigations were implemented using a range of cell wall related Arabidopsis xyloglucan and pectic arabinan mutants. *In situ* analysis was applied on those *H. schachtii* induced syncytia. The results indicated the strong adaptions during the induction and formation of the syncytia while the cell wall composition of the syncytium was stable. Besides, the syncytial wall pectin methyl-esterification status was shown to fluctuate along with the syncytium development in addition to coping with induced PEG-simulated drought stress. Further analysis was carried out on selected pectic homogalacturonan related mutants, and the fluorescence-based quantifications revealed the complexity of the forming and regulating pectin methyl esterification.

Transgenic wheat lines with a root-cap-specific promoter were made via biolistics, in the hope of using this system to further investigate the syncytia formed in wheat, which were shown to be different from the other syncytia analysed.

Table of Contents

List of Figures

List of Tables

List of Abbreviations

AG	Arabinogalactan
AGA	Apiogalacturonan
AGP	Arabinogalactan protein
ANOVA	Analysis of variance
ATs	Acetyltransferases
bp	Base pair
Ca^{2+}	Calcium ion
CAPS	N-cyclohexyl-3-aminopropanesulfonic acid
CBM	Carbohydrate-binding module
CCN	cereal cyst nematode
cDNA	Complementary DNA
CO_2	Carbon dioxide
col	Columbia
CTAB	Cetyl trimethylammonium bromide
cv.	Cultivar
DMSO	Dimethyl sulfoxide
DNA	Deoxyribonucleic acid
DNase	Deoxyribonuclease
dpi	Days post infection
EDTA	Ethylenediaminetetraacetic acid
EGTA	Ethylene glycol-bis(2-aminoethylether)-N,N,N',N'-tetraacetic acid
ER	Endoplasmic reticulum
EtOH	Ethanol
FITC	Fluorescein isothiocyanate
g	Gravity
g	Gram
GalA	D-Galacturonic acid
GAX	Glucuronoarabinoxylan
GFP	Green fluorescent protein
GRP	Glycine-rich protein
GTs	Glycosyltransferases
GUS	β-glucuronidase
GX	Glucuronoxylan
h	Hour
H_2O_2	Hydrogen peroxide
HG	Homogalacturonan
HRGP	Hydroxyproline-rich glycoprotein
IAA	Indole-3-acetic acid
IPTG	Isopropyl β-D-1-thiogalactopyranoside
ISC	Initial syncytial cell
J1	First stage juvenile
J2	Second stage juvenile
kb	Kilobase

M	Molar
mAb	Monoclonal antibody
mg	Milligram
Mg^{2+}	Magnesium ion
mL	Milliliter
MLG	Mixed-linkage glucan
mM	millimolar
Mr	molecular mass
mRNA	Messenger RNA
MS	Murashige and Skoog medium
MTs	Methyltransferases
nm	Nanometre
OD_{600}	optical density of a sample at 600 nanometres
ORF	open reading frame
PCR	Polymerase chain reaction
PEG	Polyethylene glycol
PIPES	piperazine-N,N'-bis(2-ethanesulfonic acid)
PME	Pectin methylesterases
PMEI	pectin methylesterase inhibitor
PMT	Pectin methyltransferase
RCP	Root-cap-specific protein
rDNA	Ribosomal DNA
RG	Rhamnogalacturonan
RNA	Ribonucleic acid
rpm	Revolutions per minute
RT-PCR	Reverse transcription PCR
SOB	Super optimal broth
TPM	Transcripts per million
µL	Microliter
µm	Micrometer
USD	United States dollar
UV	Ultraviolet
v	Volume
w	Weight
XGA	Xylogalacturonan
X-gal	5-bromo-4-chloro-3-indolyl-β-D-galactopyranoside
XyG	Xyloglucan

Chapter 1 Introduction

1.1 Plant parasitic nematodes

Plant pathogens, including viruses, fungi, bacteria and nematodes, can attack all major cultivated crops. Among those pathogens, plant parasitic nematodes are responsible for important constraints on crop production worldwide. It has been reported that there are over 4100 species of plant parasitic nematodes that are a great threat to global food security (Perry and Moens 2013), with estimated economic loss between $80 billion annually (Nicol, Turner *et al.* 2011) and $157 billion annually (Abad, Gouzy *et al.* 2008). However, due to the misdiagnosis of symptoms in the field, the damage caused by nematode infestation may still be largely underestimated.

In terms of taxonomy, plant parasitic nematodes are in the phylum Nematoda (roundworms, Figure 1.1), with over 23,000 species described and an estimate of up to a million in total (Blaxter 2011). Most nematodes are free-living (nonparasitic) in freshwater, marine, or soil ecosystems and only a comparatively small fraction of nematode species are animal or plant parasites (Baldwin, Nadler *et al.* 2004, Quist, Smant *et al.* 2015). Those that feed on plants during a portion of their life cycles, are primarily from three orders, Triplonchida, Dorylaimida, and Tylenchida (Blaxter, De Ley *et al.* 1998, Baldwin, Nadler *et al.* 2004, van Megen, van den Elsen *et al.* 2009, Quist, Smant *et al.* 2015). Generally, plant parasitic nematodes have hollow, protrusible stylets to penetrate cells and can be classified into three types of parasitism: ectoparasitic, never enter the host and use roots as a source of nutrient while remaining in the soil; semi-endoparasitic, only the anterior part of the nematodes penetrate the root while posterior part is external to the root; endoparastic, the whole nematode penetrates root cells and enter host tissue (Perry and Moens 2013). The migratory endoparasites can enter hosts and migrate through host tissues, retain their mobility and have no fixed feeding site, while sedentary endoparasites induce feeding structures, such as syncytia or giant cells, within host roots and feed on the roots via these feeding structures. The female lose locomotory ability once feeding is established (Jones, Haegeman *et al.* 2013). The most economically important plant parasitic nematodes are root-knot nematodes (*Meloidogyne* spp.) and cyst nematodes (*Heterodera* and *Globodera* spp.), all from the order, Tylenchida.

Both root-knot nematodes and cyst nematodes comprise approximately 100 known species. Root knot nematodes have, in general, a wide host range whereas cyst nematode species tend to have a more restricted host range. While root knot nematodes are the most economically important group of plant parasitic nematodes, cyst nematodes also cause huge agronomic losses on a global scale (Jones, Haegeman *et al.* 2013).

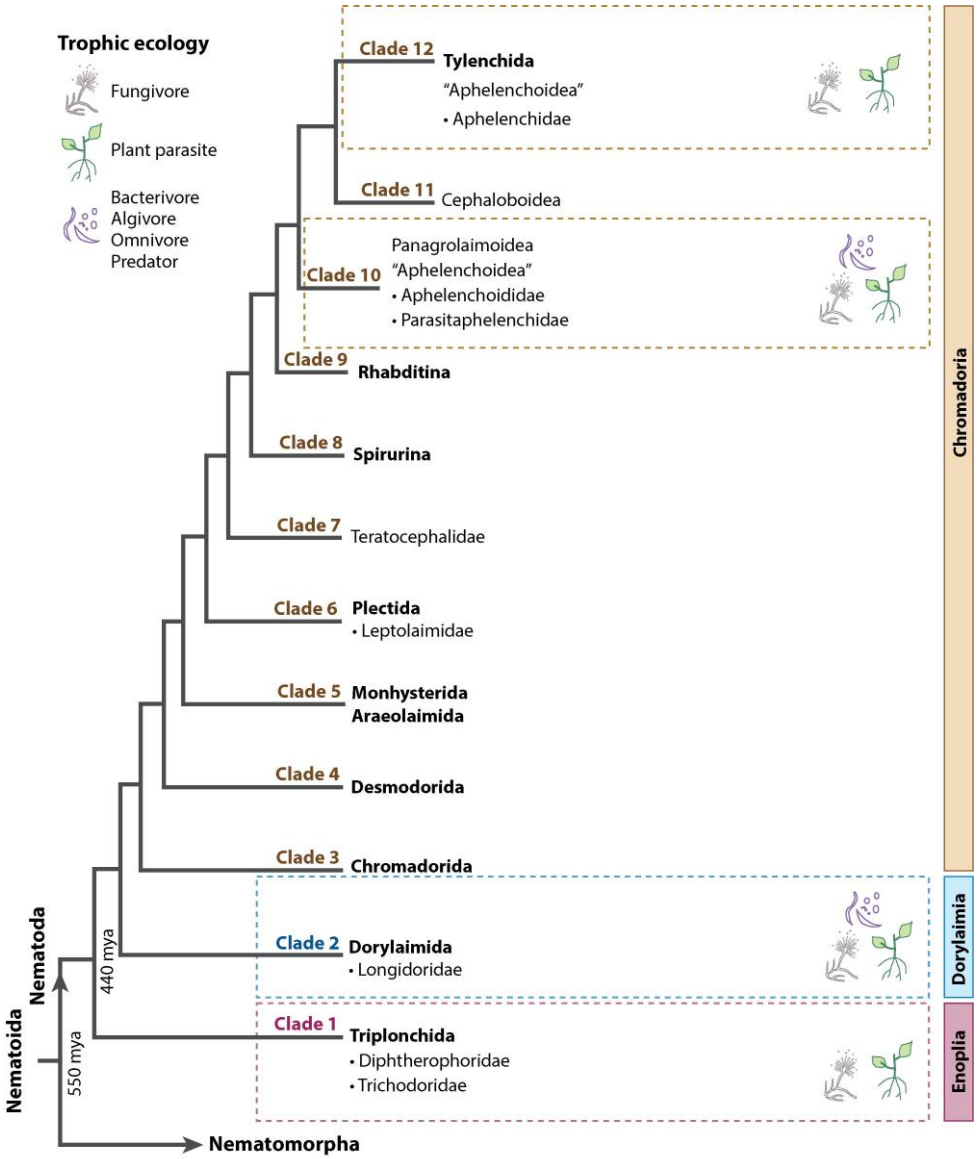

Figure 1.1 Schematic overview of the phylum Nematoda. Division of the 12 major clades is based on the sequence data of small-subunit rDNA (Holterman, van der Wurff *et al.* 2006). (Sub)order names (with the suffix –ina and –ida, respectively) and subclass names (-ia) are given. The superfamily Aphelenchoidea is marked in quotation marks, as it is probably not monophyletic. Trophic ecologies and nematode head regions relevant in the context are labelled by icons and shown. Modified from (Quist, Smant *et al.* 2015).

1.1.1 Root-knot nematodes

Root-knot nematodes are obligate plant parasites, distributed worldwide, and parasitize almost every vascular plant species (Jones, Haegeman *et al.* 2013). Known for the galls (root-knots) induced on the roots of host plants, root-knot nematode infestation causes reduced water and nutrient uptake in host plants, resulting in lower crop productivity. The most widespread and economically damaging nematodes species in the *Meloidogyne* genus include the tropical species *M. incognita*, *M. arenaria*, and *M. javanica* and the temperate species *M. hapla*, and increasingly important species such as *M. enterolobii* and *M. chitwoodi*, all together responsible for the vast majority of crop damage, which is estimated to be multibillion USD annually worldwide (Castagnone-Sereno, Danchin *et al.* 2013, García and Sánchez-Puerta 2015).

1.1.1.1 Root knot nematodes life cycle

The root-knot nematode life cycle takes three to six weeks to complete, depending on host species and environmental conditions, and comprises four juvenile stages (separated by moults) in addition to the adult stage (Castagnone-Sereno, Danchin *et al.* 2013). Mature females lay eggs in a protective gelatinous matrix which forms an egg mass, found on the root surface or embedded in galls or plant tissues, and can contain up to 1000 eggs (Jones, Haegeman *et al.* 2013). The first-stage juvenile (J1) moults within the egg to the infective second-stage juvenile (J2) after embryogenesis. Due to the broad host range of many *Meloidogyne* species, the hatching is solely dependent on suitable environmental conditions, such as temperature and moisture conditions, no stimulus from host plants usually is required. Infective second stage juveniles (J2s) invade the root in the elongation zone, by both physical force through thrusting of the spear-like stylet and a combination of secreted cell wall degrading enzymes, and then migrate inter-cellularly towards the root tip. Once they reach the root meristem, they turn around in a U-shape and move upwards into the differentiating vascular cylinder. After they reach the zone of protoxylem development, they puncture a few plant cells with their stylet and induce the formation of a permanent feeding site and become sedentary (Castagnone-Sereno, Danchin *et al.* 2013). The feeding site consists several multinucleate and hypertrophied giant cells, up to 100 times the size of normal root vascular parenchyma cells. The J2, with its head embedded in the periphery of the vascular tissue, swells and moults a further three times after feeding to reach the reproductive adult stage. Sexual dimorphism is associated with the sedentary lifestyle. Males become vermiform and motile again, and finally leave the host root, while females stay sedentary and continue to feed and enlarge into saccate shape. The *Meloidogyne* spp. have a degree of reproductive plasticity and cytogenetic diversity. For instance, within the species *M. hapla*, amphimixis is facultative for the majority isolates and reproduction can also occur by meiotic parthenogenesis; while other isolates reproduce by obligate mitotic parthenogenesis (Bird, Williamson *et al.* 2009). In contrast to *M. hapla*, the other three most damaging species, *M. incognita*, *M. arenaria* and *M. javanica* reproduce exclusively by mitotic parthenogenesis (Bird, Williamson *et al.* 2009).

1.1.1.2 Giant cells

Root-knot nematodes growth and reproduction depend on the successful establishment of the feeding structure within host roots, termed giant cells. The formation of giant cells is induced by injected nematode secretions from oesophageal gland cells via the stylet. Those enlarged, multinucleate and active cells, forming through repeated nuclear divisions of the initial feeding cells without cell divisions, fulfil the nutritional requirements of nematodes. Each root-knot nematode triggers the development of five to seven giant cells and these cells are metabolically active, with a very dense cytoplasm containing numerous mitochondria, plastids, ribosomes, a well-developed Golgi apparatus and smooth endoplasmic reticulum (Castagnone-Sereno, Danchin *et al.* 2013). The central vacuole is replaced by many small vacuoles, with visible cell wall ingrowth, believed to enhance solute uptake from the vascular system.

1.1.2 Cyst nematodes

Cyst forming nematodes are obligate biotrophic sedentary plant endoparasites and are mainly found throughout temperate regions worldwide. The most agronomically damaging species include potato cyst nematodes *Globodera pallida* and *G. rostochiensis*, soybean cyst nematodes *Heterodera glycines*, cereal cyst nematodes *H. avenae* and *H. filipjevi* and beet cyst nematodes *H. schachtii* (Jones, Haegeman *et al.* 2013). It is difficult to accurately estimate the economic losses (Nicol, Turner *et al.* 2011, Jones, Haegeman *et al.* 2013) caused by those nematode species due to easy misdiagnosis in the fields of crops with similar symptoms, and losses are in the range of millions to billions USD per year for each species. For instance, *G. pallida* and *G. rostochiensis* together account for 9% of yield loss (~70 million USD) for potato production in the UK (Nicol, Turner *et al.* 2011); *H. glycines* cause damage valued at more than 1 billion USD per annum in the United States alone (Winter, Rajcan *et al.* 2006, Koenning and Wrather 2010); and yield losses due to *H. avenae* infection on wheat are estimated to be 15-20% in Pakistan, 40-92% in Saudi Arabia, 23-50% in Australia, 24% in the Pacific North West of the USA and 26-96% in Tunisia (Nicol, Turner *et al.* 2011).

1.1.2.1 Cyst nematode life cycle

The life cycles of cyst nematodes *Globodera* and *Heterodera* are very similar (Figure 1.2). They start from infective second stage juveniles (J2s) hatching under suitable conditions in the soil (I, Figure 1.2), such conditions include constant temperature, sufficient moisture and the existence of root exudates from suitable host roots. Hatched J2s migrate towards host roots as a response to the gradients of a variety of stimuli, including CO_2, amino acids, pH and sugars around the roots (II, Figure 1.2) (Lilley, Atkinson *et al.* 2005). The epidermal cells of the root elongation zone are penetrated by J2s using repeated thrusts of their stylets and the cortical cells are disrupted by both mechanical force and nematode secreted cell wall digestion enzymes during their intracellular migration towards the vascular cylinder. An initial syncytial cell (ISC) is then selected and injected with nematode

secretions through the hollow stylet to trigger the syncytium forming process (III, Figure 1.2) (Grundler, Golinowski *et al.* 1999). For *Globodera* spp., one cell among the inner cortex or the endodermal cells will be chosen as ISC; while for *H. schachtii*, the ISC is usually among cambial or procambial cells within the vascular bundle (Bohlmann and Sobczak 2014). After the initiation of a syncytium, the neighboring cells will go through cell wall dissolutions and successively fuse with the ISC to become one multinuclear syncytium, with numerous organelles. It acts as a nutrient sink and keeps functioning throughout the nematode feeding periods. A feeding tube will be assembled at the tip of the stylet each time the nematode begins a cycle of feeding (Grundler, Golinowski *et al.* 1999). After three moults, the J2s reach adult stage and the males will regain locomotion, leave the root and fertilize the females. Most cyst nematodes are amphimictic and the females are polymandrous (Triantaphyllou and Esbenshade 1990, Hoolahan, Blok *et al.* 2011, den Akker, Lilley *et al.* 2015) and their body will eventually turn into a tough leather-like cyst (IV, Figure 1.2). Each cyst can contain around 200-500 eggs (*Globodera* sp.) and the egg to egg life cycle for most cyst nematode species is completed within 30 days.

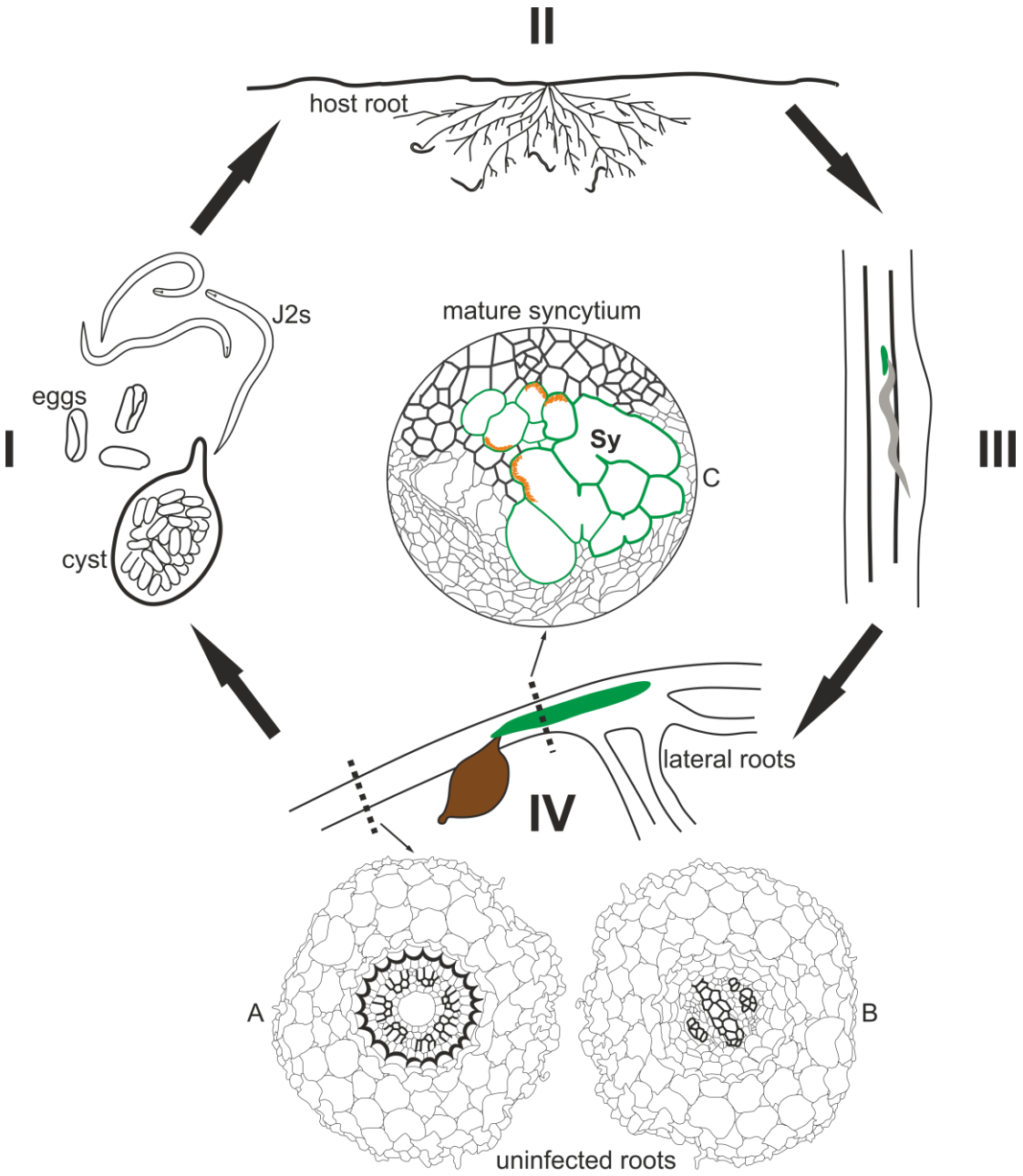

Figure 1.2 Schematic of a typical cyst nematode life cycle. I. Infective J2s hatch from eggs in a cyst; **II**. Nematodes migrate towards host root system; **III**. The initiation and formation of a syncytium within host root vascular cylinder induced by a J2; **IV**. A cyst is formed after adult female matures and dies. Transverse sections of syncytium (marked as green) containing region (C, syncytium cell walls in green, xylem in bold black, phloem in light black, cell wall ingrowth marked in orange) as well as the normal roots (A, monocot wheat root; B, dicot Arabidopsis root) were shown. Sy: syncytium.

1.1.2.2 Syncytium

As the sole nutrient supply, the successful initiation and formation of a functional syncytium (Figure 1.3) is vital for cyst nematode survival and reproduction. After the ISC is selected, secretions produced in nematode oesophageal glands are injected into the ISC through the hollow stylet to trigger the formation process of the syncytium (Jones and Northcote 1972, Sijmons, Grundler *et al.* 1991, Grundler, Golinowski *et al.* 1999, Bohlmann and Sobczak 2014). By consistently incorporating neighbouring pro-/cambial cells located between xylem and phloem bundles via local cell wall dissolutions, the syncytial region expands longitudinally along with the vascular cylinder.

Initiation and formation in general

At the beginning of syncytium induction, there is a preparation phase when the juvenile is motionless with its stylet inserted in the selected ISC (Wyss 1992). During this time, electron translucent callose-like material is deposited around the stylet tip inside the wall of the ISC as well as other parts of the ISC and neighbouring cells (Grundler, Sobczak *et al.* 1998). The first cell wall dissolution is then caused by the gradual widening of plasmodesmata between the ISC and the neighbouring cells at the end of the preparation phase (Grundler, Sobczak *et al.* 1998). Eventually, a syncytium composed of several cells possessing cytoplasmic continuity is formed by the cell wall openings and meanwhile the outer syncytial walls begin to slightly thicken. Comparing with later stages of syncytium formation, cell wall openings are mostly formed by enzymatic dissolutions of intact walls involving putative cellulase activity, and the thickening of syncytial cell walls will also block existing plasmodesmata (Grundler, Sobczak *et al.* 1998, Bohlmann and Sobczak 2014). During the formation of such openings in those stages, first, the membranes of ER accumulate adjacent to the syncytial walls and the wall lesions appear, expand and the walls degrade from both sides of the adjacent sites; later, after the dissolutions of cell walls and the middle lamella, protoplasts fuse and the ER systems of the adjacent cells also extend and fuse (Grundler, Sobczak *et al.* 1998). Cellulase activity is proven to be involved in the forming of these openings (Grundler, Sobczak *et al.* 1998). The syncytium formation and enlargement consist of continuous cell fusions and stop when it is mature. In the following maintenance phase of syncytium, no additional cells are incorporated and the syncytium will keep its function of feeding the developing nematode.

Cell cycle alteration

One important cytological feature of the syncytium is the formation of several large nuclei through host root cell fusion and endoreduplication (endocycle), supporting the enhanced metabolic demands imposed by the nematode (Wildermuth 2010). The general cell cycle is composed of DNA replication (S phase), followed by chromosome and nuclear division (mitosis, M phase) and cell division (cytokinesis). Two gap phases also exist in this cycle, one (G1) precedes DNA synthesis and the other (G2) separates S phase and M phase (Stals and Inzé 2001). However, in a nematode induced syncytium, the mitosis M phase is blocked immediately after DNA synthesis, resulting unseparated chromatids, together with cell fusions, eventually leading to several enlarged nuclei (endoreduplication) (de Engler

2013).

Activation of the cell cycle has been proven to be crucial for normal feeding site development and subsequent nematode growth and reproduction (de Almeida Engler, De Vleesschauwer *et al.* 1999). ^{3}H-thymidine incorporation experiments have demonstrated that additional DNA replication cycles occur in a cyst nematode-induced syncytium, even until later stages of development. Meanwhile treatment with cell cycle inhibitors could cause the initiation of syncytia failure, showing that DNA synthesis is essential for successful parasitism (de Almeida Engler, De Vleesschauwer *et al.* 1999). Two cell-cycle switch related genes *CCS52A* (*CCS52A1*) and *CCS52B*, involved in conversion of mitotic cycles into endocycles, were characterized as endocycle activators during syncytium formation, while an atypical E2F cellular transcription factor *E2Fe/DEL1* (Inzé and De Veylder 2006) was shown to be the repressor for such alteration (de Almeida Engler, Kyndt *et al.* 2012).

Symplastic connection

Direct cell-to-cell exchange of cytoplasmic content among adjacent cells is only possible through plasmodesmata, which are highly dynamic communication channels that can undergo various structural and functional modifications. The restriction of plasmodesmata mediated cell-to-cell communication has been shown to be an essential innate immune response to microbial pathogens (Lee 2015). However, the symplasmical connectivity (through plasmodesmata) status of syncytia is still debatable (Grundler, Sobczak *et al.* 1998, Hoth, Schneidereit *et al.* 2005, Hofmann and Grundler 2006), and the certain existence of plasmodesmata are mainly found at later stages of nematode development (Hofmann, Youssef-Banora *et al.* 2010). Few plasmodesmata were observed in young syncytia along with temporal callose deposition, indicating impaired function, and later callose degradation Arabidopsis mutants were revealed to cause size reduction of *H. schachtii* induced syncytia, reflecting the importance for this process in nematode development (Hofmann, Youssef-Banora *et al.* 2010). Nevertheless, there is still a lack of direct evidence for such symplastical connection as plasmodesmata found in outer syncytial walls were generally occluded by deposition of cell wall materials (Bohlmann and Sobczak 2014).

Nematode feeding

The feeding from the initial syncytium for J2s is composed of a series of repeated cycles and each cycle contains three phases: the stylet is inserted into the syncytium and material is continuously withdrawn from within a zone of modified cytoplasm through a feeding tube, hypothesised to be a molecular sieve (Eves-van den Akker, Lilley *et al.* 2014); followed by stylet retraction, alternating withdrawal by depletion of secretory fluids from subventral oesophageal gland ampullae and reinsertion; and finally secretory material of dorsal gland is released into the initial syncytium, forming a new feeding tube inside the zone of modified cytoplasm to connect to the stylet-tip orifice (Rumpenhorst 1984, Wyss and Zunke 1986, Grundler, Golinowski *et al.* 1999). A feeding plug is formed where the nematode stylet is inserted into the syncytium (Endo 1978, Grundler, Golinowski *et al.* 1999) and an opening in the plasmalemma is formed at the orifice of the stylet. An electron

translucent layer of callose-like material is deposited to separate the stylet from the plasmalemma except for the stylet orifice (Grundler, Golinowski *et al.* 1999). This callose-like layer is then pulled inside the syncytial wall after the stylet is retracted each time the food withdrawal is completed. The feeding cycle repeats every 2-3 hours (Sobczak and Golinowski).

General structural features

Over the past four decades, ultrastructural observations have been carried out using syncytia induced by a range of agriculturally important cyst nematode species, including *G. rostochiensis* (Jones and Northcote 1972) and *G. pallida* in potato roots (Melillo, Bleve-Zacheo *et al.* 1990), *H. glycines* in soybean roots (Gipson, Kim *et al.* 1971, Riggs, Kim *et al.* 1973), *H. schachtii* in radish (*Raphanus sativus*) (Wyss, Stender *et al.* 1984), sugar beet (Bleve-Zacheo and Zacheo 1987) and rape (*Brassica napus*) (Magnusson and Golinowski 1991), and cereal cyst nematode *H. avenae* in hexaploid wheat (Grymaszewska and Golinowski 1987, Grymaszewska and Golinowski 1991).

Syncytia induced by different cyst nematode species are morphologically different. For example, in susceptible and resistant host roots such as radish (Wyss, Stender *et al.* 1984), soybean (Kim, Riggs *et al.* 1987) and wheat (Grymaszewska and Golinowski 1991), or in different varieties of potato (Melillo, Bleve-Zacheo *et al.* 1990), the syncytia might incorporate different types/amounts of cells, differ in size and position and even possess certain different ultrastructural features, such as cell wall ingrowth status.

Differences in the structure of syncytia have been shown to be dependent on the sex of the nematode. For instance, syncytia associated with *H. schachtii* females were usually induced in procambial or cambial cells (Golinowski, Grundler *et al.* 1996) while syncytia initiated in the pericycle of secondary roots were associated with male development (Sobczak, Golinowski *et al.* 1997, Grundler, Sobczak *et al.* 1998). Typically, the syncytia induced by male juveniles were inconspicuous comparing with the clearly visible, extended hypertrophied region in the vascular cylinder induced by the females. The ultrastructure of both types of syncytia are very similar apart from the structure and localization of cell wall ingrowths (Sobczak, Golinowski *et al.* 1997). At the end of the third developmental stage, the males will stop feeding and the syncytia then degenerate.

Apart from these differences, cyst nematode induced syncytia in general still possess some similar ultrastructural features characteristic of high metabolic activity such as a pronounced increase in cytoplasmic density, reduction of the central vacuole into numerous small vacuoles, abundance of ribosomes, polyribosomes, mitochondria, proliferated endoplasmic reticulum and enlargement of nuclei. Other features also include thickened cell walls, increased osmotic pressure within than the adjacent cells and possible cell wall ingrowth adjacent to xylem elements (Figure 1.3) (Jones and Northcote 1972, Riggs, Kim *et al.* 1973, Wyss, Stender *et al.* 1984, Grymaszewska and Golinowski 1987, Grymaszewska and Golinowski 1991, Böckenhoff and Grundler 1994, Golinowski, Grundler *et al.* 1996, Sobczak, Golinowski *et al.* 1997).

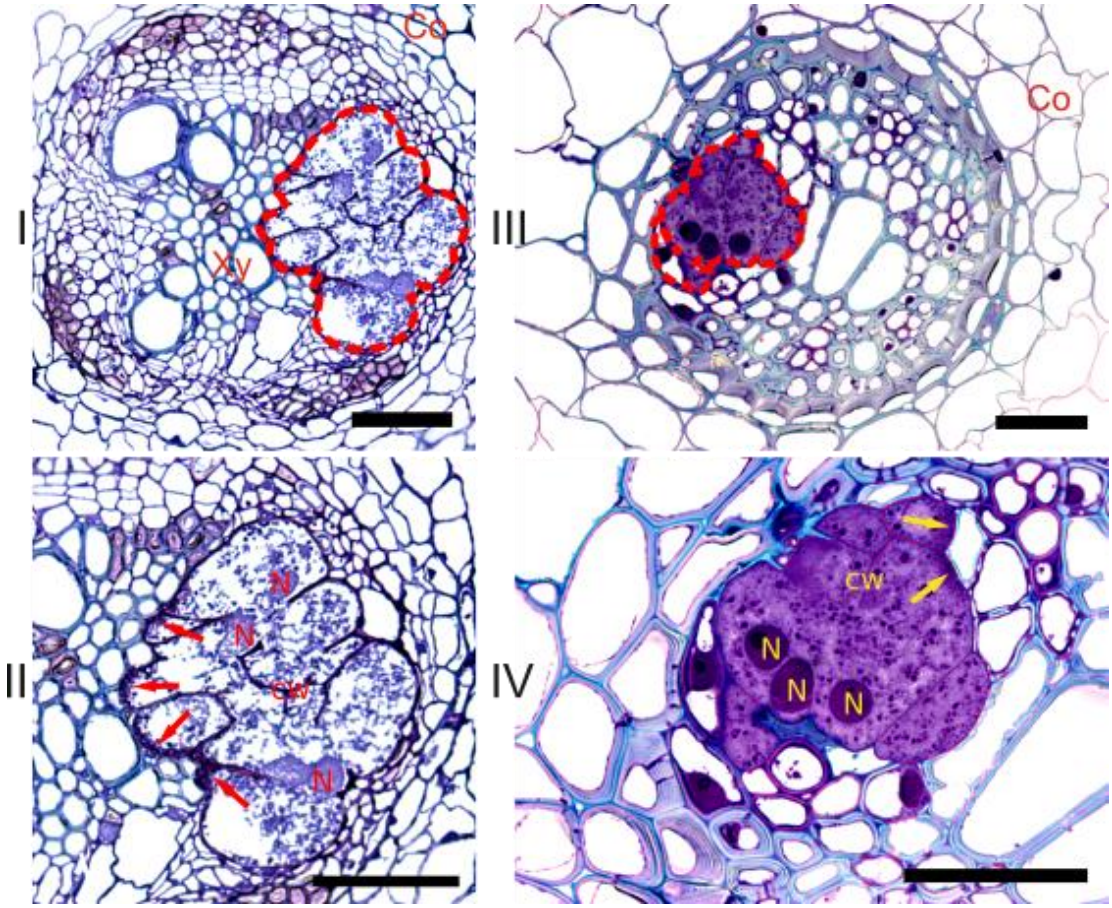

Figure 1.3 Syncytia induced by cyst nematodes within host roots vascular cylinder. Transverse sections were taken from *H. glycines* infested soybean roots (14 dpi, I & II) and *H. avenae* infested wheat roots (cv. Bobwhite, 21 dpi, III & IV), and stained with Toluidine Blue. Syncytial regions were outlined with red dash line in I & III. (Co, cortex; Xy, xylem; CW, cell walls within syncytia; N, hypertrophied nuclei; arrows indicates the cell wall ingrowth adjacent to host xylem; bar=50 µm)

1.1.2.3 Host-nematode interactions

Cyst nematode effectors

Cyst nematodes secrete numerous proteins and other molecules through the stylet into their hosts (Hussey 1989), collectively known as effectors (Hogenhout, Van der Hoorn *et al.* 2009), to exert diverse functions for facilitating parasitic colonization, including interacting against/with plant innate immune system (Jones and Dangl 2006) modulating plant signalling or hormone pathways to promote feeding sites formation (Haegeman, Mantelin *et al.* 2011, Hewezi 2015). Those effectors are produced mainly in nematode oesophageal glands, consisting of two subventral glands and one dorsal gland cell (Mitchum, Hussey *et al.* 2013), though some studies also show that effectors can originate in other glands (Eves-van den Akker, Lilley *et al.* 2014).

Some of the first and most studied effectors are plant cell wall modifying enzymes, such as β-1,4-endoglucanase from *G. rostochiensis* and *H. glycines* (Smant, Stokkermans *et al.* 1998) and pectate lyase from *G. rostochiensis* (Popeijus, Overmars *et al.* 2000), capable of degrading cellulose and pectin in plant cell walls and thus facilitating nematode invasion and migration during parasitism. Effectors with similar (Qin, Kudla *et al.* 2004, Kudla, Milac *et al.* 2007, Rehman, Butterbach *et al.* 2009, Peng, Cui *et al.* 2016) or other related cell wall degrading activities (Danchin, Rosso *et al.* 2010) were extensively reported in various nematode species (Haegeman, Mantelin *et al.* 2011).

During the successful parasitism, the suppression of the host immunity by effectors is a key step. Two venom allergen-like protein genes (VAPs) were first isolated from *H. glycines* (*Hg-VAP-1* and *Hg-VAP-2*) as putative secreted proteins and suggested to play a role during parasitism (Gao, Allen *et al.* 2001). Similarly, the *G. rostochiensis* VAP gene Gr-VAP1, also located in subventral oesophageal glands at the infective stage (Qin, Overmars *et al.* 2000), was shown to severely reduce the infection when its expression was supressed by dsRNA (Lozano-Torres, Wilbers *et al.* 2014). Heterologous expression of *Gr-VAP1* and other two *H. schachtii* VAPs (*Hs-VAP1*, *Hs-VAP2*) resulted in enhanced nematode infection (Lozano-Torres, Wilbers *et al.* 2014). In tomato, Gr-VAP1 was shown to target the papain-like cysteine protease $Rcr3^{pim}$ by perturbing its active site, which could trigger the Cf-2-mediated defence response (Lozano-Torres, Wilbers *et al.* 2012). This gives an example of how nematode secreted effectors could be involved in manipulating the host immune response during parasitism (Mitsumasu, Seto *et al.* 2015). Via different approaches, especially the use of current sequencing technology and analytical tools, this field of study has been extended enormously (Blaxter, Kumar *et al.* 2012, Rehman, Gupta *et al.* 2016). For instance, the SPRYSEC family of proteins from *G. rostochiensis* (Rehman, Postma *et al.* 2009) and *G. pallida* (Jones, Kumar *et al.* 2009, Cotton, Lilley *et al.* 2014, Thorpe, Mantelin *et al.* 2014) were discovered based on transcripts sequencing or RNAseq and proposed to interact with a range of host targets and suppress host defence. Additionally, a novel group of hyper-variable extracellular effectors were identified from the *G. pallida* RNAseq data and in planta RNAi was shown to cause reduction of successful parasitism (Eves-van den Akker, Lilley *et al.* 2014). Similar analysis were also applied to feeding female and J2 stage of *H. avenae* (Kumar, Gantasala *et al.* 2014) and J2 stage of *H. schachtii* (Fosu-Nyarko, Nicol

et al. 2016) transcriptome data, effectors with various putative functions were identified, shedding light on our understanding of nematode parasitism.

Cyst nematode secreted effectors are also responsible for modulating host root cell differentiation and remodelling in syncytia. As a class of plant signalling peptides, CLAVATA3(CLV3)/ENDOSPERM SURROUNDING REGION (ESR) (CLEs), with hallmark feature including a hydrophobic N-terminal signal peptide and a conserved 14 amino acid consensus sequence (named CLE motif) at or near the C-terminal, implicates various physiological and developmental processes by binding to cellular surface receptor-like proteins to transmit a signal in conserved signalling pathway (Betsuyaku, Sawa *et al.* 2011). Intriguingly, CLE-like proteins were identified in cyst nematode dorsal oesophageal gland cell. Over-expression of an *H. glycines* CLE gene (*HgCLE2*, formerly *4G12*) (Wang, Mitchum *et al.* 2005, Davis 2009) and *G. rostochiensis CLE* genes (Lu, Chen *et al.* 2009) caused similar phenotypes as Arabidopsis overexpressing plant *CLE* gene, meanwhile the nematode *CLE* genes could partially or fully rescue the mutant phenotype, suggesting a function as a molecular ligand mimic of endogenous plant CLE peptides, probably facilitating the formation and/or maintenance of cyst nematode induced syncytia (Mitchum, Wang *et al.* 2008, Wang, Lee *et al.* 2010). In a similar strategy, nematode effectors acting as mimics of host plant proteins during parasitism, might also apply to *Hg4F01*, an annexin-like effector gene related to cell stress response isolated from *H. glycines* (Patel, Hamamouch *et al.* 2010).

Host cell response

Host root cells undergo drastic changes during the initiation and formation of syncytium and it is clear that nematodes modulate and utilise host cell machinery in their favour.

Auxin is involved in almost every aspect of plant development and an important level of regulation in auxin action is the auxin gradients between cells of a tissue (Vanneste and Friml 2009). An enhanced auxin response has been visualized at the infection sites of cyst nematodes, where auxin signalling mutants have reduced level of nematode infection (Goverse, de Engler *et al.* 2000, Goverse, Overmars *et al.* 2000, Grunewald, Karimi *et al.* 2008), suggesting that changes in host auxin response and transport are induced by nematode infection (Grunewald, Cannoot *et al.* 2009, Grunewald, van Noorden *et al.* 2009). A proposed model was that PIN1-mediated basipetal auxin transport is hampered in the initial feeding cell, resulting auxin accumulation in this cell. Thereafter, nematodes direct PIN3 and PIN4 to the lateral membranes and auxin is transported laterally towards the surrounding cells, causing the feeding site expend radially (Grunewald, Cannoot *et al.* 2009). Another study has also shown that a nematode effector protein Hs19C07 from *H. schachtii* can cause the increased auxin influx mediated by LAX3 (an auxin influx transporter), thus stimulating cell wall hydrolysis during syncytium development (Lee, Chronis *et al.* 2011). Recently, the gene expression pattern of a set of 22 auxin response factors (ARFs) during different parasitic stages in *H. schachtii* induced Arabidopsis syncytia were analysed (Hewezi, Piya *et al.* 2014). The different and dynamic distribution of those *ARFs* indicates various roles during parasitism, for instance, ARFs predominantly expressed in neighbouring cells are probably responsible for the initiation of specific transcriptional

programmes required for incorporation into the expanding syncytium; several ARFs with a high expression level in fully developed syncytia might implicate syncytia maintaining function (Hewezi, Piya *et al.* 2014).

Cytokinin signalling is also activated in both syncytium and neighbouring cells to be incorporated into syncytium, suggesting a role of cytokinin in parasitic interactions. Cytokinin and cytokinin signalling deficient mutants revealed significantly decreased nematode susceptibility (Siddique, Radakovic *et al.* 2015). Meanwhile, it was also shown that cytokinin produced by both nematodes (Meutter, Tytgat *et al.* 2003) and manipulated host cells are all involved in feeding site formation, the highest cytokinin produced by nematodes might be sufficient to activate cell cycle at the initial stages of infection but not sufficient for optimal development and expansion of syncytium (Siddique, Radakovic *et al.* 2015). Although significant progress has been made to underpin our understanding regarding the relationship between host phytohormone modulations and syncytium development, we are just beginning to understand this conundrum (Gutierrez, Wubben *et al.* 2009, Kazan and Manners 2009).

Apart from phytohormone changes, numerous host plant genes involved in cyst nematode parasitism also affect various other aspects of this process. For instance, in terms of morphology of syncytia, the double mutant of *UGD2* and *UGD3* (UDP-glucose dehydrogenase; dominant for UDP-glucuronic acid production, the precursor for several cell wall polysaccharides) not only caused the induction of smaller syncytia, less and smaller females, but also the abnormal syncytial ultrastructure, including electron translucent cytoplasm rather than the normal dense cytoplasm and the absence of cell wall ingrowths (Siddique, Sobczak *et al.* 2012).

Using high-throughput sequencing technology, more information of host gene expression following infection were evaluated, such as, comparisons between *H. schachtii* and *H. glycines* infested Arabidopsis roots (Puthoff, Nettleton *et al.* 2003), the transcriptome analysis of *G. rostochiensis* infected tomato roots (Swiecicka, Filipecki *et al.* 2009), *H. schachtii* induced syncytia in Arabidopsis (Szakasits, Heinen *et al.* 2009), *H. avenae* infected *Aegilops variabilis* roots (Xu, Long *et al.* 2012) and *H. glycines* infested *Glycine Max* (soybean) at different stages and using different host varieties (Ithal, Recknor *et al.* 2007, Klink, Hosseini *et al.* 2010, Mazarei, Liu *et al.* 2011, Wan, Vuong *et al.* 2015). Together with novel data analysis tool like NEMATIC (Cabrera, Bustos *et al.* 2014) and a wide range of transcriptome data analysis tools, we can now illustrate the picture of host gene expression changes in fine detail, boosting our understanding of plant-nematode interactions.

1.2 Plant cell walls

Cyst nematode induced syncytia are derived from normal host root cell, expanding through continuous incorporation neighbouring cells via local cell wall dissolutions (Bohlmann and Sobczak 2014). Cyst nematodes manipulate and modulate the innate machinery of host cells to synthesise new cell wall materials onto the outer syncytial walls (Bohlmann and Sobczak 2014). Therefore, the investigation of general plant cell walls would be beneficial for further evaluation of syncytial cell walls.

As the most noticeable difference between animal cells and plant cells, plant cell walls are designated as the fibrous polysaccharide-rich outer layer outside the plant protoplast. The layers between two cells include: middle lamella, separating two cells; primary cell wall, a thin layer deposited right after cell divisions; and thicker secondary cell wall, formed within certain cell types (such as xylem, Figure 1.4 II) when cells cease growth, providing great mechanical strength and structural reinforcement (Figure 1.4 III) (Fry 2004, Fangel, Ulvskov *et al.* 2012).

1.2.1 Cell wall types

1.2.1.1 Primary cell wall

In growing cells, a typical primary cell wall is a fibrous layer, consisting predominantly of complex polysaccharides and a small amount of structural proteins (Cosgrove 2005). It is a thin flexible layer (0.1-1 µm), capable of both plastic and elastic extension, and its size and shape dictate most external features of plant development (Fry 2004). A typical model of primary cell wall is depicted as a cellulose scaffold embedded into a matrix of polysaccharides, namely hemicelluloses and pectins (Figure 1.4 IV) (Cosgrove 2005, Cosgrove 2014). This network is dynamically modified, to allow for the growth status of plants. Of this typical primary cell wall model, cellulose microfibrils are composed of unbranched cellulose as the scaffolding of the wall (Cosgrove 2014). Cell wall polysaccharides are classified into hemicelluloses, including xylans, mannans, mixed-linkage glucans (MLG) and xyloglucans (XyG), and pectins, containing various structural classes of homogalacturonan (HG), rhamnogalacturonan-I (RG-I), rhamnogalacturonan-II (RG-II), xylogalacturonan (XGA) and apiogalacturonan (AGA) (Figure 1.5) (Caffall and Mohnen 2009, Scheller and Ulvskov 2010, Atmodjo, Hao *et al.* 2013).

Based on the known differences of wall chemical structures, primary cell walls of flowering plants were described as two distinct types of walls, namely the 'type I' cell wall, a generalized cell wall of most flowering plants including the dicots and non-commelinid monocots, and 'type II' primary wall, the wall of Poaceae family (Carpita and Gibeaut 1993, Smith and Harris 1999). In this model, the type I wall is described as a network of cellulose microfibrils, crosslinked with mainly XyG and further embedded into a pectic gel matrix. Meanwhile, in the type II wall, the similar cellulose microfibrils are interlocked by mainly glucuronoarabinoxylans (GAXs). It also contains small amounts of XyG and notably less pectin (Carpita 1996, Smith and Harris 1999). However, with the extended research over other species, even across the whole kingdom plantae (Popper and Fry 2003, Popper and Fry 2004), various cell wall polysaccharide compositions were identified, indicating different plant cell wall microstructural models far beyond the classical two types in angiosperms. For instance, the discovery of MLG in horsetail *Equisetum arvense*, one of the closest relatives to seed plants (Pryer, Schneider *et al.* 2001), not only disproved the uniqueness of MLG in type II wall but also raised the possible existence of a different cell wall architecture, comprising high levels of pectin as type I wall, low levels of XyG as type II wall but a nearly complete absence of GAXs (Fry, Nesselrode *et al.* 2008, Sørensen,

Pettolino *et al.* 2008). Another cell wall study of nine fern species and one lycophyte, together with horsetail all belonging to pteridophytes, revealed another cell wall type of mannan and minor XyG and xylans (Silva, Ionashiro *et al.* 2011). With broad-range investigations, cell wall research provides more and more valuable information for plant biology and plant evolution (Popper, Michel *et al.* 2011). Narrowing down to the cell walls of flowering plants, contemporary studies still provide evidence to further retrieve and refine the two cell wall structural models.

1.2.1.2 Secondary cell wall

In certain cell types, a much thicker secondary cell wall will be formed after cells reach their final size and shape, implementing functions like providing mechanical support for the plant or for water transport (Kumar, Campbell *et al.* 2016), for instance, the xylem in Arabidopsis roots (Figure 1.4 III). Though not all secondary walls are rich in lignin; most of them are associated with woody tissue, with a typical composition of cellulose (40-80%), hemicellulose (xylan and glucomannan, 10-40 %), lignin (5-25%) and cell wall proteins. However, the composition of secondary walls do vary among different plant species, secondary walls of different cell types of the same species, or even different developmental stages or coping with environmental stimuli (Zhong and Ye 2015, Kumar, Campbell *et al.* 2016). Cellulose is the load-bearing unit, cross-linking with hemicellulose to form this network, which hydrophobic lignin is impregnated to provide additional mechanical strength, rigidity and hydrophobicity to secondary walls (Zhong and Ye 2009, Zhong and Ye 2015). At subcellular level, a typical secondary wall can be further divided into three layers, namely S1, S2 and S3, as a consequence of changed orientation of cellulose microfibrils (Zhong and Ye 2009).

In regard to the forming of plant cell walls, enormous efforts have been made, especially the use of model plant Arabidopsis (Liepman, Wightman *et al.* 2010, Strabala and Macmillan 2013), to analyse the machinery of biosynthetic pathways for those cell wall components, modulations during the formation process and eventual ways of assembling for all the polymers to form a cell wall matrix. With these knowledge, it will both improve our understandings towards cell wall functioning and utilise it in various cell wall related biological aspects.

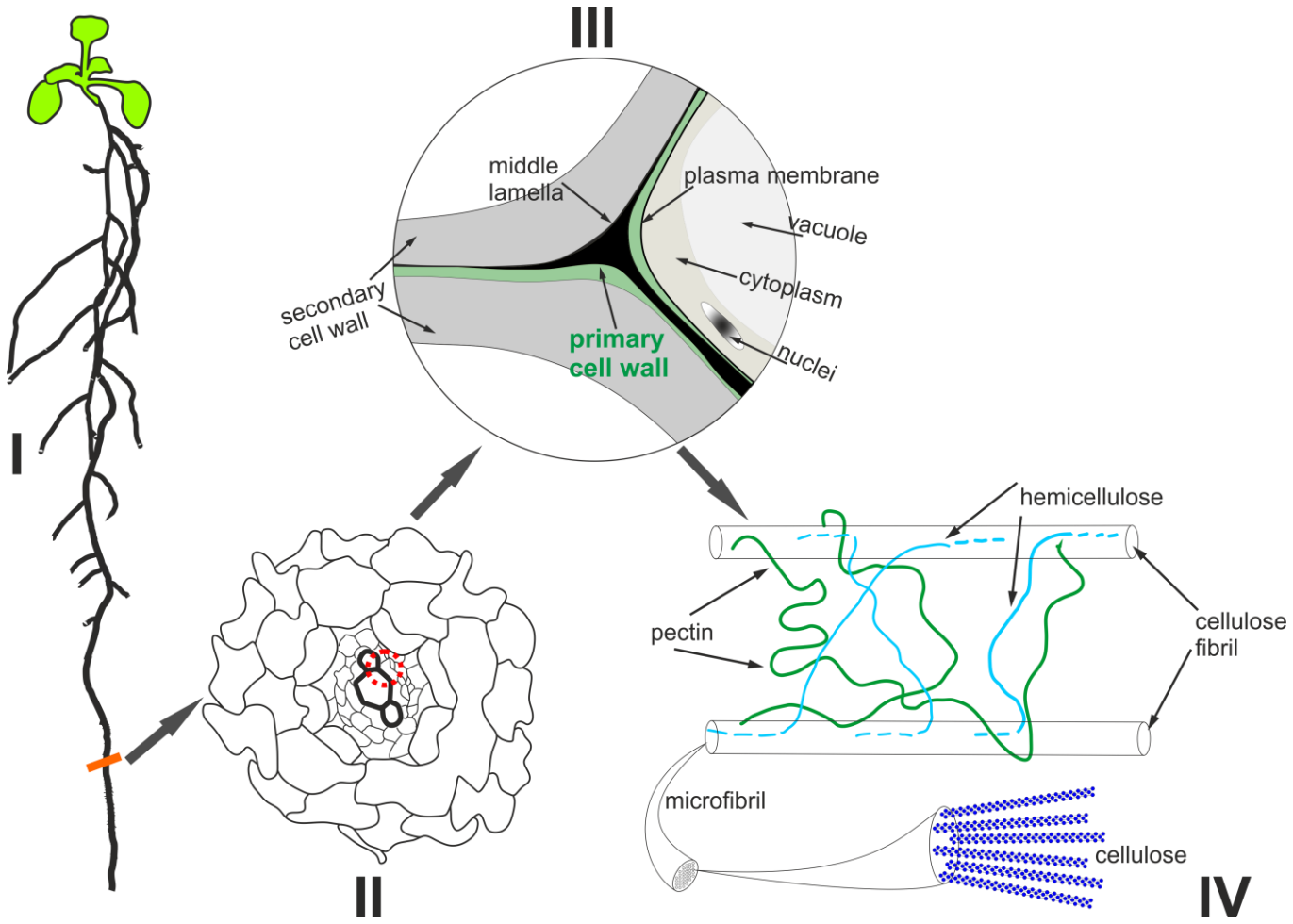

Figure 1.4 Plant cell walls. I. An Arabidopsis seedling; **II**. Root transverse section (xylem in bold line; red dash circle shown in III); **III**. Cell structures around the xylem, indicating different cell wall layers, adapted from (Caffall and Mohnen 2009); **IV**. A model of primary cell wall network, modified from (Dick‐Perez, Wang *et al.* 2012).

1.2.2 Cell wall polysaccharides

Plant cell walls, the skeletal system of plant cells, must have considerable strength to maintain cell shape and enable plant growth against gravity especially for big plants. Meanwhile they must be capable of possessing sufficient flexibility to cope with the large tensile and compressive forces, being porous to allow water and nutrients diffuse freely among cells/tissues and being impermeable in certain cells to allow only required transportations (Cosgrove 2005, Burton, Gidley *et al.* 2010). All those functional requirements are accommodated through the cell wall polymers synthesised and assembled in place properly, eventually forming a cellulose microfibril network embedded in a gel matrix consisted predominantly of cell wall polysaccharides (Burton, Gidley *et al.* 2010). Chemically, the plant cell walls are composed primarily of three classes of polysaccharides, namely cellulose, hemicelluloses and pectins, and they also contain structural proteins and other compounds as well.

1.2.2.1 Cellulose

Of all the cell wall polymers, cellulose is the most abundant biopolymer on the planet and also the most commercially utilised biological material. In plant cell walls, cellulose is present as 30-90% of wall polysaccharides, this together with other cell wall polysaccharides represent more than 90% of primary cell wall mass. Cellulose has been isolated and named nearly two centuries ago, and studied for over 150 years. However, various aspects including its biosynthesis are still not fully understood, even the fine structural model for cell wall cellulose microfibril was still modified recently and is still debated (Cosgrove 2014, Basu, Omadjela *et al.* 2016)

Cellulose is a linear chain of several hundreds to many thousands of unbranched, unsubstituted β-1,4-linked D-glucose units (Figure 1.5), packed into the so called cellulose microfibril and further assembled into a network (Figure 1.4 IV), the load-bearing scaffolding in most types of plant cell walls. The microfibril has been represented as a hexagonal arrangement of 36 glucan chains, based on estimates of microfibril diameter and partly speculation on the basis of the appearance of the cellulose synthase (CesA) complex (CSC) (Herth 1983, Cosgrove 2014, Ding, Zhao *et al.* 2014). However the actual number of chains is still debatable (Figure 1.4 IV, representing a 18-chain model), ranging from 18-36 among some recent research (Fernandes, Thomas *et al.* 2011, Ding, Liu *et al.* 2012, Newman, Hill *et al.* 2013, Thomas, Forsyth *et al.* 2013).

Cellulose biosynthesis in plants is a complex process, involving the formation of plasma membrane-located CSCs, polymerization of glucose into a β-1,4-glucan chain, translocation of glucan across the plasma membrane, and coalescence of multiple glucan chains to form paracrystalline microfibrils (Slabaugh, Davis *et al.* 2014). In higher plants, the CSCs are assembled into rosettes with sixfold symmetry (Mueller and Brown 1980, Kimura, Laosinchai *et al.* 1999) in intracellular compartments and secreted to the plasma membrane, as the functional unit of cellulose synthesis (McFarlane, Doring *et al.* 2014).

Plant *CesA* genes were first identified as homologs of the bacterial cellulose synthase genes (Pear, Kawagoe *et al.* 1996), and the recent crystal structure of bacterial CSC from *Rhodobacter sphaeroides* offered a proposed model for cellulose synthesis and translocation (Morgan, Strumillo *et al.* 2013). A computationally predicted 3D structure of a cotton CESA has also been revealed, providing new knowledge with respect to cellulose polymerization (Sethaphong, Haigler *et al.* 2013). Furthermore, structural snapshots of a complete cellulose biosynthesis cycle, from substrate binding to polymer translocation, have been revealed recently *in crystallo* using bacterial cellulose synthase BcsA-BcsB complex (Morgan, McNamara *et al.* 2016).

As the only known components of the large multimeric CSCs, there are 10 *CesA* genes (*CesA1-10*) in the Arabidopsis genome encoding proteins with similarity to bacterial cellulose synthases. The function of CESA proteins was first revealed via the use of the temperature-sensitive Arabidopsis *rsw1* mutant (*CesA1*), which show reduced amounts of cellulose synthesis, accumulation of noncrystalline β-1,4-glucan, disassembly of cellulose synthase and large morphological abnormalities (Arioli, Peng *et al.* 1998). Until now, *CesA4*, *CesA7* and *CesA8* are associated with cellulose deposition during secondary wall formation, while *CesA1*, *CesA3*, *CesA6*, *CesA2*, *CesA5* and *CesA9* are required for primary walls. Both *CesA1* and *CesA3* are necessary for plant growth and development, although the exact number and stoichiometry of CESAs in primary and secondary wall CSCs are still obscure. The role of *CesA10* is as yet uncharacterised (Endler and Persson 2011, McFarlane, Doring *et al.* 2014), although recently shown to be present in seed mucilage biosynthesis but not essential for this (Griffiths, Šola *et al.* 2015). In a proposed model of CSC functioning, sitosterol-β-glucoside acts as the possible primer for cellulose synthesis *in vitro* (Peng, Kawagoe *et al.* 2002), CSC catalytic subunits use uridine diphosphate glucose (UDP-Glc) as substrate to polymerize the β-1,4-glucan chain, and both microtubule (Paredez, Somerville *et al.* 2006) and the actin cytoskeleton are involved in this process (Wightman and Turner 2008, Endler and Persson 2011). There are still many gaps and controversy over this synthesis process, hence further resolving these issues will lead to greate comprehension of this intricate machinery.

1.2.2.2 Hemicelluloses

Hemicelluloses are traditionally defined as galacturonate-free, neutral or slightly acidic polysaccharides that are extractable from the wall with strong alkali (e.g. aqueous NaOH, 6 M at 37°C) and can be adsorbed from neutralized aqueous solutions by hydrogen-bonding to cellulose (Fry 2004, Cosgrove 2005). Its backbone resembles that of cellulose (apart from MLG), but branched or modified with other sugars, preventing them from forming microfibrils by themselves (Figure 1.5). XyG and arabinoxylan are two of the most abundant hemicelluloses. While in grass (Poales) cell walls, there are abundant MLG and xylans are more in the type of GAX. The most general biological role of hemicelluloses was believed to be contribution to strengthening the cell wall by interacting with cellulose (Scheller and Ulvskov 2010).

Mannans

The mannans, considered to be the most ancient hemicellulose of wall polysaccharides as they are abundant in early land plants (even in walls of some algae), are the major hemicellulose in the secondary wall of gymnosperms while generally less abundant in the walls of spermatophytes (Popper and Fry 2003, Popper and Fry 2004, Scheller and Ulvskov 2010, Silva, Ionashiro *et al.* 2011, Pauly, Gille *et al.* 2013). Based on the backbone composition and side chain substitution, heteromannans can be grouped into four classes: mannan, glucomannan, galactomannan and galactoglucomannan (Scheller and Ulvskov 2010), of which, both mannan and galactomannan consist of a pure β-1,4-linked mannose backbone, while glucomannan and galactoglucomannan contain backbones of β-1,4-linked mannose and glucose in a nonrepeating pattern (Figure 1.5). The biological function for mannans has been associated with cell wall rigidity, mostly functioning as seed storage polymer, and are also shown to be involved in wall signalling, embryogenesis and tissue differentiation (Pauly, Gille *et al.* 2013).

The biosynthesis of heteromannans are synthesised from activated nucleotide sugars in Golgi, similar to other cell wall polysaccharides, guanosine diphosphate mannose (GDP-mannose), GDP-glucose, and uridine diphosphate galactose (UDP-galactose) in this case. These sugars are utilised by highly specific glycosyltransferases (GTs), which facilitate the formation of special linkage between sugar units, further into the polymers (Breton, Snajdrová *et al.* 2006). The first β-mannan synthase was identified in guar seed (Dhugga, Barreiro *et al.* 2004) and shortly in Arabidopsis (Liepman, Wilkerson *et al.* 2005), all belonging to the cellulose synthase-like superfamily (*CSL*). The *CSL* superfamily contain 10 families (namely from *CSLA*, *CSLB* and so on, up to *CSLH*, *CSLJ* and *CesA*), and 31 *CSL* genes together with 10 *CesA* genes are identified in Arabidopsis genome, classified into six *CSL* families (*CSLA*/*B*/*C*/*D*/*E*/*G*) and one *CesA* gamily (Richmond and Somerville 2000, Cosgrove 2005, Yin, Huang *et al.* 2009). Until recently, identified genes responsible for Arabidopsis (gluco)mannan are mainly from the *CSLA* family, including C*SLA2*, *CSLA3*, *CSLA7* and *CSLA9* (Goubet, Barton *et al.* 2009). Three more genes from the *CSLD* family, *CSLD2*, *CSLD3* and *CSLD5*, were also shown to be involved in mannan synthesis and early development (Verhertbruggen, Yin *et al.* 2014).

Xyloglucans

Xyloglucans are the most abundant hemicellulose in the primary walls of spermatophytes except for grasses, making up to 20-25% of the wall polysaccharide in compared to 2-5% in grass primary walls and minor in secondary walls (Scheller and Ulvskov 2010, Pauly and Keegstra 2016). They have been found in every land plant species ever analysed, with a basic structure of β-1,4-glucan backbone substituted with xylosyl residues and these xylosyl residues can be further substituted with other glycosyl and nonglycosyl substituents (Figure 1.5). Those substitution variations and branching patterns stands for both functional and taxonomic significance (Scheller and Ulvskov 2010). A one-letter code, according to the substituents of XyG, has been developed (Fry, York *et al.* 1993) and update recently (Tuomivaara, Yaoi *et al.* 2015) to mark these variations. It includes: 'G' denotes an unbranched Glc residue, 'X' denotes α-D-Xyl-(1,6)-Glc, 'L' represents β-D-Gal-(1,2)-α-D-Xyl-(1,6)-Glc, and so on (Glc, glucose; Xyl, xylose; Gal, galactose) (Figure 1.5). As in Arabidopsis,

many other dicots and non-graminaceous monocots, XyG usually appear in a three-xylosyl-residue per four backbone glucosyl pattern (XXXG-type), while in Poales order and several other clades of monocots, some mosses, lycophytes, and liverworts, the XyG backbone is less xylosyl substituted, as shown in a two xylosyl residues per four or more glucosyl residues ($XXGG_n$-type) (Figure 1.5) (Scheller and Ulvskov 2010, Pauly, Gille *et al.* 2013, Pauly and Keegstra 2016).

Besides distribution and structure, wide range of studies also cover function and biosynthesis of XyG. It has long been recognised as forming a cross-linking network with microfibrils, as its ability to bind to cellulose via such as hydrogen bonds (Valent and Albersheim 1974, McCann, Wells *et al.* 1990, Cosgrove 2005). This was believed to be the main load-bearing structure, playing the leading role during chemical processes essential for wall expansion and therefore cell growth and differentiation. Enzymes, such as endo-xyloglucan transferase (EXT), a member of a larger family of xyloglucan endotransglucosylase/hydrolase (XEH), as well as expansins, are involved in modulating this network (Smith and Fry 1991, Nishitani and Tominaga 1992, McQueen-Mason and Cosgrove 1994, Cosgrove 2000, Cosgrove 2005). These concepts of XyG function emerged from a large amount of studies, summarised and extended by later results in various ways (Park and Cosgrove 2015). However, the use of an Arabidopsis mutant lacking of detectable XyG, that was found to grow essentially normal apart from being shorter and have aberrant root hairs, has challenged this conventional XyG-cellulose tether network model (Cavalier, Lerouxel *et al.* 2008). Although, the XyG is still considered to play a reinforcing role and important for wall loosening mediated by α-expansin in this mutant (Park and Cosgrove 2012), those findings indicate that XyG is not that vital for normal wall structure or function. An updated model depicts that cellulose interactions with XyG are more restricted to limited regions ('biomechanical hotspots'), whereas pectin cellulose interactions are more prevalent. Therefore, wall loosening mediated by expansins and specific endoglucanases may be limited to those limited regions where cellulose microfibrils are brought to close contact by XyG (Cosgrove 2014, Cosgrove 2014). Besides, XyG is reported to be capable of rapid shifts in molecular mass (*Mr*) under various conditions, for instance, the peak values for its relative *Mr* can vary from 9 kDa (28 glucose residues, 14 nm) to 900 kDa (2800 glucose residues, 1400 nm). These change in peak values is remarkable and thought to play a central role in cell wall architecture and mechanics (Park and Cosgrove 2015). Moreover, XyG is also deposited during seed development in certain species, generally not interact with cellulose in this case and thus being water soluble, indicating its use as storage polysaccharide that can be degraded to provide energy for seeds germination and seedling growth (Pauly and Keegstra 2016).

Similar to the synthesis of most complex carbohydrates, XyG biosynthesis occurs in Golgi, through adding a sugar residue from an activated sugar to the nascent polymer chain by glycan synthases and GTs. It is then packaged into secretory vesicles, delivered to the plasma membrane, released to the extracellular matrix and continue to be modified by various enzymes (Pauly and Keegstra 2016). Breaking down the XyG biosynthesis process, it includes synthesis of glucan backbone, xylosyl substitution and acetyl modifications, and

adding further more substituents. By analysing the transcripts of the last maturation stage of nasturtium (*Tropaeolum majus*) seeds, as a large amount of XyG is deposited as a reserve polysaccharide, a *CSLC* gene was identified and a homolog (*AtCSLC4*) revealed to be related to XyG backbone synthesis in Arabidopsis (Cocuron, Lerouxel *et al.* 2007) Golgi membrane (Davis, Brandizzi *et al.* 2010). As four barley *CSLC* genes (*HvCSLC1-4*) are located in the plasma membrane, not all *CSLCs* are involved in XyG biosynthesis (Dwivany, Yulia *et al.* 2009). The mechanism responsible for patterning of xylosyl substitutions is still elusive. Five candidate genes have been identified for XyG:xylosyltransferase (XXT) activity in Arabidopsis, not all but at least some of them are proven to be involved in XyG biosynthesis. For instance, XXT1 and XXT2 are shown to be responsible for the bulk of xylosylation of the glucan backbone and at least one of them must be present for successful XyG synthesis, while XXT5 is proven to play a significant yet not fully characterised role in this process (Zabotina, van de Ven *et al.* 2008, Zabotina, Avci *et al.* 2012, Culbertson, Chou *et al.* 2016). In the meantime, CSLC and XXT proteins are shown to be capable of forming multiprotein complexes and be able to work together to form XyG (Chou, Pogorelko *et al.* 2012, Pauly and Keegstra 2016). Further substitutions to either the backbone or the xylosyl substituents, including such as galactosyl, fucosyl and acetyl, require multiple enzymes to form, transport and add those groups of units to various positions of XyG, complex and highly variable depending on plant species (Scheller and Ulvskov 2010, Pauly, Gille *et al.* 2013, Pauly and Keegstra 2016).

Xylans

Xylan, a polymer of β-1,4-linked xylose units, is the major hemicellulose in secondary walls of dicots and walls of commelinid monocots. Its deposition in secondary walls is required for normal plant growth and development, and the cell wall recalcitrance will be increased, defending against herbivores and pathogens (Rennie and Scheller 2014). The backbone of xylose units can be further modified in various forms and a common substitution is with α-(1→2)-linked glucuronosyl and 4-*O*-methyl glucuronosyl residues. Xylans, abundant in this type substitution, are the dominating noncellulosic polysaccharide in dicots secondary walls, namely glucuronoxylan (GXs). In the reducing end of the dicot xylan molecules, there is a conserved tetrasaccharide β-D-Xyl*p*-(1,4)-β-D-Xyl*p*-(1,3)-α-L-Rha*p*-(1,2)-α-D-Gal*p*A-(1,4)-D-Xyl*p* structure, considered to be the initiator or terminator of xylan backbone synthesis (York and O'Neill 2008, Rennie and Scheller 2014). In the walls of commelinid monocots, xylans usually contain many arabinose residues, known as GAXs or arabinoxylans, and these α-(1→3)-linked residues may be further substituted with xylose or ferulic acid (Figure 1.5) (Scheller and Ulvskov 2010, Rennie and Scheller 2014). Feruloylated GAXs are found throughout the commelinid monocots and not in other groups of seed plants. The importance of ferulate esters is that it can be oxidatively cross-linked thus render the cell wall recalcitrant to digestion (Scheller and Ulvskov 2010).

Great progress has been made towards identifying the GTs that synthesise xylan. The use of *irregular xylem* (*irx*) Arabidopsis mutants has been instrumental in elucidating the mechanisms of xylan biosynthesis. *IRX9*, *IRX14* from GT43 family and *IRX10* from GT47 family, together with their homologous genes *IRX9L* (*IRX9 like*), *IRX14L* and *IRX10L*, are

thought to be responsible for xylan backbone elongation (Brown, Goubet *et al.* 2007, Lee, O'Neill *et al.* 2007, Brown, Zhang *et al.* 2009, Hu, Li *et al.* 2016). Mutations of these genes cause dwarfing and a reduction in xylan content and xylosyltransferase activity, suggesting their function in Golgi located xylan synthase complex (XSC). A study using heterologous expression of asparagus AoIRX9, AoIRX10 and AoIRX14A in *Nicotiana benthamiana* has allowed reconstituted and partially purified active XSC, and further proven that the three proteins were the core component of XSC, each with distinct roles for effective xylan biosynthesis (Zeng, Lampugnani *et al.* 2016). This agrees with other studies in wheat, indicating the presence of several GTs in the same XSC (Zeng, Jiang *et al.* 2010, Jiang, Wiemels *et al.* 2016). IRX7 (also known as FRA8), IRX8 (GAUT12) and PARVUS (GATL1) are all specifically involved in synthesizing the oligosaccharide of the conserved structure at the reducing end of xylans (Rennie and Scheller 2014). In terms of substitution of xylan backbone, enzymes should include α-glucuronsyltransferases and α-arabinofuranosyltransferases to form the most important side chains (Scheller and Ulvskov 2010). GUX1 and GUX2 are required for glucuronic acid substitution of xylan in Arabidopsis stem cells (Mortimer, Miles *et al.* 2010, Rennie, Hansen *et al.* 2012), while rice and wheat GT61 proteins are related to adding arabinose to xylan in grass (Anders, Wilkinson *et al.* 2012). Another rice GT61 family gene *XAX* was found to possess β-1,2-xylosyl transferase activity, capable of transferring xylose from UDP-xylose onto xylan. Other modifications of xylan, including such as methylation of glucuronic acid (Urbanowicz, Peña *et al.* 2012) and acetylation (Yuan, Teng *et al.* 2016, Yuan, Teng *et al.* 2016), are all being extensively studied providing increasing valuable information towards xylan biosynthesis and future bioenergy production (Pauly, Gille *et al.* 2013, Rennie and Scheller 2014).

Mixed Linkage Glucan

β-(1,4)-linked glucans with interspersed single β-(1,3)-linkages are known as MLG (Figure 1.5). It was thought to be unique to Poaceae family (grass) of type II wall, then later found in some other families in the order Poales (Smith and Harris 1999) and even in pteridophytes horsetail *Equisetum* (Fry, Nesselrode *et al.* 2008, Sørensen, Pettolino *et al.* 2008) and red algae (Popper, Michel *et al.* 2011). The abundance of MLG is regulated developmentally and changes during cell elongation, including accumulating predominantly in old tissues in the stems (Vega-Sánchez, Verhertbruggen *et al.* 2013). Recent study revealed the binding ability of MLG to cellulose *in vitro*, similar to some other hemicelluloses, including XyG, arabinoxylan and mannan (Kiemle, Zhang *et al.* 2014). Another study also pointed out the suggested correlation between silicon accumulation and MLG, indicating its ability in strengthening cell wall in the presence of silicon in rice leaf blades (Kido, Yokoyama *et al.* 2015). It also is postulated as storage polymer as well, though much detailed aspects of its role in terms of cell wall architecture remains largely obscure (Pauly, Gille *et al.* 2013).

Owning a simple structure, MLG is glucose-based unsubstituted, non-branched homopolymer, whereby randomly distributed β-1,4-linked cellotriosyl and cellotetraosyl units linked by β-1,3- linkages. Two gene classes have been identified responsible for MLG synthesis, *CSLF* and *CSLH*. The expression of a rice *CSLF* gene in Arabidopsis caused the

detection of MLG in transgenic plants, providing direct evidence for MLG biosynthesis (Burton, Wilson *et al.* 2006). Similarly, a barley *CSLH* gene was also shown to be able to mediate the synthesis of MLG in Arabidopsis, independently to the *CSLF* family (Doblin, Pettolino *et al.* 2009). Further study reveals that a single amino acid within the transmembrane domain of *CSLF6*, a major component of the MLG synthase, can control MLG structure, responsible for the structural varieties existed between different cereals and during developmental stages of plant growth (Jobling 2015). However, the exact mechanism for MLG biosynthesis remains largely theorised (Scheller and Ulvskov 2010, Pauly, Gille *et al.* 2013), especially the recent discovery that MLG synthases were localised in plasma membrane, instead of Golgi, where other hemicelluloses are assembled, suggesting a different model of MLG assembly mechanism (Wilson, Ho *et al.* 2015).

1.2.2.3 Pectins

Pectins are wall polysaccharides that are solubilized by aqueous buffers and dilute acidic solutions or calcium chelators (Cosgrove 2005), and are most abundant in plant primary walls and the middle lamellae. Apart from this conventional definition, pectin is more a family of plant cell wall polysaccharides and/or glycan domains that contain galacturonic acid (GalA) linked at both 1 and 4 positions (Atmodjo, Hao *et al.* 2013). Pectins can be grouped into three major classes on the basis of the structure: HG, RG-I and RG-II, of which RG-II is the most complex cell wall polymer (Figure 1.5). Some plant species also contain some other structural classes, known as XGA and AGA. It is worth emphasising that different pectic polysaccharides are not separate molecules but rather covalently linked domains. Similar to other matrix polysaccharides, pectins are synthesised and modified as they move through different Golgi cisternae and the *trans*-Golgi network and are transported via vesicles to the cell wall. They crosslink to hemicelluloses, phenolics and proteins, contributing to cell strength, cell adhesion, stomatal function, defence response and more (Caffall and Mohnen 2009, Atmodjo, Hao *et al.* 2013).

Homogalacturonan

Pectin is abundant in primary walls of dicots and nongrass monocots and some fruits as well, while present in much lower amounts in secondary walls and grass primary walls. Of the overall pectins, HG stands for approximately 65%. HG is a polymer of α-1,4-linked-D-GalA, and the backbone can be further decorated with methyl or acetyl groups at C-6 and *O*-2 or *O*-3 (Figure 1.5). The pattern and degree of methylesterification and acetylation vary from source to source. The unmethylated C-6 of HG GalA is negatively charged and could form a stable gel with Ca^{2+}, the so called egg-box model (Liners, Letesson *et al.* 1989), providing strength to the wall or making HG a target for pectin degrading enzymes, such as polygalacturonase (PG) and pectin/pectate lyases (PL) (Wolf, Mouille *et al.* 2009, Jolie, Duvetter *et al.* 2010). The degree of methylation also influence the elasticity and porosity of pectic gels, making such modulation of the methyl groups affect the properties of cell wall matrix in planta.

The HG is assumed to be synthesised in Golgi and secreted in a fully methyl-esterified form. The methylation status is then controlled by cell wall-localized esterase, pectin

methylesterases (PMEs). PMEs can catalyse the removal of methyl groups from HG, and their activities can be modulated in various levels and ways, such as pH, ionic strength as well as the PME inhibitors (PMEIs), specifically inhibiting plant PMEs (Wolf, Mouille *et al.* 2009, Jolie, Duvetter *et al.* 2010). Both PMEs and PMEIs are large multigene families, for instance, there are 66 and 69 ORFs have been annotated as putative PMEs and PMEIs respectively, indicating the diversity of their role in plant development (Wolf, Mouille *et al.* 2009). Besides, PMEs also cooperate with pectic enzymes, particularly PGs, in the processes of loosening and wall disassembly during organ initiation, cell elongation, pollen tube growth, and fruit softening (Lionetti, Cervone *et al.* 2012).

Rhamnogalacturonan II

As the most structurally complex polymer, RG-II has a backbone of HG substituted with various side chains comprising 13 different types of glycosyl residues, and constitutes ~10% of pectin (Atmodjo, Hao *et al.* 2013). In an RG-II molecule, a stretch of approximately 7~9 backbone residues are decorated with four well-defined side chains (Figure 1.5). Despite the complexity of substituents, there is structural conservation of RG-II across higher and lower land plants. It exists as a borate cross-linked dimer in primary cell wall and this dimer is required for a function wall assembly and normal plant growth. Reduced borate cross-linking of RG-II is usually associated with reduced growth, brittle tissues, and swollen cell walls or even deleterious in some plant species, thus reflecting the importance of forming a functional network of RG-II, HG and RG-I in plant growth (Bar-Peled, Urbanowicz *et al.* 2012).

Rhamnogalacturonan I

Unlike RG-II, RG-I makes up 20-35% of pectin and has a disaccharide repeat backbone of [α-D-GalA*p*-(1,2)-α-L-Rha*p*-(1,4)-]$_n$ rather than an HG backbone, in which GalA residues are highly acetylated at *O*-2 or *O*-3 position (Rha, rhamanose) (Atmodjo, Hao *et al.* 2013). The extended conformation of RG-I reveals that the RG-I isolated from cell walls is highly branched by arabinan, galactan, or Type-I AG and Type-II AG (AG, arabinanogalactan) side chains at C-4 of the Rha residues (Figure 1.5), while isolated seed mucilage RG-I is unbranched. About half of the Rha residues of the RG-I backbone are substituted with α-(1,5)-linked-L-Ara*f* or β-(1,4)-linked-D-Gal*p* side chains (Ara, arabinose). The arabinan chain consists of α-(1,5)-L-Ara*f* backbone, with possible Ara*f* and/or arabinan branched at *O*-3; galactan and Type-I AG are composed with β-(1,4)-D-Gal*p* backbone and Type-I AG is characterised by single interspersed α-(1,5)-L-Ara*f* residue and galactan chain is branched with one or more Ara*f* residue or a single terminal Ara*p*. Comparing with Type-I AG, Type-II AG is in much smaller amounts over all RG-I related AGs, and it is composed of a β-(1,3)-D-Gal*p* backbone with branch points of 6-linked β-D-Gal of one to three residues. These side chains of RG-I are found to be developmentally regulated and with great heterogeneity among different sources (Caffall and Mohnen 2009).

The RG-I related arabinans are shown to be affecting the opening and closing of the stomata, with a hypothesis that arabinans work as spatial regulators of the proximity HG thus preventing the formation of HG and Ca^{2+} interaction (Jones, Milne *et al.* 2003),

supported by studies using cells under extreme water deficit stress (Moore, Farrant *et al.* 2008). As arabinans together with galactan are highly mobile comparing with other pectic components, the mobility of these side chains will be largely affected facing hydration and they will thus retain mobility longer upon desiccation (Ulvskov, Wium *et al.* 2005, Moore, Nguema-Ona *et al.* 2013). Later, reduction of arabinan is shown to cause collapse of pollen in its late developmental stage, indicating an important role for arabinan in pollen grain maturing and dehydrating (Cankar, Kortstee *et al.* 2014). These all together indicate that the RG-I components play a role of transmitting stress in the wall, maintain flexibility and integrity of the wall, and hence directly affect wall rheological property.

As complex macromolecules, if unique enzymes are needed to catalyse the formation of each unique pectic glycosidic linkage (as illustrated in Figure 1.5), pectin biosynthesis requires at least 67 different transferases, including GTs, methyltransferases (MTs) and acetyltransferases (ATs). Two hypothetical models are proposed for this overall process, the consecutive GT model and the domain synthesis model. In the consecutive GT model, GTs work independently and sequentially to add sugar residues to the nonreducing end of the backbone or sidechain of pectin; while in the other data-supported domain synthesis model, it includes elongation of oligosaccharide domains, en bloc transfer of a domain onto another domain (might happen repeatedly), and eventually transfer the mature polysaccharide to the wall (Atmodjo, Hao *et al.* 2013). However, same as revealing the structural complexity and diversity of pectins, further studies are needed to solve this conundrum.

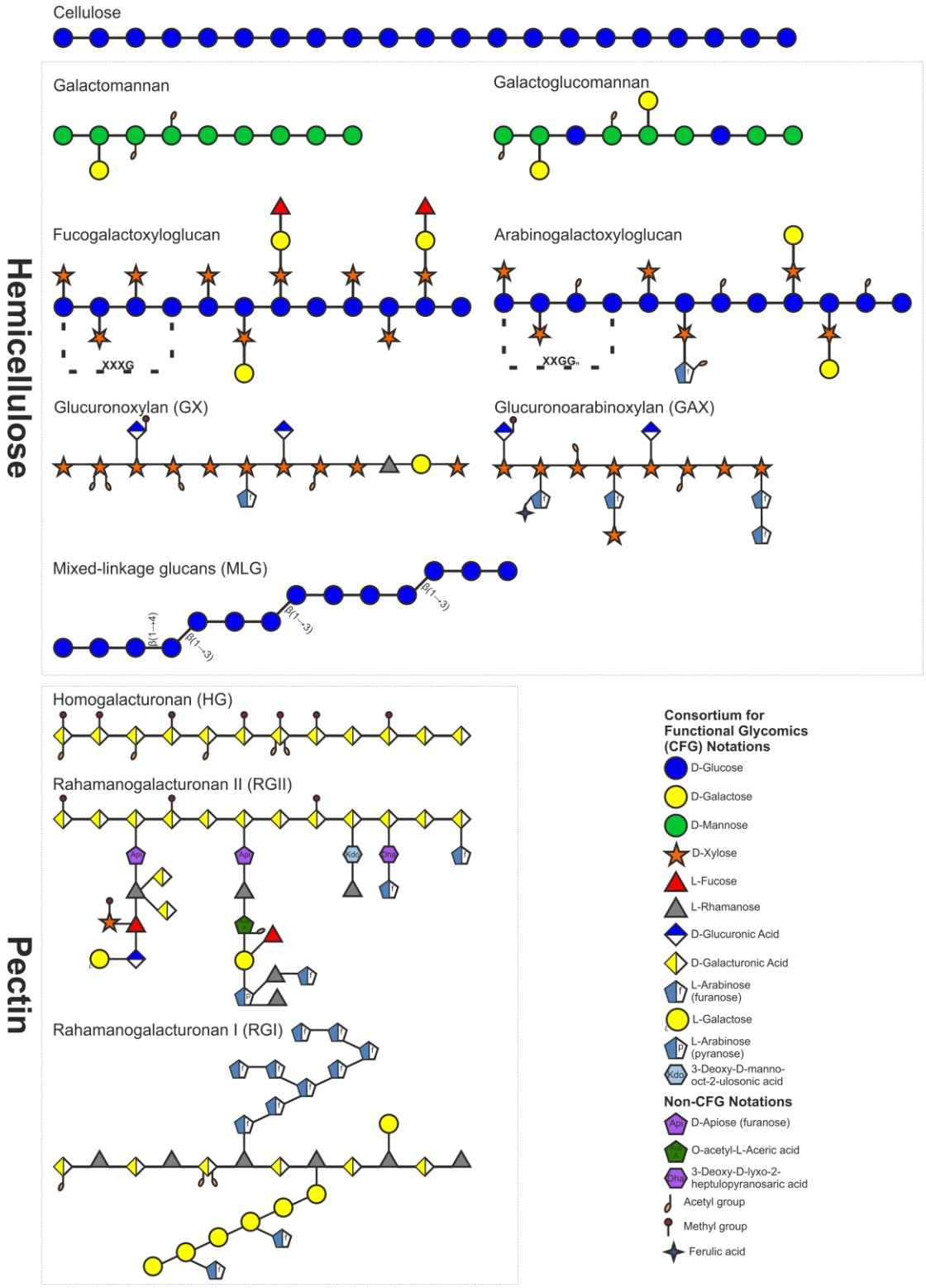

Figure 1.5 Schematics of chemical structures of plant cell wall polysaccharides. Composed and redrawn from (Scheller and Ulvskov 2010, Pauly, Gille *et al.* 2013, Kumar and Turner 2015). For pectins, only the most general structural classes are listed.

1.2.3 Cell wall proteins

Apart from abundant complex polysaccharides, plant cell wall still possess ubiquitous proteins. They are usually rich in one or two amino acids, contain highly repetitive sequence domains, and are glycosylated to various extent, such as hydroxyproline-rich glycoproteins (HRGPs) and glycine-rich proteins (GRPs) (Cassab 1998). These proteins are essential constituents of plant cell walls and involved in different biological functions, such as cell wall polymer and/or cell wall structure modifications and signalling and interactions with plasma membrane proteins (Jamet, Canut *et al.* 2006).

HRGPs

HRGPs are a superfamily of plant cell wall proteins with diverse functions in plant growth and development. It consists of three members: hyperglycosylated arabinogalactan proteins (AGPs), moderately glycosylated extensins (EXTs), and lightly glycosylated proline-rich proteins (PRPs). Besides, hybrid HRGPs, composed of HRGP modules from different families, and chimeric HRGPs, composed of one or more HRGP modules within a non-HRGP protein, can also be considered part of the HRGP superfamily (Showalter, Keppler *et al.* 2010).

AGPs are a family of proteoglycans identified on plasma membrane and the cell walls of various plant species. Generally, they contain repetitive dipeptide motifs, such as Ala-Pro, Ser-Pro, Thr-Pro, and Val-Pro, which are distinguishable comparing with EXTs sequence motifs. Moreover, many AGPs are attached to the plasma membrane via one glycosylphosphatidylinositol anchor, but can be cleaved by phospholipases. The glycan moiety of AGPs accounts for over 90% of their total mass and is shown to possess various structures, of which the common structural feature is a backbone of β-1,3-galactan. It can be further decorated to great complexity and it is suggested to play an key role in AGPs function (Knoch, Dilokpimol *et al.* 2014).

EXT is the most well-studied cell wall structural protein of plants. The classical EXTs can be defined as wall-located, Hyp-rich structural glycoproteins with alternating hydrophilic and hydrophobic motifs whose alignment as self-assembling amphiphiles likely drives extensin work assembly. The hydrophilic motifs comprise arabinosylated X-Hyp_n, where X usually is Ser and n is mostly 4 and occasionally 5, while the hydrophobic part varies, may be a single amino acid or dipeptide and often containing Tyr residues as potential cross-link sites (Lamport, Kieliszewski *et al.* 2011). They are well known to be able to form an insolubilized, covalent network in cell walls therefore affect cell walls physical properties.

PRPs contain one repetitive motif (Pro-Hyp-Val-Tyr-Lys)$_n$, lacking Ser and lightly glycosylated. The expression of PRP genes is shown to be influenced by wounding, drought, light and more, meanwhile the expression pattern is proven to be tissue or cell specific. Functional studies indicate that PRPs are also implicated in various aspects of plant development, ranging from germination, pod formation, to the early stages of nodulation (Cassab 1998).

GRPs

GRPs are characterised by the presence of semi-repetitive glycine-rich motifs in plants. They are further classified based on their general structure, as well as the arrangement of the glycine repeats and the presence of conserved motifs (Mangeon, Junqueira *et al.* 2010). Functions of GRPs in plant cell wall include acting as cell wall constituents, involved in secondary cell wall formation and lignin biosynthesis or a structural role in cell wall (Mangeon, Junqueira *et al.* 2010).

Expansin

Expansins are cell wall proteins that mediate acid-induced growth by catalysing loosening of plant cell walls without lysis of wall polymer (Cosgrove 2000, Cosgrove 2015). Classified by sequence-based phylogeny, plant expansins are grouped into two major families, namely EXPA (α-expansins) and EXPB (β-expansins). Additionally, expansins also include two smaller families, expansin-like A and B (EXLA, EXLB), also with proposed function as targeting the cell wall for modification (Cosgrove 2015). Expansins are required in almost all plant physiological development aspects, from germination, roots and leaf growth, to stem elongation and fruiting (Marowa, Ding *et al.* 2016).

1.2.4 Other cell wall components

Apart from the abundant polysaccharides, plant cell walls still possess other chemical components, such as phenolic compounds, lignin, and callose. However, they are either found in much lower abundance, or only present in restricted regions or cell types.

Ferulic acid

Ferulic acid, 4-hydroxy-3-methoxy-cinnamic acid, can represent up to 3% of the dry weight of graminaceous cell walls. It is commonly found in both primary and secondary grass cell walls, and is most abundant in the epidermis, xylem vessels, bundle sheaths, and sclerenchyma. Ferulic acid residues are mainly introduced into the grass cell wall polysaccharides via an ester linkage between the carboxylic group of ferulic acid and the C-5 alcohol of the arabinose side chain of arabinoxylans. Additionally, it can also be covalently linked to lignin monomers. In grass cell wall, it could form dehydrodiferulate dimers, cross-linking polysaccharide chains, and feruloylation of arabinoxylan may facilitate lignin formation and the linkage of lignin to the xylan/cellulose network (Buanafina 2009). The cross-links has also been postulated to play important roles in modulating cell wall extensibility and protecting against pathogen invasion (Ishii 1997, Buanafina 2009).

Lignin

Lignin is a major component of most secondary cell walls, representing the second most abundant biopolymer on the planet. Chemically, it is a heterogeneous and complex polymer largely derived from three hydroxycinnamyl alcohol precursors, *p*-coumaryl, coniferyl, and sinapyl alcohol. These polymers are deposited predominantly in walls of

secondarily thicken cells, providing rigidity and imperviousness. Its biosynthesis can also be induced upon various biotic and abiotic stress conditions, such as pathogen invasion and metabolic stress (Vanholme, Demedts *et al.* 2010).

Callose

Callose is a linear polymer of glucose units like cellulose, but linked by β-(1,3)-linkage rather than β-(1,4) of cellulose. It is synthesised at the plasma membrane, and it is present in cell walls in minor quantities comparing with other hemicellulose. Its biological function involves cell plate formation, pollen development, plasmodesmata regulation, pathogen resistance and stress response (Kumar and Turner 2015)

1.2.5 Syncytial cell walls

Great efforts have been made in plant nematode parasitism research, making huge progress in further comprehension of host-nematode interactions (as discussed above). However, as the 'result' of host-cyst nematode interaction, apart from the fine structural observations of syncytia made in the past few decades, most of the recent revealed plant cell wall related effectors, e.g. cellulase, pectate lyase and expansins, are more responsible for cell wall degrading and facilitating the migration of nematodes . Even though, the formation of syncytia also requires new cell wall materials synthesis, and this is believed to be completed through nematode manipulating host cell machinery (Bohlmann and Sobczak 2014), the actual cell wall microstructures of mature syncytia are still largely unknown.

Frist research in this topic was carried out via *H. schachtii* female induced syncytium in Arabidopsis roots and the study revealed the general chemical compositions of syncytial cell walls (Davies, Lilley *et al.* 2012). Immunohistochemical results show that the syncytial walls are composed with cellulose, hemicellulose XyG and heteromannan, lack of xylan and galactan and rich in methyl esterified homogalacturonan (methyl-HG) (Davies, Lilley *et al.* 2012). Part of the results, the presence of HG and methyl-HG, is later confirmed in other research using the same materials (Wieczorek, Elashry *et al.* 2014). Similar work has also been involved in a recent study using cereal cyst nematode *H. avenae* induced syncytia in both susceptible and resistant barley cultivars, and the results conclude that the syncytial walls contain barely detectable levels of HG, methyl-HG and heteroxylan, and with confirmed presence of MLG, callose and cellulose (Aditya, Lewis *et al.* 2015).

These studies provide us a new insight of this unique feeding structure. However, due to certain limitations, especially the range of cell wall probes used, these results are yet not capable of drawing a general picture of how the microstructure of syncytium could fulfil its functional role. Especially when considering the significantly thickened outer syncytial walls, withstanding the high turgor pressure within (usually 9000-10000 hPa comparing to about 2000 hPa in cortex cells and 4000 hPa in vascular parenchyma cells) (Böckenhoff and Grundler 1994), and the large volumes of nutrients withdrawal by the nematode (about four times of the syncytium size per day) (Muller, Rehbock *et al.* 1981), the chemical

compositions should be able to provide the syncytium enough strength whilst maintain certain level of flexibility. Therefore, fine chemical microstructures of syncytia induced by major cyst nematode species in their preferred hosts are needed to help us to get broader comprehension.

1.3 Project overview

In order to investigate the cell wall microstructure of cyst nematode induced syncytia, some of the most economically important cyst nematode species, including *G. pallida*, *H. glycines*, *H. avenae* and *H. filipjevi*, together with their natural hosts have been chosen. Immunohistochemical analysis has been applied, using of a set of cell-wall-polymer specific probes, to reveal the general microstructures of cyst nematode syncytial walls.

Based on the general microstructures of cyst nematode syncytia, selected Arabidopsis mutants, (potentially) targeting important cell wall components, have been used to reveal the relation between syncytial cell wall chemical compositions and nematode parasitism.

Finally, the expression pattern of a root-cap-specific protein (RCP) promoter will be investigated in hexaploid wheat by either bombardment or *Agrobacterium tumefaciens* mediated transformation, hoping to evaluate its potential usage in furture studies of wheat-cereal cyst nematode interactions.

Chapter 2 Materials and methods

2.1 Biological materials

2.1.1 Cyst nematodes stock maintenance

Potato cyst nematode *Globodera pallida* was maintained by growing susceptible potato plants (*Solanum tuberosum* L. cv. Désirée) in infected soil containing approximately 50 eggs per gram in a greenhouse, at 18-20 °C under 16 h/8 h photoperiod. Dry soil with cysts were collected after 2-3 months and kept at 4 °C until needed.

Soybean cyst nematode *Heterodera glycines* was maintained in the greenhouse on cultivated soybean plants (*Glycine max* (L.) Merr. cv. Williams) in pots filled with infested soil, containing approximately 10 *H. glycines* eggs per gram soil. Plant tops were removed after about 40 days and the root systems were left in pots for a further 2 weeks. The soil was then collected at stored at 4 °C until required.

Beet cyst nematode *H. schachtii* was maintained through planting 4-week-old cabbage (*Brassica oleracea* cv. Primo II) in infected soil containing approximately 20 *H. schachtii* eggs per gram soil. Damp soil was collected after about 2-3 months and stored at 4 °C until required.

Cereal cyst nematodes *H. avenae* and *H. filipjevi* cysts were extracted from field soil sourced from Turkey. Cysts stock were then kept in water at 4 °C until required.

2.1.2 Nematode cysts sterilization and hatching

H. glycines and *H. schachtii* cysts were extracted from infected soil using a Fenwick can method and incubated in 0.1% malachite green solution for one hour at room temperature on a rotating sample mixer. The cysts were rinsed in tap water overnight until water became clear and then treated with antibiotic cocktail (streptomycin sulfate 8.00 mg/mL, penicillin G 6.00 mg/mL, polymyxin B 6.13 mg/mL, tetracycline 5.00 mg/mL, amphotericin B 1.00mg/mL) at 4 °C for 24 hours. Cysts were then rinsed in sterile tap water and transferred into autoclaved hatching jars in dark at 25 °C and 20 °C respectively. 2mM $ZnCl_2$ was used to stimulate nematodes hatching. Newly hatched second-stage juveniles (J2s) were collected in a non-stick 15 mL polystyrene tube (Sarstedt, Germany) every other day and could be stored at 10 °C for future use.

G. pallida cysts were extracted from infected soil and soaked in 1% sodium hypochlorite for 5 minutes. Cysts were then transferred into 100% ethanol for 30 seconds and rinsed in sterile tap water for 3 times. Finally, cysts were placed in an autoclaved hatching jar with

added potato root diffusate and incubated at 20 °C in dark to hatch. Newly hatched J2s were collected every other day and were stored in 10 ° until needed.

H. avenae and *H. filipjevi* cysts were rinsed in sterile tap water and stored in a 1.5 mL tube at 4 °C for a month before hatching. Cysts were then placed into a sterile hatching jar and stored at 10 °C or 4 °C in dark. If fungi were found during hatching, a 0.1 % chlorhexidine gluconate and 0.5 mg/mL cetyl trimethyl ammonium bromide (CTAB) solution could be applied to sterilize J2s and/or eggs for 25-32 minutes. After rinsing in sterile tap water for 3 times, they were placed back to the hatching jar. Newly hatched J2s were collected and stored in 4 °C until required.

2.1.3 Potato, soybean and wheat hydroponic culture

In order to obtain clean nematode infected root samples, host plants were cultivated in cyg germination pouches (Mega-International) in a plant growth chamber.

Potato (cv. Desiree) chits of similar age were taken off from potatoes stored at room temperature and transferred to cyg germination pouches. Cultivation was then carried out at 20 °C under 16 h/8 h photoperiod. Soybean (cv. Toliman) seedlings, germinated in Petri dishes at room temperature, were transplanted in pouches and the following cultivation were carried out at 25 °C, 16 h/8 h photoperiod. Fresh tap water was added every other day for both potato and soybean seedlings and the roots growth status were monitored.

Spring wheat (*Triticum aestivum* L. cv. Bobwhite, Cadenza and Fielder) seeds were soaked in 0.5% H_2O_2 (v/v) overnight and then thoroughly washed and placed in a Petri dish with wet filter paper for germination at room temperature. 5-day-old seedlings with healthy roots were transferred to pouches and cultivated at 20 °C under 16 h/8 h photoperiod. The seedlings were supplied with full-strength Hoagland nutrient solution (MP Biomedicals) when the third leaf was about to emerge. Water was added daily to make up for the evaporation losses and the pH of the solution was monitored. The replacement of the nutrient solutions was done every other week for the first two weeks and then once per week afterwards (Gorham, Bridges *et al.* 1997).

2.1.4 Nematode inoculation

Collected J2s were suspended in autoclaved tap water at one J2 per µL. Selected root tips (approximately 7-day old) of cultured host plants were marked and approximately 20 J2s were pipetted onto each root tip, covered by a piece of glass microfiber filter paper (GF/A grade, GE Healthcare). Filter papers were taken off 2 days after inoculation and roots were inspected after 2 weeks for successful infection.

2.1.5 Wheat greenhouse maintenance

Wheat seeds were germinated as above and the seedlings were transplanted to pots filled with 50:50 sand/loam: compost in greenhouses, one plant per pot. Water daily and maintain glasshouse temperature at 22 °C day 15 °C night. After 7-8 weeks, the anthesis (yellow anthers appeared out of the glume) would start and record the date for each spike. Harvest spikes at 12-14 days post anthesis and the immature seeds were used in following experiments. Spikes with flag leaves could be kept in dark at 4 °C for up to one week before use.

For seeds production, seeds were harvested, dried for 2-3 weeks at 37 °C and stored at 16 °C with a relative humidity of 15% for future use.

2.2 Molecular cloning methods

2.2.1 DNA extraction

According to different types of materials, two DNA extraction methods were applied.

A rapid DNA extraction method was used for most of the occasions (Weining and Langridge 1991, Weining, Ko *et al.* 1994), including wheat leaves and Arabidopsis leaves. Plant tissue was ground in liquid nitrogen with sterilized blue pestles in a 1.5 mL tube, keeping tissue frozen the entire time. 500 µL DS DNA extraction buffer (2% Sodium Lauroylsarcosine, 0.1M Tris-HCl, 10 mM EDTA, pH 8.0) was added and the tube was well vortexed. Followed by adding 550 µL phenol:chloroform:isoamyl alcohol (25:24:1, v/v) and vortex for 30 sec, the mixture was incubated on ice for 20 minutes and then centrifuged at 4 °C, 12000 *g* for 5 minutes. The aqueous phase was transferred into a new labeled tube with equal volume of chloroform, mixed well and centrifuged same as above. The top layer was then pipetted into a new tube with adding 0.7 volume of isopropanol and 0.1 volume of 3M NaAc (pH 5.2). The solution was mixed by inverting several times and left at room temperature for around 10-15 minutes. Centrifuge at 12000 *g* for 5 minutes and the DNA pellet was washed using 75% EtOH and 100% EtOH, 1 minute each. The DNA pellet was left drying thoroughly for 20 minutes and then dissolved in 50 µL TE buffer (10 mM Tris pH 8.0, 1 mM EDTA) or sterile deionized water (dd H_2O). For removal of RNA contamination, 4 µL RNase A (10 mg/mL) could be added to the aqueous phase after the first centrifugation and incubated at 37 °C for 20 minutes before carrying on the following steps. For obtaining best quality and quantity of DNA as well as easy pipetting, tubes preloaded with 100 mg phase separation grease (Dow Corning® high-vacuum silicone grease, USA) could be used instead of normal tubes for better separation of each layers (Mukhopadhyay and Roth 1993).

A CTAB solution based method was used for DNA extraction from small amount of materials, such as 5-10 Arabidopsis seeds. The plant materials were ground in liquid nitrogen and 100 µL CTAB DNA extraction buffer (100 mM Tris-Cl pH 8.0, 20 mM EDTA pH 8.0, 1.4 M NaCl, 2% (w/v) CTAB and 1% polyvinyl pyrrolidone) was added to resuspend the

resultant powder. The mixture was incubated at 55 °C for over 1 hour and equal volume of phenol:chloroform:isoamyl alcohol (25:24:1, v/v) was added, mixed and then centrifuged at 12000 *g* for 10 minutes. The supernatant layer was kept and the same precipitating and purification methods as described above were applied. In order to harvest sufficient DNA, longer incubation at 55 °C and precipitation at room temperature might be necessary. The DNA pellet was then dissolved in 20 µL TE buffer or dd H_2O and stored at -20 °C.

An assessment of extracted DNA was carried out using Nanodrop (Thermo Fisher scientific) if necessary.

2.2.2 RNA extraction using column based kit

RNeasy Mini Kit (Qiagen) was used for total RNA extraction following manufacturer's instructions. This silica-membrane RNeasy spin columns could bind up to 100 µg RNA and in-tube DNase I digestion was also carried out based on the Qiagen handbook. An assessment of extracted RNA was carried out using Nanodrop (Thermo Fisher scientific) and samples were stored at -80 °C.

2.2.3 Polymerase Chain Reaction (PCR)

PCR was carried out for amplifying target genes using MyTaq™ Red Mix (Bioline) following the manufacturer's instructions. This is a ready-to-use PCR mix containing DNA polymerase, buffer, dNTPs, $MgCl_2$, enhancers and stabilizers. Template and specific primers were added to the mix, making up to a final working solution for a standard 50 µL reaction. The reaction volume could be reduced down to 10 µL for large-scale screening. PCR cycling conditions were: initial denaturation 95 °C 1 minute, followed by 34 cycles of 95 °C 15 seconds, specific annealing temperature for each primer pair 15 seconds and target extension 72 °C 1 minute per kilobase (kb). A final 5 minutes extension at 72 °C was added and the product was used in agarose gel electrophoresis, target purification or other downstream processes.

For amplification of DNA fragments used for downstream cloning, Phusion DNA polymerase (New England Biolabs) with proof reading activity was used following manufacturer's protocols, offering high-fidelity and better performance. A typical 20 µL reaction included 1X Phusion HF buffer, 0.4 µL 10 mM dNTPs, 10 mM primers 1 µL for each, 0.2 µL Phusion DNA polymerase, 100 ng template DNA and nuclease-free water to final volume. Thermocycling conditions were: initial denaturation 98 °C 30 seconds, followed by 25-35 cycles of 98 °C 10 seconds, customized annealing temperature for 10-30 seconds and amplifying target 15-30 seconds per kb at 72 °C, ended with additional extension at 72 °C for 5-10 minutes. If a cloning vector with 3´ terminal thymidine at both ends was used, add extra 1 unit general *Taq* DNA polymerase to the completed reaction and incubate at 72 °C for a further 10 minutes.

2.2.4 Agarose gel electrophoresis and gel extraction

To separate nucleic acid fragments as well as determine the size of the DNA of interest, agarose gel electrophoresis was carried out. The gel was made by melting 1.2 % (w/v) agarose into TAE buffer (40 mM Tris, 20 mM acetate acid and 1 mM EDTA). Gel Red nucleic acid gel stain (Biotium) was added into the gel to help visualize DNA before the gel solidified. Samples were loaded and gel was electrophoresed at 80-100 volts for appropriate time, depending on gel size and target size. The gel was photographed under UV light and target band was excised using a scalpel if needed. The recovery of target fragments was carried out using QIAquick gel extraction kit (Qiagen), following manufacturer's manual.

2.2.5 Restriction enzyme digestion and DNA ligation

Type II restriction enzyme digestion was generally used for gene cloning and routine DNA analysis. A standard restriction enzyme digestion was carried out using a 50 µL reaction containing 10 units restriction enzyme (NEB), appropriate NEBuffer and template DNA, following 1 hour incubation at 37 °C or other specified temperature. Double digest of a DNA substrate could be set up in one reaction if the two restriction enzymes were both active in one buffer system. If not, sequential digest should be performed. Template DNA could be plasmid, genomic DNA or PCR products and digested fragments were separated via gel electrophoresis or other DNA clean-up reagents if applicable.

DNA ligation was used to join dsDNA fragments with blunt or cohesive ends to form new recombinant DNA in gene cloning. A typical 20 µL DNA ligation reaction included T_4 DNA ligase buffer, vector DNA and insert DNA (recommended molar ratio of 1:3 vector to insert) and 1 µL T_4 DNA ligase. The mix was incubated at 16 °C overnight or room temperature for 10-60 minutes and 5 µL of the reaction was used to transform competent cells.

2.2.6 Preparation and transformation of *Escherichia coli* competent cells

Preparation of *Escherichia coli* (*E. coli*) ultra-competent cells was carried out in the lab (Inoue, Nojima *et al.* 1990). Luria Broth (LB) agar plate (1% tryptone, 0.5% yeast extract, 1% NaCl plus 1.5% agar) with *E. coli* DH5α was incubated at 37 °C overnight and single *E. coli* colony was picked and cultured in 250 mL SOB solution (0.5% yeast extract, 2% tryptone, 10 mM NaCl, 2.5 mM KCl, 10 mM $MgCl_2$ and 10 mM $MgSO_4$) in a 1 liter flask at 19 °C with vigorous shaking to OD_{600}=0.5. The culture was chilled on ice for 10 minutes followed by centrifuging at 4000 rpm for 10 minutes at 4 °C. The collected cells were gently suspended by swirling in 80 mL ice-cold TB solution (10 mM PIPES, 15 mM $CaCl_2$ and 250 mM KCl) and

stored on ice for 10 minutes, centrifuged again as above and resuspend the cell pellet in 20 mL ice-cold TB and add 1.4 mL DMSO. Cells were aliquoted into 100 µL or 200 µL, frozen in liquid nitrogen and stored at -80 °C until required.

E. coli transformation was carried out using the competent cells made above. Place the tube with frozen competent cells on ice and let it thaw. Add half of DNA ligation or 1 µL plasmid DNA to the cells and keep it on ice for 5 minutes. The cell mix was pipetted onto pre-warmed LB agar plates with appropriate selection and spread. For *lacZ* gene selection, 40 µL 0.1 M IPTG (isopropyl β-D-1-thiogalactopyranoside) and 40 µL X-gal (5-bromo-4-chloro-3-indolyl-β-D-galactopyranoside) (20 mg/mL) were spread on each plate prior to the cell mixture. Incubation was carried out at 37 °C overnight and successful transformants were verified by PCR, plasmid digestion or sequencing.

2.2.7 Column based plasmid extraction

A commercial silica membrane based plasmid extraction kit (QIAprep Spin Miniprep, Qiagen) was used for extracting plasmids from *E. coli*. In general, bacterial cultures were lysed and the cleared lysates were then applied to the column tube where plasmid DNA adsorbed to the silica membrane. Impurities were then washed away and pure plasmid DNA was eluted in water or TE buffer.

2.2.8 Preparation and transformation of *Agrobacterium tumefaciens* cells

Agrobacterium tumefaciens freeze-thaw competent cells were made for transformation procedure. *Agrobacterium* was cultured in 5 mL LB with 50 µg/mL rifampicin at 28 °C overnight. 2 mL of the culture was transferred to 50 mL LB in a 250 mL flask, cultured at 28 °C with vigorous shaking until OD_{600}=0.5-1.0. The cell culture was chilled on ice and then centrifuged at 4000 rpm, 4 °C for 5 minutes. The cell pellet was resuspended in 1 mL ice cold 20 mM $CaCl_2$ by gentle shaking. The cells were aliquoted in 100-200 µL, frozen in liquid nitrogen and stored at -80 °C.

Transformation was carried out by adding 1 µL DNA (10-100 ng) into competent cells and incubating the mixture in 37 °C water bath for 5 minutes. 1 mL LB was added into the mixture and the tube shaken at 28 °C for 2 hours. The cells were spreaded onto LB agar plates with appropriate antibiotic selection and incubate at 28 °C for 48 hours. Colonies were verified by colony PCR using short heating step lysed bacteria (bacteria suspended in water, incubated at 99 °C for 10 minutes) as template. PCR amplicon and size of the product were determined by electrophoresis alongside a DNA size marker on an agarose gel.

2.3 Immunolabelling methods

2.3.1 Sample preparation

Root samples were cut off using a clean scalpel, washed in distilled water and then placed in a 1.5 mL centrifuge tube containing fresh fixative solutions (4% paraformaldehyde (16% solution, EM grade, VWR international) in PEM buffer (50 mM PIPES (1,4-piperazinediethanesulfonic acid), 5 mM EGTA (Ethylene glycol-bis(2-aminoethylether)-N,N,N',N'-tetraacetic acid), 5 mM Magnesium sulfate, pH 6.9)) at 4 °C overnight. The root samples were washed three times using 1X PBS buffer (137 mM NaCl, 2.7 mM KCl, 10 mM Na_2HPO_4 and 1.8 mM KH_2PO_4, pH 7.4) and dehydrated with a series of ethanol solutions (10%, 20%, 30% and 50% for 30 minutes each, 70%, 90% and 100% for 60 minutes each) at 4 °C. Root samples were then incubated in a series of LR white resin (hard grade, London Resin Company) solutions (10%, 20%, 30% and 50% for 30 minutes each, 70%, 90% and 100% for 60 minutes each) at 4 °C. The root samples were then kept in 100% resin at 4 °C for 2 days (replace with fresh resin every 8 hours) before being embedded in gelatin capsules (Agar Scientific) filled with resin. Embedded samples were left still at 37 °C for at least 5 days to allow the resin to set and successfully embedded samples could then be stored at room temperature for future use.

2.3.2 Slide pre-treatment and sample sectioning

8-well or 12-well MultiTest Slide (MP Biomedicals) were thoroughly washed using distilled water, dried and then coated with VECTABOND reagent (SP-1800, Vector laboratories) in order to increase the adherence of tissue sections to glass slides following manufacturer's instructions: slides were first immersed in acetone for 5 minutes, then transferred to prepared VECTABOND reagent solution (add the entire bottle 7 mL of reagent to 350 mL acetone) for 5 minutes and then gently washed in distilled water. Slides were then left dry at room temperature or 37 °C and were wrapped in cling film and stored at room temperature until needed.

Gelatin capsules were removed from embedded samples and the blocks were carefully trimmed using single edge razor blades (VWR International) and sectioned at 0.5 µm thickness with a diamond knife (DiATOME Diamond Knives) by an ultramicrotome (Reichert Ultracut E, Leica Microsystems). Sections were placed on the coated slides, preloaded with a drop of deionized water and heated dry using a slide warmer. Dried slides could be stored at room temperature in Micro Slide Trays (VWR International) until required.

2.3.3 Immunolabelling and imaging

Sections were blocked using 5% (w/v) PBS/milk solution at room temperature for 30 minutes followed by 1X PBS washing and replaced with primary antibodies diluted 5 times in fresh 5% (w/v) PBS/milk solution. Slides were incubated at room temperature or 37 °C for 2 hours and washed for 5 minutes in 1X PBS. Secondary antibody (Anti-Rat IgG (whole molecule)-FITC antibody produced in rabbit, Sigma-Aldrich) was applied on sections at 1000-fold dilution in 5% (w/v) PBS/milk solution. Following incubation was carried out at room temperature for 1.5 hours in dark. Slides were washed in 1X PBS for 5 minutes and could be incubated in Calcofluor White solution (Fluorescent Brightener 28, Sigma-Aldrich, 0.2 mg/mL in 1X PBS) for 5 minutes at room temperature or directly mounted with antifadent solution (Citifluor Glycerol Pbs Solution AF1, Agar scientific) to prevent photobleaching and covered with a coverslip. If background autofluorescence was observed, a 0.1% Toluidine Blue O (pH 5.5, 0.2 M sodium phosphate buffer) incubation for 5 minutes should be used. Sections without primary antibody labelling were used as negative control and all the rest of the experimental steps stayed the same. This was carried out together with other antibody labelling simultaneously in all analysed samples.

Sections were observed using Leica Leitz DMRB Fluorescence Microscope (Leica Microsystems) and images were taken by QImaging QICAM digital camera (QImaging) using QCapture Pro 7 (QImaging). Further necessary image editing was carried out using CorelDRAW Graphics Suite X7 (Corel) and PaintShop Pro X7 Ultimate (Corel). Immunolabelled slides could be stored temporarily at 4 °C in dark.

Pectate lyase (*Aspergillus sp.*) (Megazyme International Ireland) was applied to remove pectic HG when applicable. To apply this, root sections were first treated with 0.1 M Na_2CO_3 (pH 11.4) for 2 hours at room temperature and then applied with 25 µg/mL pectate lyase solution (diluted in 50 mM CAPS buffer (pH 10.0) with 1 mM $CaCl_2$) and incubated at room temperature for 2 hours. Slides were washed using distilled water and could be used immediately or left to air dry.

2.3.4 Plant cell wall probes

A set of plant cell wall probes, mainly monoclonal antibodies, were used in this study, targeting the major known cell wall chemical components. Table 2.1 listed the major antibodies used throughout the whole study.

Table 2.1 Primary antibodies used throughout the study

Primary antibody	Epitopes revealed	Reference
LM10, LM11	heteroxylan	(McCartney, Marcus *et al.* 2005)
LM12	feruloylated xylans	(Pedersen, Fangel *et al.* 2012)
LM15	XXXG motif of xyloglucans	(Marcus, Verhertbruggen *et al.* 2008)
LM25	XXXG/galactosylated xyloglucan	(Pedersen, Fangel *et al.* 2012)
LM19	partially methyl-HG/de-esterified HG	(Verhertbruggen, Marcus *et al.* 2009)
LM20	methyl-HG	(Verhertbruggen, Marcus *et al.* 2009)
LM5	(1→4)-β-D-galactan	(Jones, Seymour *et al.* 1997)
LM6	(1→5)-α-L-arabinan	(Willats, Marcus *et al.* 1998)
JIM20	extensins	(Smallwood, Beven *et al.* 1994, Knox, Peart *et al.* 1995)
MLG	mixed linkage glucans	(Meikle, Hoogenraad *et al.* 1994)

Chapter 3 Cell wall microstructures of syncytia induced by cyst nematodes in potato, soybean and wheat

3.1 Introduction

Cyst nematodes (*Heterodera* and *Globodera* spp.) are some of the most specialized plant-parasitic pests in agriculture, normally with a narrow host range (Nicol, Turner *et al.* 2011). However, these sedentary endoparasites can cause great economical losses to crop production globally and thus of scientific interest. The most damaging species include soybean cyst nematode *H. glycines*, potato cyst nematodes *G. pallida* and *G. rostochiensis* and cereal cyst nematodes (CCNs) *H. avenae* and *H. filipjevi* (Jones, Haegeman *et al.* 2013).

In a typical cyst nematode life cycle, the successful initiation and formation of a feeding site as the sole nutrient supply, termed a syncytium, is a vital step for nematode survival and reproduction. Great efforts have been made in the past few decades to investigate this transformation, providing valuable information in regard to this sophisticated process (reviewed in 1.1.2.2). The syncytium has been revealed to possess unique structural features, including enlarged multinucleate, dense cytoplasm with numerous organelles and thickened outer cell walls with wall ingrowth in certain region. However, the chemical structures of the syncytial cell wall, which might reflect its forming process, affecting the structural and physiological properties and function, are still largely unknown.

Revealing the chemical compositions of a plant cell wall requires the use of several plant probes, of which monoclonal antibodies (mAbs) developed against a broad range of cell wall polymers are widely used (Knox 2008, Pattathil, Avci *et al.* 2010). Combined with other analytical techniques, it can then provide either very fine structures at nanometre scale or ultra-sensitive quantifications. Meanwhile, due to the technical difficulties, although dissecting intact syncytia is possible (Juergensen, Scholz-Starke *et al.* 2003) but not applicable to just the syncytial walls, *in situ* analysis becomes the optimal choice. Previous studies have given valuable first looks at the chemical structures of cyst nematode induced feeding sites, for instance, the *H. schachtii* induced syncytial walls in Arabidopsis possess cellulose, XyG, heteromannan, abundant methyl-HG and lack of xylan and galactan (Davies, Lilley *et al.* 2012, Wieczorek, Elashry *et al.* 2014); the syncytial walls induced by *H. avenae* in barley contain cellulose, callose and MLG and only barely detectable low levels of HG, methyl-HG and heteroxylan (Aditya, Lewis *et al.* 2015). However, due to technical reasons, such as the selection of cell wall probes used, it is not yet clear to draw a general picture over the syncytial wall chemical structures especially the ones induced in their natural hosts.

In this study, four of the most damaging cyst nematode species together with their hosts,

G. pallida, *H. glycines*, *H. avenae* and *H. filipjevi* in potato, soybean and wheat roots respectively, were chosen and the microstructures of their syncytial walls were analysed with the use of a set of plant cell wall mAbs and fluorescence imaging technique.

3.2 Materials and methods

Potato (*Solanum tuberosum* L. cv. Désirée) and soybean (*Glycine max* (L.) Merr. cv. Toliman) seedlings were inoculated with cyst nematodes *G. pallida* and *H. glycines* respectively. Infection status was checked after 7 days post inoculation (dpi). Roots with mature developing females of both species as well as early developing stage females of *G. pallida* were fixed and embedded as described (2.3). Three spring wheat (*Triticum aestivum* L.) cultivars, Bobwhite, Fielder and Cadenza, together with two CCNs *H. avenae* and *H. filipjevi* were used in this study. The hydroponic culture and nematode inoculation were carried out as described (2.1.3). Infection were checked every week after inoculation. Successful forming females together with the roots were cut off, fixed and embedded as described (2.3).

Transverse sections were collected around the middle point of the longitudinal syncytial region. Immunolabelling methods were applied (2.3) and bright field optical images were taken on sections, stained with Toluidine Blue O solution (1% Toluidine Blue O dissolved in 1% sodium borate aqueous solution, filtered with filter paper) for 5-10 minutes at room temperature and excessive dye was washed off using water or ethanol dilution.

When using a recombinant carbohydrate-binding module (CBM) probe instead of mAbs, sections were incubated in 5% PBS/milk solution containing 10 μg/mL CBM for 1 hour and then washed in 1X PBS for 3X 5 minutes. The subsequent incubation was carried out using a 1000-fold diluted monoclonal 'Anti-polyHistidine' antibody (produced in mouse, Sigma) for 1 hour and washing for 3X 5 minutes using 1X PBS. Then, the sections were incubated in 100-fold diluted Anti-Mouse IgG (whole molecule)-FITC antibody (produced in goat, Sigma) for 1 hour and then washed 3X 5 minutes in 1xPBS. Finally, sections were mounted with antifadent solution, covered with a coverslip and visualised as described (2.3.3).

Essential photo editing process, including combination, cropping and alignment, were applied to immunolabelling images where needed. For bright field images, additional background correction and colour adjustment, not concerning the image content, were used apart from the above photo editing procedures. All adjustments above were carried out using CorelDRAW Graphics Suite X7 (Corel) and PaintShop Pro X7 Ultimate (Corel). Fluorescence intensity measurements were carried out using ImageJ.

3.3 Results

The *in situ* analysis of syncytial walls, induced by *G. pallida*, *H. glycines* and two CCNs in potato, soybean and spring wheat respectively, were carried out using a set of plant cell wall probes, mainly mAbs. They target various general plant cell wall polymers, such as hemicelluloses, pectins and cell wall structural proteins, as well as differentiate their specific modifications. Together with fluorescence imaging and image analysis, this study

provides a systematic look at the syncytial wall chemical features induced by those important cyst nematode species in their natural hosts.

Immunolabelling results of all tested antibodies were summarized in tables in this section while only parts of the most representative images were shown below. All images are included in the supplementary dataset. Due to the different binding performances of mAbs, fluorescence images were not taken under the exact same parameters, for instance at variable exposure time, in order to gain optimal display quality. As the scaffolding of cell walls, the presence of cellulose microfibrils were tested using both Calcofluor White staining and plant cell wall probe CBM3a (Blake, McCartney *et al.* 2006). Their availability was verified and related results are included in the supplementary data, thus no further depiction is made in the following context. As most of the attention has been paid to the actual syncytial wall microstructures, the majority of the listed figures may only represent parts of the whole root transverse sections, such as the syncytium-containing vascular cylinder or even only the syncytium together with a few surrounding cells, in order to display in higher definition. Sections with no primary antibody labelling were used as control and no nonspecific fluorescence was observed in the syncytial walls (figures included in supplementary data).

3.3.1 *G. pallida* induced syncytial cell walls in potato

Immunolabelling and downstream data processing were carried out as described. Most of the attention was paid to the syncytial walls induced by developing females of around mature stages. The results listed including mainly the mature stage syncytia at 14 dpi, as well as a few representative results of 21 dpi. Some other time-points were also assessed, to further evaluate the consistency of syncytial cell wall chemical compositions throughout nematode parasitism.

Anti-xylan antibody LM11, an indicator for root vascular structures

One of the initial challenges for *in situ* analysis is the ability to identify the host root internal structure in dark field images after the drastic changes caused by nematode invasion and syncytium formation. For instance, as shown in the bright field images in Figure 3.3.1.1, the much thickened xylem is pushed aside rather than staying in the centre of the vascular bundle as in normal roots, and the nematode induced syncytium takes more than half of the vascular cylinder space. The anti-xylan antibody LM11 was revealed to bind primarily to the root epidermis cell walls and the xylem whilst absent in syncytial walls, and similar binding patterns were also observed in other assessed potato root samples (included in supplementary datasets). As the syncytium was generally initiated and formed within the vascular cylinder, the anti-xylan LM11 can then be used as an indicator in telling root basic structures in dark field images of nematode infested samples. Together with the Toluidine Blue O staining of equivalent sections, this clear identification of the syncytial boundaries validates further wall related analysis and comparison in downstream steps. The following listed figures are all from close equivalent sections as to both the bright field and the LM11

labelled sections in Figure 3.3.1.1.

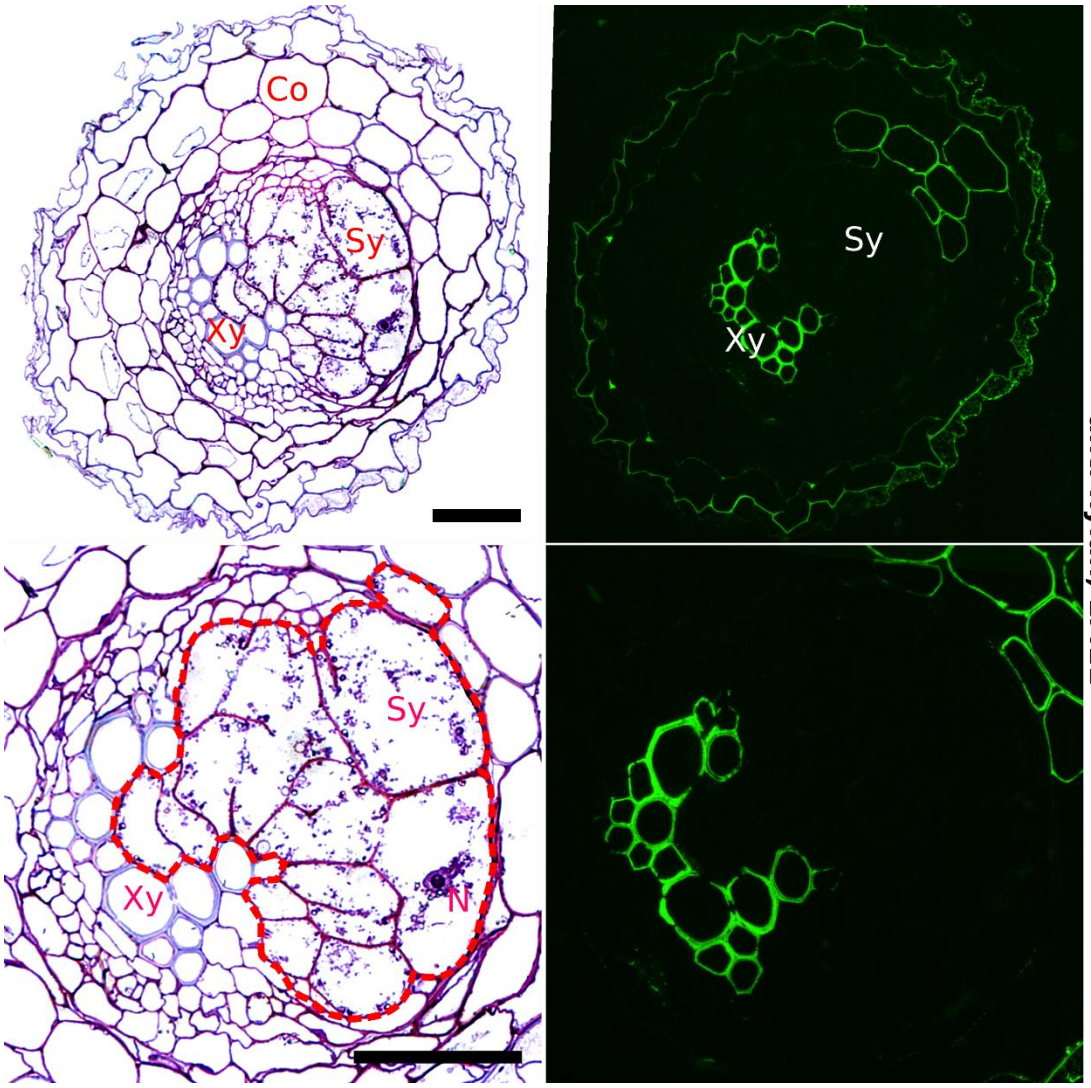

Figure 3.3.1.1 Transverse sections of potato roots, infested with *G. pallida* (14 dpi). Bright field images are captured from the same section at different magnifications, stained with Toluidine Blue O. Syncytial region is outlined with red dash line. Immunofluorescence (green) images are from the specific binding of anti-xylan mAb LM11 to an equivalent section. (Co, cortex; Xy, xylem; Sy, syncytium; N, enlarged nuclei; bar=50 µm)

Hemicellulosic XyG in syncytial walls

The distribution of XyG, the major non-cellulosic polysaccharide in eudicot primary walls, was revealed with the use of different anti-XyG antibodies, targeting various substitution and branching patterns of the basic XyG backbone. The mAbs binding within the vascular cylinder was shown in Figure 3.3.1.2, and the clear binding of LM25 in the syncytium, with stronger targeting ability to galactosylated XyGs than LM15, indicated the existence of XyG in syncytial walls. The removal of pectin using pectate lyase largely improved the performance of LM25 in the whole root, reflecting the anti-XyG epitopes were partially masked, similar to previous studies (Marcus, Verhertbruggen *et al.* 2008, Davies, Lilley *et al.* 2012). As shown in the pectate lyase pre-treated section, the binding of LM25 was found in almost all types of cell walls, among which the syncytium gave the strongest binding, suggesting that XyG is abundant in the nematode induced syncytial walls.

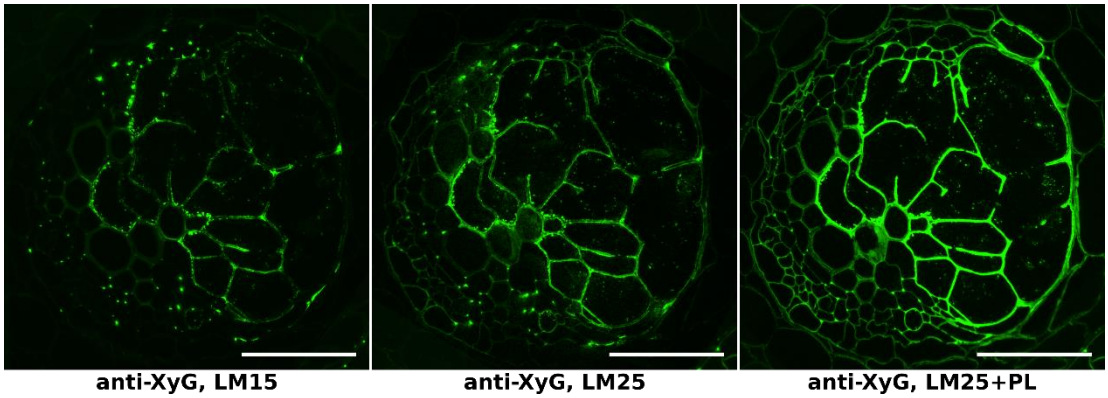

Figure 3.3.1.2 Immunolocalization of XyG in syncytial walls induced by *G. pallida* in potato roots (14 dpi). Immunofluorescence (green) images are from the specific binding of anti-XyG mAbs LM15 and LM25 using equivalent sections. (PL, sections pre-treated with pectate lyase; bar=50 µm)

Pectic HG in syncytial walls

As the major structural class of pectin, HG was tested over syncytium sections using antibodies LM19 and LM20, designated to non/low-methyl HG and heavily methyl-esterified HG respectively. In the listed results of the vascular regions (Figure 3.3.1.3), the antibody LM19 bound to the walls of almost all cells including the syncytium apart from the xylem elements (structure indicated by LM11 in Figure 3.3.1.1) and its epitopes also appeared in the cytoplasmic content. The removal of methyl groups via pre-treatment with Na_2CO_3 to the sections largely increased the binding affinity of LM19, as revealed by the significantly higher fluorescence intensity. Further with the clear and abundant binding of LM20, it is clear that the *G. pallida* induced syncytial walls in potato roots contain large amount of pectic HGs and they are prominently methyl esterified.

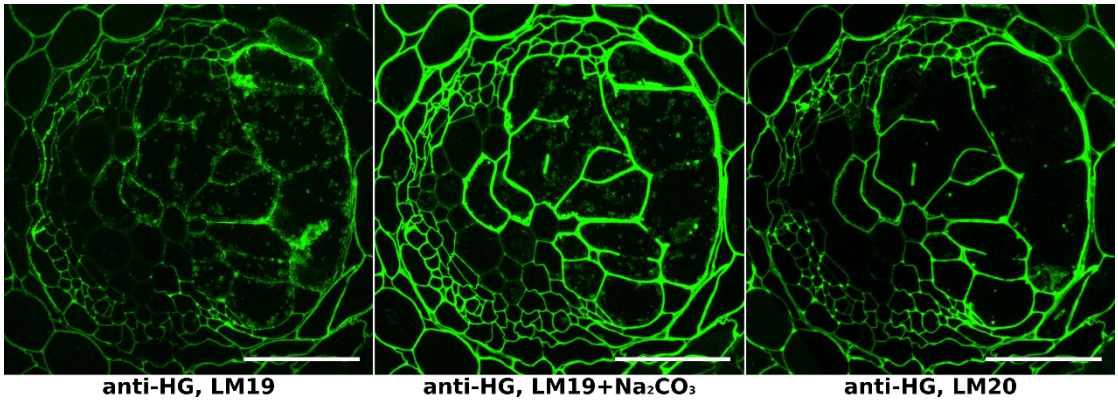

Figure 3.3.1.3 Immunolocalization of pectic HG in syncytial walls induced by *G. pallida* in potato roots (14 dpi). Indirect immunofluorescence (green) images are from the specific binding of anti-HG mAbs LM19 and LM20 using equivalent sections. (Na_2CO_3, sections pre-treated with Na_2CO_3; bar=50 µm)

Other pectic polymers and wall proteins of syncytial walls

Apart from pectic HG, two other related mAbs LM5 and LM6, recognising the neutral sugar side chains of the rhamnose residues of the RG-I backbone, were applied to equivalent sections, similar as above. The two antibodies revealed almost inverse binding patterns within the vascular bundle as well as the surrounding cells, apart from the absence of both antibodies in xylem (Figure 3.3.1.4). The anti-arabinan LM6 bound strongly to the syncytial walls whilst in much lower amount in the walls of other types of cells. Conversely, the epitopes of the anti-galactan LM5 were shown to be abundant in all cell walls except the xylem and close to absent in syncytial walls. These results together gave the modification features of the syncytial wall pectic RG-I, rich in arabinans whilst largely lack of galactan sidechains.

In order to further investigate the cell wall structural proteins, several mAbs targeting mainly AGPs were applied to the equivalent sections, and the epitopes of one anti-AGP mAb JIM13 were found to exist in different cells including the syncytium in an unevenly distributed fashion. Within the syncytial walls, it displayed some strong binding close to the cell wall ingrowth region, right adjacent to the xylem, as well as certain cell content in the cytoplasm.

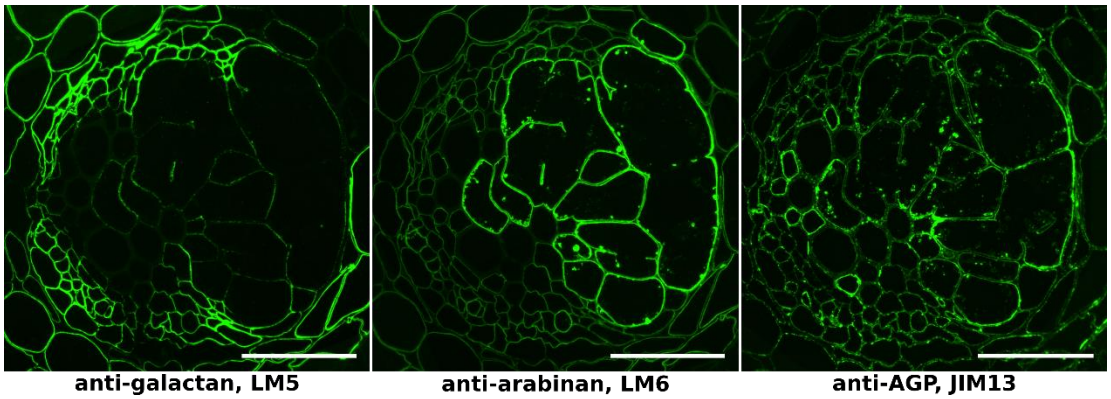

Figure 3.3.1.4 Immunolocalization of pectic polymers and cell wall proteins in syncytial walls induced by *G. pallida* in potato roots (14 dpi). Indirect immunofluorescence (green) images are from the specific binding of anti-galactan LM5, anti-arabinan LM6 and anti-AGP JIM13 mAbs respectively using equivalent sections. (bar=50 µm)

Among cell walls of the entire root sections, the syncytial walls are distinctive from a chemical composition perspective

Expanding the wall analysis from only the syncytial region to a larger whole-root scale, it is obvious that the syncytial walls possess different cell wall chemical compositions, as shown in Figure 3.3.1.5, from the rest of the root cells, either within or outside the vascular bundle. For instance, the anti-XyG LM25 gave bright binding in the syncytial walls whilst looking much dimmer in the rest of the root cells. Meanwhile, the RG-I related LM5 and LM6 gave strikingly different binding patterns: with anti-galactan epitopes being almost completely absent in syncytial region, xylem, the epidermis and its adjacent cortex layer whilst being abundant in the rest of the cell walls; while for anti-arabinan epitopes, they were revealed to be rich in syncytial walls whilst displaying a lower content in the rest of all root cell walls. For the generally abundant cell wall pectic HG, the LM20, targeting the heavily methyl esterified HG, gave strong binding in almost all cell walls, including the syncytial walls, apart from the much weaker binding in the walls of xylem, epidermis and the outer layer of cortex cells.

Visual distinctions in terms of antibody binding patterns were then tested over further image analysis of the walls in different cell types, including the syncytium, host xylem, phloem elements, cortex cells and epidermis. For fluorescence intensity measurement, mean values of at least 50 representative wall portions from each of the cell types were measured except for the around 30 measurements taken over the xylem. The outer cell layer of the cortex, adjacent to the epidermis, show distinctive binding patterns from the rest and they were eliminated from the fluorescence quantification. As shown in the respective diagrams, the syncytium walls possess abundant XyG, RG-I arabinan and methyl-HG, same as shown in the fluorescence images. Overall, comparing with other walls of the host root, the syncytial walls were chemically distinguishable.

Previous high definition imaging, from Toluidine Blue O stained sections at bright field, makes it possible to clearly differentiate the boundaries of *G. pallida* induced feeding sites from the rest of the host root cells. Additionally, based on the chemical structure difference, it is also feasible to tell the syncytium from the other host root cells, adding uniqueness beyond the visual structural difference.

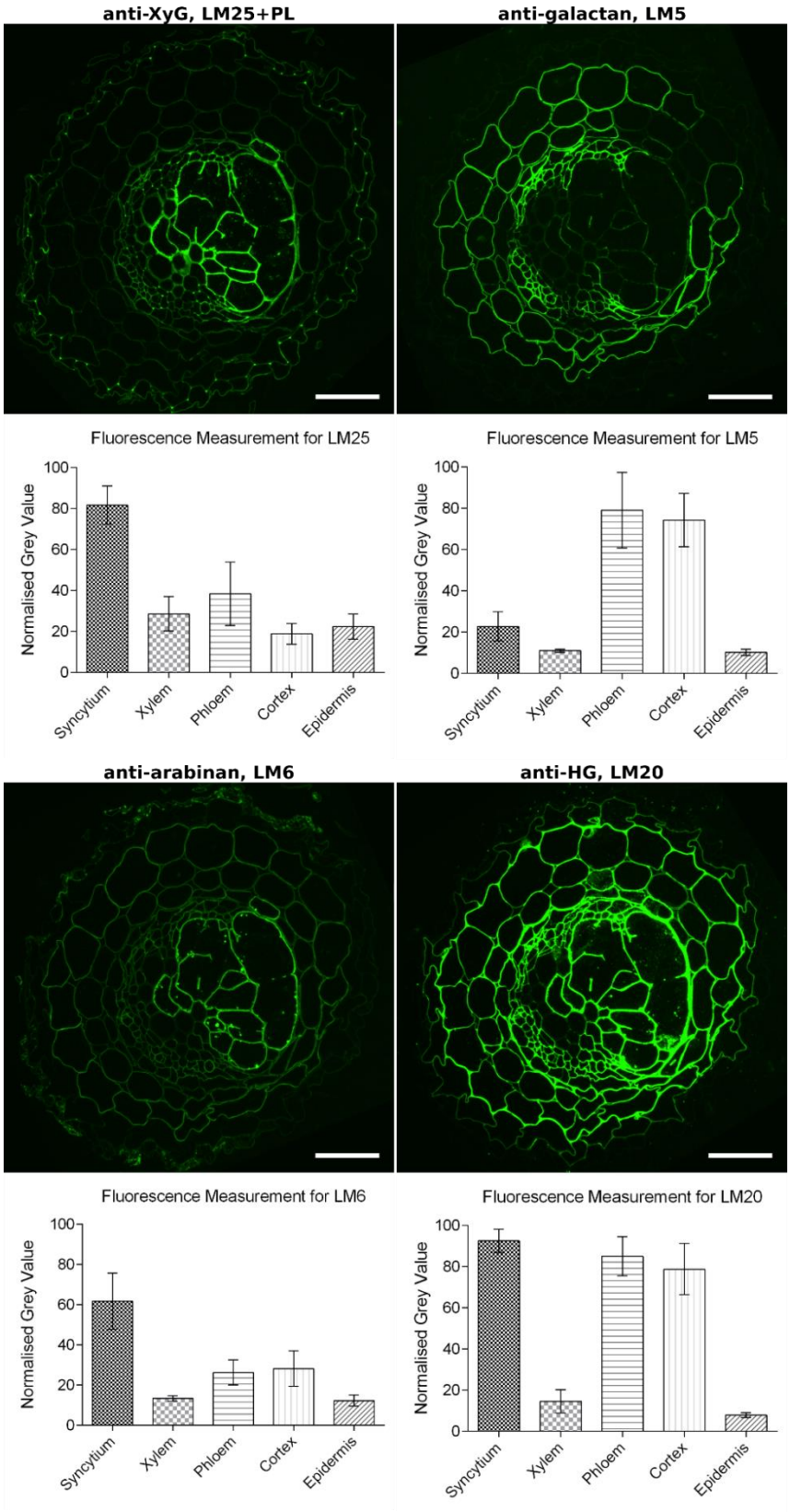

Figure 3.3.1.5 Immunolocalization of general cell wall polymers in transverse sections of potato root infested with *G. pallida* (14 dpi) and fluorescence analysis. Fluorescence (green) images are from the specific binding of mAbs, LM25 to XyG, LM5 to galactan, LM6 to arabinan and LM20 to HG, on equivalent sections; graphs are based on respective fluorescence measurements (mean values ± SD). (PL, sections pre-treated with pectate lyase; bar=50 µm)

The consistency of syncytial cell wall chemical compositions during parasitism

Apart from the above analysis over syncytium samples taken at mature stage of the *G. pallida* life cycle (14 dpi), more work has been done over both earlier and later stages of nematode development. As shown in Figure 3.3.1.6, the syncytial walls of 21 dpi samples possess largely similar mAb binding patterns as observed in 14 dpi samples, indicating consistency of wall chemical compositions during nematode parasitism. The anti-xylan LM11 still bound strongly to the xylem and absent from the syncytial walls. The pectate lyase pre-treatment over the slides improved the binding performance of anti-XyG LM25, indicating epitopes masked by rich pectin. The binding comparison between LM5 and LM6 over the syncytial walls clearly show the RG-I sidechain modifications, meanwhile the pectic HG was shown to be largely methyl esterified judging by the bright fluorescence of anti-HG LM20. Structural AGPs were also revealed to be present by JIM13, similar to previous results as well. Such chemical structure consistency was also observed at other earlier stages (7 dpi and 17 dpi) of nematode development, as later summarised in Table 3.1.

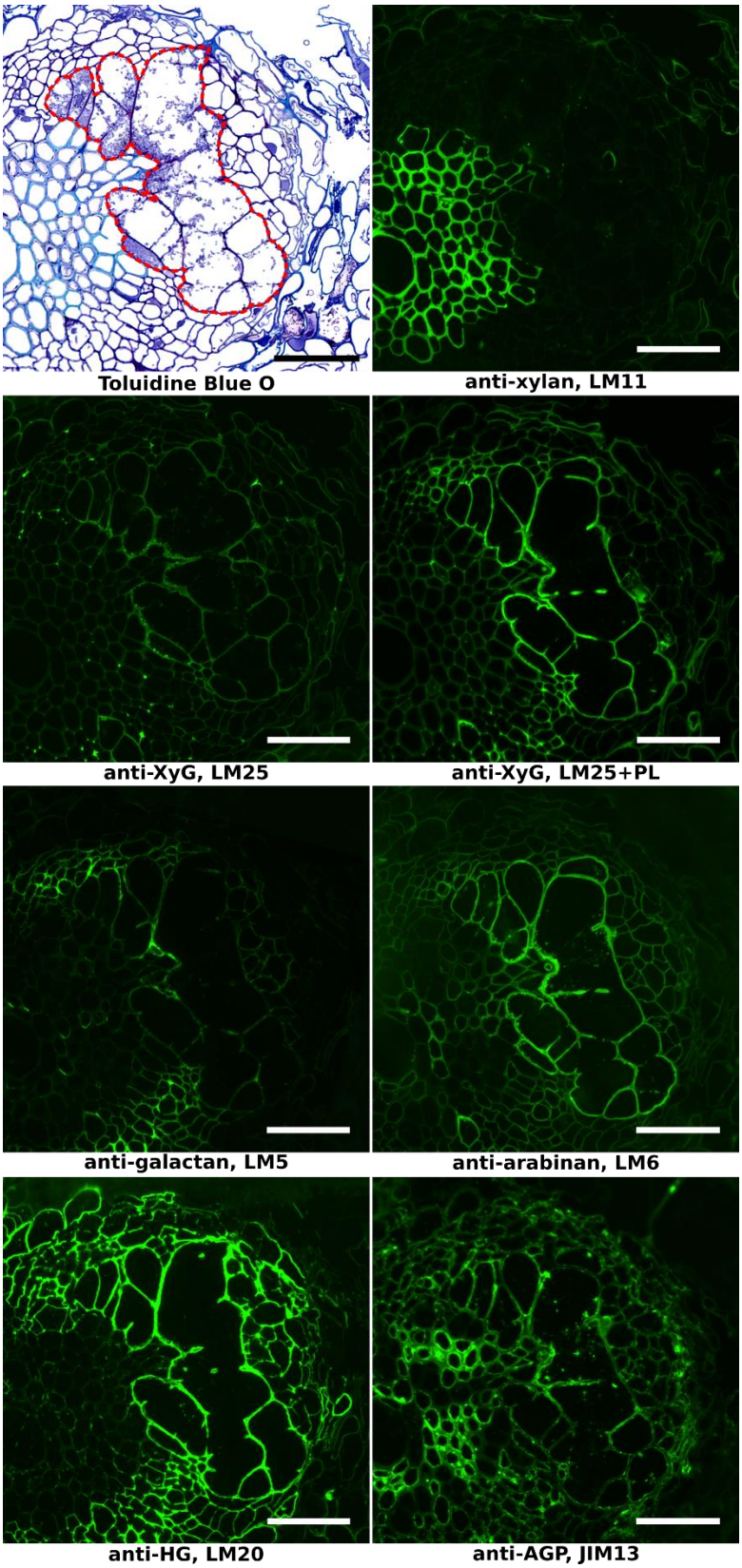

Figure 3.3.1.6 Immunolocalization of general cell wall polymers in syncytial walls induced by *G. pallida* in potato roots (21 dpi). Bright field image is captured from the Toluidine Blue O stained section. Syncytial region is outlined with red dash line. Fluorescence (green) images are from the specific binding of mAbs using equivalent sections. (PL, sections pre-treated with pectate lyase; bar=50 µm)

3.3.2 *H. glycines* induced syncytial cell walls in soybean

As the most serious nematode pest on soybean, *H. glycines* infests most of the soybean producing countries in the world. In this study, the cell walls of the feeding site induced by *H. glycines* within its host root were analysed, using the same experimental procedures as for *G. pallida*.

Mature syncytium samples were taken at 14 dpi and the results listed mainly represented the syncytial regions together with few surrounding cells due to size limitation. Antibodies targeting general cell wall polysaccharides were used, including mainly hemicelluloses and pectins.

Anti-xylan antibody LM11, an indicator for root xylem elements

The anti-xylan LM11, targeting specifically to un/low-branched heteroxylans, was revealed to bind exclusively to the xylem within the vascular cylinder in *G. pallida* infested potato root. The same binding patterns were also observed in *H. glycines* infected soybean roots, as shown in Figure 3.3.2.1. It gives clear indications of the root vascular structure after the drastic changes caused by the formation of the syncytium. Together with the bright field staining, it helps to distinguish the syncytial boundaries, which are essential in telling the binding patterns of the tested cell wall probes. All other listed figures are from equivalent sections as the ones used in Figure 3.3.2.1, thus direct comparisons can be made over the root structures.

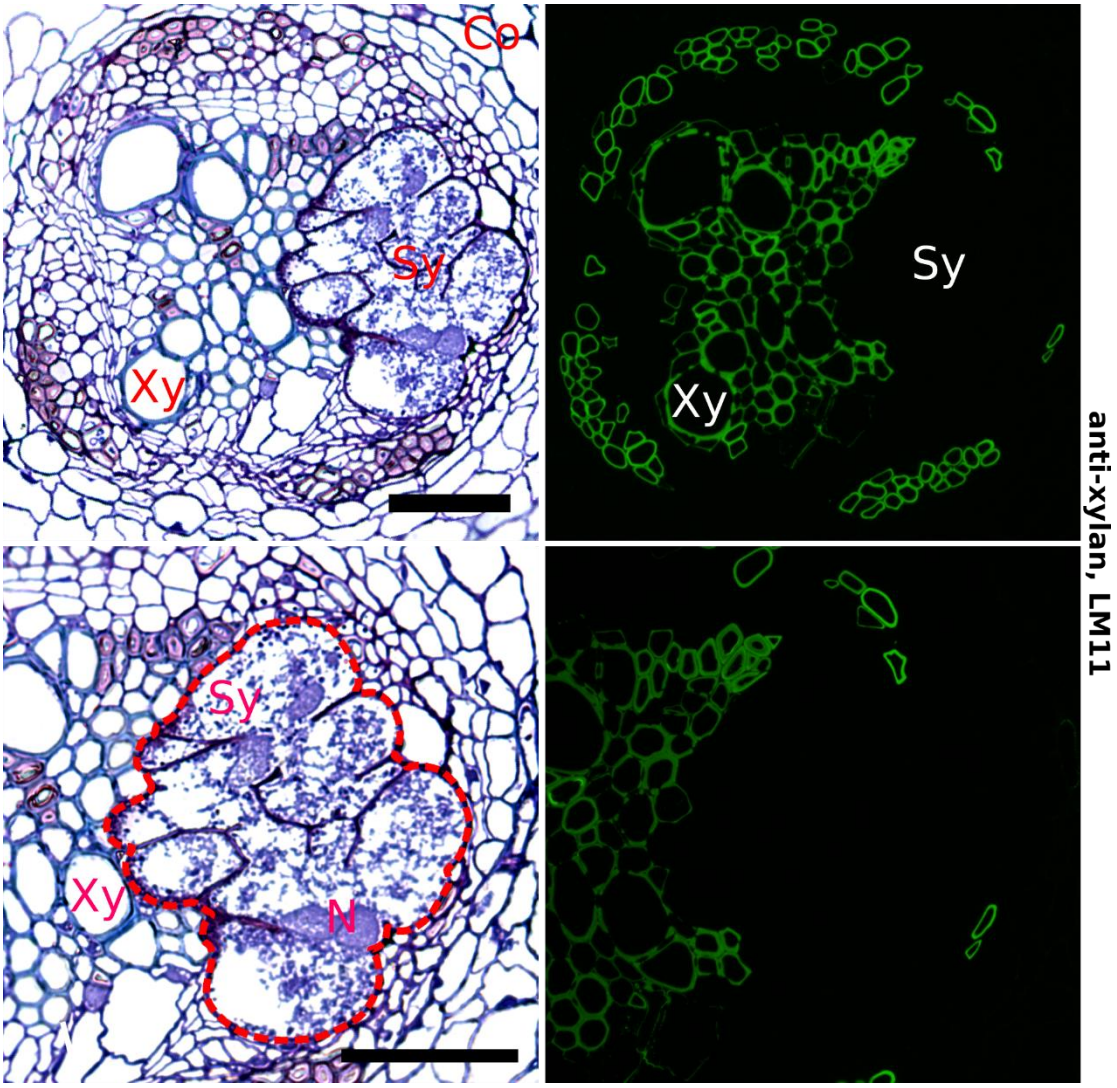

Figure 3.3.2.1 Transverse sections of the vascular bundles in soybean root, infested with *H. glycines* (14 dpi). Bright field images are captured from the same section at different magnifications, stained with Toluidine Blue O. Syncytial region is outlined with red dash line. Indirect immunofluorescence (green) images are from the specific binding of anti-xylan mAb LM11. (Co, cortex; Xy, xylem; Sy, syncytium; N, enlarged nuclei; bar=50 µm)

Hemicellulosic XyG is abundant in soybean syncytial walls

In order to detect the major non-cellulosic polysaccharide, three anti-XyG mAbs LM15, LM24 and LM25 were used to target the XyGs in syncytial walls. As shown in Figure 3.3.2.2, both the LM15 and LM25 epitopes were revealed to be abundant in the syncytial walls, with LM25 targeting wider range of galactosylated XyG bound to more walls of some other cell types within the vascular cylinder than LM15. Meanwhile, the LM24, with slightly narrower range of recognition of galactosylated XyG, displayed weak binding patterns comparing with LM15 and LM25 as listed in Table 3.1 (image data included in the supplements). Altogether, this revealed the abundance of XyG in nematode induced syncytial walls in soybean.

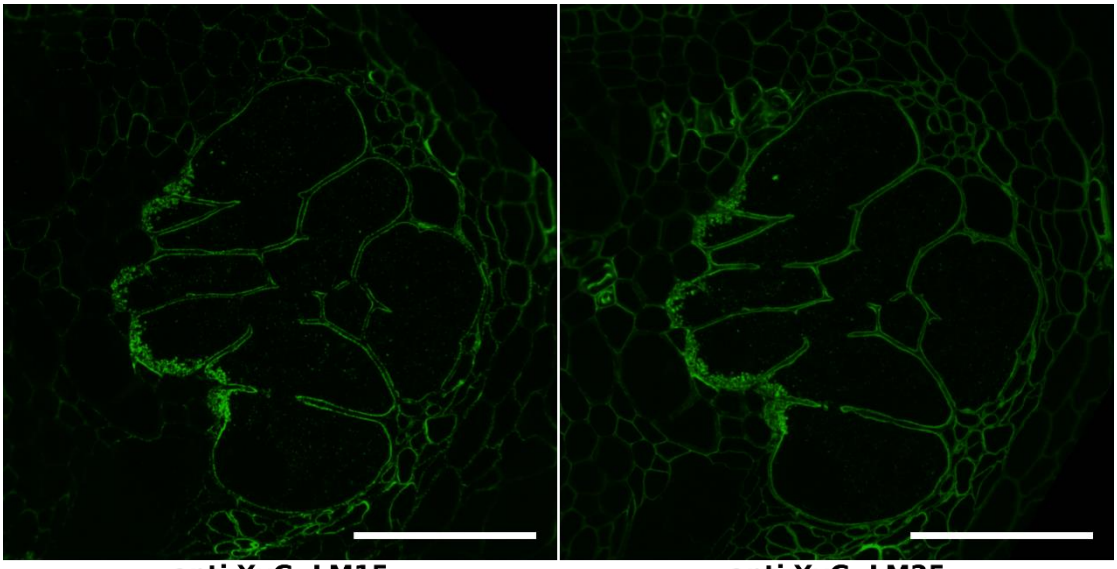

Figure 3.3.2.2 Immunolocalization of XyG in *H. glycines* infested soybean roots (14 dpi). Indirect immunofluorescence (green) images are from the specific binding of anti-XyG mAbs LM15 and LM25 using equivalent sections. (bar=50 µm)

Pectic polymers and wall proteins in soybean syncytial walls

Derived from pectin-rich host root cells, the cell wall of *H. glycines* induced syncytium was revealed to contain abundant pectic arabinans and methyl-HG while completely lack of RG-I related galactan, as indicated by the binding of LM6, LM20 and LM5 respectively in Figure 3.3.2.3. This was also similar to the binding in *G. pallida* induced potato syncytial walls. Apart from the syncytial region, the anti-galactan LM5 also bound to limited phloem elements inside the vascular cylinder whilst the anti-arabinan LM6 recognised more cell types apart from the almost absence in primary xylem. Meanwhile, the methyl-HG was also found to be abundant in other cell walls, especially the corners of those intercellular space, but not in xylem. For wall structural proteins, the anti-extensin JIM20 was shown to bind more clearly to the wall fragments within the syncytial content and some adjacent phloem elements, but not to the outer syncytial walls including the cell wall ingrowth, representing a distinctive distribution pattern might reflect different developmental status of the syncytial walls.

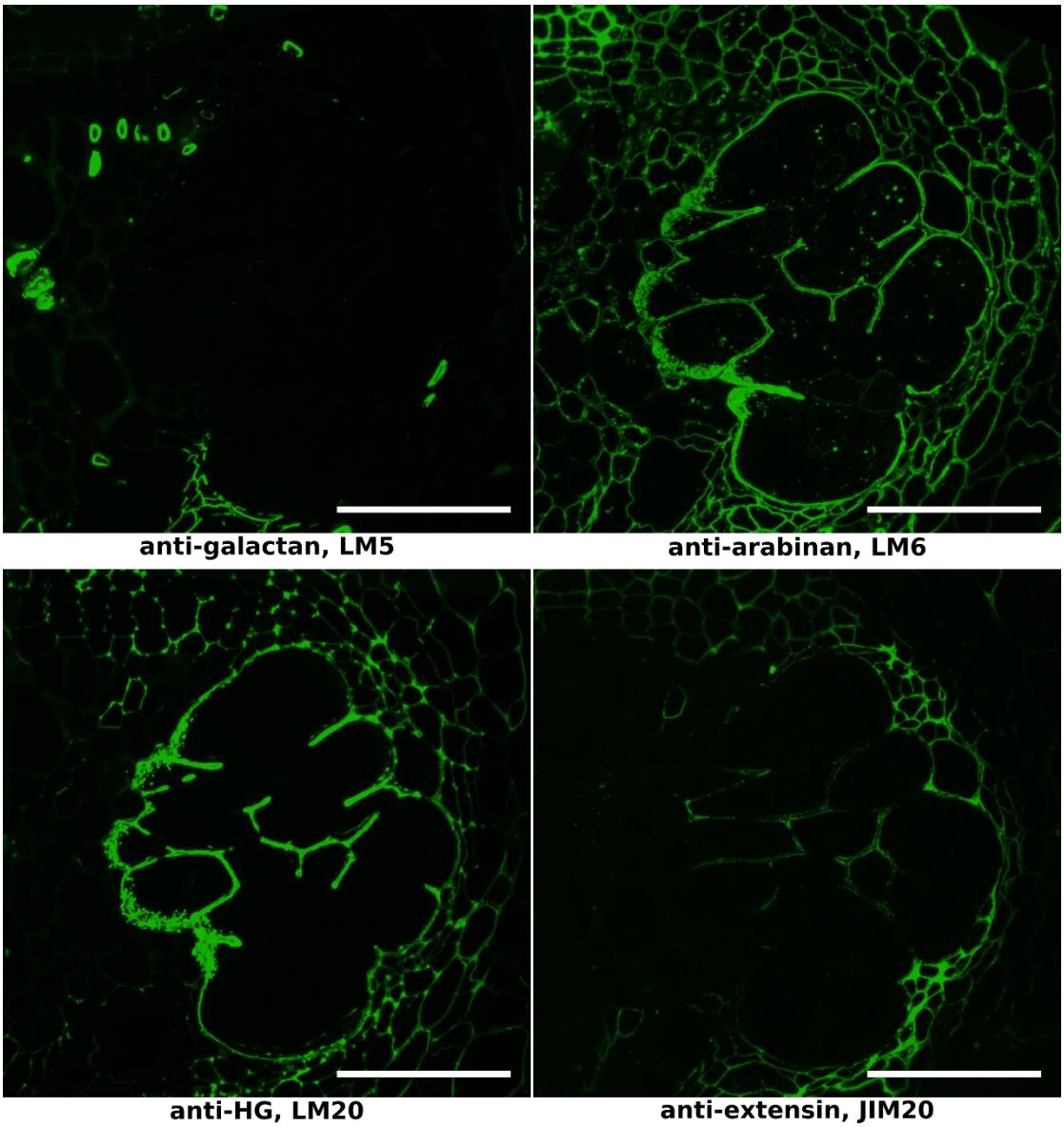

Figure 3.3.2.3 Immunolocalization of pectic glycans and proteins in syncytial walls induced by *H. glycines* in soybean roots (14 dpi). Indirect immunofluorescence (green) images are from the specific binding of mAbs, LM5 to galactan, LM6 to arabinan, LM20 to HG and anti-extensin JIM20, using equivalent sections. (bar=50 µm)

The cell walls of syncytia induced by *G. pallida* in potato and *H. glycines* in soybean

Cell wall architectures of syncytia induced by *G. pallida* and *H. glycines* in dicotyledonous hosts, potato and soybean respectively, were analysed. As summarised in Table 3.1, various antibodies were used to cover the most general cell wall components, not only revealing their existence but also the possible substitution/modification of these polymers as well (full set results could be found in supplemented material).

As listed in the table, potato syncytium samples of 4 different time points, 7 dpi, 14 dpi, 17 dpi and 21 dpi, were taken and analysed. The syncytia of different life stages all have distinctive structures and could be identified from the rest of the host root cells in Toluidine Blue O stained sections. Additionally, the distinction of their chemical compositions also makes it possible to distinguish them over mAbs labelled fluorescence images. Among those *in situ* results, no antibody binding pattern difference has been found, reflecting the stableness of cell wall microstructures of *G. pallida* induced syncytia during parasitism. For syncytia formed in soybean, only the mature stage 14 dpi sample was analysed. It also possesses distinctions at both structural level and chemical composition level.

Comparing the antibody binding patterns of syncytia across these two species, even the known results from beet cyst nematode *H. schachtii* induced syncytia (Davies, Lilley *et al.* 2012), the syncytial walls all possess diverse polysaccharides, including the abundant XyG, methyl-esterified HG and pectic arabinan, and lack of heteroxylan. Overall, for most of the mAbs applied, they share high similarities in terms of binding in syncytia formed within both host species. For instance, the anti-xylan antibody LM11, was used to visualize xylem within the vascular bundles and allow the orientation of key root structures in spite of the gross changes in morphology after syncytia formation. The distribution of XyG, the major non-cellulosic polysaccharides in dicots, was revealed by three antibodies and it was proven to be abundant in syncytial cell walls. The removal of pectin could unmask the epitopes of anti-XyG LM25 in potato syncytia, similar as described in previous studies (Marcus, Verhertbruggen *et al.* 2008, Davies, Lilley *et al.* 2012). The presence of pectic HG was visualized using two antibodies, directed towards lower/non-methyl-esterified HG and highly methyl-esterified HG. Differential binding patterns of these two antibodies together with the effect of Na_2CO_3 pre-treatment to remove methyl suggested that the syncytial cell walls possessed abundant pectic HG and it was heavily methyl esterified. For another group of pectic polymers, RG-I related two mAbs recognising 1,5-α-arabinan and 1,4-β-galactan sidechains of RG-I backbone respectively, were revealed to have strikingly different binding patterns in both plant species: anti-arabinan epitopes were abundant within syncytial cell walls in both plants while the anti-galactan epitopes were barely detectable in syncytia formed in potato and completely absent in soybean syncytia.

Apart from polysaccharides, plant cell walls also possess many structural proteins. Extensin, a type of HRGPs, was detected at a low level in syncytial cell walls of soybean, especially the wall fragments insider the syncytium. Cell surface AGPs were also analysed using several antibodies and the epitopes of anti-AGP JIM13 were observed in potato syncytial elements whilst largely absent in soybean syncytia.

Table 3.1 Summary of immunolocalization of primary antibodies in syncytial cell walls induced by *G. pallida* in potato roots and *H. glycines* in soybean roots

Antibody epitopes		mAbs	Potato syncytia				Soybean syncytia 14 dpi	Reference
			7 dpi	14 dpi	17 dpi	21 dpi		
Xyloglucan	XXXG motif	LM15	++(PL)	N/A	+++(PL)	N/A	+++	(Marcus, Verhertbruggen *et al.* 2008)
	galactosylated	LM24	-	N/A	-	N/A	- / +(PL)	(Pedersen, Fangel *et al.* 2012)
	XXXG / galactosylated	LM25	+++	+++	+++	+++	+++	(Pedersen, Fangel *et al.* 2012)
Mannan	heteromannan	LM21	-	-	-	-	+(PL)	(Marcus, Blake *et al.* 2010)
Xylan	(1→4)-β-D-xylan	LM10	-	-	-	-	-	(McCartney, Marcus *et al.* 2005)
	(1→4)-β-D-xylan / arabinoxylan	LM11	-	-	-	-	-	(McCartney, Marcus *et al.* 2005)
	feruloylated xylan	LM12	-	N/A	-	N/A	-	(Pedersen, Fangel *et al.* 2012)
Homogalacturonan	partially methyl-HG / de-esterified HG	LM19	+ / +++(Na_2CO_3)	-	+ / +++(Na_2CO_3)	- / +++(Na_2CO_3)	++	(Verhertbruggen, Marcus *et al.* 2009)
	partially methyl-HG	LM20	+++	+++	+++	+++	+++	(Verhertbruggen, Marcus *et al.* 2009)
RG-I related	(1→4)-β-D-galactan	LM5	+	+	+	+	-	(Jones, Seymour *et al.* 1997)
	(1→5)-α-L-arabinan	LM6	+++	+++	+++	+++	+++	(Willats, Marcus *et al.* 1998)
	processed arabinan	LM16	-	N/A	-	N/A	-	(Verhertbruggen, Marcus *et al.* 2009)
Arabinogalactan-protein	GlcA in AGP glycan	LM14	-	N/A	-	N/A	+(PL)	(Moller, Marcus *et al.* 2008)
	β-linked-GlcA in AGP glycan	LM2	-	N/A	-	N/A	-	(Yates, Valdor *et al.* 1996)
	AGP glycan	JIM4	-	N/A	-	N/A	-	(Yates, Valdor *et al.* 1996)
	AGP glycan	JIM13	++	+++	++	+++	-	(Yates, Valdor *et al.* 1996)
	AGP glycan	JIM14	+	-	+	+	-	(Yates, Valdor *et al.* 1996)
	AGP glycan	JIM15	-	N/A	-	N/A	-	(Yates, Valdor *et al.* 1996)
	AGP glycan	JIM16	-	N/A	-	N/A	-	(Yates, Valdor *et al.* 1996)
Extensin		LM1	-	N/A	-	N/A	N/A	(Smallwood, Martin *et al.* 1995)
		JIM19	-	N/A	-	N/A	N/A	(Wang, Heimovaara-Dijkstra *et al.* 1995)
		JIM20	+	+	+	-	++	(Knox, Peart *et al.* 1995)
Glycophospholipid		JIM18	-	N/A	-	N/A	-	(Knox, Peart *et al.* 1995)

* -, no binding; +, slight binding; ++, clear binding; +++, significant binding; N/A, not tested; PL, antibody epitope partly/fully masked by pectin; Na_2CO_3, sections pre-treated with Na_2CO_3.

** mAbs binding performance was marked visually, ranks not to be used for precise comparisons.

3.3.3 Cereal cyst nematodes induced syncytial walls in wheat

As the major staple cultivated worldwide, wheat production is also threatened by cyst nematode pests. Of which, two cereal cyst nematodes *H. avenae* and *H. filipjevi* are the most widespread and damaging. In this study, those two nematode species together with three spring wheat cultivars were used to analyse the cell wall chemical structures of the established feeding sites.

Root samples of all three wheat cultivars (Bobwhite, Cadenza and Fielder), infested with J2s of *H. avenae* and *H. filipjevi*, were taken at 21 dpi and 28 dpi respectively, with comparable size of developing females shown on the root surface. The same experimental procedures were applied, using a collection of specific mAbs. Immunolabelling results of the three wheat cultivars did not show clear host-cultivar-related differences in terms of syncytial wall microstructures for each nematode species, and the figures shown below are only a part of the whole representative dataset. Sections without primary antibody treatment were used as background control and no nonspecific fluorescence was observed in plant cell walls after blocking the background autofluorescence as described before (figures included in supplementary data).

Anti-xylan antibodies target non-cellulosic xylans in wheat syncytial walls

As revealed in the above sections, the anti-heteroxylan LM11 binds specifically to the xylem elements but not the syncytial walls inside the vascular cylinder of both potato and soybean roots and is used as an indicator in telling host root vascular structures. While as in wheat, a type of grass with distinct type II primary walls, xylans are the major cross-linking glycans in its primary walls. Therefore, an extensive selection of mAbs targeting heteroxylans were applied. As revealed by antibody binding patterns in Figure 3.3.3.1 for *H. avenae* induced syncytia and Figure 3.3.3.2 for *H. filipjevi* induced syncytia, the syncytial walls induced by both nematode species all possess abundant levels of substituted xylans, indicated by the fine binding of LM12 and LM28, while absent of unbranched/low-branched xylans, as indicated by LM10 and LM11. Judging by the binding patterns of those mAbs, the syncytium-surrounding cells, regardless of cell types, mainly maintain much more low-branched xylans in walls, as given by the strong binding of LM10 and LM11 in comparison with the much weaker affinity to LM12 and LM28.

Bright field images were taken over Toluidine Blue O stained sections to aid the structural identifications of syncytial regions. Fluorescence images were obtained using equivalent sections as the ones in bright field, thus direct discrimination of syncytial walls shall be made accordingly. Due to size limitations, only the nematode induced syncytial regions and few surrounding cells are shown in most of the listed fluorescence images.

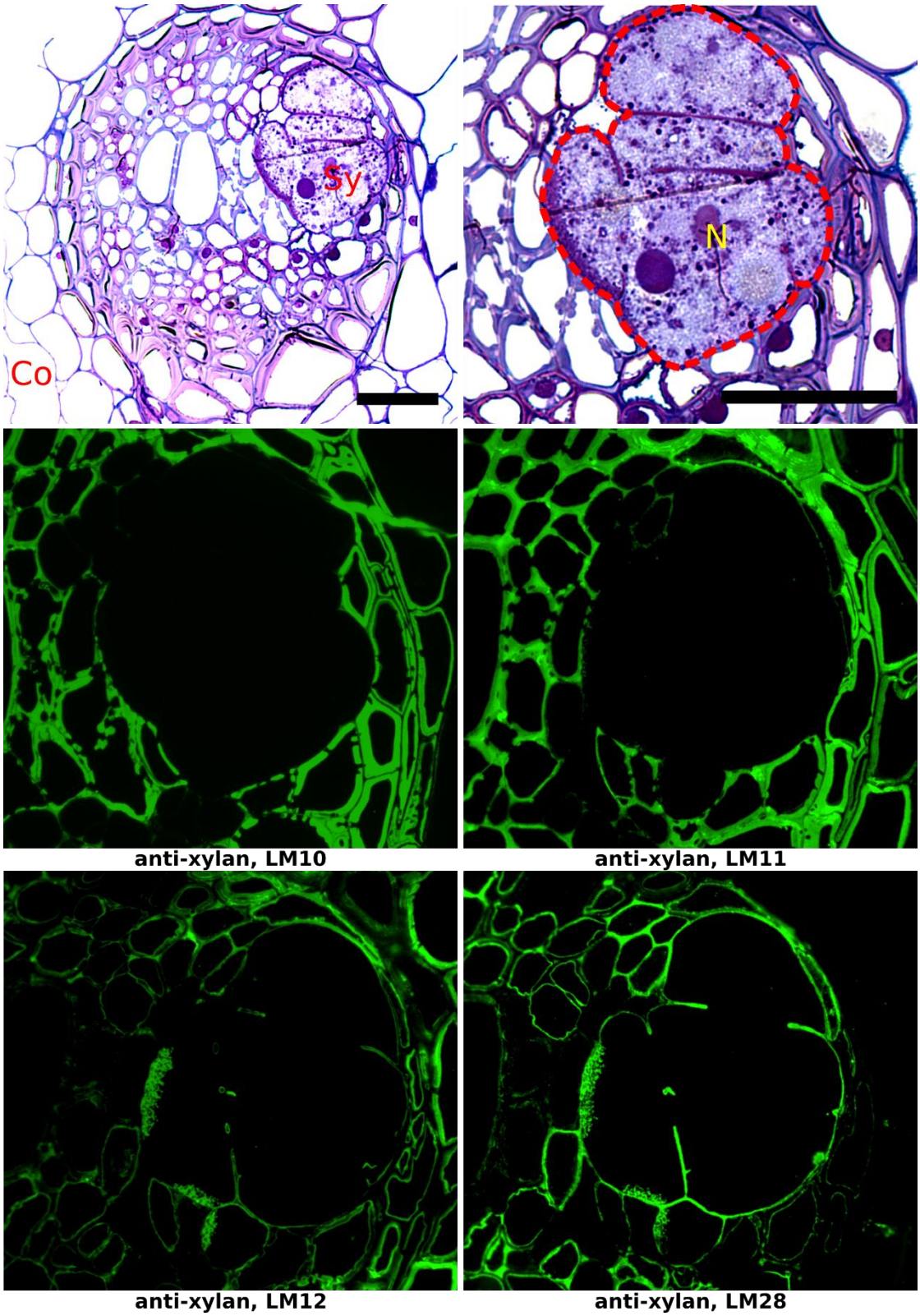

Figure 3.3.3.1 Immunolocalization of xylan in *H. avenae* induced syncytial walls in wheat roots (Bobwhite, 21 dpi). Bright field images are captured from the section stained with Toluidine Blue O. Syncytial region is outlined in red dash line. Indirect immunofluorescence (green) images are from the specific binding of anti-xylan mAbs LM10, LM11, LM12 and LM28 using equivalent sections. (Co, cortex; Sy, syncytium; N, enlarged nuclei; bar=50 µm)

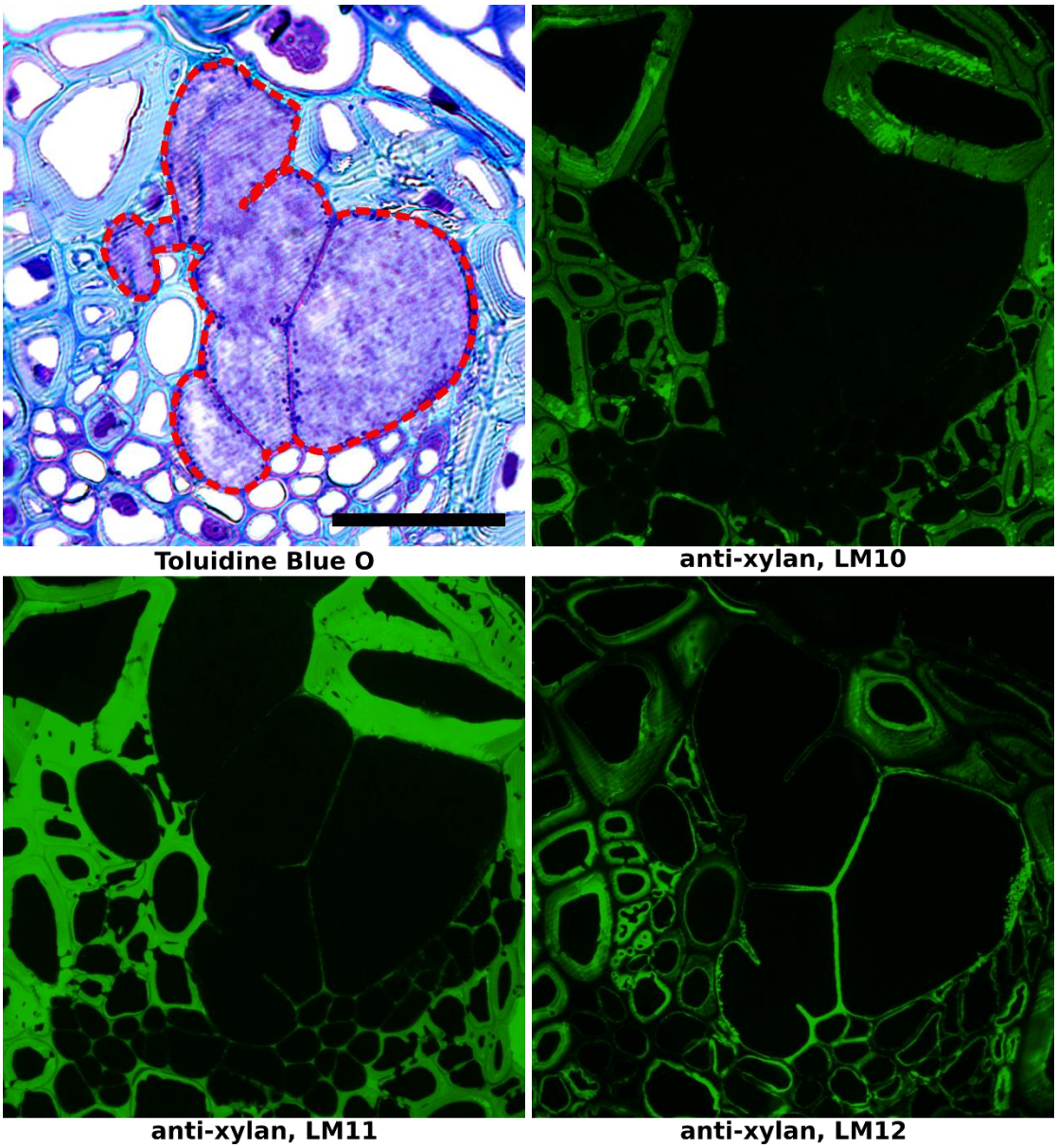

Figure 3.3.3.2 Immunolocalization of xylan in *H. filipjevi* induced syncytial walls in wheat roots (Cadenza 28 dpi). Bright field image is captured from the section stained with Toluidine Blue O. Syncytial region is outlined with red dash line. Indirect immunofluorescence (green) images are from the specific binding of anti-xylan mAbs LM10, LM11 and LM12 using equivalent sections. (bar=50 µm)

Non-cellulosic XyG and MLG in wheat syncytial walls

The analysis of other cross-linking glycans were carried out using LM15 and LM25 against XyG and the MLG specific antibody, as shown in Figure 3.3.3.3. Although the type II primary walls naturally possess less XyG, it was still proven to be present in the syncytial walls of both nematode species, with LM25 giving relatively stronger binding. However, the binding properties of anti-MLG mAb was different between the two nematode species, with the absence in *H. avenae* induced syncytial walls in Bobwhite and weak presence in *H. filipjevi* induced syncytial walls in Cadenza. This type of difference is consistent among all tested wheat cultivars (as summarised in Table 3.2), thus reflecting it is more likely to be related to nematode species rather than the different cultivars used.

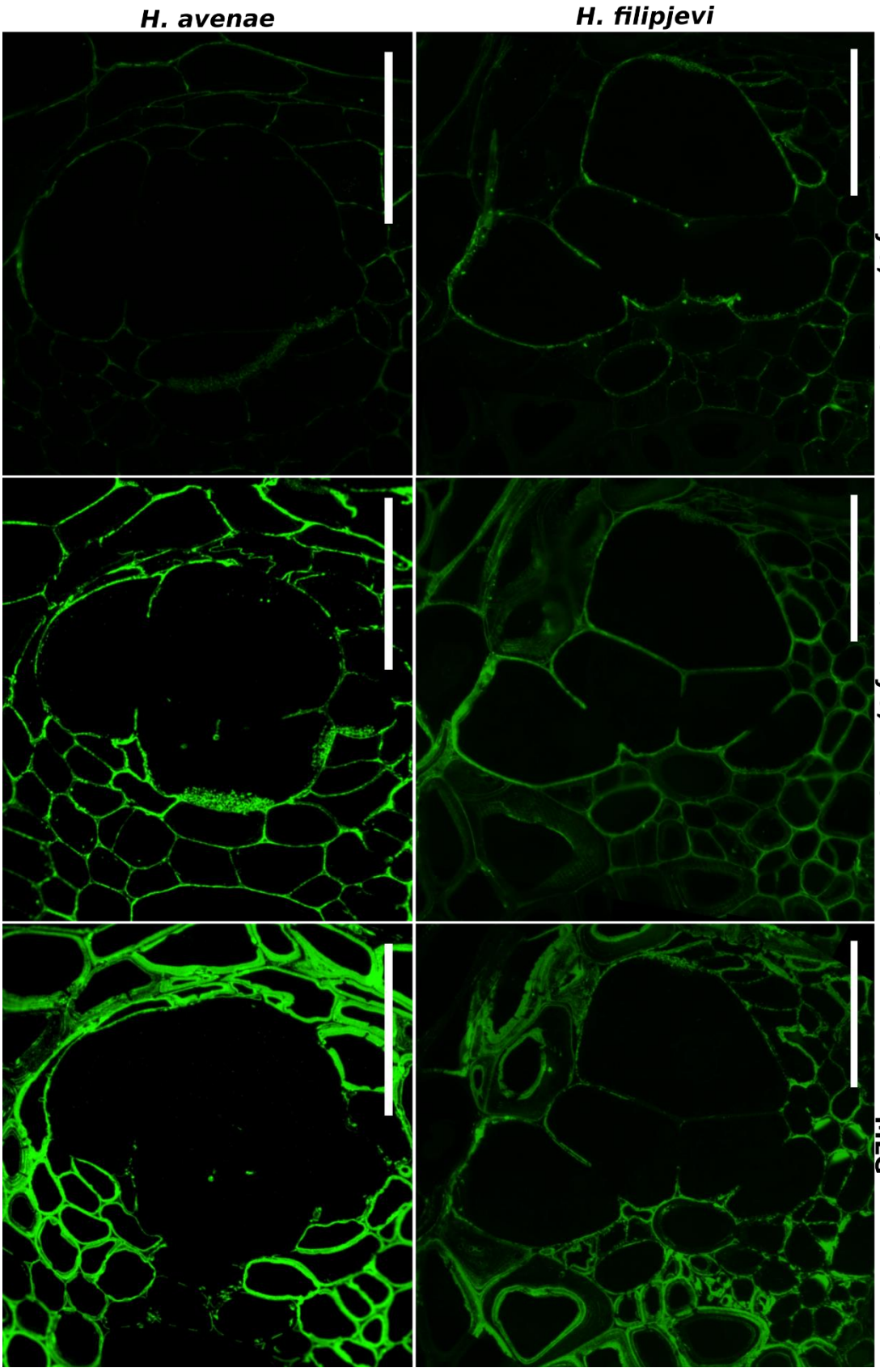

Figure 3.3.3.3 Immunolocalization of XyG and MLG in syncytial walls induced by *H. avenae* (Bobwhite, 21 dpi) and *H. filipjevi* (Cadenza, 28 dpi). Immunofluorescence (green) images are from the specific binding of anti-XyG mAbs LM15 and LM25 and MLG antibody using equivalent sections. (bar=50 µm)

Pectic polymers in wheat syncytial walls

Analysis of the pectic polymers, including RG-I and HG, was performed by applying specific mAbs, LM5 to 1,4-galactan, LM6 to 1,5-arabinan and LM20 to methyl-HG. As revealed by antibody binding properties in Figure 3.3.3.4, the wheat syncytial walls contain abundant arabinans whilst close to absent of galactans. Both epitopes are thought to be linked to the heterogeneous RG-I. The epitopes of LM20, representing pectic methyl-HG, were also found in syncytial walls at a very low yet detectable level as it is naturally low in grass cell walls. All these binding patterns were also observed in syncytia formed in other tested cultivars.

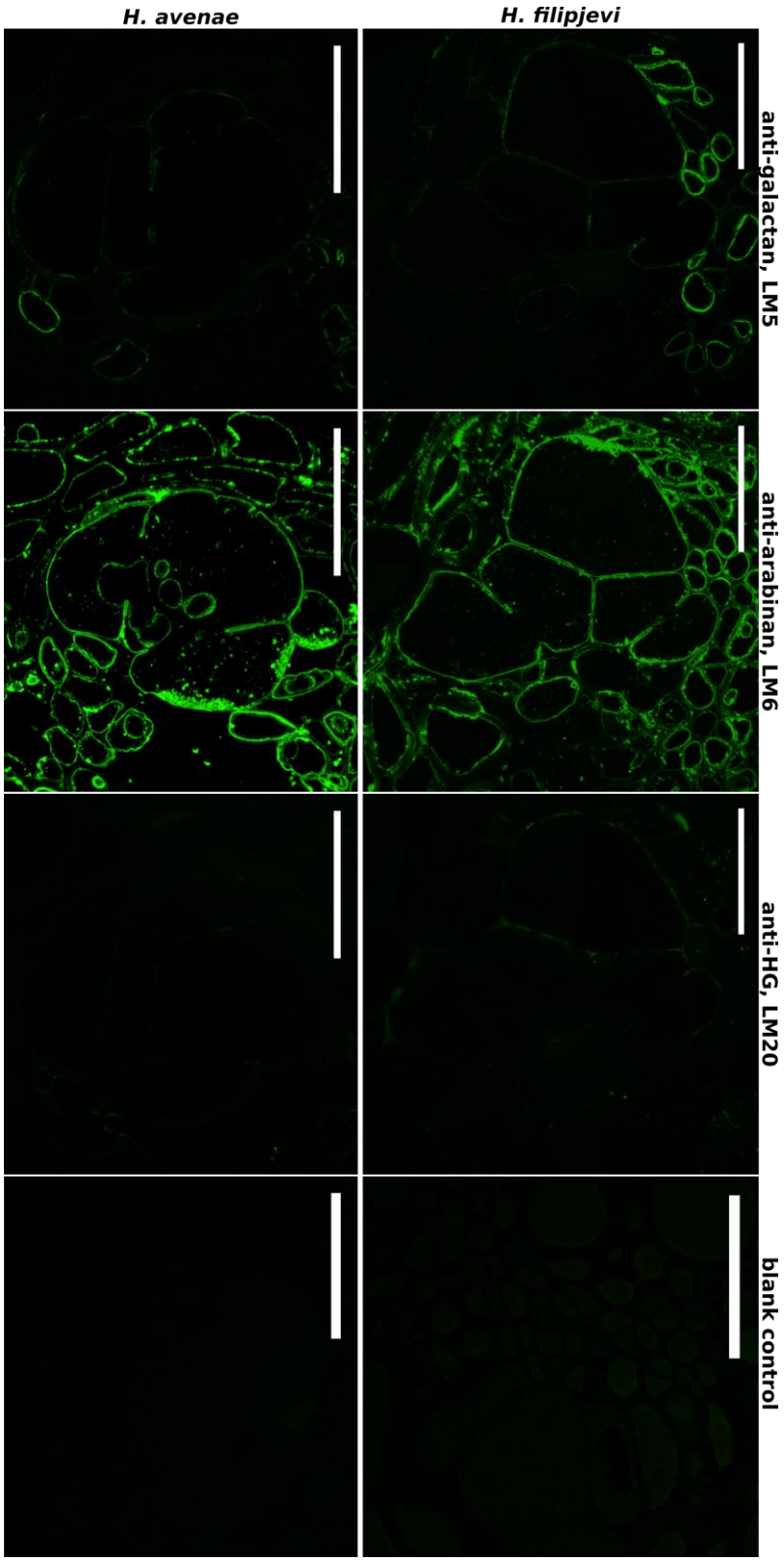

Figure 3.3.3.4 Immunolocalization of pectic polymers in syncytial walls induced by *H. avenae* (Bobwhite, 21 dpi) and *H. filipjevi* (Cadenza, 28 dpi). Indirect immunofluorescence (green) images are from the specific binding of anti-galactan LM5, anti-arabinan LM6 and anti-HG LM20 using equivalent sections. Sections without primary antibody labelling were used as negative control. (bar=50 µm)

The chemical structures of syncytial walls induced by *H. avenae* and *H. filipjevi* in wheat

The investigation of the wall chemical structures of syncytia induced by *H. avenae* and *H. filipjevi* in wheat was carried out using a set of mAbs targeting specific wall polymers. In order to eliminate possible cultivar related differences, three spring wheat cultivars were used, including Bobwhite, Cadenza and Fielder, for both nematode species. Successful infections at a comparable stage, for instance 21 dpi for *H. avenae* and 28 dpi for *H. filipjevi* both with observed developing females on the root surface, were taken and the results are summarised in the following Table 3.2.

As listed in the table, the syncytia induced in the three cultivars by both CCNs all possess abundant amount of feruloylated heteroxylans and arabinans, small amount of XyG as well as trace level of pectic galactan and marginal levels of methyl-HG. The major difference between those two types of syncytial walls was observed when using the MLG specific antibody.

As the major cross-linking glycans in primary cell walls of grass, four anti-xylan antibodies LM10, LM11, LM12 and LM28 were used to reveal both the presence and substitutions of xylans in syncytia. They recognise unsubstituted xylan, unsubstituted xylan/arabinoxylan, feruloylated xylan and glucuronosyl-containing heteroxylan respectively. Antibody binding patterns revealed the absence of unbranched xylans and low levels of arabinoxylan within syncytial cell walls. Meanwhile, significant strong binding was observed using LM12 and LM28, suggesting that the xylans of syncytial walls were predominantly substituted with ferulic acid and glucuronic acid. The XyG was present in both types of syncytial cell walls, with the epitopes of anti-XyG LM25 relatively more abundant. MLG is mainly restricted to the grass family and was evident in a range of cell types in the root sections. However, whilst MLG was present in the cell walls of syncytia induced by *H. filipjevi*, it was almost entirely absent from *H. avenae* induced syncytial walls. The prevalence of pectic polymers in the syncytial cell walls was analysed. Trace levels of methyl-esterified HG were found within syncytia, indicated by the slight binding of LM20 comparing with the absence of LM19 targeting non/low-methyl HG. Low levels of galactan were detected whilst anti-arabinan epitopes were much more abundant in the walls of syncytia.

No antibody binding pattern differences were observed among syncytia induced by the same nematode species in the three analysed wheat cultivars. This allows the use of one cultivar, Bobwhite, to further investigate the syncytium cell walls at different parasitic stages for both CCNs.

Table 3.2 Summary of immunolocalization of primary antibodies in syncytial cell walls induced by *H. avenae* and *H. filipjevi* in wheat roots

Antibody epitopes		mAbs	*H. avenae* induced syncytia 21 dpi			*H. filipjevi* induced syncytia 28 dpi			Reference
			Bobwhite	Cadenza	Fielder	Bobwhite	Cadenza	Fielder	
Xyloglucan	XXXG motif	LM15	++	++	+	++	++	++	(Marcus, Verhertbruggen *et al.* 2008)
	galactosylated	LM24	-	-	-	-	-	-	(Pedersen, Fangel *et al.* 2012)
	XXXG / galactosylated	LM25	++	++	++	+++	+++	+++	(Pedersen, Fangel *et al.* 2012)
Xylan	(1→4)-β-D-xylan	LM10	-	-	-	-	-	-	(McCartney, Marcus *et al.* 2005)
	(1→4)-β-D-xylan / arabinoxylan	LM11	+	+	+	+	+	+	(McCartney, Marcus *et al.* 2005)
	feruloylated xylan	LM12	+++	+++	+++	+++	+++	+++	(Pedersen, Fangel *et al.* 2012)
	heteroxylan	LM28	+++	+++	+++	+++	+++	+++	(Cornuault, Buffetto *et al.* 2015)
Mixed-Linkage (1→3),(1→4)-β-D-Glucans		MLG	-	-	-	+++	+++	+++	(Meikle, Hoogenraad *et al.* 1994)
Homogalacturonan	partially methyl-HG / de-esterified HG	LM19	-	-	-	-	-	-	(Verhertbruggen, Marcus *et al.* 2009)
	partially methyl-HG	LM20	+	+	+	+	+	+	(Verhertbruggen, Marcus *et al.* 2009)
RG-I related	(1→4)-β-D-galactan	LM5	+	+	+	+	+	+	(Jones, Seymour *et al.* 1997)
	(1→5)-α-L-arabinan	LM6	+++	+++	+++	+++	+++	+++	(Willats, Marcus *et al.* 1998)
Arabinogalactan-protein	β-linked-GlcA in AGP glycan	LM2	-	-	-	-	-	-	(Yates, Valdor *et al.* 1996)
Extensin		JIM19	-	-	-	-	-	-	(Wang, Heimovaara-Dijkstra *et al.* 1995)
		JIM20	-	-	-	-	-	-	(Knox, Peart *et al.* 1995)

* -, no binding; +, slight binding; ++, clear binding; +++, significant binding. Ranks of mAbs binding are not to be used for precise comparisons.

** Plant cell wall probe CBM2b1-2, targeting the backbone of linear and substituted xylans, is not included in this table and results can be found in the supplement dataset.

3.3.4 *H. avenae* and *H. filipjevi* induced syncytial walls in wheat at different nematode developmental stages

Based on the above analysis over both *H. avenae* and *H. filipjevi* infested spring wheat cultivars, further investigations were carried out to evaluate the stableness of syncytial cell wall chemical structures during parasitism. More samples of continuous parasitism stages were collected using Bobwhite infested with both CCNs. Immuno-histochemical analysis was then proceeded using a refined range of cell wall mAbs (CBM probes were also used and the results are included in supplementary data) to obtain representative results. The most representative images are listed below (full results were summarised in the relative table) and only parts of the whole root sections are shown due to size limitations.

The wheat syncytial walls possess abundant heteroxylans during nematode parasitism

As listed in Figure 3.3.4.1, the walls of syncytia induced by *H. avenae* in Bobwhite contain abundant substituted xylans, indicated by LM12 and LM28 binding (LM28 results were included in supplementary data), throughout parasitism, from early forming stage 7 dpi to later mature stage 35 dpi. Similar results were also observed in *H. filipjevi* induced syncytia at various stages, as later summarised in Table 3.3.

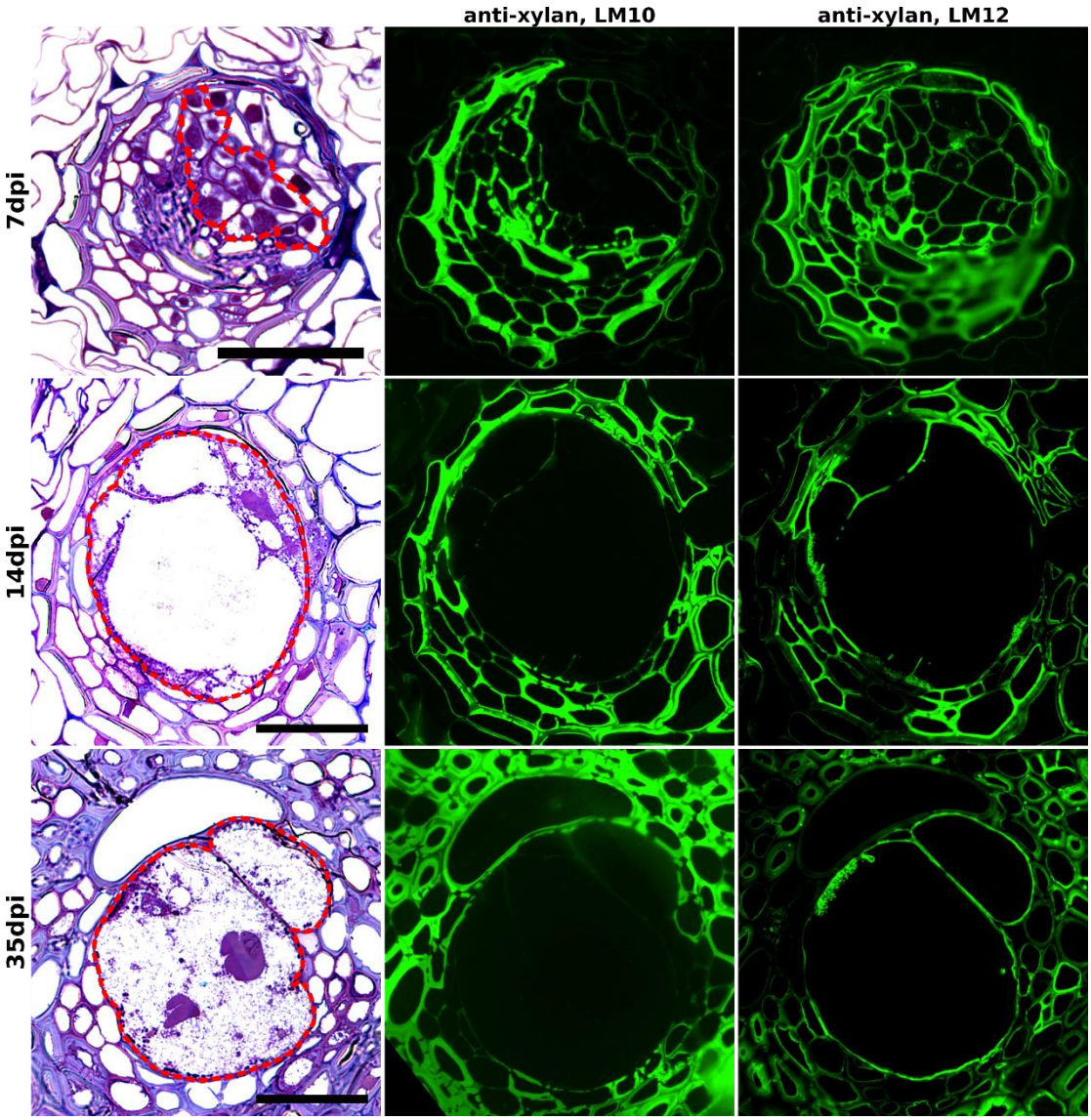

Figure 3.3.4.1 Immunolocalization of xylan in *H. avenae* induced syncytial walls in Bobwhite roots (7 dpi, 14 dpi and 35 dpi). Bright field images are captured from the sections stained with Toluidine Blue O. Syncytial regions are outlined with red dash line. Indirect immunofluorescence (green) images are from the specific binding of anti-xylan mAbs LM10 and LM12 over equivalent sections respectively. (bar=50 µm)

Other non-cellulosic and pectic polysaccharides in wheat syncytial walls

Further analysis, in searching for other cross-linking as well as pectic wall polymers, was implemented using equivalent sections as above.

As revealed by the fluorescence distribution, the *H. avenae* induced syncytial walls contain XyG and arabinans consistently, while the galactan and MLG epitopes, known to be largely absent in the last section, were present as in Figure 3.3.4.2. The MLG appeared to be largely absent in the initial 7 dpi and 14 dpi samples, while show clear existence in the 35 dpi syncytial walls except the cell wall ingrowth region. The LM5 epitopes were shown to be in an unpredictable pattern, with marginal or low binding in 7 dpi and 35 dpi whilst gave clear binding at 14 dpi.

In comparison, the *H. filipjevi* induced syncytia were also analysed at 14 dpi, 21 dpi and 35 dpi as shown in Figure 3.3.4.3. The anti-arabinan LM6 epitopes were abundant among all samples, while the binding of MLG and anti-galactan LM5 was shown to be much less or absent.

The consistency and variation of wheat syncytial cell wall chemical structures

As summarised in Table 3.3, in order to further investigate the consistency of wall compositions during syncytium development, syncytial samples from additional stages of nematode development were studied using the wheat cultivar Bobwhite. The antibody binding patterns in syncytia induced by the same nematode species were generally stable among different parasitism stages and both types of syncytia shared high similarities in terms of cell wall chemical compositions.

Adding results from the previous section, the cell walls of syncytia induced by both *H. avenae* and *H. filipjevi* in wheat roots were all rich in feruloylated heteroxylans and arabinans. Besides, XyG was also shown to be present in all wheat syncytial walls. Syncytia induced by the same nematode species were generally stable at the cell wall chemical composition level, both among different host cultivars and among various developmental stages within the same cultivar. Apart from the fluctuating binding of pectic galactan and MLG, wheat syncytia of both nematode species possess similar cell wall microstructures. As analysed using syncytia induced in the same host cultivar at a series of developmental stages, those differences of galactan and MLG were more likely related to the different development of both nematode species, although the fine reasons were yet to be elucidated.

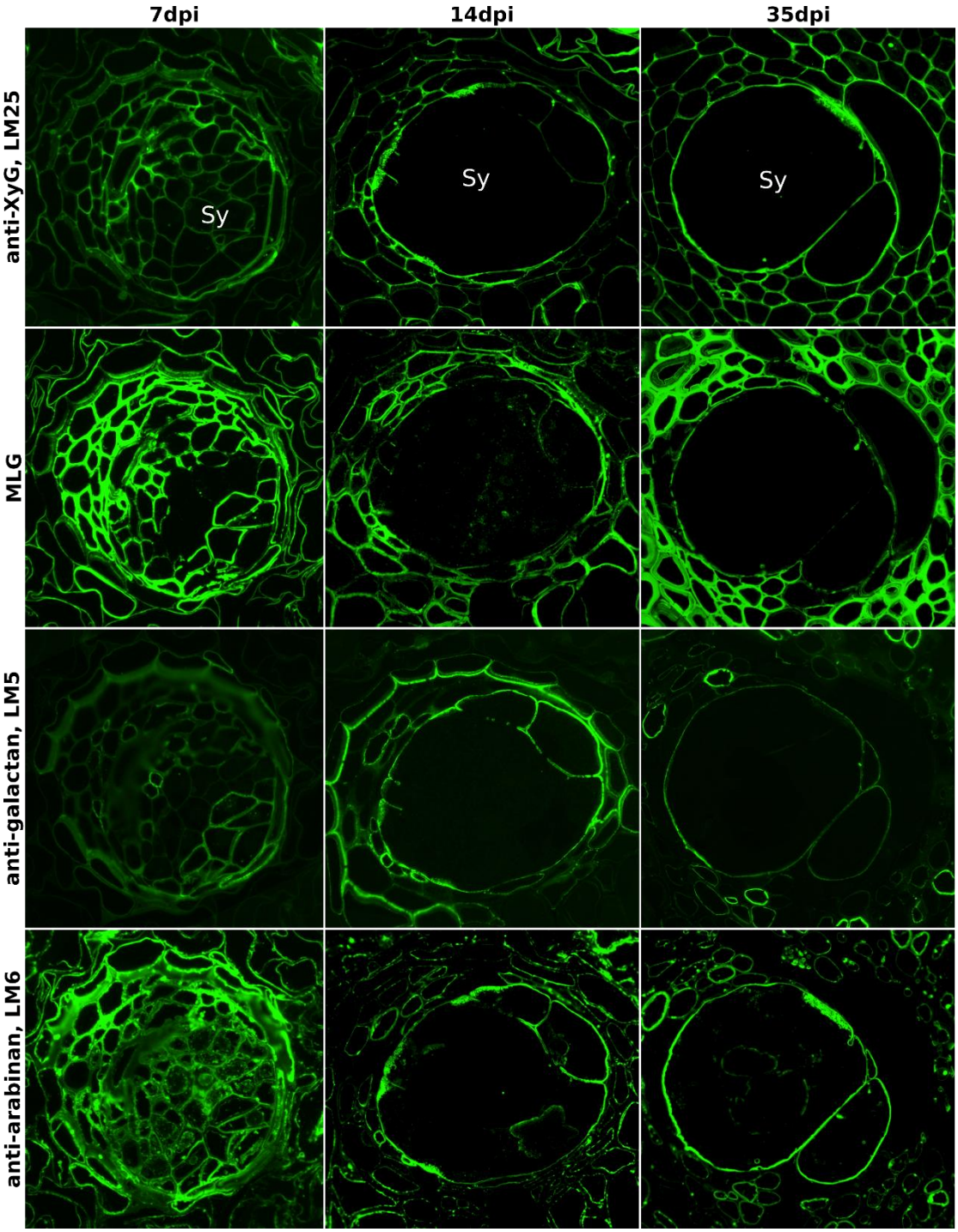

Figure 3.3.4.2 Immuno-fluorescence imaging of syncytial walls induced by *H. avenae* in Bobwhite roots (7 dpi, 14 dpi and 35 dpi). Indirect immunofluorescence (green) images are from the specific binding of mAbs, anti-XyG LM25, MLG antibody, anti-galactan LM5 and anti-arabinan LM6, using equivalent sections respectively. (Sy, syncytium; bar=50 µm)

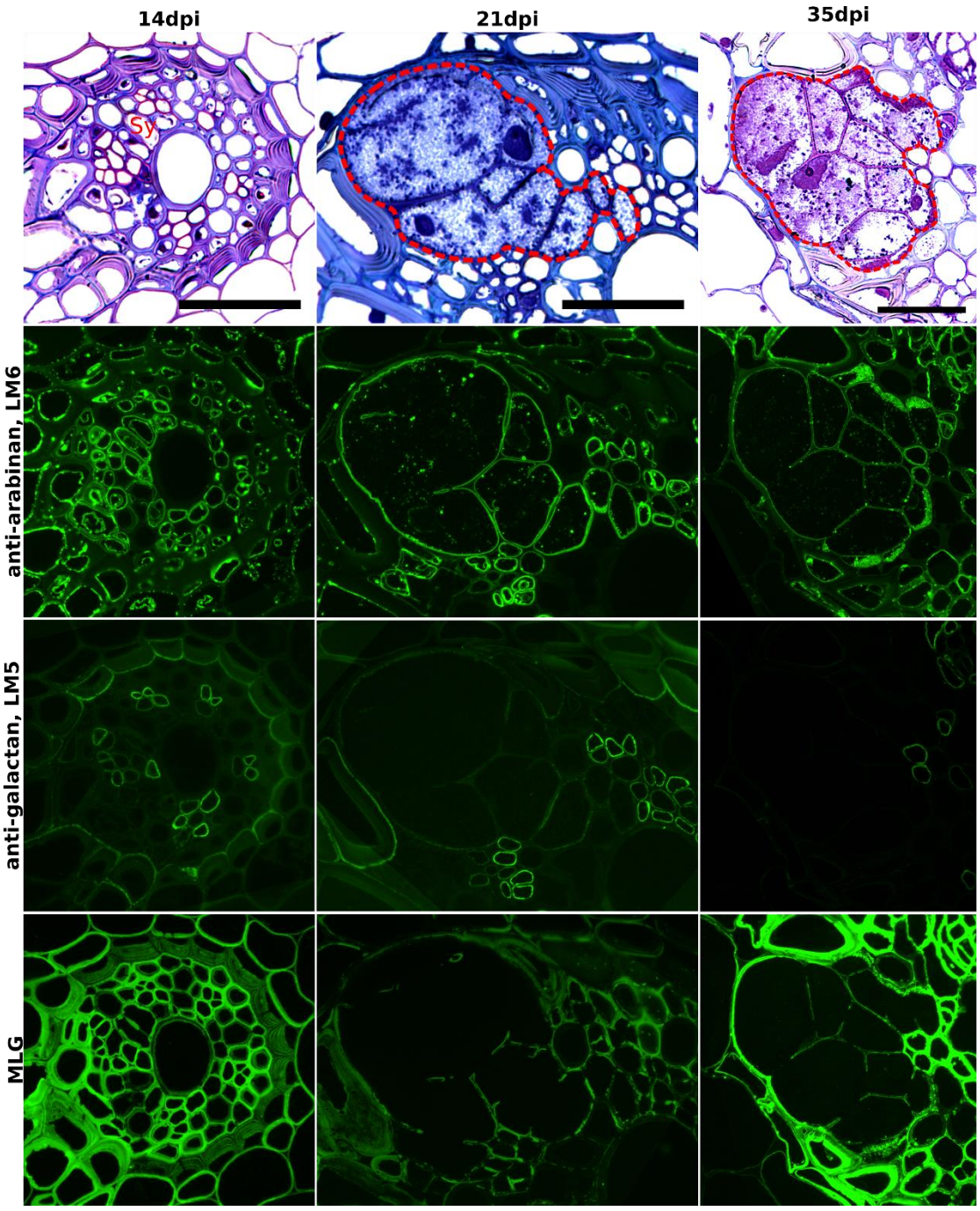

Figure 3.3.4.3 Immuno-fluorescence imaging of syncytial walls induced by *H. filipjevi* in Bobwhite roots (14 dpi, 21 dpi and 35 dpi). Bright field images are captured from the sections stained with Toluidine Blue O. Syncytial regions are outlined with red dash line. Indirect immunofluorescence (green) images are from the specific binding of mAbs, LM6 to arabinan, LM5 to galactan and MLG antibody, using equivalent sections respectively. (Sy, syncytium; bar=50 µm)

Table 3.3 Summary of immunolocalization of primary antibodies in syncytial cell walls induced by *H. avenae* and *H. filipjevi* in Bobwhite

Antibody epitopes		mAbs	*H. avenae* induced syncytia			*H. filipjevi* induced syncytia			Reference
			7 dpi	14 dpi	35 dpi	14 dpi	21 dpi	35 dpi	
Xyloglucan	XXXG motif	LM15	++	+	+	+	+	+	(Marcus, Verhertbruggen *et al.* 2008)
	XXXG / galactosylated	LM25	++	++	+++	+++	+++	+++	(Pedersen, Fangel *et al.* 2012)
Xylan	(1→4)-β-D-xylan	LM10	-	-	-	-	-	-	(McCartney, Marcus *et al.* 2005)
	(1→4)-β-D-xylan / arabinoxylan	LM11	-	+	+	-	+	+	(McCartney, Marcus *et al.* 2005)
	feruloylated xylan	LM12	+++	+++	+++	++	+++	+++	(Pedersen, Fangel *et al.* 2012)
	heteroxylan	LM28	++	+++	+++	+++	+++	+++	(Cornuault, Buffetto *et al.* 2015)
Mixed-Linkage (1→3),(1→4)-β-D-Glucans		MLG	+	++	+	++	++	++	(Meikle, Hoogenraad *et al.* 1994)
Methyl esterified Homogalacturonan		LM20	+	+	+	+	+	+	(Verhertbruggen, Marcus *et al.* 2009)
RG-I related	(1→4)-β-D-galactan	LM5	+	++	++	-	+	-	(Jones, Seymour *et al.* 1997)
	(1→5)-α-L-arabinan	LM6	+++	+++	+++	+++	+++	+++	(Willats, Marcus *et al.* 1998)

* -, no binding; +, slight binding; ++, clear binding; +++, significant binding. Ranks of mAbs binding are not to be used for precise comparisons.

** Plant cell wall probe CBM2b1-2 against xylan is not included in this table; results are included in the supplementary dataset.

The cell wall microstructures of syncytia induced by cyst nematodes in their natural hosts

Based on the immunolabelling results in all tested nematode species and host types, the major syncytial cell wall components were summarised in the following Table 3.4. Overall, cyst nematode induced syncytial walls maintain stable chemical compositions throughout their life stages, as depicted above.

Apart from the cell wall scaffolding cellulose microfibrils, the syncytial cell walls studied all possess XyGs and abundant arabinans. Syncytia formed within eudicot potato and soybean roots also contain large amount of methyl-HG whilst wheat syncytia induced by both CCNs contain large amount of feruloylated/glucuronosyl-containing heteroxylans. Noticeable variations, in terms of antibody binding directed to MLG and galactan, were observed in wheat syncytia, and these differences are more likely due to the different development between the two nematode species.

Table 3.4 Summary of cell wall composition of syncytia induced by cyst nematodes *G. pallida*, *H. glycines, H. avenae* and *H. filipjevi* in their host roots

Cell wall components	Potato	Soybean	Wheat	
	G. pallida	*H. glycines*	*H. avenae*	*H. filipjevi*
Xyloglucan, XXXG motif	++	++	++	++
Xylan, (1→4)-β-D-xylan	-	-	-	-
Xylan, arabinoxylan	-	-	+	+
Xylan, feruloylated	-	-	++	++
Xylan, glucuronosyl-heteroxylan	N/A	N/A	++	++
Mixed-Linkage (1→3),(1→4)-β-D-Glucans	-	-	++, noticeable variation	++, noticeable variation
Homogalacturonan, methyl esterified	++	++	+	+
RG-I related, (1→4)-β-D-galactan	+	-	+, noticeable variation	+, noticeable variation
RG-I related, (1→5)-α-L-arabinan	++	++	++	++

* Results derived from immunolocalization of plant cell wall probes in various nematode development stages. Ranks of mAbs binding are not to be used for precise comparisons.

** -, absent; +, low level of existence; ++, abundant level

3.3.5 Distribution analysis of cell wall polymers in syncytia

The syncytium formation process encompasses the transformation of a host root cell into the ISC and further continuous cell wall dissolutions of neighbouring cells. Comparing with the general structures of plant cell walls (Figure 1.4 III), the walls of a functioning syncytium can be further divided into different layers/partitions under high definition microscopy, including the cell wall ingrowth, the syncytial primary walls with direct contact to the syncytium cytoplasmic content and the syncytial middle lamella layer (Figure 3.3.5.1). This middle lamella layer separates the syncytium primary walls and the adjacent host cell primary walls (Figure 3.3.5.1 B), and it usually 'branches' to the inside of the syncytial region as part of the wall fractions (Figure 3.3.5.1 C). However, this type of differentiation of wall layers is not always fully distinguishable due to technical reasons, especially in the Immunohistochemical analysis. Therefore, the including of the middle lamella layer as part of the whole syncytium cell walls is practical and meanwhile make space for further analysis where possible. This definition of the range of total syncytial cell walls was used in previous results and will be used continuously in the following text, unless specified.

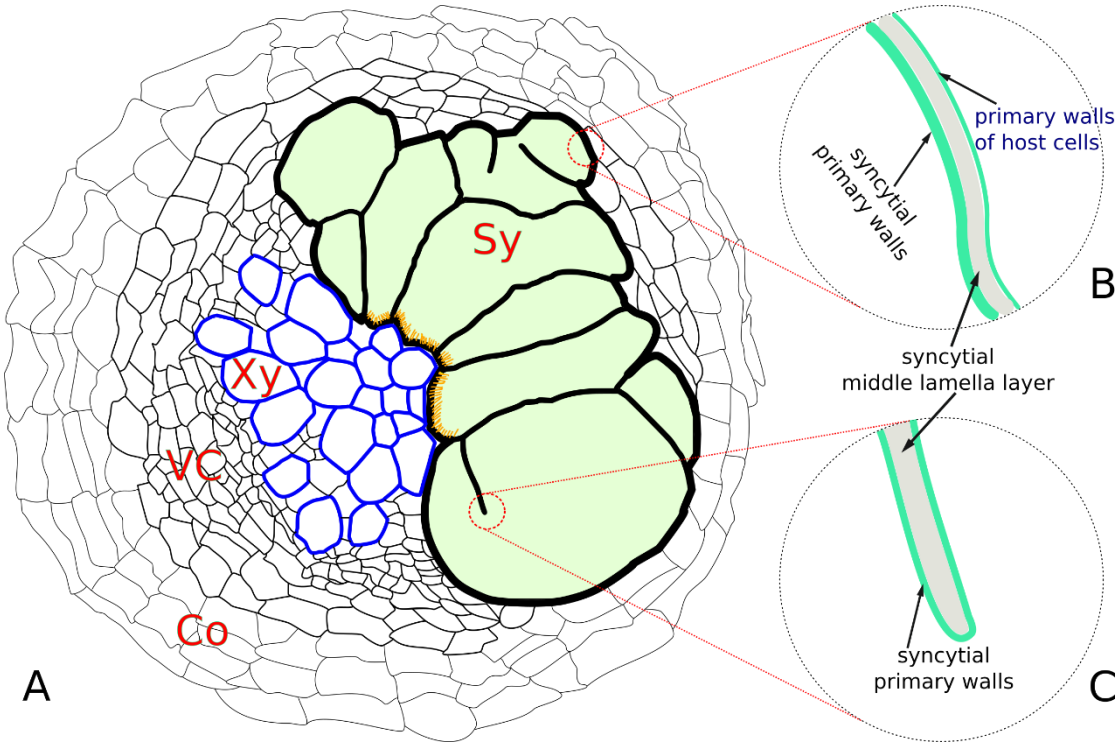

Figure 3.3.5.1. A cyst nematode induced syncytium within the host root. A. A transverse section of a syncytium within the host root (Xy, xylem, in blue; VC, vascular cylinder; Co, cortex; Sy, syncytium region, in green; cell wall ingrowth marked in yellow); **B**, **C**. Different cell wall layers of syncytial walls at high resolution.

Observed under higher magnification, fluorescence distribution analysis was carried out, providing the syncytial wall study greater details. It show that the unresolved wall layers of the syncytium, occasionally observed in bright field images, are also 'separable' from each other from a wall chemical composition angle. As revealed in previous results, the syncytial walls share high similarities in chemical compositions as well as having distinctiveness, for instance, both potato and soybean syncytial walls possess abundant XyG and methyl-HG, and together with wheat syncytia, all syncytial walls contain rich arabinans. Comparisons were made among different mAbs targeting those wall polymers at higher magnification.

The distribution of epitopes of mAbs in potato syncytial walls

As shown in Figure 3.3.5.2, the syncytial walls contain abundant XyG, arabinans, methyl-HG and clear JIM13 designated structural proteins. The comparison of fluorescence clearly indicates that the epitopes of those mAbs are not distributed evenly in the syncytial walls, instead there are clear differentiated 'layers' with less binding for anti-XyG LM25, anti-arabinan LM6 and anti-AGP JIM13. This suggests that the syncytial walls have chemical distinctive layers, with the syncytial primary walls (as illustrated in Figure 3.3.5.1) contain most of the XyG, arabinans and AGPs meanwhile the syncytial middle lamella layer more likely contain mainly pectic HGs as shown by the strong binding of LM19 (sections pre-treated to remove methyl groups) and LM20.

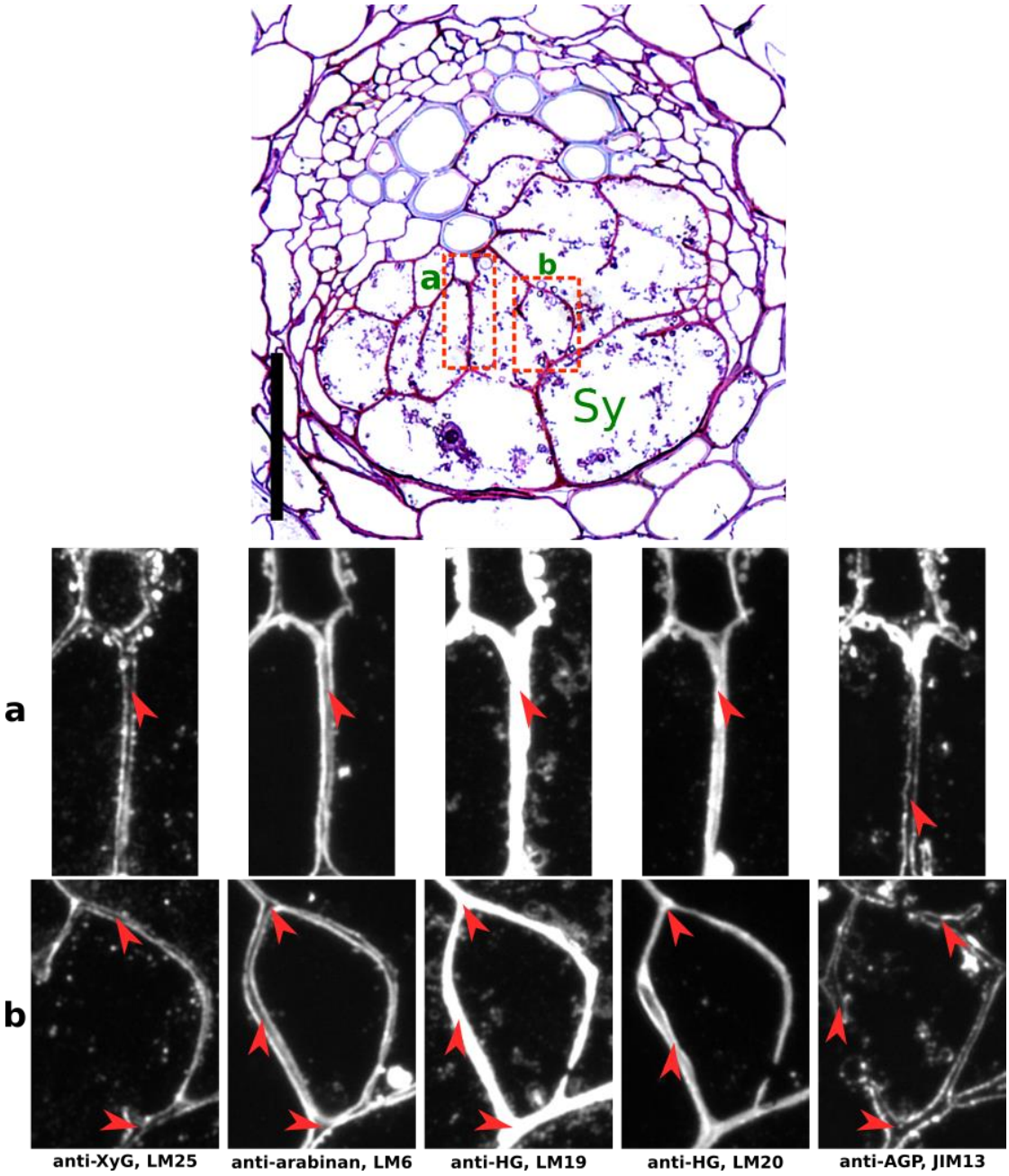

Figure 3.3.5.2 Antibody binding analysis of syncytial walls induced by *G. pallida* in potato roots (14 dpi). Fluorescence images (dark field) of group 'a' and 'b' are parts of the syncytial cell walls from sections labelled with specific mAbs, equivalent to the 'a' and 'b' regions marked with red dash line in the bright field image (stained with Toluidine Blue O). Epitope distribution pattern in syncytial walls is indicated with red arrows. Antibodies used include anti-XyG LM25, anti-arabinan LM6, anti-HG LM19 and LM20 and anti-AGP JIM13. LM19 labelled section is pre-treated with Na_2CO_3 to remove methyl groups. (Sy, syncytium; bar=50 µm)

The distribution of epitopes of mAbs in soybean syncytial walls

Similar fluorescence analysis was also carried out in soybean induced syncytial walls. As revealed in Figure 3.3.5.3, the syncytial middle lamella layer clearly possess less XyG and arabinan than the syncytial primary walls and wall ingrowth as represented by anti-XyG LM15 and LM25 and anti-arabinan LM6 respectively. The anti-HG LM20 was shown to be binding strongly overall while the anti-extensin JIM20 epitopes were found exclusively in the wall fragments within the syncytia. This might reflect the chemical heterogeneity in syncytial walls.

Due to the size difference of syncytia, this type of differentiation was easily distinguished in those largely thickened syncytial walls formed in potato and soybean, while in wheat syncytia often with a much thinner syncytial wall, this phenomenon was only observed mostly for anti-arabinan LM6 labelled sections in several samples (see full dataset).

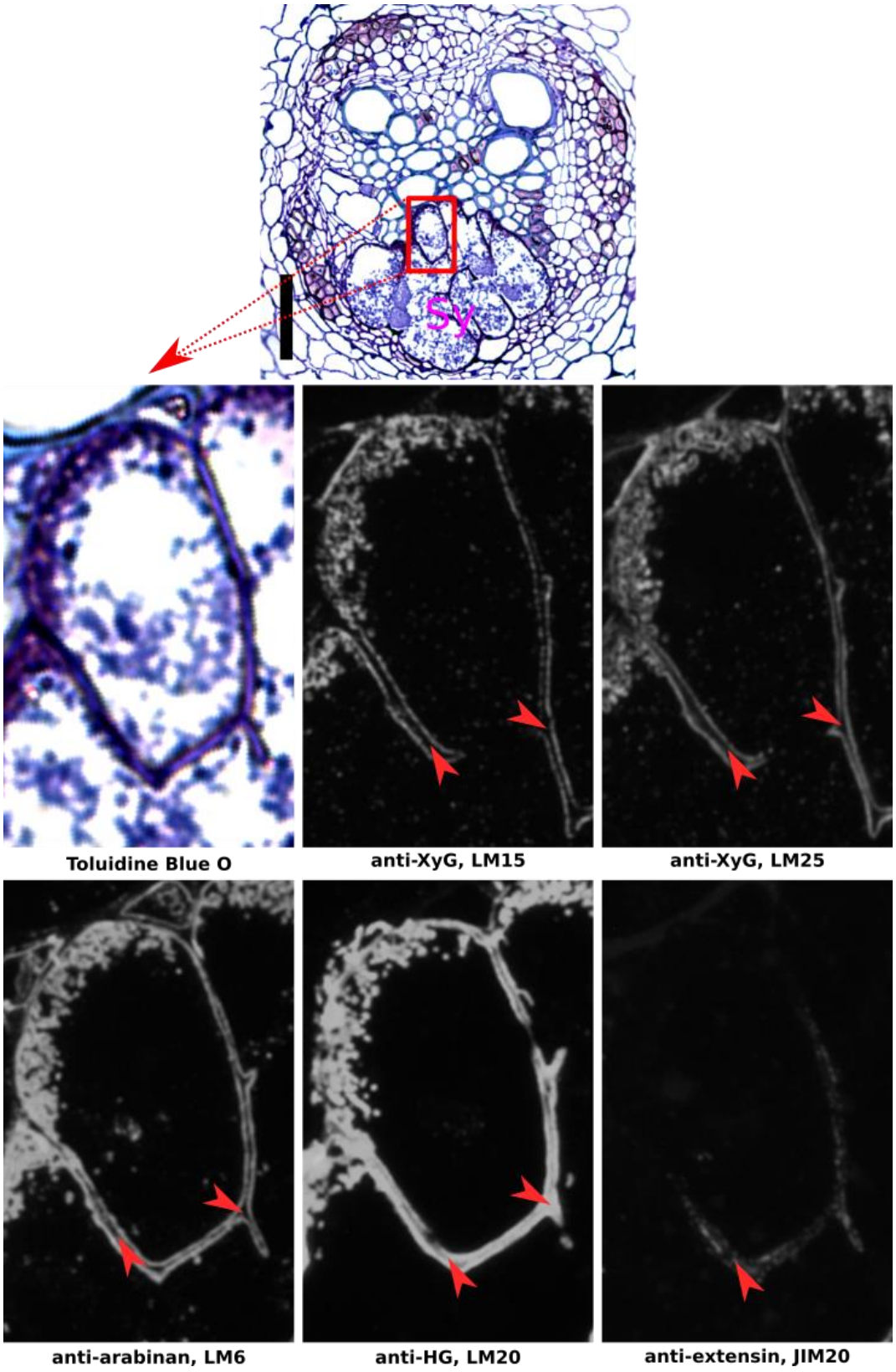

Figure 3.3.5.3 Antibody binding analysis of syncytial walls induced by *H. glycines* in soybean roots (14 dpi). Fluorescence images (dark field) are parts of the syncytial cell walls in sections labelled with specific mAbs, equivalent to the regions marked with red dash line in the bright field image (stained with Toluidine Blue O). Epitope distribution pattern in syncytial walls is indicated with red arrows. Antibodies used include anti-XyG LM15 and LM25, anti-arabinan LM6, anti-methyl-HG LM20 and anti-extensin JIM20. (Sy, syncytium; bar=50 µm)

3.4 Discussion

The chemical structures of syncytial cell walls induced by cyst nematodes in potato, soybean and wheat roots have been revealed using a set of plant cell wall probes, targeting a wide range of plant cell wall components.

Wall layer differentiation of cyst nematode induced syncytia

The syncytium is formed via host root cell wall dissolutions and differentiated cells such as xylem and phloem cells won't be incorporated.

Outside the growing cells are primary cell walls, thin flexible layers (0.1-1 μm) generating turgor pressure (Cosgrove 2005); whilst secondary cell walls are more restricted to specific differentiated cells and more resistant to compressive forces (Lee, Marcus *et al.* 2011). During a normal cell division, a cell plate is formed between new cells, followed by the arriving cellulose synthase and hemicellulose delivery, and eventually a new wall is generated for each cell with a pectin-rich area between them, named middle lamella (Daher and Braybrook 2015). In comparison, the primary cell walls are typically composed by cellulose microfibrils, forming a network with hemicelluloses, and this network is then further embedded in a pectic polysaccharide matrix (as illustrated in Figure 1.4 III) (Scheller and Ulvskov 2010, Fangel, Ulvskov *et al.* 2012). Using high definition imaging of cyst nematode induced syncytia, it is clear that the syncytial middle lamella layer between the syncytial primary wall and neighbouring cell wall is largely 'extended' into the wall fragments inside the syncytial region (as illustrated in Figure 3.3.5.1). Meanwhile, the immunolabelling results also demonstrate clear differentiations in terms of antibody binding patterns among these layers. For instance, the anti-XyG LM25 have a significant drop of binding in this layer in soybean syncytia (Figure 3.3.5.3). Similar binding patterns have also been observed for other mAbs in soybean syncytia and the potato syncytia (Figure 3.3.5.2), even in wheat syncytia as well. This clearly indicates the necessity of the awareness of such wall differentiation at both structural and chemical levels.

However, this phenomena is not always uniformly observed due to certain experimental difficulties, such as the small syncytium size at early nematode developmental stages, the nematode species related structural differences, or even the different microtome implementations. In order to neglect any possible misinterpretations of those not-so-clear differentiated layers, the syncytial middle lamella layer has been taken as part of the whole syncytial walls throughout this study, only detailed where further data available. In fact, those depicted as 'thickened syncytial walls' in soybean syncytia are much more those syncytial middle lamella layers rather than the much thinner syncytial primary walls, as shown in Figure 3.3.5.3. Based on those successfully performed analysis, this layer of a syncytium could still be considered as a pectin-rich middle lamella layer separating the primary walls, from both the un-incorporated neighbouring cells and the syncytium itself.

As the pectin-rich middle lamella is generally considered as a physical mediator of cell adhesion and separation among normal cells (Daher and Braybrook 2015), the syncytial middle lamella layer might also account for such a role during syncytium function, at least representing a different role from other syncytial primary walls or wall ingrowth as hinted

by the large chemical compositional distinctions.

Cell wall microstructures of cyst nematode induced syncytia

In comparison with the relatively 'simple' chemical compositions of the syncytial middle lamella, the syncytial 'primary wall' together with wall ingrowth possess more chemical complexity as revealed by the plant cell wall probes.

XyG is the major non-cellulosic polymer in both *G. pallida* and *H. glycines* induced syncytial cell walls, while highly substituted heteroxylans are abundant in wheat syncytia

XyG has been found in almost every land plant species analysed and is the most abundant hemicellulose in primary walls of spermatophytes except for grasses (Scheller and Ulvskov 2010, Pauly, Gille *et al.* 2013). Syncytial cell wall analysis show that XyG is present in all of the syncytia tested, though it is relatively abundant in those within potato and soybean roots in comparison to the ones in wheat roots.

The function of XyG is described by the classic load-bearing XyG/cellulose framework model: increasing XyG tethers between the cellulose microfibrils causes the increased rigidity, while the degradation of these tethers causes the walls to loosen (Hayashi and Kaida 2011, Pauly, Gille *et al.* 2013). The dynamic changes of XyG cross-linking, catalyzed by certain enzymes, such as xyloglucan endo-transglycosylase/hydrolase (XTH), could mediate the cell wall construction and restructure to cope with the functional requirements of cells. In cyst nematode induced syncytial cell walls, XyG might also perform such a role through this mechanism. For instance, the expression of Arabidopsis *XTH9* and an endo-xyloglucan transferase *XTR6* were revealed to be both upregulated in *H. schachtii* induced syncytia comparing with host root cells, whilst *XTR9* was marked as downregulated (Szakasits, Heinen *et al.* 2009), reflecting the reconstructions of host cell walls during syncytium formation and functioning. However, although soybean syncytial walls also possess XyG, an Arabidopsis *XTR6* homolog was found to be slightly downregulated in *H. glycines* induced soybean syncytium (Ithal, Recknor *et al.* 2007). Especially when the actual role of XyG in this "tethered network" model was recently questioned (Peaucelle, Braybrook *et al.* 2012, Pauly, Gille *et al.* 2013) due to the creation of XyG-absent Arabidopsis mutants (Cavalier, Lerouxel *et al.* 2008), the syncytial wall XyG might still play a role in syncytium formation and integrity, while at what extent or in which manner remain to be ambiguous.

The diverse group of xylans comprises the dominant noncellulosic polysaccharide in the secondary cell walls of dicots. They are commonly substituted with glucuronosyl residues, known as glucuronoxylans. Previous research has shown that syncytia formed in Arabidopsis roots possess no secondary cell walls and correspondingly contain no xylans (Davies, Lilley *et al.* 2012, Wieczorek, Elashry *et al.* 2014). Similarly, no xylan epitopes were detected within syncytial cell walls in potato and soybean roots, indicated by the absence of mAbs LM10 and LM11 binding. Conversely, in commelinid monocots (such as Poales, including wheat, rice, maize), xylans are the dominating noncellulosic polysaccharides in primary walls and usually contain many arabinose residues attached to the backbone,

forming arabinoxylans (AXs) and glucuronoarabinoxylans (GAXs) (Buanafina 2009, Scheller and Ulvskov 2010). The AXs serve an important role by cross linking cellulose microfibrils as well as oxidatively linked with each other. The walls of growing cells predominantly contain highly substituted AXs rather than the less branched xylans (Buanafina 2009). Syncytial cell walls in wheat contain no unsubstituted xylans, as revealed by a lack of binding with mAb LM10, but a small amount of low-substituted heteroxylan as targeted by LM11. The mAb LM12, derived to recognize feruloyl residues attached to a range of sugars (Pedersen, Fangel *et al.* 2012), show strong binding within the wheat syncytial cell walls, most likely to feruloylated xylans. Meanwhile, the LM28, targeting glucuronosyl-containing epitopes widely present in heteroxylans, also show strong binding in the same pattern as LM12. These anti-xylan mAbs all together revealed the abundance of highly substituted xylans in syncytial cell walls throughout the nematode developmental stages, indicating the importance of the xylan substitution in syncytium formation and functioning. Known to be very important for the cell wall structure, ferulate esters can be oxidatively cross-linked in a variety of ways and this could cause cell wall stiffening, growth deceleration and also is correlated with cell wall degradability (Buanafina 2009). Transgenic plants, expressing a fungal feruloyl esterase *AnFAE* and resulting in a deduction of ferulica acids, were found to have compromised cell wall integrity and more susceptible to fungal pathogens (Reem, Pogorelko *et al.* 2016). A similar study has also shown the link between the expression of fungal ferulic acid esterase and the cell wall digestibility (Badhan, Jin *et al.* 2014). Meanwhile, the common substitution of glucuronic acid could be further decorated, and the substituted and unsubstituted xylans enable the interactions with different cell wall polymers, such as cellulose and other plant cell wall glycans (Cornuault, Buffetto *et al.* 2015, Mortimer, Faria-Blanc *et al.* 2015). Therefore, the abundance of xylan substitutions within wheat syncytial cell walls may indicate similar functions in maintaining syncytial wall integrity as well as providing sufficient mechanical strength by forming cross-linked networks. Although, in a recent study over *H. avenae* induced syncytia in barley, a host also with type II primary walls (Aditya, Lewis *et al.* 2015), it draw the conclusion that the syncytial walls did not contain heteroxylan as indicated by the weak binding of anti-xylan LM11, which could worth further evaluation using wider range of anti-xylan probes.

β-(1-3,1-4)-glucan (known as mixed linkage glucan, MLG) is abundant in Poales cell walls whilst generally absent from the rest of the flowering plants. The proportion of MLG changes at different plant growth stage (Gibeaut, Pauly *et al.* 2005), while its function in cell wall cross-linking and cell growth remains largely unknown. MLG was present in the cell walls of syncytia formed by both *H. avenae* and *H. filipjevi* in wheat roots. However its abundance varies in relation to nematode species as well as different syncytia developing stages.

Pectic HGs are highly methyl-esterified in both potato and soybean syncytial cell walls

Pectic polysaccharides, of which HG is the major group, are abundant in plant cell walls, comprising as much as 30% of dicot, gymnosperm, and non-Poales monocot cell walls, but considerably less in cell walls of grasses (Caffall and Mohnen 2009). HG was abundant and predominantly methyl-esterified in the syncytial cell walls of *G. pallida* and *H. glycines*.

Most intriguingly, methyl-HG was detectable within the syncytial cell walls formed in wheat roots, despite that host generally lacking abundant pectin in primary cell walls. The methylesterification status of HG in syncytial cell walls formed in potato, soybean and wheat is similar to that previously described for mature syncytia in Arabidopsis (Davies, Lilley *et al.* 2012, Wieczorek, Elashry *et al.* 2014) and later in barely (Aditya, Lewis *et al.* 2015), although HG was reported to be largely unmethylated at the earlier stages of Arabidopsis syncytium formation (Wieczorek, Elashry *et al.* 2014).

Pectic HGs are highly methyl-esterified when secreted into the walls and can subsequently be de-methyl-esterified to facilitate the conformation of the HG-calcium complexes, form the so called 'egg-box' model (Micheli 2001, Pelloux, Rustérucci *et al.* 2007, Caffall and Mohnen 2009, Wolf, Mouille *et al.* 2009). According to the correlation between cell wall stiffness and the methyl-esterification level of HG, the presence of the HG-calcium is postulated to induce the pectic gel formation and thus cause the cell wall stiffening. However, the abundant methyl-HG in syncytia should still be able to keep syncytial walls possessing enough mechanical strength for withstanding the content, especially for the much higher turgor pressure within in the feeding sites (Böckenhoff and Grundler 1994). Moreover, the methylesterification status was also known to affect the degrading ability of pectin and the rheological properties of the cell wall, including its porosity and extensibility, meanwhile could be modulated accordingly by the spatially distributed modifying enzymes such as PMEs and PMEIs (Bosch and Hepler 2005). In this case, the large amount of methyl-HG might attribute to the formation and maintaining of a functional syncytium. Further investigations should be made to elucidate the methyl-HG forming mechanism in syncytial walls as well as its impact for nematode parasitism, especially considering the innate complexity of the role of pectin cross-links (Peaucelle, Braybrook *et al.* 2011, Peaucelle, Braybrook *et al.* 2012).

Pectic arabinans are abundant in all cyst nematodes induced syncytial cell walls analysed

Large amount of arabinosyl residues were localised in syncytial cell walls in all three tested plants by mAb LM6, which bound strongly to pectic arabinans and/or arabinogalactan proteins (AGPs), in this case more likely to be pectic arabinans (Pedersen, Fangel *et al.* 2012). As revealed in previous studies, the large amount of arabinan chains could provide flexibility to *Commelina* guard cell walls coping with water stress (Jones, Milne *et al.* 2003), later similar phenomena was also revealed in the leaf cell walls of *Myrothamnus flabellifolia* (Moore, Nguema-Ona *et al.* 2006). A hypothetical model was then proposed based on those findings, suggesting that it is the arabinan side chains that are responsible for coping with the dehydration by preventing the formation of tight junctions such as HG-calcium complex and/or interactions with other wall polysaccharides (Moore, Farrant *et al.* 2008). Although large differences of other syncytial wall polysaccharides have been found, plus the abundant methyl-HG in potato and soybean syncytia would not eventually form the wall-rigidity junctions as in this hypothetical model, the rich arabinan side chains could still play the role of maintaining cell wall flexibility in certain way for both types of hosts. Especially, considering the large amount of nutrients withdrawal by the nematode (Muller, Rehbock *et al.* 1981) and the high turgor pressure within syncytium (Böckenhoff and Grundler 1994), such wall flexibility seems to be more essential to general syncytium

function.

In comparison with the abundant arabinans detected, pectic galactan (indicated by LM5) was found to be absent in soybean root syncytia, the same as in Arabidopsis (Davies, Lilley *et al.* 2012), while very weak yet detectable in potato and wheat root syncytia. It was also believed to be related to mechanical rigidity of cell walls (McCartney, Ormerod *et al.* 2000). In potato and soybean syncytia, together with previous results in Arabidopsis, the differences might be correlated to the host cell types as there are naturally more abundant pectin-galactan in potato. Meanwhile, in wheat root syncytia, the different presence of galactan might be related to different nematode species, as there appears to be relatively clear binding in *H. avenae* induced syncytia at certain time points comparing with the almost complete absence in *H. filipjevi* induced syncytia of all tested stages.

Other major antibody binding include the anti-extensin JIM20, binding to cell walls inside the soybean syncytium region and the anti-AGPs JIM13 binding to both potato and soybean syncytial walls. As an important type of HRGPs, extensin is related to plant growth and development and its distribution pattern within the soybean syncytium may reflect the distinguishing developmental status of different parts of syncytial walls. While AGPs are a highly diverse class of cell surface proteoglycans, the precise function of the JIM13 indicated AGPs presence is much more uncertain.

Models of syncytial walls and the syncytia

As analysed above, the complexity of the cell wall microstructures of cyst nematode induced syncytia was elucidated using mAbs, targeting a wide range of cell wall polymers. The results, together with previous studies, show distinctive cell wall architectures of syncytia: 1) cell walls of syncytia induced by *G. pallida* and *H. glycines* in eudicot hosts potato and soybean respectively, as well as *H. schachtii* infested Arabidopsis (full results are listed in chapter 4), contain abundant XyG, pectic methyl-HG and arabinans. Pectic galactan was found at low level in potato syncytial regions whilst absent in soybean syncytia. 2) Syncytia cell walls in wheat roots, induced by *H. avenae* and *H. filipjevi*, are composed with abundant highly substituted heteroxylans and arabinans, whilst possess low levels of XyG, methyl-HG, galactan and MLG with certain level of variability.

Comparing with other host vascular cells, the chemical compositions of syncytial cell walls, represented by the mAb binding, are distinguishable. Further analysis, using the high definition fluorescence images, shows that these cell wall polymers have unevenly-distributed patterns in syncytial walls, reflecting the structural complexity from a chemical perspective. Meanwhile, taking the host cell wall types into consideration, the syncytial wall microstructures illustrate clear impact from host cell walls. After all, they originate from host root cells.

As a nutrient sink and the sole supply for cyst nematodes parasitism, the syncytia use a composition of complex polysaccharides to maintain functioning and also in general have stable wall chemical structures during parasitism. In the roughly depicted ‘two types’ of syncytial walls, the abundant wall arabinans may add flexibility to the walls of syncytia whilst the XyG in soybean and potato syncytia and heteroxylans in wheat syncytia help

creating/maintaining certain level of mechanical strength by crosslinking, substitution, and forming various links even with these low-abundance wall glycans discovered. Together with the pectin rich ‘between-wall’ middle lamella, thick or thin; and the largely thickened walls of those surrounding cells, especially those around wheat syncytia; this complex is capable of providing both sufficient mechanical support, withstanding the high turgor pressure inside the syncytium, and adequate flexibility, in coping with the nematode feeding as well as environmental fluctuation.

Chapter 4 Investigation of cell wall chemical structures of syncytia induced by *H. schachtii* in *Arabidopsis thaliana*

4.1 Introduction

The cell wall chemical structures of syncytia induced by some of the most economically important cyst nematode species in their host roots have been revealed using a range of monoclonal antibodies targeting general cell wall polymers. As indicated by antibody binding, the syncytial cell walls in eudicot hosts, potato and soybean in this study, contain abundant XyG, highly methyl-esterified HG and pectic arabinans, meanwhile low/absent in pectic galactan and lack of xylans, similar to previous results in *H. schachtii* induced mature syncytia in Arabidopsis (Davies, Lilley *et al.* 2012). Based on these findings, as well as the syncytial walls formed in wheat, a type of grass with distinct primary cell walls, a general model of cell wall microstructures of syncytia induced in both types of hosts has been proposed. Possible functions of those polysaccharides have also been postulated based on related research.

As a model plant with well-defined root anatomy (Dolan, Janmaat *et al.* 1993), Arabidopsis infested with *H. schachtii* has long been used as a model system for plant parasitic nematodes related studies, resulting in valuable information in almost every aspect of nematode parasitism research (Sijmons, Grundler *et al.* 1991). The study of syncytial cell walls induced by cyst nematode has also been initially revealed using this system (Davies, Lilley *et al.* 2012). Later, a related study carried out over both early forming stage and later mature stage of syncytia has mentioned that there are some changes in terms of syncytial wall chemical structures during nematode development (Wieczorek, Elashry *et al.* 2014). Therefore, it is worth evaluating the structural variations of syncytial walls in this model system before further investigating the functions of syncytial wall polymers using related cell wall mutants.

In cyst nematode induced syncytial walls, hemicellulose XyGs and pectic arabinans are widely distributed in both types of hosts. As the most abundant hemicellulose in eudicot primary cell walls, XyG was also rich in both potato and soybean syncytial walls. It was depicted as playing important roles in the “tethered network model”: XyGs coat cellulose surfaces to prevent direct cellulose-cellulose contacts and function as tethers to cross-link adjacent cellulose microfibrils, forming a load-bearing network further embedded in an independent pectin gel matrix (Albersheim, Darvill *et al.* 2010). This model has been dominant for over two decades until recent discovers have shaken its validity, with proposing a new ‘hotspot hypothesis’: cellulose microfibrils are linked with one another via direct load-bearing junctions, mediated by intimate bonding by XyGs in some scenarios (biomechanical hotspot) (Cavalier, Lerouxel *et al.* 2008, Dick-Pérez, Zhang *et al.* 2011,

Dick‐Perez, Wang *et al.* 2012, Park and Cosgrove 2012, Wang, Zabotina *et al.* 2012, Cosgrove 2014, Zhang, Mahgsoudy-Louyeh *et al.* 2014, Park and Cosgrove 2015, Wang, Park *et al.* 2015). One most shocking discovery of those is the Arabidopsis double mutant (*xxt1*/*xxt2*), XXT1 and XXT2 are xylosyl transferases that add xylose side chains to the glucan backbone of XyG, was revealed to be lack of detectable XyGs whilst possessing only minor phenotype changes (Cavalier, Lerouxel *et al.* 2008). In consideration of the abundance of XyG in syncytial walls, this mutant has also been used in this study to evaluate whether XyG could affect cyst nematodes infestation in the first place or the properties of syncytial cell walls in any successful infections.

Another widely found cell wall polymer in syncytial walls is pectic arabinan, sidechains of pectins. Pectins are the most complex polysaccharides found in nature, playing a key role in cell wall porosity and thickness (Yapo 2011). They are the primary targets of attack by invading microbes and the breakdown products are potent plant-defense response elicitors (Cosgrove 2005). The structural classes of pectins include HG, RG-II and RG-I, and arabinan is an important sidechain branching RG-I (Figure 1.5). It was found to be rich in syncytial cell walls formed in both eudicots and commelinoid monocots hosts. The role of pectic arabinan was possibly related to cell wall flexibility as shown in stomatal guard cells (Jones, Milne *et al.* 2003) and *Myrothamnus flabellifolia* (Moore, Farrant *et al.* 2008), and cell wall integrity during pollen development (Cankar, Kortstee *et al.* 2014). The use of two arabinan deficiency mutants, *arad1* (Harholt, Jensen *et al.* 2006) and *arad2* (also include double mutant *arad1/arad2*) (Harholt, Jensen *et al.* 2012), helped to demonstrate the biosynthesis of pectic arabinan and its relation to mechanical properties of Arabidopsis inflorescence stems (Verhertbruggen, Marcus *et al.* 2013). With the use of *H. schachtii* infesting those mutants, we can further evaluate the impact of pectic arabinan in syncytial cell walls.

Another important pectin structural class discovered in syncytial walls is pectic HG, mostly highly methyl esterified. It was also proven to be present in syncytial walls formed in wheat, a host naturally low in pectins. The methyl esterification status can influence the property of pectic gels, thus affecting the cell wall functions throughout plant development. The HG is assumed to be secreted in a fully methyl-esterified form and later de-esterification is modulated by cell wall-located PMEs. Meanwhile, PMEIs can specifically inhibit PMEs and they are both large multigene families in Arabidopsis, indicating the various roles can be played. Another group, known as pectin methyltransferases (PMTs), can transfer the methyl groups from methyl donors to pectin, may also take part in defining the degree of methylesterification of pectin though still lack of experimental evidence (Wolf, Mouille *et al.* 2009, Kim, Held *et al.* 2015). Therefore, the laying obstacles for further investigation of syncytial wall pectic HG are the large amount of candidate mutants representing those large gene families with little or no previous functional validation, meanwhile the lack of a quantification method to assess the syncytial wall methyl esterification status will also restrict the study. Based on the hypothetical functional roles these gene families may play, a range of Arabidopsis mutants, representing the genes with a reasonable expression level in syncytial regions from a previous microarray study (Szakasits, Heinen *et al.* 2009), have been chosen and a quantification procedure has also been applied.

In this study, the structural variations has been assessed over syncytia formed at different developmental stages with the use of a set of plant cell wall mAbs. Next, considering the major wall polymers in cyst nematode induced syncytial walls and the availability of cell wall related Arabidopsis mutants, hemicellulose XyG and pectic arabinan deficiency mutants were selected and later pectic HG related mutants were chosen, screened and used based on previous microarray data in hoping to provide further look at the syncytial wall microstructures.

4.2 Materials and methods

Arabidopsis seeds were surface sterilised under the following procedure: 75% EtOH for 60s; ddH_2O washing thoroughly; 10% (v/v) household bleach for 30 mins in a rotator and finally washed 5 times in ddH_2O. Seeds were then kept in a 1.5 mL tube with ddH_2O at 4 °C overnight. Sterilised Arabidopsis seeds were sowed (using sterile toothpicks or pipette tips) on square plates (Corning) supplied with ½ MS medium (1% plant agar, 1% sucrose, pH 5.8). Culture was carried out at 20 °C in tissue culture room. After about 10 days, the seedlings with robust root systems were ready to be inoculated.

Freshly hatched *H. schachtii* J2s were collected and sterilised by soaking in 0.1% chlorhexidine gluconate, 0.5 mg/ml CTAB and 0.01% Tween-20 solutions (filtered by sterile filter, pore size 0.22 µm, Merck Millipore). Nematodes were then resuspended in sterile tap water at a concentration of 1 J2 per µL. On average 10 J2s were pipetted on one selected root tip and each plant was infected with around 100 J2s. Root sections with successful developing females were cut off and following procedures were described as before (2.3).

For nematode infection assay, a minimum of 50 individual 10-day old seedlings were used. Each plant was inoculated with 200 J2s, sterilised as above. Infection was then checked and counted at 14 dpi. Statistical tests (ANOVA) were performed to determine the statistical significance ($P<0.05$) (GraphPad Prism 7.0).

For poly(ethylene glycol) (PEG) test used plant culture plates in this study, 1%, 2%, 3% and 5% (w/v) PEG 6000 was added to the medium before sterilisation (over 10% PEG could cause medium unable to solidify). Seeds were first sowed on general ½ MS plates to germinate for 7 days. Seedlings were then carefully transferred to PEG supplied plates and cultured for another 7 days. Plants with robust root systems were chosen and inoculated with nematodes as described above.

Before Arabidopsis mutants were used, homozygosity was checked using a homozygous test (primers listed in relative sections).

For fluorescence images used for quantification, sections were labelled simultaneously and images were taken under the same parameters (16bit, monocolour). Quantification was carried out on raw images using ImageJ.

4.3 Results

The *in situ* analysis was carried out over *H. schachtii* infested Arabidopsis roots, both wildtype of different developmental stages and a range of selected cell wall mutants. The

most representative figures are shown and the full results are summarized in relative tables. In order to gain optimal display quality, the listed fluorescence images are not taken under exact same parameters, and they are not used for fluorescence quantification and downstream comparisons.

4.3.1 Syncytial walls induced in Arabidopsis roots at different developmental stages

In order to evaluate the consistency and fluctuations of plant cell wall polymers in *H. schachtii* induced syncytia, a set of antibodies were used over samples collected at three time points, 7 dpi, 14 dpi and 21 dpi. Same immunolabelling methods were applied and the results listed below cover the major findings

Hemicellulosic xylan and XyG in syncytial walls

As known in previous results, the anti-xylan LM11 binds mainly to the xylem within the root vascular cylinder. Although with formed syncytia of different size and shape as shown in Figure 4.3.1.1, the anti-xylan LM11 still mainly bound to the xylem elements in all three tested samples, therefore being used to tell root basic structures after nematode invasions. Meanwhile, another hemicellulose, XyG was present in the walls of almost all the cell types within the vascular bundle, as indicated by the binding of LM25. The following figures in this section are from equivalent sections, thus direct structural comparisons can be made accordingly.

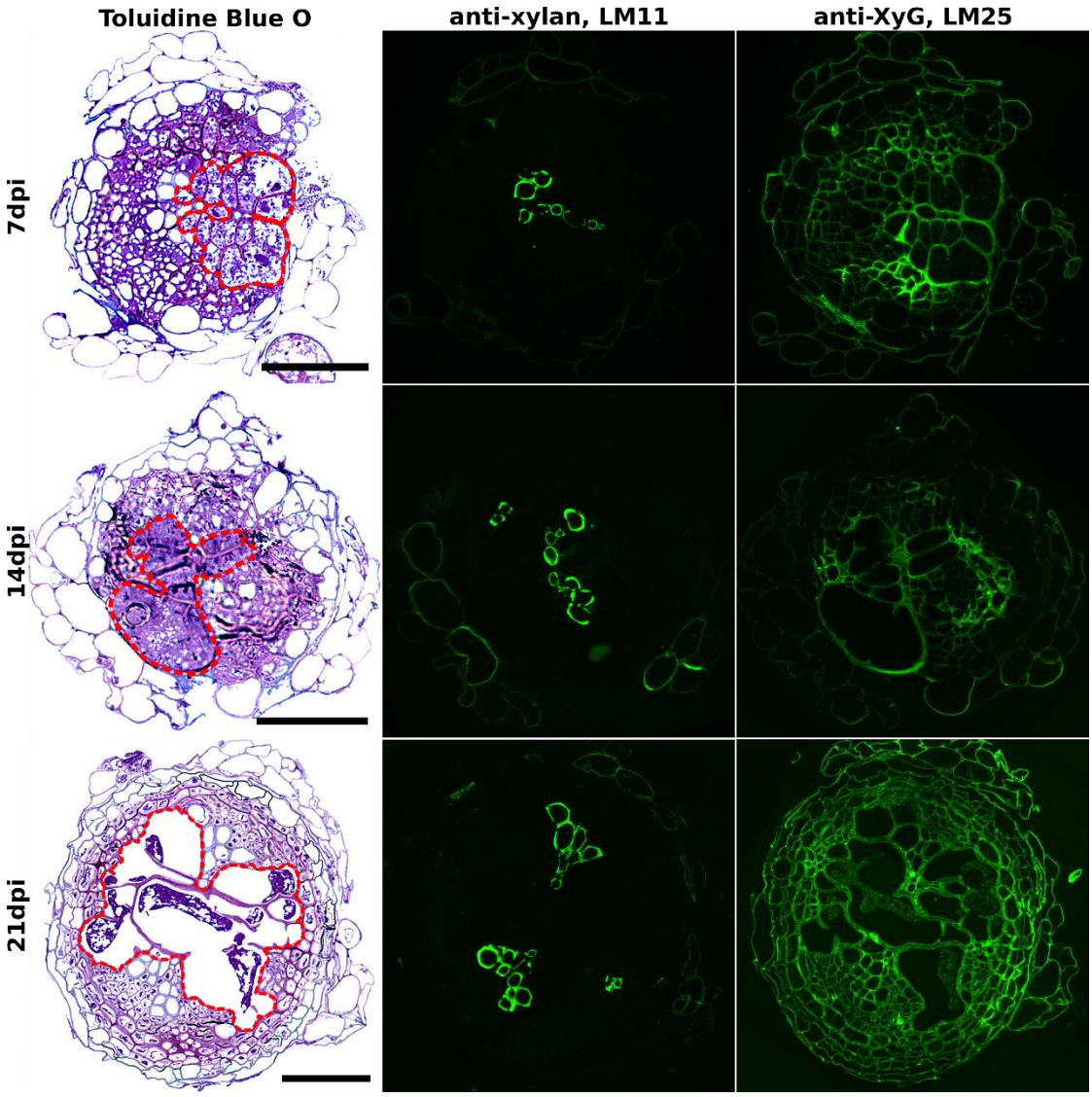

Figure 4.3.1.1 Immunolocalization of hemicelluloses in the walls of *H. schachtii* infested Arabidopsis roots (wild type, Columbia). Bright field images are captured from sections stained with Toluidine Blue O. Syncytial regions are outlined with red dash line. Indirect immunofluorescence (green) images are from the specific binding of anti-xylan LM11 and anti-XyG LM25 using equivalent sections. (bar=50 µm)

Pectic HG in syncytial walls

Two anti-HG antibodies were used to reveal the existence and methyl-esterification status of HGs in syncytial walls. As shown in Figure 4.3.1.2, the LM19 targeting mainly non/low methyl-HG was shown to bind clearly to the vascular cylinder cells including the syncytial regions at 7 dpi, whilst show almost absence in 14 dpi and low abundance in 21 dpi syncytial walls. This partially agrees with previous findings that the HG in initial stage of syncytial walls are predominantly non-methyl esterified (Wieczorek, Elashry *et al.* 2014). In comparison, the LM20 indicated methyl-HG was found to be largely abundant in the syncytial walls throughout the tested samples. This together proves that the methyl esterification status of pectic HGs in syncytial walls change along with the nematode development.

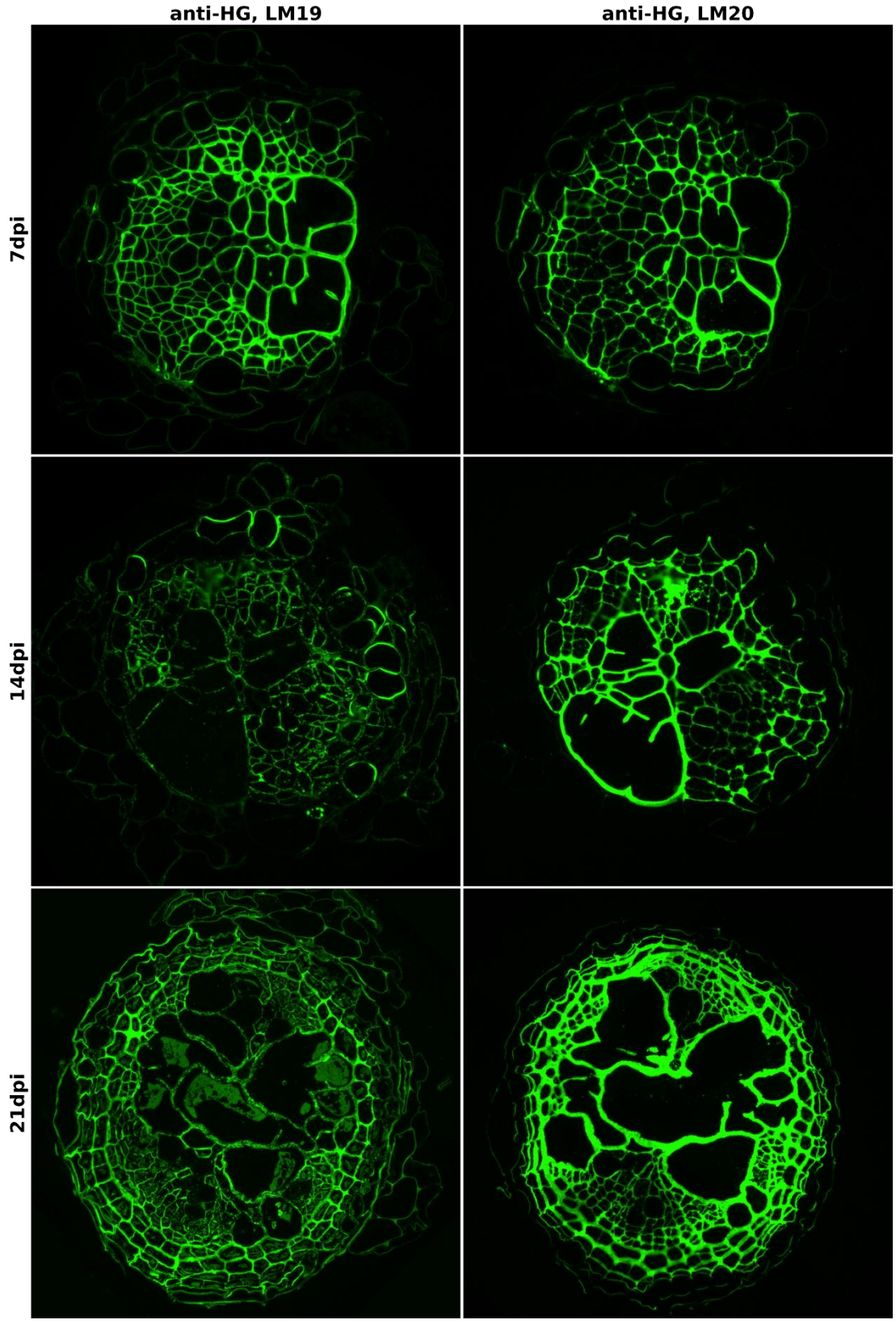

Figure 4.3.1.2 Immunolocalization of pectic HG in the walls of *H. schachtii* infested Arabidopsis roots (wild type, Columbia). Indirect immunofluorescence (green) images are from the specific binding of anti-HG LM19 and LM20, targeting non/low-methyl-HG and methyl-HG respectively, using equivalent sections.

RG-I related galactans and arabinans in syncytial walls

Another important structural class of pectin is analysed using RG-I related probes, LM5 to galactan, LM6 and LM16 to arabinan. Similar to previous results, the galactan epitopes were mainly found in cell walls within the vascular cylinder apart from the xylem and nematode induced syncytial walls in all three samples (Figure 4.3.1.3). Three anti-arabinan mAbs, direct to different aspects of arabinans, were used and the LM16 binding pattern is shown in Figure 4.3.1.3. The LM16, targeting processed arabinans, has weak yet still clear binding within the syncytial walls at 7 dpi, with stronger binding in the rest of the cells apart from xylem. However, the binding is blur in 14 dpi syncytial walls and almost entirely absent in the 21 dpi syncytia. Meanwhile, the LM13 recognising long linearized arabinans is shown to be largely absent and another anti-arabinan LM6 epitopes are proven to be present/abundant in the syncytial walls (as summarised in Table 4.1).

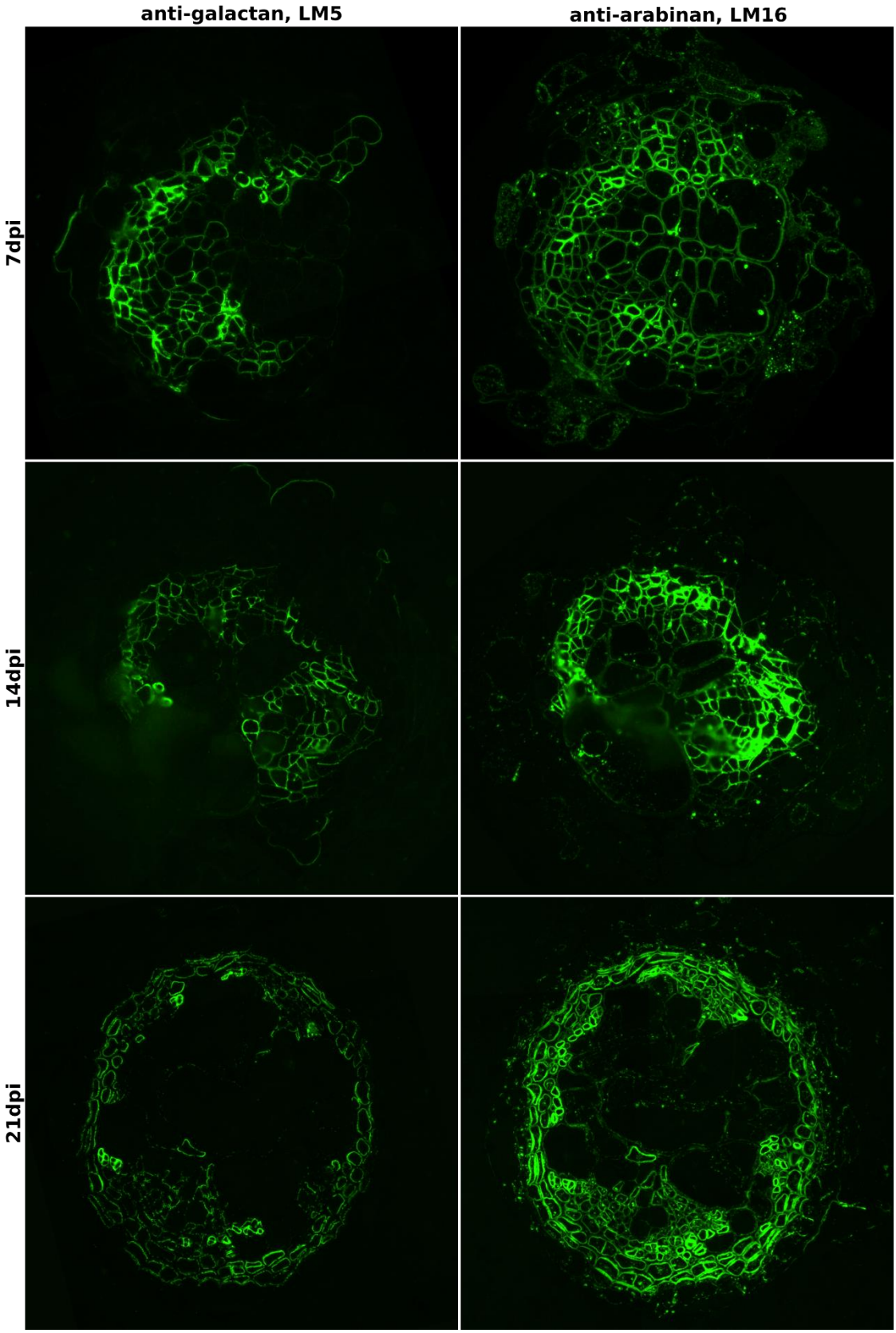

Figure 4.3.1.3 Immunolocalization of RG-I related polymers in the walls of *H. schachtii* infested Arabidopsis roots (wild type, Columbia). Indirect immunofluorescence (green) images are from the specific binding of anti-RG-I LM5 and LM16, targeting galactans and arabinans respectively, using equivalent sections.

Distribution analysis of cell wall polymers in syncytial cell walls

Previous study has shown that the distribution of antibody epitopes are not even over the whole syncytial walls. Similar phenomenon has also been found in *H. schachtii* induced syncytial walls in Arabidopsis. For instance, in Figure 4.3.1.4, the binding of LM25 and LM16 in syncytial walls has clear differentiation comparing with the binding of LM20, even for the wall fragments branched inside the syncytium. This was also clear in the other two tested samples, indicating that the syncytial walls include a pectin rich middle lamella layer.

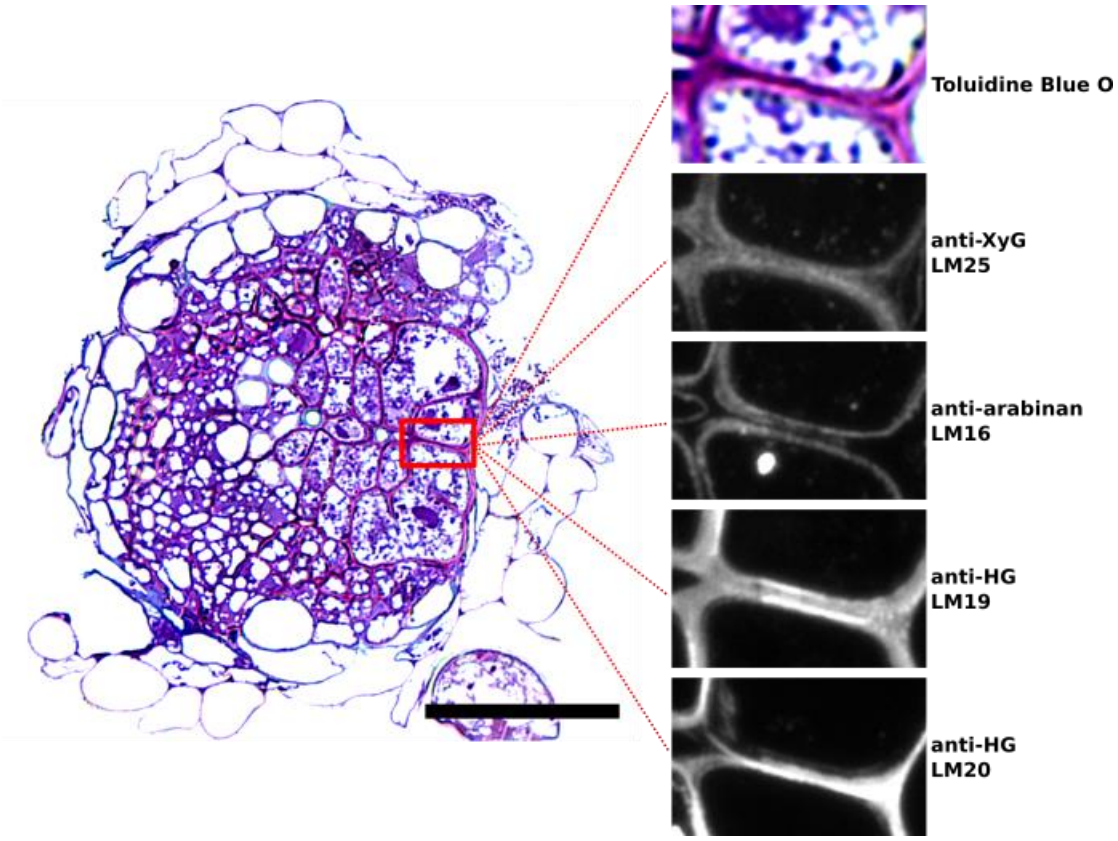

Figure 4.3.1.4 Antibody binding analysis of syncytial walls induced by *H. schachtii* in Arabidopsis (wildtype Columbia, 7 dpi). Fluorescence images (dark field) are parts of the syncytial cell walls from sections labelled with specific mAbs, equivalent to the regions marked with red line in the bright field image ,stained with Toluidine Blue O. (bar=50 µm)

The consistency of syncytial wall chemical structures in Arabidopsis

The microstructure of syncytia induced by female *H. schachtii* in Arabidopsis at three different developmental stages has been revealed (partial results shown above) and summarised in Table 4.1.

The immunolabelling results clearly demonstrated that the syncytial cell walls contain non-cellulosic XyG, lack of xylan, abundant pectic methyl-HG and arabinans and small amount of extensin. Throughout the three stages analysed, 7 dpi, 14 dpi and 21 dpi, the binding patterns of antibodies stay stable and this is similar to the results in potato and wheat syncytia. The most obvious change in terms of antibody binding is the anti-HG antibody LM19. It was shown to be binding strongly to syncytial walls at 7 dpi whilst decreased significantly in the other two parasitism stages assessed. In comparison, the binding of LM20 was constantly clear and abundant in all syncytial walls. Another change is the weak binding of LM16 targeting processed arabinans at 7 dpi also decreased to almost absent at 21 dpi. In general, the results agree with previous study (Davies, Lilley *et al.* 2012) and we can also find clues for the changes of HG methyl esterification, indicated by LM19 and LM20, in a previous research (Wieczorek, Elashry *et al.* 2014).

In order to clearly demonstrate such changes in the binding of anti-HG antibodies within syncytial regions and reveal the trend during nematode parasitism, a quantification method tailored for this purpose is needed. The most used quantification methods (Lee, Cornuault *et al.* 2013, Cornuault, Manfield *et al.* 2014), such as sandwich ELISA, generally involve chemical extraction of plant tissues and this is not suitable for getting representative results of the syncytial walls. Therefore, *in situ* immunolabelling together with appropriate quantification of fluorescence signals within only syncytial walls should make such comparison possible.

Table 4.1 Summary of immunolocalization of primary antibodies in syncytial walls induced by *H. schachtii* in Arabidopsis roots

Antibody epitopes		mAbs	*H. schachtii* induced syncytial walls in *Arabidopsis thaliana*			Reference
			21 dpi	14 dpi	7 dpi	
Xyloglucan	XXXG motif	LM15	-	N/A	N/A	(Marcus, Verhertbruggen *et al.* 2008)
	galactosylated	LM24	-	N/A	N/A	(Pedersen, Fangel *et al.* 2012)
	XXXG / galactosylated	LM25	++	++	+++	(Pedersen, Fangel *et al.* 2012)
Mannan	heteromannan	LM21	-	N/A	N/A	(Marcus, Blake *et al.* 2010)
Xylan	(1→4)-β-D-xylan	LM10	-	N/A	N/A	(McCartney, Marcus *et al.* 2005)
	(1→4)-β-D-xylan / arabinoxylan	LM11	-	-	-	(McCartney, Marcus *et al.* 2005)
	feruloylated xylan	LM12	-	N/A	N/A	(Pedersen, Fangel *et al.* 2012)
Xylogalacturonan		LM8	-	N/A	N/A	(Willats, McCartney *et al.* 2004)
Homogalacturonan	partially methyl-HG / non methyl-HG	LM19	++	+	+++	(Verhertbruggen, Marcus *et al.* 2009)
	partially methyl-HG	LM20	+++	+++	+++	(Verhertbruggen, Marcus *et al.* 2009)
	non-blockwise partially methyl-HG	LM7	-	N/A	N/A	(Clausen, Willats *et al.* 2003)
	partially methyl-HG / de-esterified HG	JIM5	-	N/A	N/A	(Clausen, Willats *et al.* 2003)
	partially methyl-HG	JIM7	+++	N/A	N/A	(Clausen, Willats *et al.* 2003)
RG-I related	linearised (1→5)-α-L-arabinan	LM13	-	+/-	+/-	(Verhertbruggen, Marcus *et al.* 2009)
	processed arabinan	LM16	+	++	++	(Verhertbruggen, Marcus *et al.* 2009)
	(1→4)-β-D-galactan	LM5	-	+	+	(Jones, Seymour *et al.* 1997)
	(1→5)-α-L-arabinan	LM6	+++	+	+	(Willats, Marcus *et al.* 1998)
Arabinogalactan-protein	AGP glycan	JIM13	-	N/A	N/A	(Yates, Valdor *et al.* 1996)
Extensin		JIM20	+	N/A	N/A	(Knox, Peart *et al.* 1995)

* -, no binding; +, slight binding; ++, clear binding; +++, significant binding; N/A, not tested

4.3.2 Syncytial walls induced in Arabidopsis cell wall mutants

With extensive investigations over the syncytial walls formed in different developmental stages in Arabidopsis, several cell wall related mutants were chosen to further study the role of these syncytial cell wall polymers. This include the XyG deficiency mutant with no detectable levels of XyG and three arabinan deficiency mutants. The focus of this section is to investigate whether the absence or lack of these cell wall polymers in the hosts could affect the formation of functional syncytia and the actual wall chemical structures of those syncytia if successfully induced.

4.3.2.1 Homozygosity test of Arabidopsis cell wall mutant

Homozygosity test was first carried out over the selected mutant lines. As summarised in Table 4.2, primers were designed for the targeted genes and the test results were shown by gel electrophoresis in Figure 4.3.2.1. The two genes *XXT1* and *XXT2* were tested separately using a two-primer test in the XyG double mutant (NASC ID N16349): gene specific primers failed to amplify the target genes in mutants as in wildtype meanwhile the T-DNA border sequences were successfully amplified. In arabinan deficiency mutants, tests were proceed in a three-primer fashion with mixed gene specific primers and T-DNA border primer. The mutants only successfully amplified amplicons containing T-DNA flanking sequences while the wildtype sample amplified part of the target genes with a different size. Tested mutants were then used in the following *in situ* analysis.

Table 4.2 Brief information of *Arabidopsis thaliana* cell wall mutants

Targeted cell wall component	Stock ID	Polymorphism	Locus	Description	Primers used for homozygosity tests
Xyloglucan	N16349	*XYLOSYLTRANSFERASE 1* (*XXT1*)	AT3G62720	Plants lack detectable xyloglucan	LP: TAAACGTGTGTCCCCTAAACG RP: AGAGAAATCTCGAGACCGGAC
		XYLOSYLTRANSFERASE 2 (*XXT2*)	AT4G02500		LP: TAAATTGTTTCCGCGGTACAC RP: AGTCACCAAAAGAACACGTGG
Pectic arabinan	SAIL_189_F10	*ARABINAN DEFICIENT 1* (*ARAD1*)	AT2G35100	Reduced level of arabinose content	LP: TATGTGTTCAGGGTGGAAAAGT RP: GGGAGACTTGACGCCAGATT
	SAIL_881_C10	*ARABINAN DEFICIENT 2* (*ARAD2*)	AT5G44930		LP: GTAGTTGTGTATACCCTAGACT RP: CGCCTCAGCCGGGTCAAAA
		ARAD1 X ARAD2			

* Left border primers (LB) for the T-DNA insertion:

For SALK lines: ATTTTGCCGATTTCGGAAC

For SAIL lines: TAGCATCTGAATTTCATAACCAATCTCGATACAC

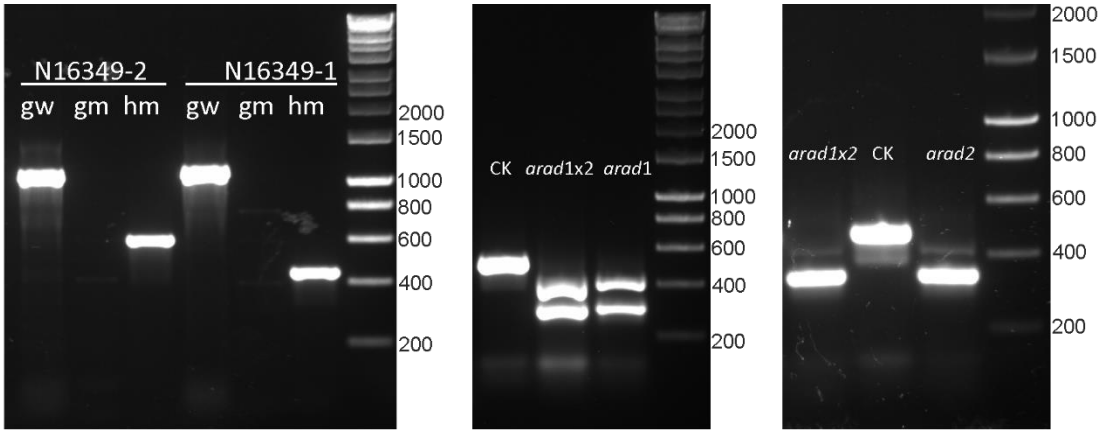

gw: gene specific primers (GSPs) in wildtype; gm: GSPs in mutants; hm: LB+RP in mutants; CK: wildtype

Figure 4.3.2.1 Homozygosity test results of Arabidopsis cell wall mutants. Two-primer test was carried out on XyG deficiency mutant (*xxt1/xxt2*, NASC ID N16349): two target genes were tested separately with GSPs amplified target genes in wildtype (>1kb bands) while T-DNA borders were successfully amplified in the mutants (bands of smaller size). Three-primer method was applied on arabinan deficiency mutants *arad1*, *arad2* and *arad1/2*. T-DNA border sequences were amplified in the mutants (smaller sized bands) while the wildtype only gave amplification with a different size of the target gene (bands with larger size).

4.3.2.2 The cell wall microstructures of syncytia induced by *H. schachtii* in Arabidopsis XyG deficiency mutant

As one of the most widely discovered cell wall polymers, XyG was proven to be abundant or present in all analysed cyst nematodes induced syncytial walls. Although, the XyG deficiency mutant was known to be lack of detectable levels of XyG, *H. schachtii* still managed to induce syncytia and developed as normal. Root samples were taken over the successful infections and *in situ* analysis was performed as before using a core list of mAbs.

Hemicelluloses in the cell walls of XyG deficiency mutant

The anti-xylan LM11, known to bind specifically to the xylem in other eudicot hosts, still only recognised the xylem vessels within the vascular cylinder in the *H. schachtii* infested XyG mutant, shown in Figure 4.3.2.2. The anti-XyG LM25 was shown to be completely absent from the whole root section. Other XyG related mAbs have also been tested, giving no binding across the whole root (data not shown). This clearly proves that XyG is not essential to the fundamental structure of syncytium induced in Arabidopsis, challenging its proposed role in crosslinking to provide cell wall mechanical support.

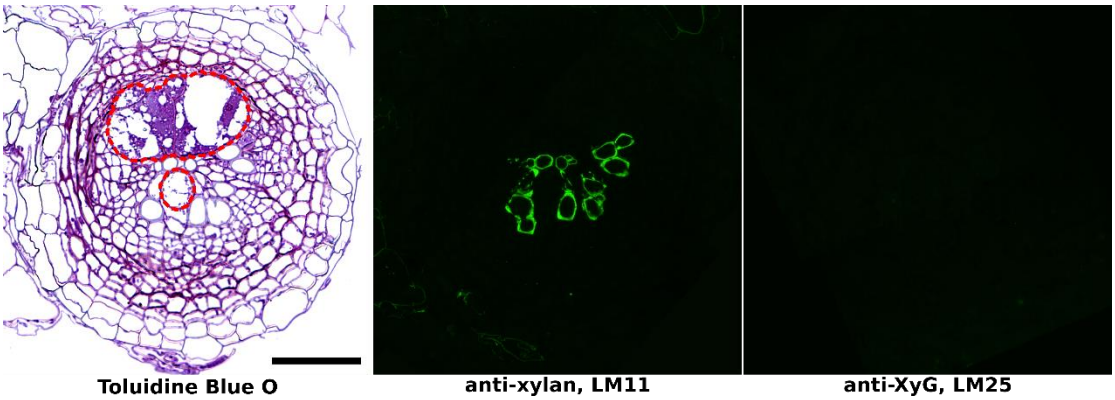

Figure 4.3.2.2 Immunolocalization of hemicelluloses in the walls of *H. schachtii* infested Arabidopsis XyG deficiency mutant (21 dpi). Bright field image is captured over Toluidine Blue O stained section. Syncytial region is outlined with red dash line. Immunofluorescence (green) images are from the specific binding of anti-xylan LM11 and anti-XyG LM25 using equivalent sections. (bar=50 µm)

Pectic polymers in the cell walls of XyG deficiency mutant

Other pectic polymers were analysed over the syncytial walls formed in XyG mutant, shown in Figure 4.3.2.3. This included the use of three anti-arabinan mAbs, LM13, LM16 and LM6. Both LM13 and LM6 gave clear binding over the vascular region including the syncytia, with LM6 epitopes relatively more abundant in the syncytial walls. Anti-galactan LM5 only gave minor binding inside the vascular bundle with no presence in the syncytial walls. Anti-HG LM19 and LM20 gave different binding over the syncytial walls, indicating the syncytial wall HG in the XyG mutant was also predominantly methyl esterified.

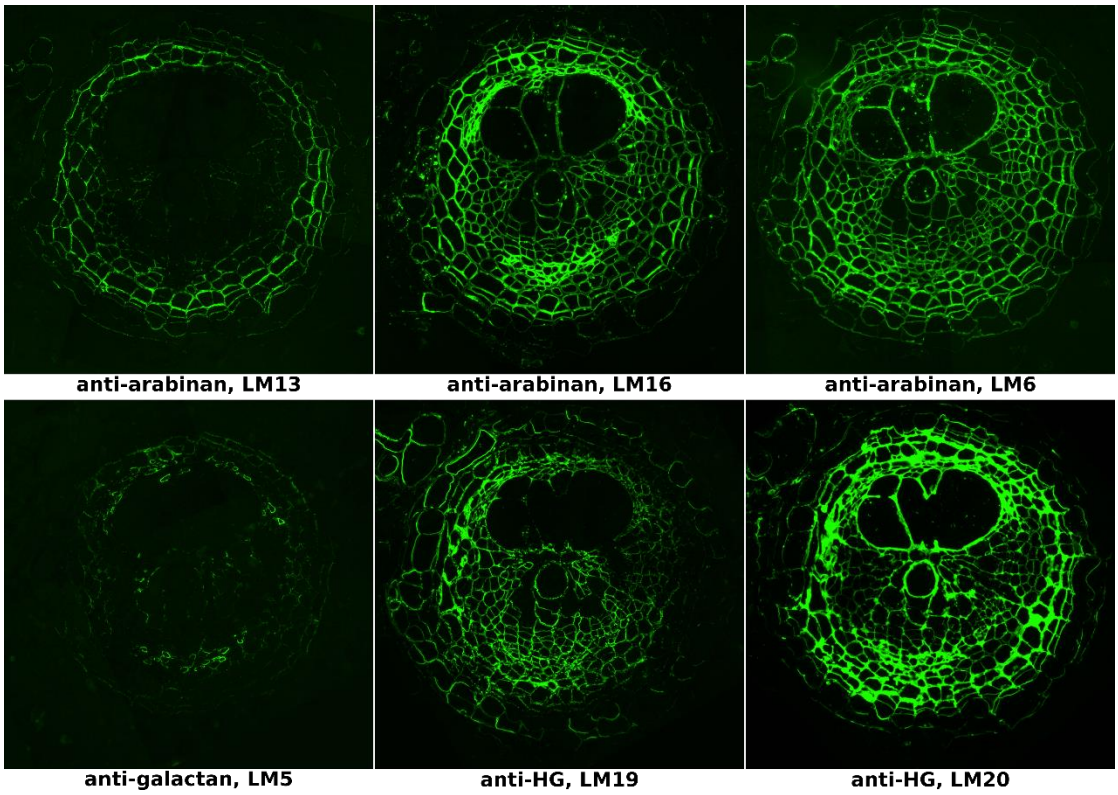

Figure 4.3.2.3 Immunolocalization of pectic polymers in the walls of *H. schachtii* infested Arabidopsis XyG deficiency mutant (21 dpi). Indirect immunofluorescence (green) images are from the specific binding of mAbs, anti-arabinan LM13, LM16 and LM6, anti-galactan LM5 and anti-HG LM19 and LM20, using equivalent sections.

Comparing with previous results, the syncytial wall chemical compositions do not differ largely from the ones formed in wildtype plants, still possessing abundant pectic arabinans and methyl-HG, whilst lack of xylan and pectic galactan. The only obvious change is the loss of XyG along with other host root cells. This clearly shows the adaptations in the syncytia formation process at a chemical composition level.

4.3.2.3 The cell wall microstructures of syncytia induced by *H. schachtii* in Arabidopsis arabinan deficiency mutants

Another widely distributed syncytial wall polymer is the pectic arabinan. To assess the syncytial wall chemical structures formed within hosts possessing naturally less arabinans, three arabinan deficiency mutants were chosen. Nematode J2s infected these mutants successfully and the structure of the syncytia was not different to those formed in wild-type plants. *In situ* analysis was then carried out over the induced syncytial walls.

Hemicelluloses in the cell walls of arabinan deficiency mutant

Hemicellulosic xylan and XyG were first analysed using LM11 and LM25 respectively in all three mutants, as shown in Figure 4.3.2.4. The anti-xylan LM11 still recognise specially to the xylem within the vascular bundle. Meanwhile, the anti-XyG LM25 epitopes were found to be clearly present in almost all the cell walls of the whole root sections, including the syncytial regions.

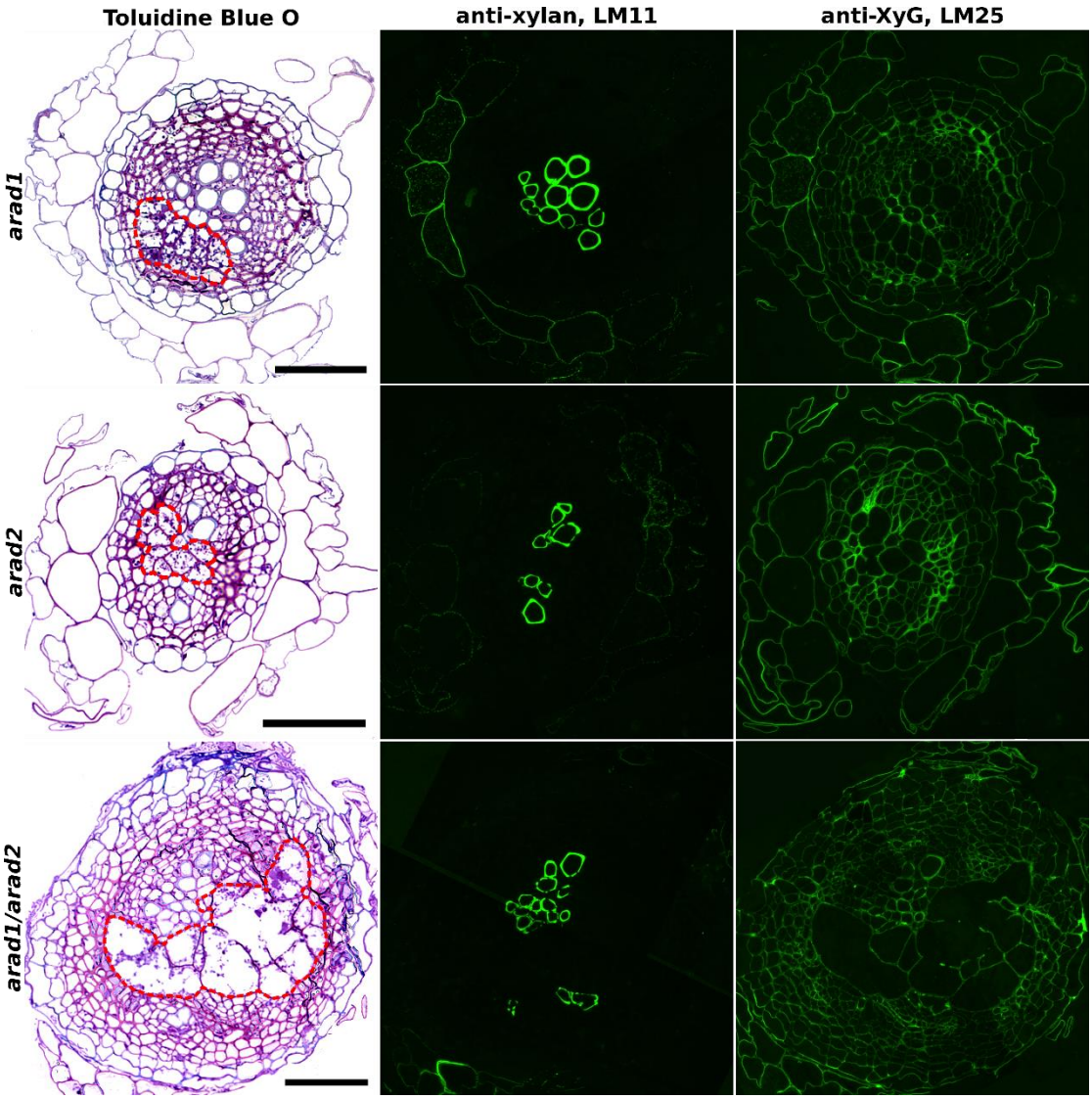

Figure 4.3.2.4 Immunolocalization of hemicelluloses in the walls of *H. schachtii* infested Arabidopsis arabinan deficiency mutants (21 dpi). Bright field images are captured over Toluidine Blue O stained sections. Syncytial regions are outlined with red dash line. Indirect immunofluorescence (green) images are from the specific binding of anti-xylan LM11 and anti-XyG LM25 using equivalent sections. (bar=50 µm)

Pectic arabinans in the cell walls of arabinan deficiency mutants

With reduced level of arabinans, three anti-arabinan mAbs were used with different recognition properties. As shown in Figure 4.3.2.5, the LM13, recognising preferentially long linearized arabinan, was largely absent in *arad1* and the double mutants. It was proven to be absent in syncytial walls in previous results and was again absent from syncytial regions in these two mutants. Meanwhile, the LM16 targeting branched arabinans was shown to be abundant in the walls of almost the whole vascular cylinder, including clear binding over the syncytial walls, especially in *arad1* and the double mutants. In comparison, the LM6 epitopes were clear in all the formed syncytial walls, with relative stronger binding in *arad2* mutant. This all together suggested that the syncytial walls formed in arabinan deficiency mutants still possess rich arabinan, indicating the important role it played in maintaining the normal function in cyst nematode induced syncytia.

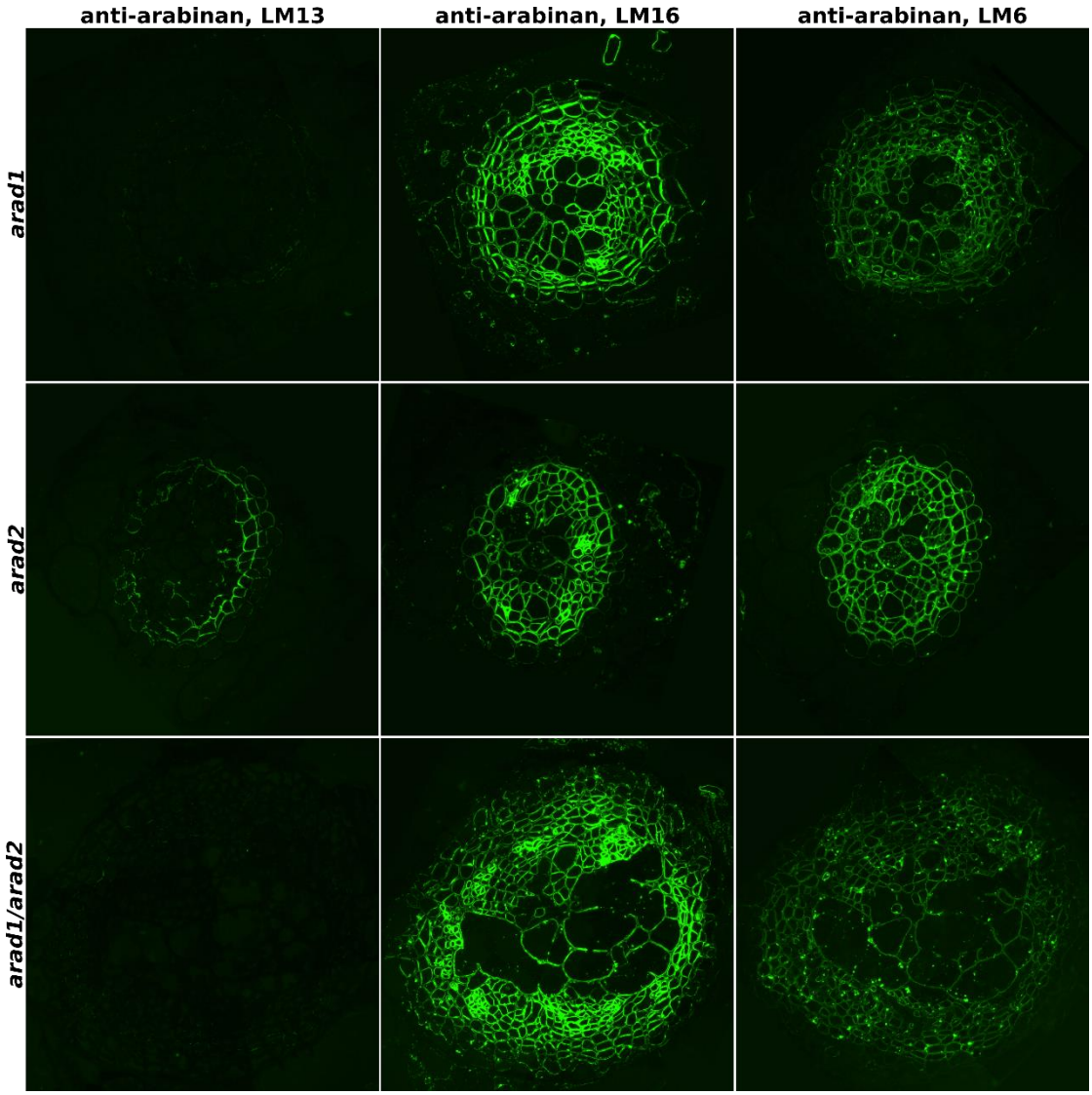

Figure 4.3.2.5 Immunolocalization of pectic arabinans in the walls of *H. schachtii* infested Arabidopsis arabinan deficiency mutants (21 dpi). Immunofluorescence (green) images are from the specific binding of anti-arabinan LM13, LM16 and LM6 using equivalent sections.

Pectic HG in the cell walls of arabinan deficiency mutants

LM19 and LM20 were used to evaluate the abundance of pectic HG in the syncytial walls formed in arabinan deficiency mutants. As shown in Figure 4.3.2.6, the LM19 bound to more cell types in and out of the vascular cylinder, comparing with the equivalent section labelled with LM20. However, the LM20 bound significantly stronger than LM19 inside the vascular region, including the abundance in syncytial walls, similar to previous results. This proves that the arabinan deficiency mutants did not change the presence of pectic HGs in the syncytial walls nor the methyl esterification status.

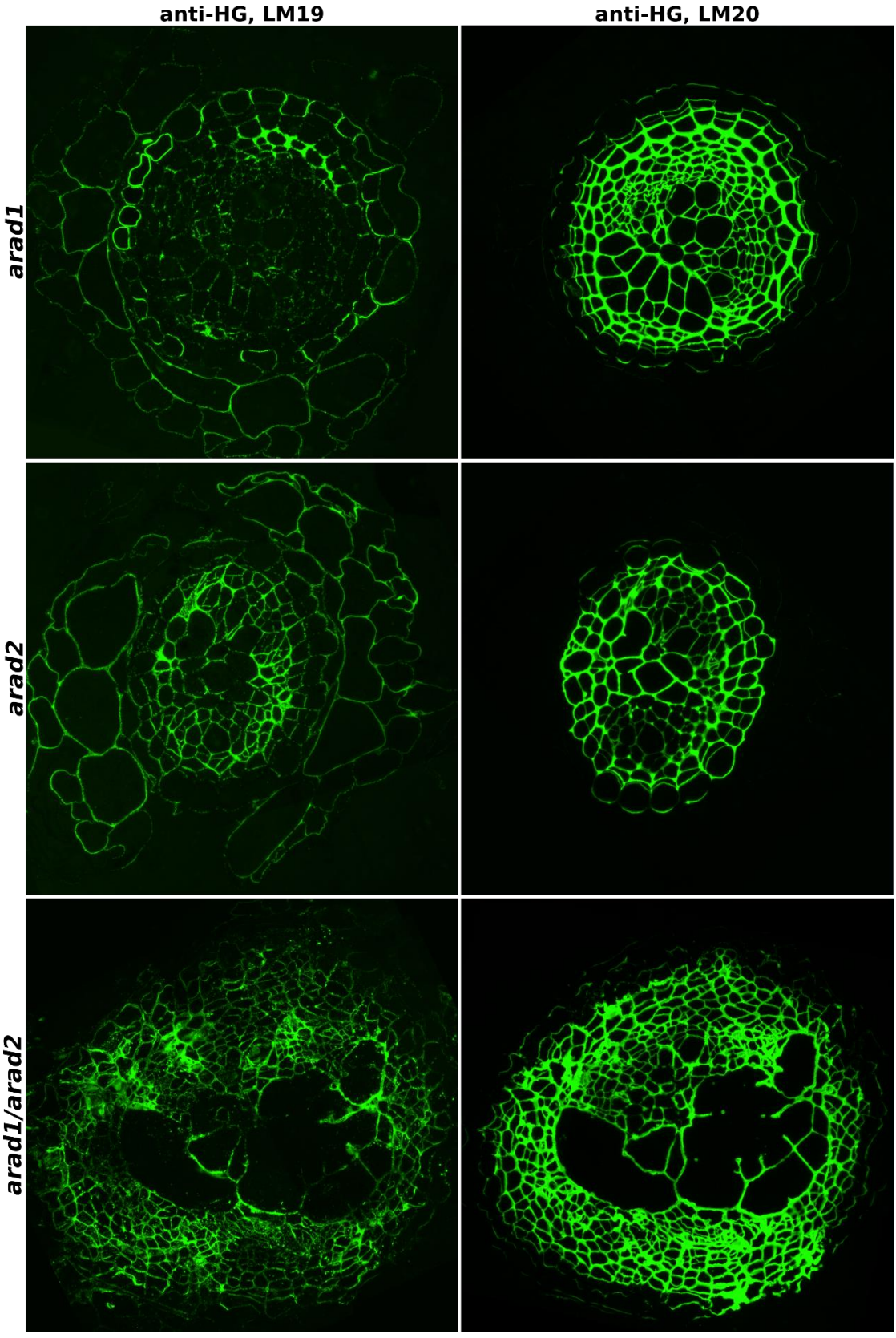

Figure 4.3.2.6 Immunolocalization of pectic HG in the walls of *H. schachtii* infested Arabidopsis arabinan deficiency mutants (21 dpi). Immunofluorescence (green) images are from the specific binding of anti-HG LM19 and LM20 using equivalent sections.

Table 4.3 Summary of immunolocalization of primary antibodies in syncytial walls induced by *H. schachtii* in *Arabidopsis thaliana* cell wall mutants

Antibody epitopes		mAbs	*H. schachtii* induced syncytia				Reference
			arad1	*arad2*	*arad 1x2*	*xxt1/xxt2*	
Xyloglucan	XXXG / galactosylated	LM25	++	++	++	-	(Pedersen, Fangel *et al.* 2012)
Xylan	(1→4)-β-D-xylan / arabinoxylan	LM11	-	-	-	-	(McCartney, Marcus *et al.* 2005)
Homogalacturonan	partially methyl-HG / de-esterified HG	LM19	+	++	++	+	(Verhertbruggen, Marcus *et al.* 2009)
	partially methyl-HG	LM20	+++	+++	+++	+++	(Verhertbruggen, Marcus *et al.* 2009)
RG-I related	linearised (1→5)-α-L-arabinan	LM13	-	-	-	-	(Verhertbruggen, Marcus *et al.* 2009)
	processed arabinan	LM16	++	++	++	++	(Verhertbruggen, Marcus *et al.* 2009)
	(1→4)-β-D-galactan	LM5	+	+	+	-	(Jones, Seymour *et al.* 1997)
	(1→5)-α-L-arabinan	LM6	++	++	+++	+++	(Willats, Marcus *et al.* 1998)

* -, no binding; +, slight binding; ++, clear binding; +++, significant binding

The syncytial cell walls formed in XyG and arabinan deficiency Arabidopsis mutants

H. schachtii infection and immunolabelling were carried out over selected Arabidopsis cell wall mutants. As summarised in Table 4.3, *H. schachtii* successfully infested all the tested mutant lines. The changes of host cell wall properties did not eliminate the nematode infection, though to what extent the infection was affected needs further investigation.

Comparing with syncytia formed in Arabidopsis wildtype, the syncytia in all the tested mutants still possess abundant methyl-HG and lack of xylan. In the three arabinan deficiency mutants, with reduced levels of arabinans, the presence of pectic arabinan was still clear and abundant in syncytial walls. Due to the lack of absolute quantification, if the level of syncytial cell wall arabinan was also reduced alongside with their host cells was yet unknown. In the XyG deficiency mutant *xxt1*/*xxt2*, the syncytial walls were completely lack of detectable levels of XyGs, the same pattern depicted by the mutant host. Due to the raised questions towards the XyG-cellulose tethered network model and the ongoing investigations to a new cell wall model, the function of XyG in syncytia in wildtype hosts is yet to be determined. However, one thing is that the role of XyG in syncytial cell wall functioning might be overestimated based on its wide distribution in all the tested syncytia induced by cyst nematodes (see Chapter 3).

4.3.3 Syncytial walls formed in PEG treated Arabidopsis roots

Based on previous research, the methyl esterification status of HG can affect the cell wall rheological properties such as porosity and extensibility as well as wall strength. In cyst nematode induced syncytia, the pectic HG was revealed to be predominantly methyl-esterified, apart from the coexisted abundant non-methyl HG at the initial syncytium forming stage. In the proposed model, this largely methyl-esterification might contribute to wall porosity and integrity thus facilitate nematode feeding.

In order to further evaluate the importance of methyl-HG, a fluorescence quantification method capable of cross-sample comparisons was introduced and validated. Together with different PEG concentrations to simulate different water stress levels, the effects of drought, potentially affect syncytium integrity and nematode feeding, to cell wall pectic HGs was assessed.

4.3.3.1 Fluorescence quantification methodology

The need for comparable quantifications of antibody binding among syncytia is raised when the changes of anti-HG probe LM19 performance during parasitism were observed. Previous researchers used transects across cell walls in adhered regions of cells in some plants (Lee, Cornuault *et al.* 2013). This is suitable to compare certain types of tissue with relatively identical cells among individuals, groups or even populations and it also indicates the clear differences, in terms of antibody bindings of cell walls versus the background noise. While adopting this method for syncytial cell wall measurements, its validity faces the following challenges: firstly, it's hard to find certain single point to represent the whole syncytial region, as within a syncytium, the cell wall thickness varies, even the different parts of the cell walls might differ, as previous research show the heterogeneity of syncytial wall composition (Davies, Lilley *et al.* 2012). Moreover, syncytia formed in different individual host plant differ in size, shape and other aspects, not to mention those formed in "different hosts", i.e. wildtype versus mutants. Choosing certain portion to represent the whole syncytium is inevitably misleading. So only the whole syncytial regions were measured under identical parameters could provide more representative data (Figure 4.3.3.1, A). In this section, for each antibody, four identical sections were used to minimize the possible deviations of antibody performance.

The choosing of appropriate exposure time is another major factor needs to be considered. As shown in Figure 4.3.3.1 B, the mean values will increase, not exactly proportionally but steadily, along with the prolonged exposure time. Images in this study were captured and stored as 16bit format images, with a fluorescence signal value of 4095 at "saturation" per pixel. This means the exposure time should be chosen not too high to cover the differences among good binding, nor too low to make circulating the syncytial cell wall boundaries too hard when antibody binding performances were poor.

Based on the above considerations, a fixed exposure time was chosen and applied throughout the study. Under such circumstances, the images are bright enough for weak binding, for example, LM19, and not way too bright for strong binding like LM20. All the

images were taken under the same parameters after all the sections were pre-labelled at the same time. Background corrections were made to all the images ahead of further analysis. The images of syncytia induced by *H. schachtii* in Arabidopsis at different parasitism stages were first analysed using this procedure, as illustrated in Figure 4.3.3.2, and the data were shown in the following section.

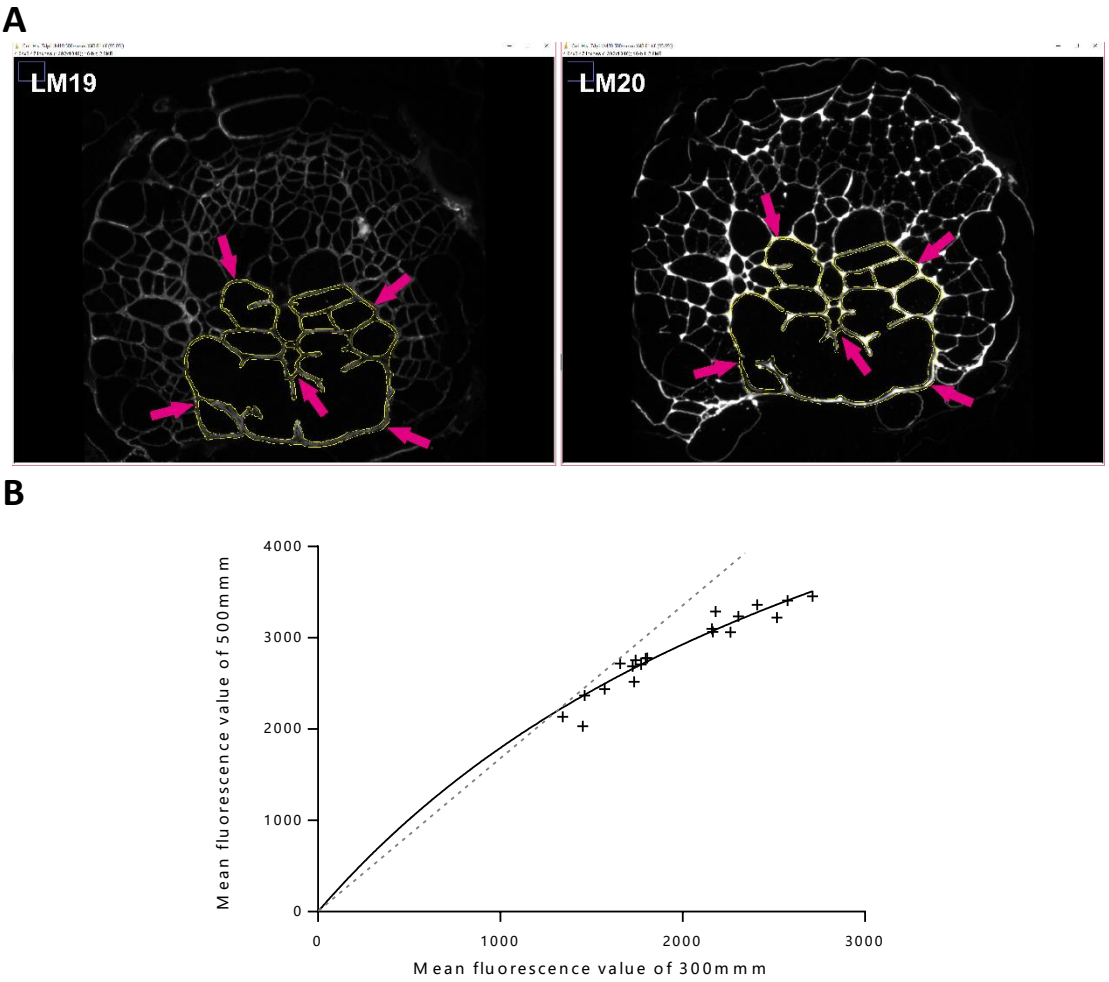

Figure 4.3.3.1 Fluorescence quantification in syncytial cell walls. A. Immunofluorescence signals within syncytial regions (indicated by arrows) were quantified using ImageJ. Identical sections were labelled simultaneously and images used were captured under the same parameters. **B**. The graph shows the correlation between mean fluorescence values and exposure time when taken images. Solid line is generated by non-linear regression analysis and the dash line is when the mean fluorescence values are only proportionally related to the exposure time. Each dot stands for two measured values of the same section at different exposure time (300mmm and 500mmm).

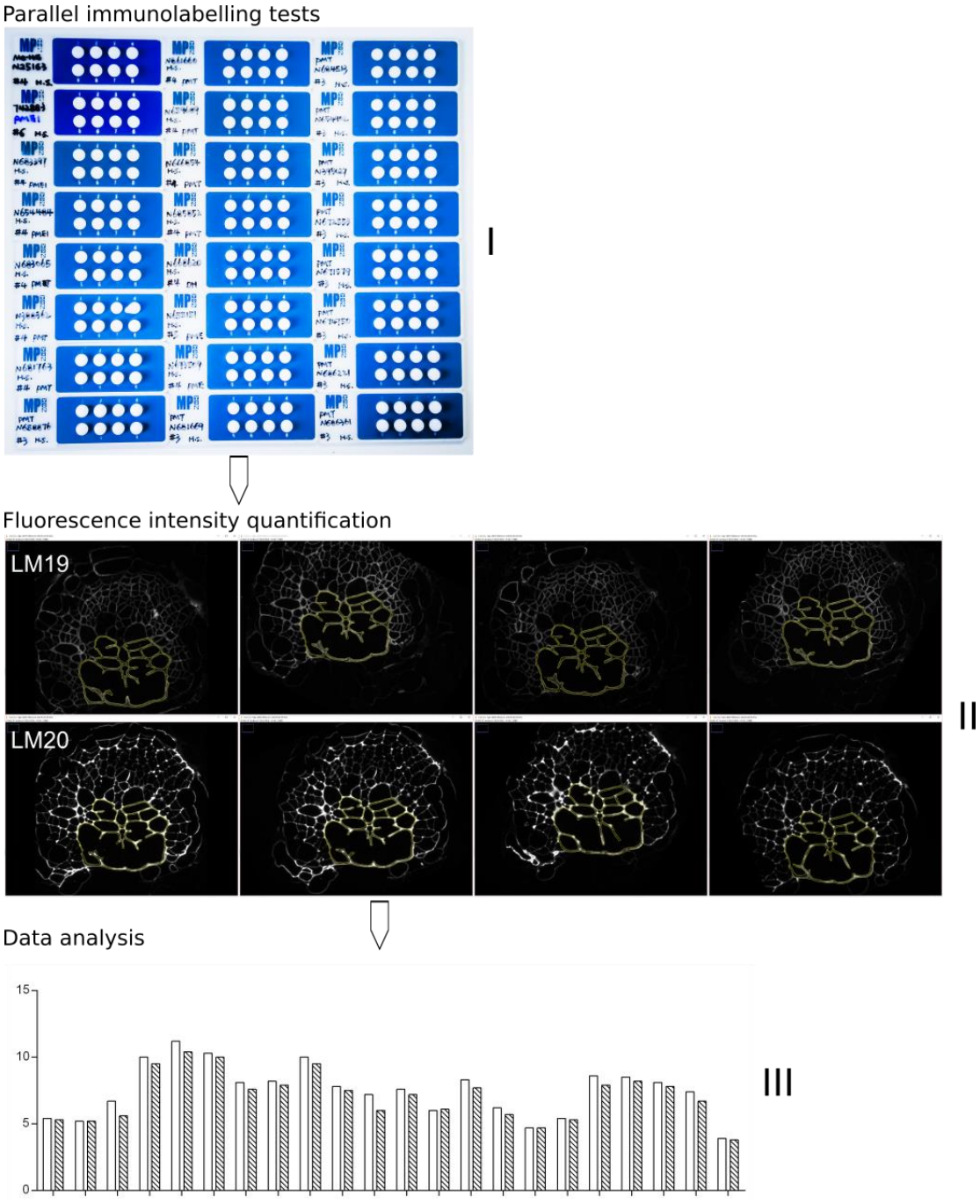

Figure 4.3.3.2 Experimental procedure for pectic HG analysis in syncytial cell walls formed in Arabidopsis. I. Parallel immunolabelling tests were carried out under the same experimental conditions simultaneously. Fluorescence images were taken under the same parameters. **II**. Fluorescence intensity quantification was proceeded over the images from step I using ImageJ. **III**. Data analysis was performed using the values generated in step II.

4.3.3.2 The pectic HGs in syncytial cell walls induced in Arabidopsis roots

Based on the proposed quantification method, as illustrated in Figure 4.3.3.2, the methyl esterification status of pectic HGs were assessed over the samples collected in previous section.

As shown in Figure 4.3.3.3, the fluorescence intensity of anti-HG antibodies LM19 and LM20, representing the low/non methyl-HG and methyl-HG respectively, in syncytia formed in Arabidopsis wildtype at 7 dpi, 14 dpi and 21 dpi were analysed. The graphs plotted by the mean values of fluorescence signals in specific syncytial walls represent the binding performance for both antibodies, making the noticeable changes shown in previous images much easier to interpret. As indicated in Figure 4.3.3.3, from early forming syncytium (7 dpi) to fully mature stage (14 dpi), the methyl-esterification level increased (represented by LM20) meanwhile the amount of non-methyl HG significantly decreased (indicated by LM19). Towards the end of nematodes feeding (21 dpi), the content of methyl-HG slightly dropped whilst non-methyl HG increased. Based on such changing trends for both LM19 and LM20 binding, we could hypothesize that the overall HG level in syncytial cell walls stay stable in general throughout parasitism, not greatly affected by the syncytium expanding, while the degree of methyl esterification of HG are altering. This indicates that the methyl esterification levels are likely to be regulated during the nematode parasitism, in order to fulfill its developmental requirements. However, we have to admit that more repeats should be carried out to avoid possible fluctuations among these randomly sectioned samples as well as test our hypothesis in a statistical way.

The methyl esterification status of HG was shown to have fluctuation during parasitism in the above results. What known is this type of modification was related to cell wall extensibility and the balance between cell wall extensibility and turgor pressure controls plant cell growth (Wolf and Greiner 2012). In a functioning syncytium, there's much higher turgor pressure than that in other types of cells among the host tissue (Böckenhoff and Grundler 1994). This raised the question if we pose drought stress onto the host roots, affecting turgor pressure and the extensibility (Moore, Vicré‐Gibouin *et al.* 2008) of those surrounding cells, will the syncytium make any structural changes to maintain its normal functioning in response? As obviously, the syncytia will also face such challenge in the field, acclimating their growth and development to the variable environment. Here, we use a range of PEG supplemented culture medium to simulate water stress, and the syncytia formed under such conditions were collected at 14 dpi and 21 dpi. Immunolabelling as well as the fluorescence quantification were applied as above and the results are listed in the following section.

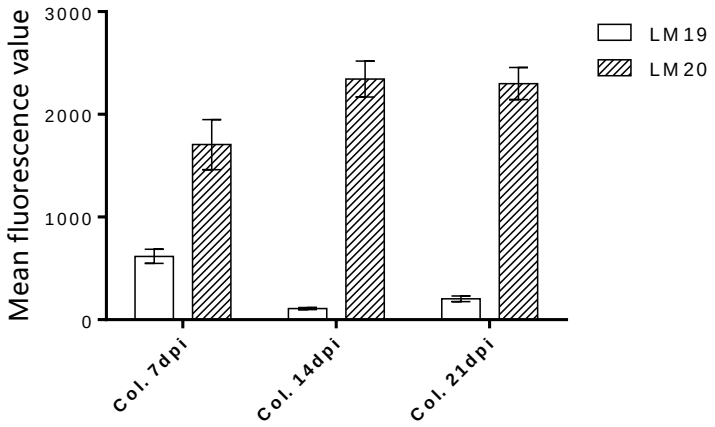

Figure 4.3.3.3 Fluorescence quantification of anti-HG LM19 and LM20 in syncytial cell walls formed in Arabidopsis roots at different development stages. Graphs were plotted from the fluorescence intensity quantification data of the two antibodies, showing the changing trends of HG levels along with nematode developmental stages. Error bars stand for standard deviations generated from technical replicates.

4.3.3.3 The syncytial cell walls induced in Arabidopsis roots, cultured with PEG

The samples of syncytia formed in Arabidopsis with PEG simulated stress were collected as described in methods. With increased PEG concentration from 1% to 5%, the seedlings gradually lose growth vigor. At 5% PEG, the whole plant could barely survive until reach the 21 dpi time point after nematode inoculation.

in situ analysis was first performed as before to check if any structural alterations occurred in syncytial walls when facing water stress. Further analysis was then carried out to evaluate the pectic HG content as well as the methyl esterification status.

The syncytial walls induced in PEG treated Arabidopsis roots

Same experimental procedure has been proceeded to the syncytia formed in Arabidopsis cultured with supplemented PEG using a core set of mAbs. As shown in Figure 4.3.3.4, the binding patterns of anti-hemicellulose LM11 and LM25 did not differ from previous results nor between the samples of different PEG concentrations. Within the vascular cylinder, the anti-xylan LM11 still represented the xylem elements whilst the anti-XyG LM25 bound to all the cells including the nematode induced syncytial walls.

As for pectic polymers, RG-I related galactan and arabinan were tested using LM5, LM16 and LM6, as shown in Figure 4.3.3.5, and pectic HGs were evaluated using LM19 and LM20, as shown in Figure 4.3.3.6.

The anti-galactan LM5 and anti-arabinan LM16 share similar binding patterns, both show strong binding over the vascular cells apart from the xylem. Comparatively, the syncytial walls possess clear binding of LM16 indicating the presence of arabinans, whilst the LM5 targeted galactan was only visible in the 1% PEG sample. The epitopes for LM6 were still present in almost all cells in the vascular bundle, with the syncytial walls show relatively stronger affinity.

Clear differences were observed over the syncytial walls in Figure 4.3.3.6 when using anti-HG LM19 and LM20, with LM20 consistently had strong binding whilst LM19 had strong binding in the 1% and 3% PEG samples meanwhile almost absent in 5% PEG treatment. The syncytial walls in 2% PEG sample also had strong binding of both LM19 and LM20 (images can be found in supplementary data), indicating a drop of non-methyl HG content represented by LM19 in syncytial walls formed under high water stress.

Quantification was then carried out over the binding performance of the anti-HG LM19 and LM20 in those samples, allowing clear comparisons over the content of both forms of pectic HGs.

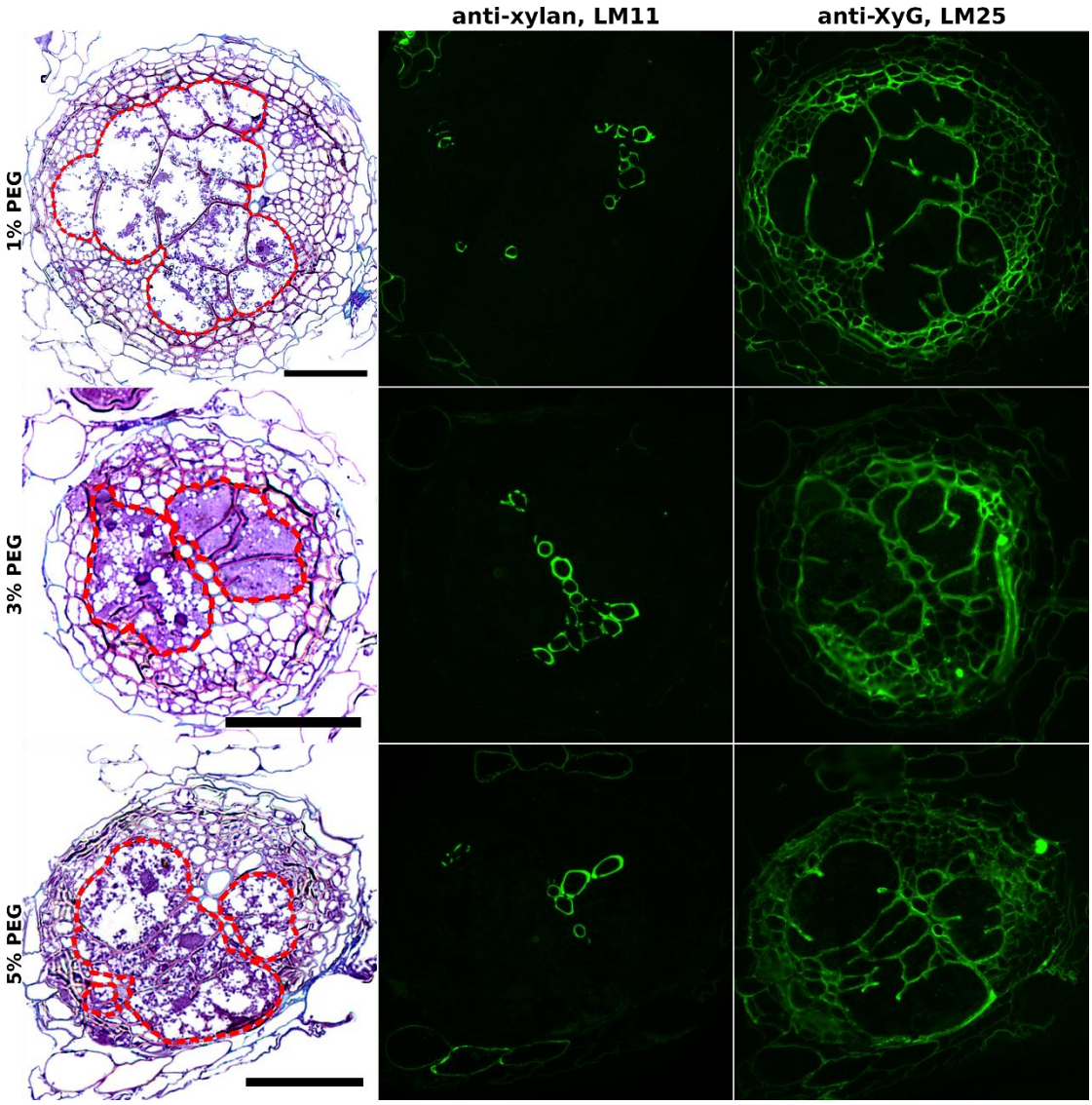

Figure 4.3.3.4 Immunolocalization of hemicelluloses in the walls of *H. schachtii* infested Arabidopsis, cultured with PEG (14 dpi). Bright field images are captured over Toluidine Blue O stained sections. Syncytial regions are outlined with red dash line. Immunofluorescence (green) images are from the specific binding of anti-xylan LM11 and anti-XyG LM25 using equivalent sections. (bar=50 µm)

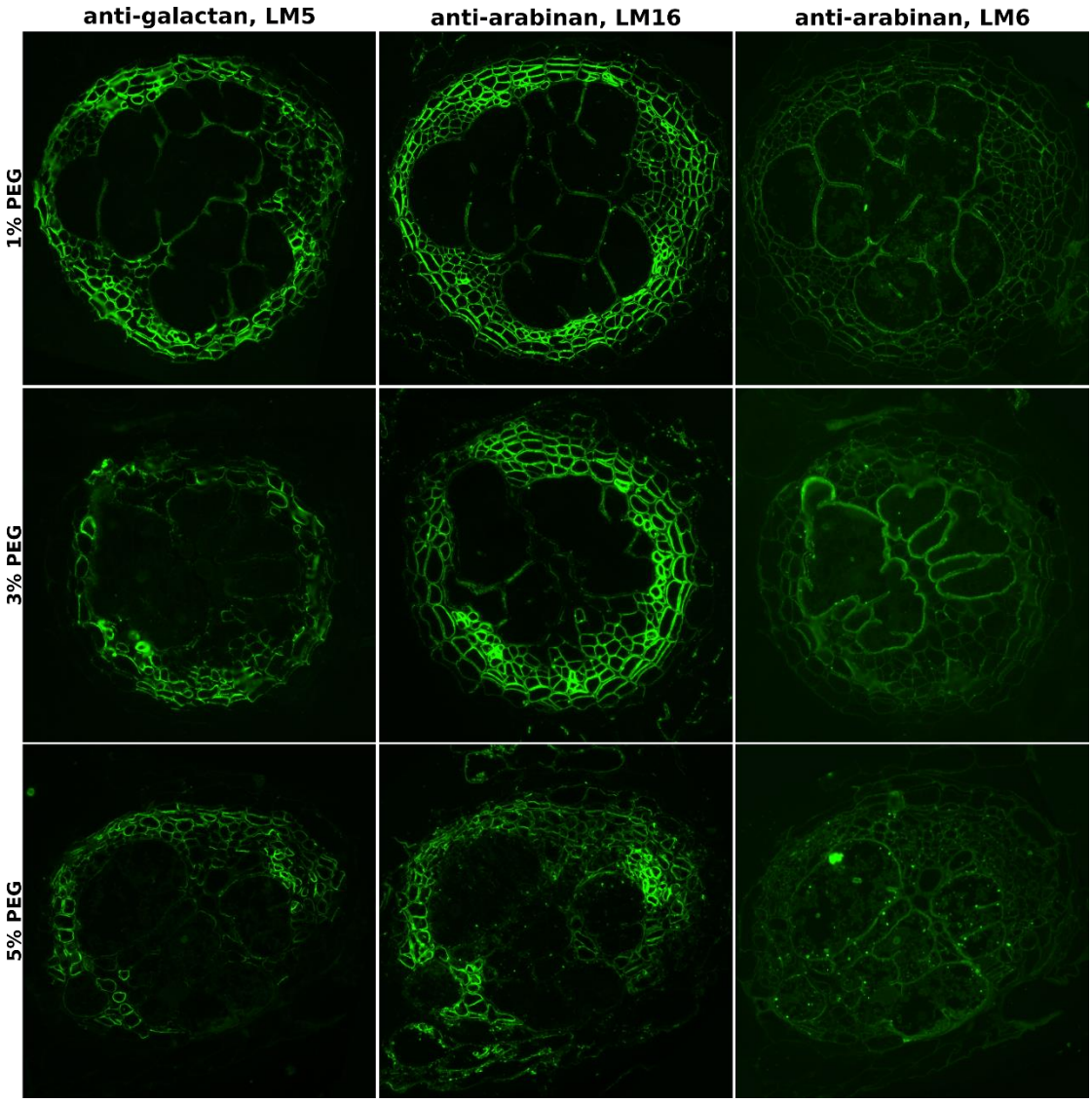

Figure 4.3.3.5 Immunolocalization of galactan and arabinan in the walls of *H. schachtii* infested Arabidopsis, cultured with PEG (14 dpi). Immunofluorescence (green) images are from the specific binding of anti-galactan LM5 and anti-arabinan LM16 and LM6 using equivalent sections.

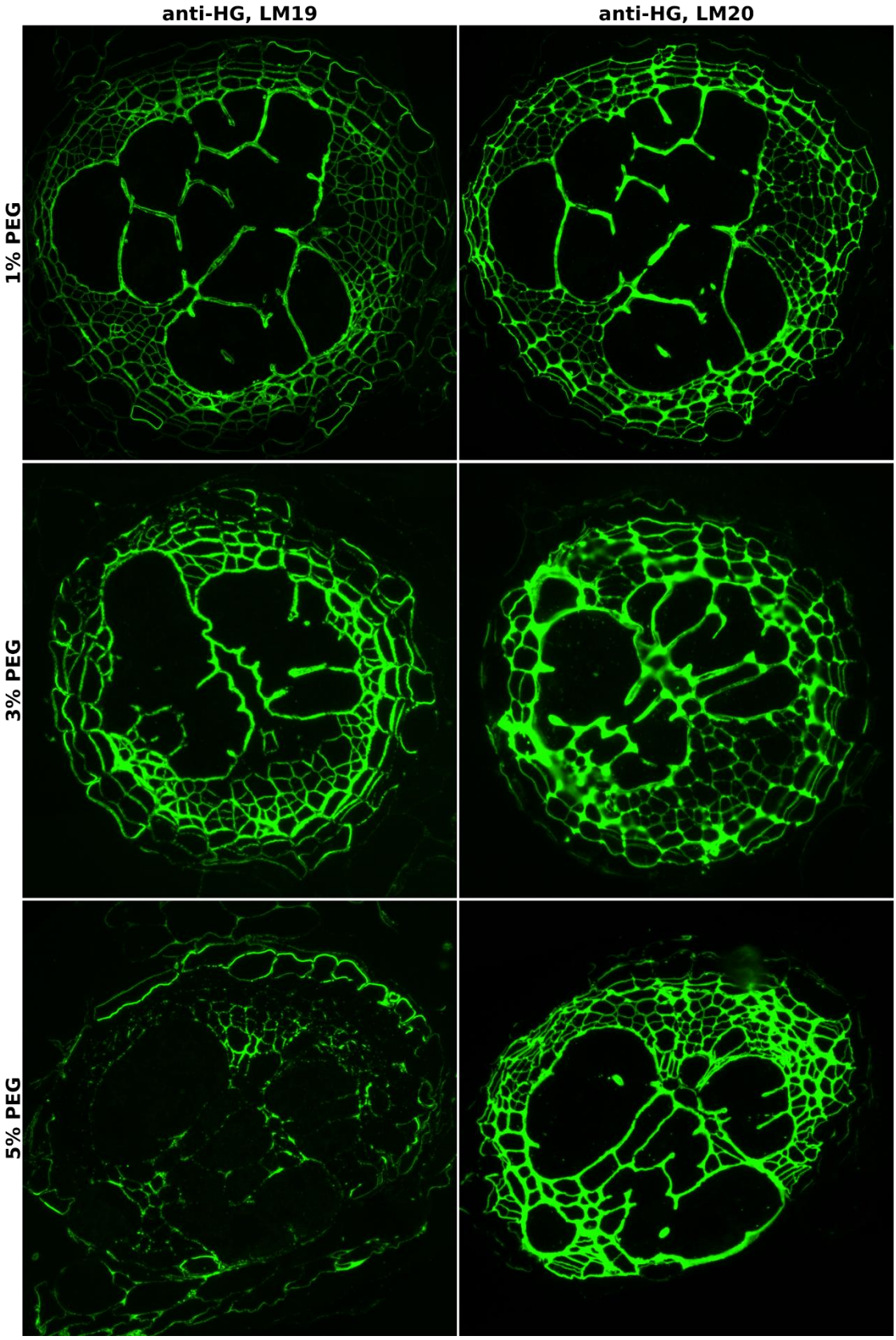

Figure 4.3.3.6 Immunolocalization of pectic HG in the walls of *H. schachtii* infested Arabidopsis, cultured with PEG (14 dpi). Immunofluorescence (green) images are from the specific binding of anti-HG LM19 and LM20 using equivalent sections.

The pectic HGs of syncytial walls induced in PEG treated Arabidopsis roots

The quantification analysis over the samples show clear changes of anti-HG LM19 and LM20 binding along with PEG simulated stress levels, data plotted in Figure 4.3.3.7.

For LM19 represented non/low-methyl HG, it was shown to be at very low level in previous quantifications. However, under light water stress, the content of non-methyl HG was shown to have a great rise at 1% PEG treatment followed by continuous decrease along with the increasing stress levels. This change might be caused by the delayed syncytium development after transferring plants from normal conditions to stress treatment. This overall decreasing trend, from 14 dpi to 21 dpi, also matched up with the decreasing levels of non-methyl HG along with aging shown in the last section.

For LM20 binding, apart from the 5% PEG treatment when the plants grew significantly smaller and could barely survive until 21 dpi with leaf chlorosis and nearly dried root system, the levels of methyl-HG along with PEG treatment show clear decrease for younger mature syncytia but steady increase for post-mature syncytia. For the walls of 14 dpi syncytia, this change might also be caused by the restrained host cell growth which might contribute to the initial fast increase of fully methyl-HG during the syncytium formation process. As for samples at 21 dpi, the methyl-HG all reached a significantly high amount regardless of stress levels indicating the essentiality of HG methyl esterification in functioning syncytia.

These analysis in all agreed with the changing path of methyl esterification status of pectic HGs in syncytial walls during parasitism. The additional water stress might have changed the developmental pace for *H. schachtii* induced syncytia, resulting in different pectic HG contents at the same timeline, however, the overall trend stayed stable: the syncytial walls possess decreasing amounts of non-methyl HG from initiation to mature stage whilst the fully methyl-HG levels go steadily up.

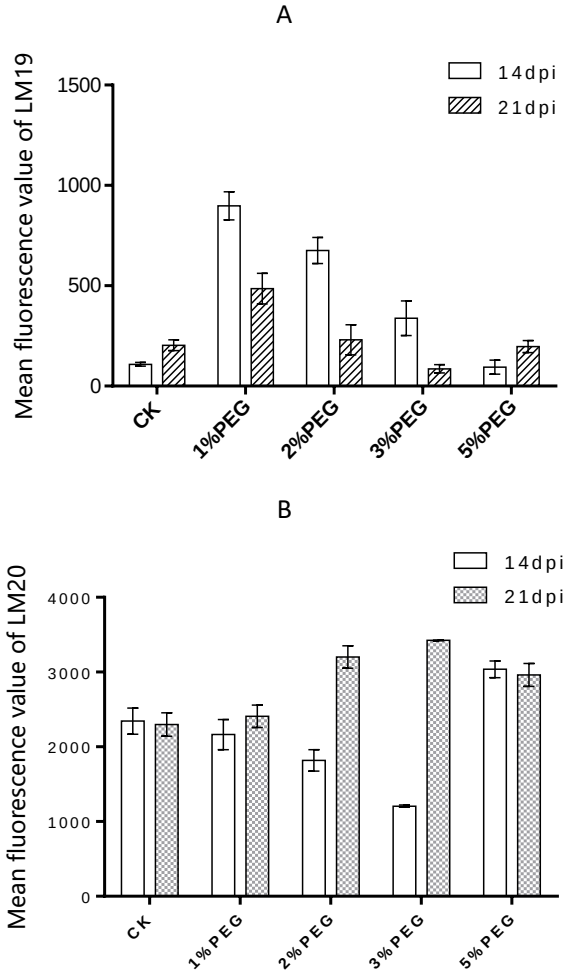

Figure 4.3.3.7 Fluorescence quantification of anti-HG LM19 and LM20 in syncytial cell walls formed in Arabidopsis roots, cultured with PEG. A. Fluorescence quantification of LM19, representing non/low-methyl HG content, were plotted for samples taken at 14 dpi and 21 dpi. **B**. Fluorescence quantification of LM20, representing methyl-HG content, were plotted for samples taken at 14 dpi and 21 dpi. CK stands for syncytia formed in untreated plants. Error bars stand for standard deviations generated from technical replicates.

The syncytial cell wall pectic HGs and drought stress

In this section, with the introducing of a standard experimental procedure, comparisons of antibody binding performances were made possible across samples. Such quantification assay show clear changing trends for syncytial pectic HGs throughout syncytium forming process, with decreasing non-methyl HG and increasing methyl-HG from initiation towards fully mature.

The chemical structures of syncytia induced in drought stressed Arabidopsis roots were analysed, using PEG simulated water stress. Immunolabelling and further quantification analysis gave clear evidence that the syncytium formed under stress still possessed the essential wall microstructures. Meanwhile, the changing process of methyl esterification status of pectic HG has be affected but eventually all reached similar levels as in control, thus indicating the importance of this alteration during syncytium formation and normal functioning.

4.3.4 Syncytial walls formed in pectic HG related Arabidopsis mutants

Based on the revealed syncytial wall microstructures in Arabidopsis as well as the ones formed in potato and soybean, one key feature is the syncytial walls of mature stages always possess large amount of highly methyl esterified pectic HG. As mentioned in previous context, the methyl esterification status is mostly related to several large gene families, including PMEs, PMEIs and probably PMTs. In order to further investigate the role of pectic methyl-HG during nematode infestation and syncytium formation, a range of Arabidopsis mutants were selected, with targeted candidate genes fall into these categories.

Due to the lack of such cell wall mutants, the selection was largely based on a previous microarray dataset (Szakasits, Heinen *et al.* 2009). The candidate genes with a reasonable level of expression inside the syncytial content were first chosen, and then related Arabidopsis mutants were ordered. After homozygosity tests, all the homozygous lines were used for nematode infection and syncytial wall analysis. The syncytial walls of all the mutants were analysed with a core set of mAbs, targeting any possible syncytial wall polymers. Quantification of pectic HGs was then accomplished for the syncytia formed in all the mutants. Eventually, several lines were chosen and nematode infection assay was carried out to evaluate the impact of pectic HGs toward nematode infestation. Restricted by the page limit, only a few immunolabelling figures were shown in the following context, all the figures can be found in supplemented dataset.

4.3.4.1 The selection of pectic HG related mutants

Candidate genes and related mutant lines

Relying on the microarray data, candidate genes and related mutant lines were chosen. Table 4.4 summarised the main information related to this process, including the possible gene name and locus, mutant stock ID, gene specific primers designed for homozygosity tests and the expected sizes of amplicons in both the mutant and wildtype plants.

Table 4.4 List of pectic Homogalacturonan related *Arabidopsis thaliana* mutants

Category	Stock ID	Polymorphism	Locus	Gene specific primers for homozygosity tests and Tm	Amplicon size in wildtype (LP+RP)	Amplicon size in mutant (LB+RP)
PMT	N676255	*PMT4*	AT1G13860	LP: CATTTGACATGGTCCACTGTG 55.0°C RP: TCATCACCCAAACTGATTTCC 54.1°C	951bp	N/S
	N683065	*PMT6*	AT3G10200	LP: TCCATTGTTTGGATTCGAAAG 59.92°C RP: TTGGGAGCAAATGAAATTGTC 59.93°C	1081bp	558-858bp
	N388362	*PMT21*	AT4G19120	LP: TCAATGGCTGTGCGTATA 62.22°C RP: TCCTTTGTTTCCTCAACTTTCG 60.82°C	1013bp	N/S
	N681763	*PMT14*	AT4G18030	LP: ACACAGAATCGGATCTCGTTG 60.13°C RP: CTCGACAGGAATGCAAAGAAC 59.87°C	1264bp	576-876bp
	N861660	*PMT8*	AT1G04430	LP: TAATGGTGGAATTGAAAACGC 59.82°C RP: CCTCCATCAGATCTCCCTCTC 60.16°C	1010bp	451-751bp
	N659689	*PMT12*	AT5G06050	LP: TCCAGCTCTCATGTCCAAGAC 60.40°C RP: GTGCTTTGGTAGCTGTTTTGC 59.94°C	1163bp	559-859bp
	N666854	*PMT23*	AT2G40280	LP: TTACCCATAGGGGGTGGTTAC 59.82°C RP: AAGCTGATCAAGAGCAGCAAC 59.78°C	1086bp	482-782bp
	N685852	*PMT20*	AT1G31850	LP: AACCTACCAAAGAAACCACGG 60.26°C RP: CCAAACTTTCATTGCTGATCC 59.56°C	985bp	468-768bp
	N668620	*PMT25*	AT2G34300	LP: ACTGACGCAGGGTTTATGTTG 60.04°C RP: TCTGGTACAACAATGTTCCCC 59.70°C	993bp	431-731bp
	N677818	*PMT3*	AT4G14360	LP: ATTCAATCGCGGTGATTACAC 59.84°C RP: GTTCCTGAGGACGGACCTAAC 59.99°C	1248bp	566-866bp
	N681669	*PMT16*	AT2G45750	LP: GTTTCCAGTCCAATGTCATGG 60.23°C RP: TACCGTCTGAATCATCGAAGG 60.08°C	1045bp	492-792bp
	N684513	*QUA2*	AT1G78240	LP: GATCACTCGTTTTCTTGCGAG 60.01°C RP: TTGGTAAACTCGTGGAAATCG 59.98°C	1268bp	591-891bp
	N654902	*PMT7*	AT5G04060	LP: GCCTCCTTCAAATTCTCCATC 60.03°C RP: GGGTCATGAACGTTGTACCTG 60.28°C	1028bp	460-760bp
	N395027	*PMT1*	AT3G23300	LP: ATCACTAATATACACAACGGCGG 60.16°C RP: TCTTTGAAGCCAATCGATA 61.08°C	1137bp	N/S
	N658876	*PMT18*	AT1G33170	LP: ATTGGTTACCAAATCGGAAGG 60.06°C	1168bp	532-832bp

				RP: CGTCTGAACTGTTTGCTTCTG 58.71°C		
	N672553	*PMT2*	AT1G26850	LP: TACAGGCCAGTCTCAATTTCC 59.18°C RP: AACATATGACCTGATCCACGC 59.83°C	971bp	452-752bp
	N671579	*PMT13*	AT4G00740	LP: TTTGGGTAACCGATAATATCCG 59.93°C RP: GAGTCTCCTCAGGCAAAGGAC 60.39°C	1030bp	433-733bp
	N674750	*PMT11*	AT2G39750	LP: CCATTTGATACATACCCACGG 59.95°C RP: AAATGCAGCAAAATTGGTCAC 60.00°C	1058bp	450-750bp
	N686221	*PMT28*	AT1G19430	LP: AGAGAGCTTTGACGAAGACCC 60.01°C RP: CGGGAGAAAAGAACGAAACAC 61.00°C	1238bp	592-892bp
	N686361	*PMT9*	AT5G14430	LP: TGGGTATGTGTCAAAGGCTTC 59.99°C RP: TTCCCTGGTGACAAACTCAAC 60.00°C	1212bp	553-853bp
	N665994	*PMT10*	AT1G77260	LP: CCATAAATGCATGATCCCAAC 60.03°C RP: ACAACGTCTAATCCAACGTCG 60.04°C	1140bp	547-847bp
PME	N25163	*PME31*	AT3G29090	LP: TCAAATTTCACCTAGGTGATTTG 51.8°C RP: CACAACCAAACGTACCAGTCC 57.6°C	1117bp	N/S
	N658293			LP: TCAAATTTCACCTAGGTGATTTG 58.18°C RP: CACAACCAAACGTACCAGTCC 60.32°C	1117bp	455-755bp
	N655151	*PME12*	AT2G26440	LP: ATGAGTAACGACAGGGTGCTG 60.19°C RP: CTGTTGCCGTGAAGTTAAAGG 59.79°C	1159bp	598-898bp
	N673509	*PME64*	AT5G64640	LP: ACTGTCCCTGGTTCCACTAGG 60.41°C RP: TGGCACCTTATTCATCACTGTC 60.00°C	1272bp	606-906bp
	N681052	*PME7*	AT1G02810	LP: TCAGTAAGCCCATGAGGTGTC 60.13°C RP: TGATTGGATTTGGAAGACAGG 59.92°C	1125bp	440-740bp
	N664100	*PME53*	AT5G19730	LP: AAAGAAAGGAGAGTTGACCGC 59.88°C RP: GCCATTGATTCTCTCCCTCTC 60.17°C	1116bp	512-812bp
	N675408	*PME17*	AT2G45220	LP: AGCTGGGTTCTTAGAGCTTGG 60.03°C RP: CGACCCGGATCTTAGAGCTAC 60.24°C	1101bp	448-748bp
	N674325	*PME8*	AT1G05310	LP: ACGTCTCCTGGCTTTGGTATC 60.51°C RP: TAATTTGCAAGGCATTCCAAC 59.96°C	1227bp	588-888bp
	N676344	*PME34*	AT3G49220	LP: GCATGAGCAAGAAAAAGTTGG 59.87°C RP: GCGTCATTTGGTGAGTTTTTC 59.61°C	962bp	441-741bp
	N660716	*PME32*	AT3G43270	LP: CTGCCCTTTTAAGGGAAGATG 60.08°C RP: TGTTTTGGAAGGTGATATCGC 59.95°C	1121bp	576-876bp

	N681327	*PME51*	AT5G09760	LP: TCCTTCAGATTTCTTTCTAGTTTAACG 59.78°C RP: GAGTTGCGTTACAAGCGAGAC 60.07°C	1220bp	598-898bp
PMEI	N742883	*AT5G20740*	AT5G20740	LP: ACACGTGTCGTCATCCGTAA 60.03°C RP: TTTTTCACACAATTGACCTGACTC 60.42°C	1294bp	N/S
	N683397	*AT1G10770*	AT1G10770	LP: ATTTGGTGTTTTTGTGTGGTG 58.30°C RP: ACCTCTGGTGAAACGTGTCAC 60.06°C	1206bp	523-823bp
	N654484	*AT3G47670*	AT3G47670	LP: GTCTCTGGGTAACGAGTCACG 59.78°C RP: TTTAGTACTCCGAACCGACCC 60.36°C	1167bp	555-855bp
	N660291	*AT1G62760*	AT1G62760	LP: CGAATCTTGAAGCGAAGTCAC 60.01°C RP: TCCATTGCTAAAATTTCACGC 60.09°C	1236bp	596-896bp

* N/S, not specified
* Left border primers (LB) for the T-DNA insertion:

For SALK lines: ATTTTGCCGATTTCGGAAC

For SAIL lines: TAGCATCTGAATTTCATAACCAATCTCGATACAC

For GABI-Kat lines: ATAATAACGCTGCGGACATCTACATTTT

Homozygosity test results

Homozygosity tests were carried out in a two-primer fashion. As shown in Figure 4.3.4.1, the gene specific primers in mutants failed to amplify amplicons as in wildtype, meanwhile the left border primer together with right gene specific primer all gave clear amplifications of the T-DNA border sequences. All the used mutants passed this test and only some of the gel electrophoresis results were shown below.

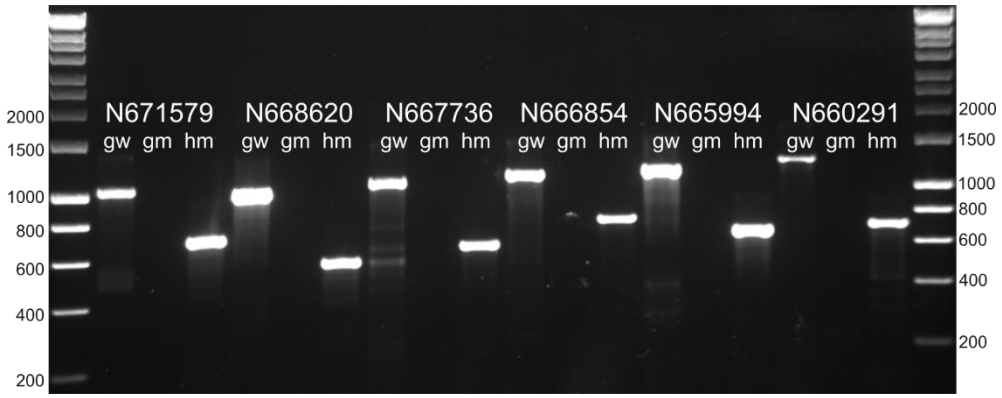

gw: gene specific primers (GSPs) in wildtype; gm: GSPs in mutants; hm: LB+RP in mutants

Figure 4.3.4.1 Homozygosity test results of selected Arabidopsis mutants. Two-primer test was carried out on selected HG-related Arabidopsis mutants, stock IDs were specified. Gene specific primers all failed to amplify amplicons in mutants as in wildtype (bands around 1kb), meanwhile all the T-DNA border primers successfully amplified parts of the insertions (bands around 600-800bp).

4.3.4.2 Syncytial walls induced in pectic HG related mutants

In situ analysis was carried out over all the mutants used and no significant change in terms of wall chemical compositions has been observed, comparing with wildtype results. The antibody binding patterns did not vary significantly among these mutants (apart from anti-HG LM19), thus only a few images were listed below. All images are included in supplementary materials.

The syncytial wall chemical structures induced in pectic HG related mutants

As shown in Figure 4.3.4.2, all the images were from equivalent sections thus direct structural comparisons can be made. As outlined in the Toluidine Blue O stained bright field image, the syncytial regions occupied over half of the whole vascular bundle. The anti-xylan LM11 gave clear binding to the xylem while hemicellulosic XyGs were universally distributed in all types of root cell walls, including the fine binding in syncytial walls. The LM6 arabinan epitopes were mainly located inside the vascular cells, with clear binding to the syncytial walls. The two anti-HG antibodies all gave strong binding over the root sections including the whole syncytia, with LM19 targeting more cell types comparing with LM20. The antibody epitopes, including LM25, LM6 and even LM19, distributed unevenly among the marked syncytial walls with visible layer differentiations.

For the antibodies used in all the mutants, they gave similar binding performance under most of the circumstances, indicating the structural constancy of nematode induced syncytial walls. However, the binding of anti-HG LM19 occasionally fluctuated to a visibly different level, thus requiring further quantifications.

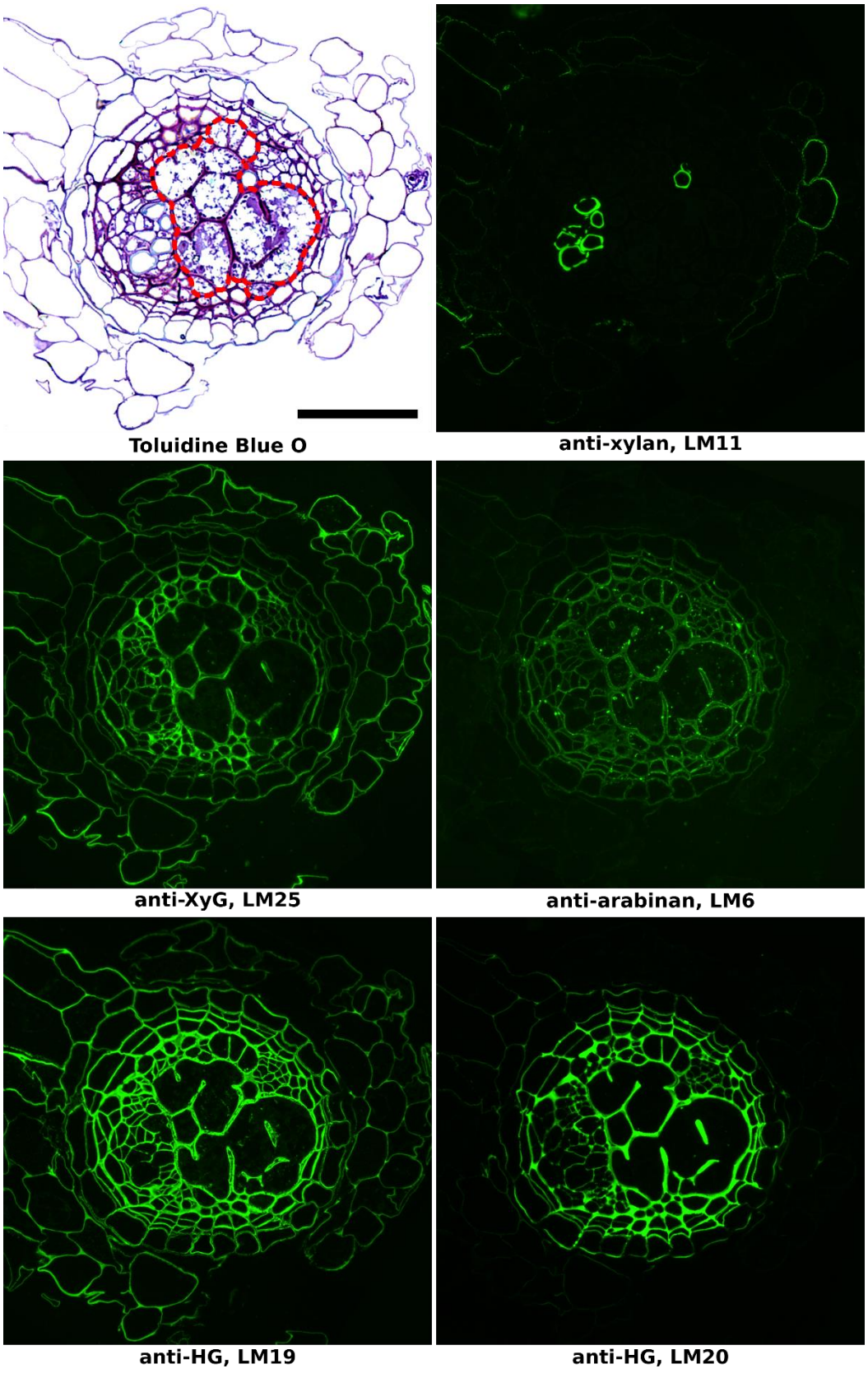

Figure 4.3.4.2 Immunolocalization of wall polymers in *H. schachtii* infested Arabidopsis mutant (21 dpi, *PMEI AT1G10770*). Bright field image is captured over Toluidine Blue O stained section. Syncytial regions are outlined with red dash line. Immunofluorescence (green) images are from the specific binding of anti-xylan LM11, anti-XyG LM25, anti-arabinan LM6 and anti-HG LM19 and LM20 using equivalent sections. (bar=50 µm)

The epitopes of anti-HG LM19 and LM20 are largely different

The two anti-HG antibodies LM19 and LM20 has been used throughout the whole study, designated to low/non-methyl HG and methyl-HG respectively.

As shown in Figure 4.3.4.3, apart from XyG indicated by LM25, the syncytial walls possess large amount of HGs of both forms indicated by the strong binding of both LM19 and LM20. When sections were pre-treated with Na_2CO_3 to remove the methyl groups, the binding of LM20 was eliminated and the binding of LM19 stayed strong. When sections were pre-incubated with pectate lyase, targeting non-methyl HG, the binding of LM19 was wiped out whilst the binding of LM20 largely unaffected. This all together show that the epitopes for both antibodies did not overlap, reassuring the reliability of the conclusions made over previous analysis.

Further quantifications of LM19 and LM20 binding have been made over all the tested mutants and the results are listed in the following sections.

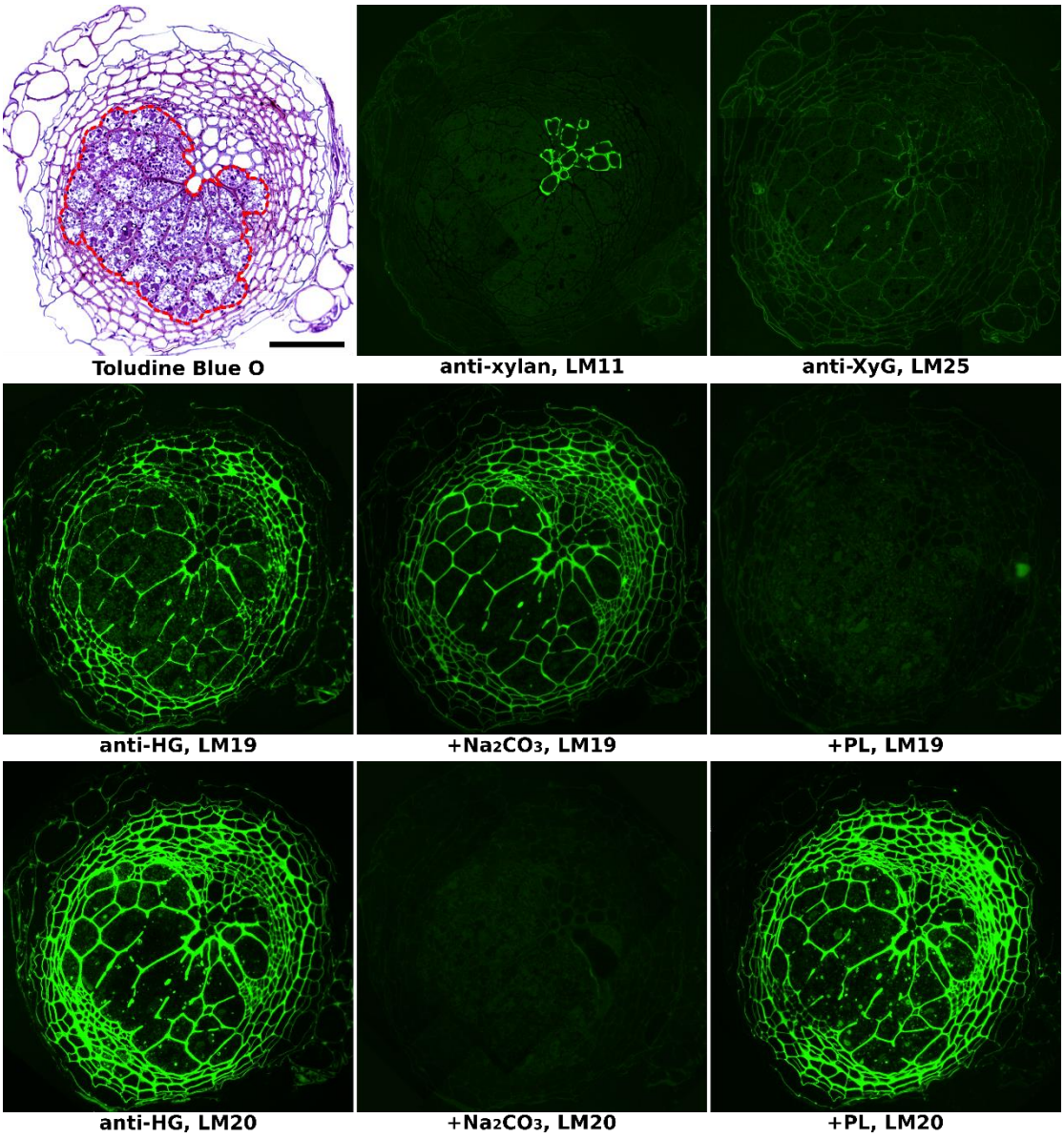

Figure 4.3.4.3 Immunolocalization of wall polymers in *H. schachtii* infested Arabidopsis mutant (21 dpi, *PMT4 AT1G13860*). Bright field image is captured over Toluidine Blue O stained section. Syncytial regions are outlined with red dash line. Immunofluorescence (green) images are from the specific binding of anti-xylan LM11, anti-XyG LM25 and anti-HG LM19 and LM20 using equivalent sections.Na_2CO_3, sections pre-treated with Na_2CO_3 to remove methyl; PL, sections pre-treated with only pectate lyase. (bar=50 µm)

Pectic HGs in the syncytial walls induced in pectic HG related mutants

Large scale of fluorescence quantifications have been carried out over all the mutant lines. The samples of different developmental stages, collected in previous section, were also include in this analysis. All the measurements were summarised in box and whiskers style plots, as listed below.

As shown in Figure 4.3.4.4 and Figure 4.3.4.5, the content of both non-methyl HG and methyl-HG varied among the tested mutant lines, though the LM19 represented non-methyl HG stayed at a much lower level in comparison with the values of LM20 targeted methyl-HG. The range of values obtained in wildtype controls as well as samples collected in previous section were taken as the 'normal range', capable of covering the syncytial wall HG values in most of the mutant lines, with only a few 'outliners'. This indicated that most of the mutant lines did not have significant impact to completely alter the syncytial wall HG properties. Therefore, the need of a dynamic yet mainly stable syncytial wall chemical compositions must be essential for successful nematode infections. Another possible reason might be the selection of candidate genes and mutant lines. Taking the complexity and largely unknown aspects of the pectic HG methyl esterification into consideration, choosing mutants mainly based on a microarray dataset might not be efficient enough. Therefore, expecting one single gene could alter the syncytial wall HG properties seemed to be unrealistic.

For the few mutant lines displaying outside-normal-range pectic HGs, nematode infection assays were performed to evaluate the impact of those targeted genes to nematode parasitism.

A

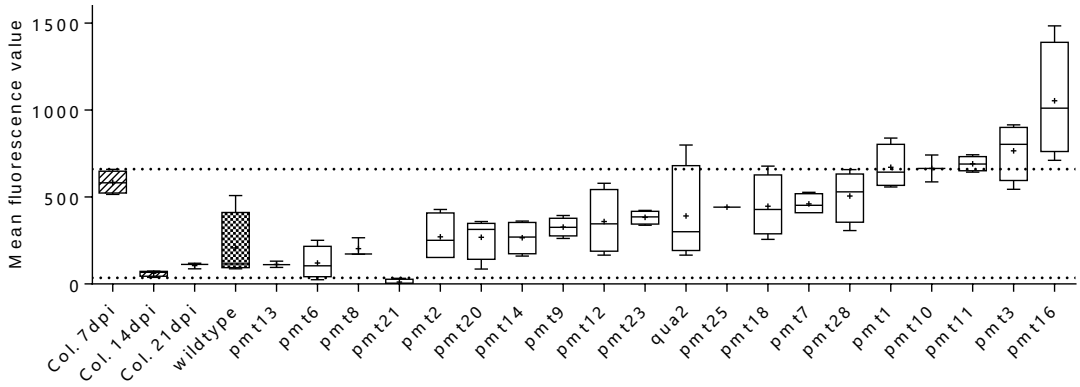

B

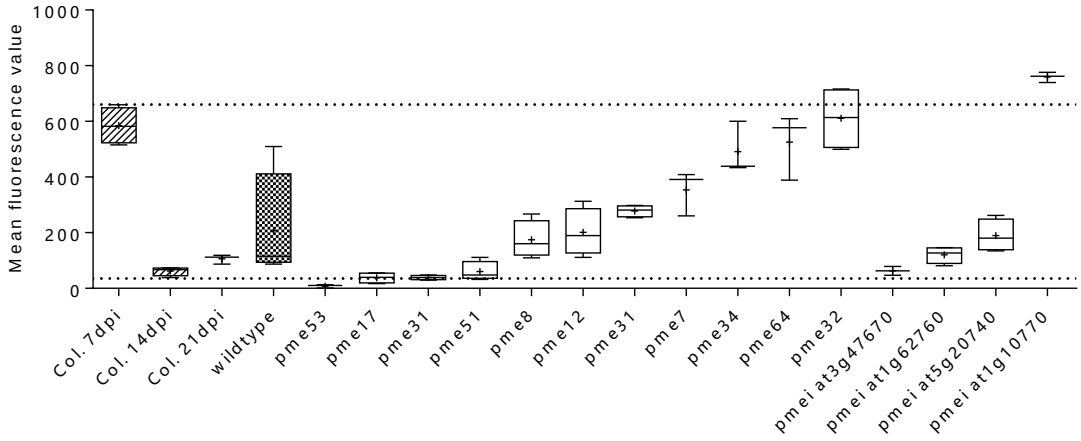

Figure 4.3.4.4 Fluorescence quantification of anti-HG LM19 in syncytial cell walls formed in Arabidopsis pectic HG related mutants. Values from mutants of probable PMTs were plotted as A. Values from mutants of PMEs and PMEIs were plotted as B. Wildtype stands for syncytia formed in wildtype control plants. Measurements were also taken over the samples collected in previous section 4.3.1, marked as Col. Whiskers stand for min to max and '+' stands for the mean. Grid lines indicate the range of obtained values in all wildtypes.

A

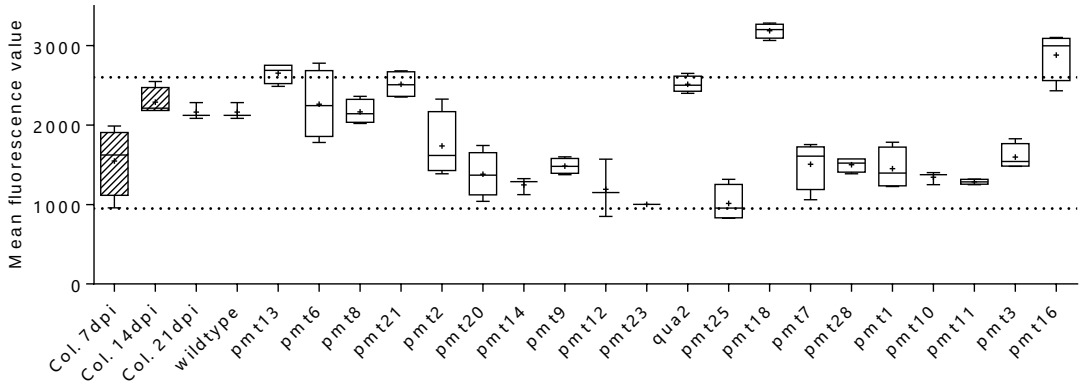

B

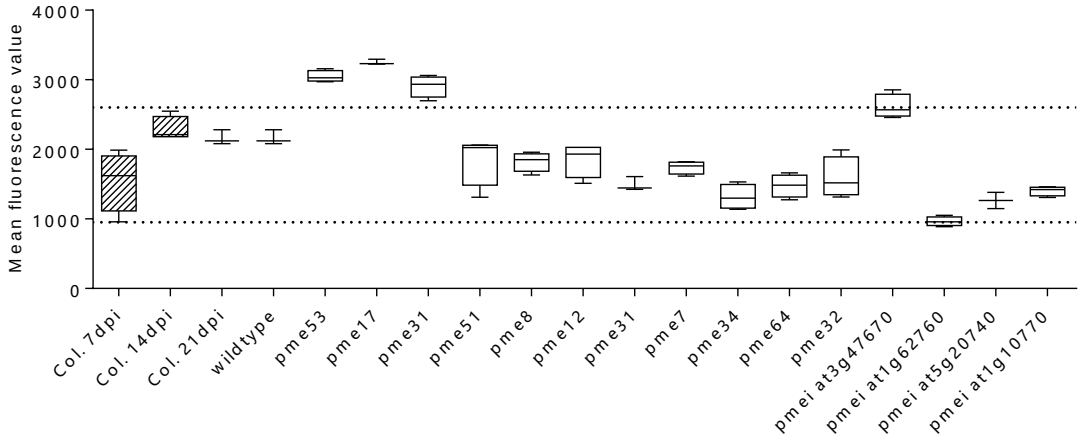

Figure 4.3.4.5 Fluorescence quantification of anti-HG LM20 in syncytial cell walls formed in Arabidopsis pectic HG related mutants. Values from mutants of probable PMTs were plotted as A. Values from mutants of PMEs and PMEIs were plotted as B. Wildtype stands for syncytia formed in wildtype control plants. Measurements were also taken over the samples collected in previous section 4.3.1, marked as Col. Whiskers stand for min to max and '+' stands for the mean. Grid lines indicate the range of obtained values in all wildtypes.

PME, PMEI and PMT genes expression analysis

The mutant lines used in this section were selected largely based on a previous microarray dataset (Szakasits, Heinen *et al.* 2009) and further cell wall analysis was proceeded using *H. schachtii* induced syncytia in those mutants. As given by the quantification results of pectic HG immunolabelling, the complexity of the formation and transformation process of syncytial wall pectic HG methyl esterification was revealed. Large genes families are postulated to be involved in this development, however only a few of them are annotated with clear functions. A recent study has included the new transcriptome data from *H. schachtii* infected Arabidopsis using RNA-seq (Shanks, Rice *et al.* 2015), a technology with advances over microarray, capable of providing precise measurements of gene expression at high dynamic range (Mortazavi, Williams *et al.* 2008, Wang, Gerstein *et al.* 2009). In this section, the RNA-seq raw data of both infected and uninfected Arabidopsis at 4 dpi and 10 dpi were retrieved from this study (Shanks, Rice *et al.* 2015), in order to assess the gene expression change during syncytium forming from those pectic HG related large families.

Raw sequencing data were first download from NCBI (BioProject Accession: PRJNA294313). Reads quality check was performed using FastQC (Andrews) and quality trimming was proceeded using Trimmomatic (Bolger, Lohse *et al.* 2014). *De novo* transcriptome assembly was then performed using Trinity (Haas, Papanicolaou *et al.* 2013) with in silicon normalisations. Sequence redundancy of the transcriptome assembly was reduced using CD-HIT (Fu, Niu *et al.* 2012). Transcript annotation was performed by local BLAST (Altschul, Gish *et al.* 1990) and expression estimation was carried out using Kallisto, estimating TPM (transcripts per million) values for each transcript in each of the data sets (Bray, Pimentel *et al.* 2016). Genes of interests were manually picked and gene-level TPM estimates were obtained by summing the corresponding transcript-level TPM estimates (Soneson, Love *et al.* 2015). Overall, in Arabidopsis, there are 67 PMEs (PF01095, EC 3.1.1.11) as shown in the carbohydrate-active enzymes database (Lombard, Golaconda Ramulu *et al.* 2014), 69 PMEIs (Saez-Aguayo, Ralet *et al.* 2013) and PMTs are chosen largely based on predicted S-adenosylmethionine-dependent methyltransferase activity in NCBI as there are only two PMTs with clear functions reported currently. The expression change was then calculated as a log2 fold change for genes with valid abundance estimation values and plotted in Figure 4.3.4.6 for PMEs, Figure 4.3.4.7 for PMEIs and probable PMTs in Figure 4.3.4.8.

As shown in the following figures, only a few genes displayed significant expression change among these large gene families. However, it was worth mention that the gene expression profile did not match well with the syncytial wall analysis data over selected mutants. For instance, the *PME53* (*AT5G19730*), *PME31* (*AT3G29090*) and *PME17* (*AT2G45220*) did show significant impact on syncytial wall pectic HGs over other mutant lines, meanwhile only had slight expression change after parasitism. Mutant *pmt16* (*AT2G45750*) displayed increased levels of both forms of HGs among all the PMT mutants, also only show slightly down regulated gene expression. The reasons for such mismatch probably was due to the complexity of pectic HG synthesis and transformation. For example, the PMEs can spatially de-methyl esterify methyl-HG where required, thus its expression level did not necessarily fluctuate hugely. Meanwhile, PMEIs can also be expressed spatially to participate such specific regulation of PME activities. Another reason might be the way the samples were

collected, using the infected whole roots instead of just the syncytial content as in the microarray study (Szakasits, Heinen *et al.* 2009) might cover the possible small expression changes meanwhile overpower the precision benefits of RNA-seq technology. Overall, choosing mutants for further investigation based on the actual syncytial wall structural changes obtained via *in situ* analysis and quantifications seems to be an optimal option at this stage.

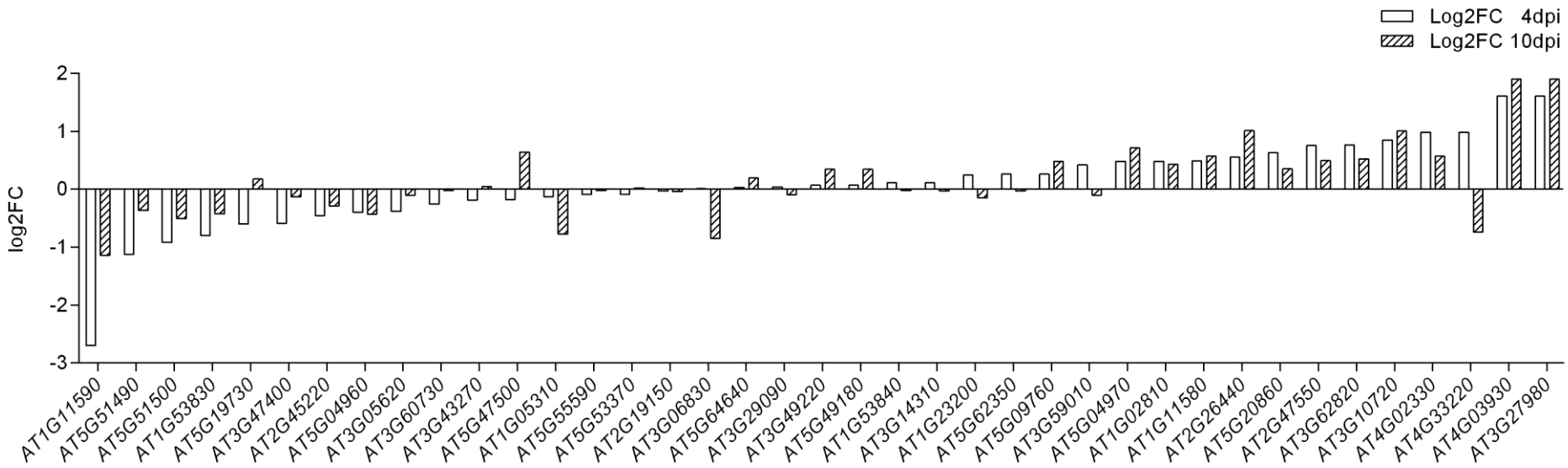

Figure 4.3.4.6 Expression of PME genes. Gene expression is shown as fold change (FC) between average normalised infected sample and uninfected sample on a per gene basis.

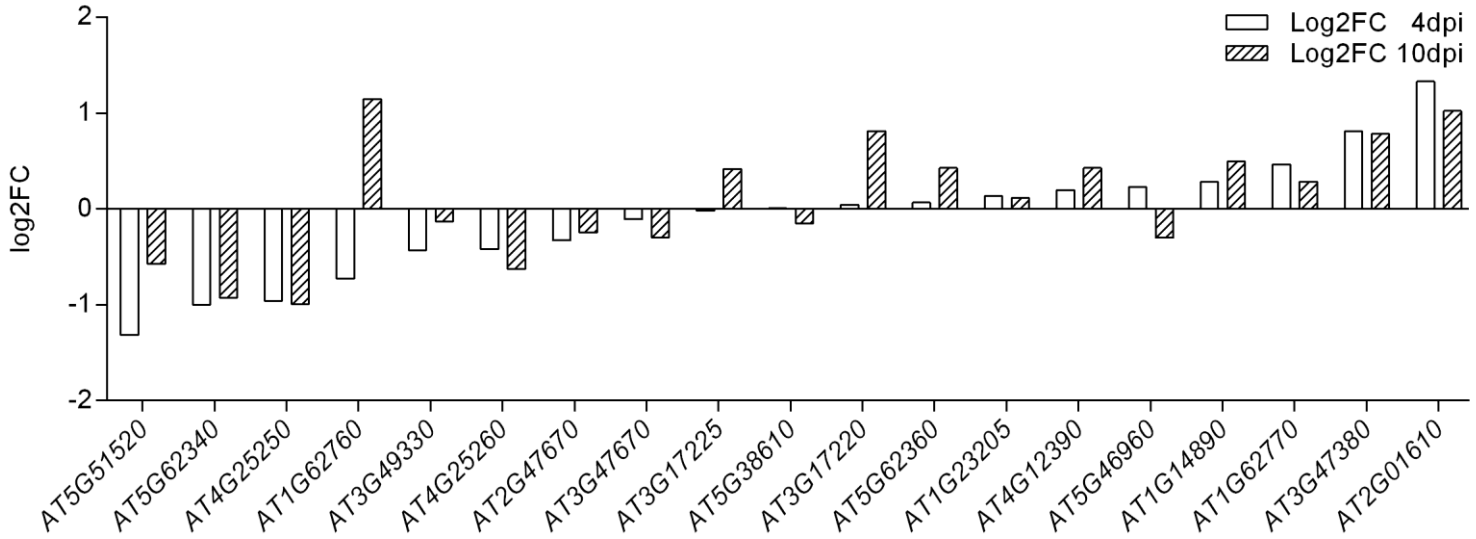

Figure 4.3.4.7 Expression of PMEI genes. Gene expression is shown as fold change (FC) between average normalised infected sample and uninfected sample on a per gene basis.

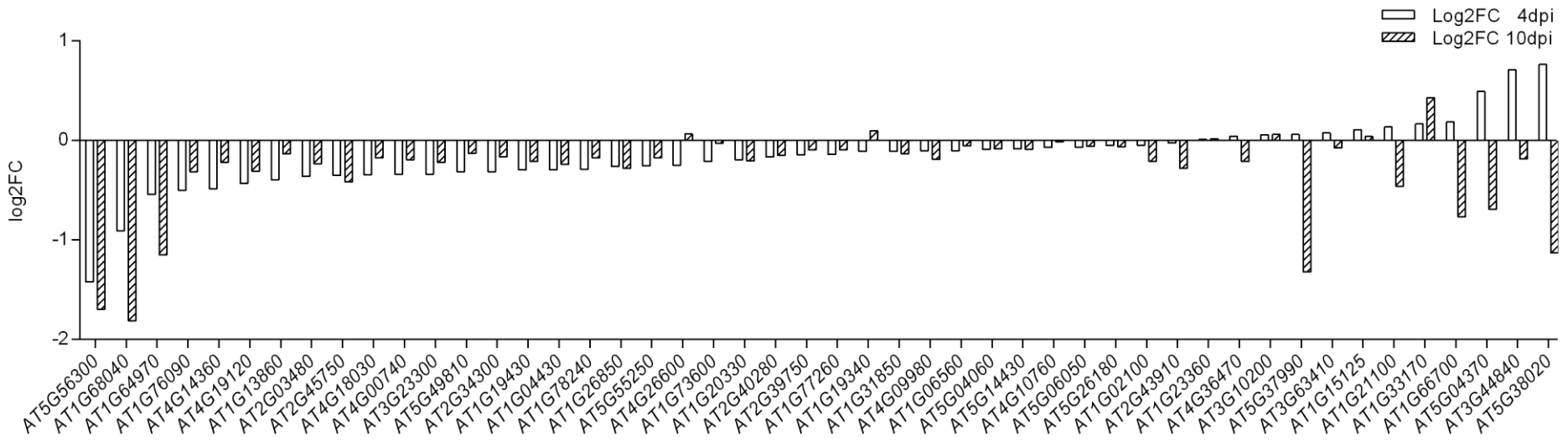

Figure 4.3.4.8 Expression of probable PMT genes (S-adenosyl-L-methionine-dependent methyltransferases activity). Gene expression is shown as fold change (FC) between average normalised infected sample and uninfected sample on a per gene basis.

Nematode infection assay for selected mutants

Based on the syncytial wall microstructures, meanwhile referring the microarray and RNA-seq data, several mutant lines were chosen to further investigate nematode susceptibility, including *PME53* (*AT5G19730*), *PME31* (*AT3G29090*), *PME17* (*AT2G45220*), *PMEI AT1G10770*, *PMT16* (*AT2G45750*) and *PMT11* (*AT2G39750*).

As shown in Figure 4.3.4.9, the nematode infection assay suggested significant changes in susceptibility among these mutants, though it was still hard to clearly interpret the causes. For instance, *PMT16*, *PME53* and *PME17*, all with a slightly decreased expression within syncytial content along with parasitism and revealed to be possessing high levels of methyl-HG, show different nematode susceptibility change in mutants. *PME31*, reported to be related to plant immunity against pathogen (Bethke, Grundman *et al.* 2014) also show increased susceptibility to nematode infection, though its expression has hardly changed in syncytium. The nematode infection assay showed that those pectic HG related genes might function in different ways and this also indicated that the correlation among syncytial wall pectic HGs, related gene expression levels and the function in nematode successful infestation were complex and largely obscure.

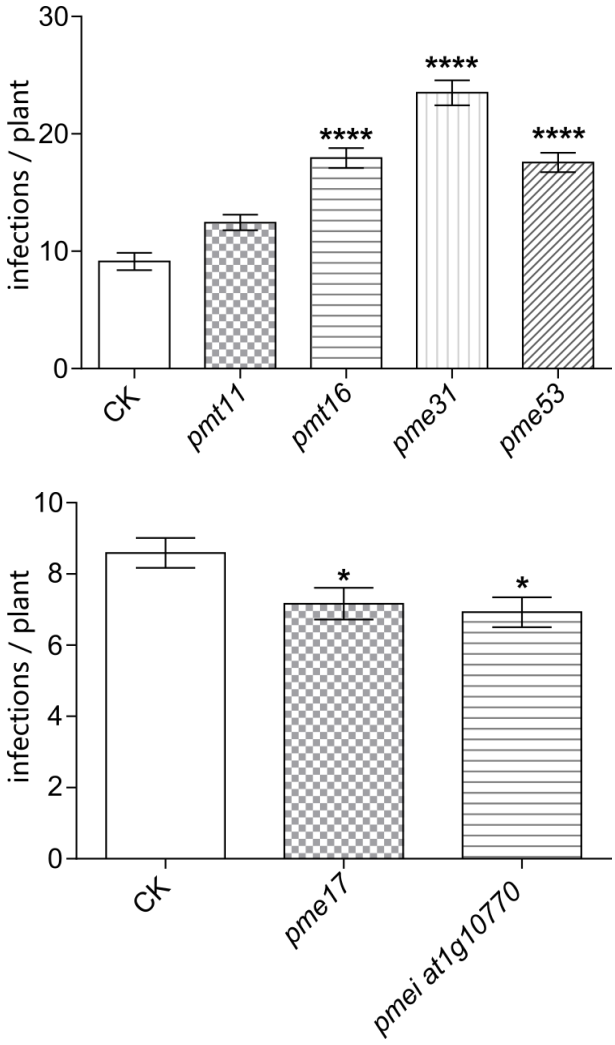

Figure 4.3.4.9 Nematode infection assay performed in Arabidopsis pectic HG related mutants. CK stands for infections in wildtype plants. Mutants targeted genes include *PMT11* (*AT2G39750*), *PMT16* (*AT2G45750*), *PME31* (*AT3G29090*), *PME53* (*AT5G19730*), *PME17* (*AT2G45220*) and *PMEI AT1G10770*. Error bars show standard error of mean. One-way ANOVA analysis was performed and asterisks represent significant differences (P<0.0001 level, ****; P<0.05 level, *).

The cell wall chemical structures of syncytia induced in pectic HG related mutants

Large scale of immunolabelling based tests were carried out over syncytial walls formed in a range of pectic HG related Arabidopsis mutants. The results all together show the complexity as well as dynamics of syncytial wall chemical compositions. The mature syncytia required a general stable wall compositions and the methyl esterification status change was among the key features during nematode parasitism. Although, no single gene was yet discovered responsible for this transformation, the data still provide support for previous proposed conclusions as well as pointing out reasons from different aspects which could jointly cause this change.

4.4 Discussion

The cell wall chemical structures of syncytia formed in XyG and arabinan deficiency mutants, as well as a range of pectic HG related Arabidopsis mutants, have been analysed. Meanwhile, the structural changes, especially the methyl esterification levels of pectic HG, were then further investigated via quantification of antibody binding in the syncytial regions formed in these mutants and wildtype Arabidopsis cultured with simulated stress.

***H. schachtii* induced syncytial cell walls maintain general structural consistency and fluctuated methyl esterification levels of pectic HG during parasitism**

Three different stages of syncytia were analysed and the main cell wall components, XyG, methyl-HG and pectic arabinans, were shown to be stable. The only obvious change observed was the non-methyl esterified HG, represented by LM19 binding. The following quantification revealed that the level of methyl esterification fluctuated during syncytium development.

The modifications of pectic HG, the major pectin, was correlated to cell wall physical properties, affecting cell growth. One of these general modifications was methyl esterifying, which influenced the forming of the pectin gel with the presence of Ca^{2+} (Palin and Geitmann 2012). The removal of methyl groups would cause increased stiffness of the cell wall and its specific regulation was correlated with such as Arabidopsis hypocotyl cell elongation (Derbyshire, McCann *et al.* 2007), phyllotaxis (Peaucelle, Louvet *et al.* 2008) and the well-studied pollen tube growth model (Bosch and Hepler 2005, Palin and Geitmann 2012). In this study, monitoring the changes of methyl esterification status along with syncytium developmental stages has been performed via local fluorescence quantification within syncytial walls. The syncytial cell wall HG was reported to be heavily methyl esterified (Davies, Lilley *et al.* 2012) when fully mature, then later proved to be transformed from non-methyl HG to methyl-HG along with its development (Wieczorek, Elashry *et al.* 2014). Although the changes have been recorded, due to the magnification of those images and lack of quantification, until this study we could then further confirm such alteration.

The pectic HG was secreted into the walls as highly methyl-esterified forms, subsequent de-esterification could be mediated spatially by PMEs, even interacting with PMEIs in various ways. In plant-parasitic nematodes interaction, such modifying enzyme was also reported to be involved. For instance, Arabidopsis overexpress *PME3* was shown to produce longer roots and exhibit increased susceptibility to *H. schachtii*, meanwhile *pme3* knockout mutant exhibit the opposite phenotypes, as a nematode produced cellulose binding protein was shown to target and activate PME3 (Hewezi, Howe *et al.* 2008). Now, the fact that syncytial cell walls contain abundant methyl-HG was revealed (Davies, Lilley *et al.* 2012, Wieczorek, Elashry *et al.* 2014), thus the relation between nematode infection and these HG methyl esterification status related genes should be paid more attention, as researches have been covering lots of other aspects such as cell wall degrading/degrading-related enzymes (Hewezi 2015). However, the lack of direct evidence makes the functional assumptions for this structure entirely based on researches in other areas (see Chapter 3),

not to mention the causes for the fluctuations of methyl esterification degrees observed in this study.

From the early forming stage to fully functioning stage, the syncytium expand mainly through incorporating neighbouring cells via local cell wall dissolutions. However, the synthesis of new cell wall materials are also required concomitantly with the cell wall degradation (Bohlmann and Sobczak 2014). The cell modifying enzymes reported, such as *PME3* (Hewezi, Howe *et al.* 2008) and pectate lyase-like (PLL) *PLL18* & *PLL19* (Wieczorek, Elashry *et al.* 2014), are more related to either remove methyl esters from methyl-HG or do not digest highly methyl-HG, leaving the origin of the abundant methyl-HG in syncytial walls obscure. The drop of non-methyl HG level could due to the pectate degrading enzymes, either secreted by nematodes or from host plant cells, coping with reducing cell wall stiffness in favor of syncytium expending. Meanwhile, those reported enzymes are unlikely to affect the heavily methyl-HG in mature syncytia, as this feature was observed among all successfully established syncytia in different plant species (see Chapter 3) and different types of mutants. How this structure was formed and retained during the parasitism remains to be elucidated. The comparative importance of cell wall degrading versus new cell wall materials synthesis in syncytium forming certainly requires more scientific attention.

The methyl esterification level in *H. schachtii* induced syncytia could be affected by water stress

Water stress was posed during nematode infestation, the immunolabelling results once again proved that the functioning syncytia would maintain general stable cell wall compositions. While the changes of pectic HG methyl esterification level was observed via local fluorescence quantification, shown to be affected by the level of stress exposed to. Light water deficiency would cause increased amounts of non-methyl HG in syncytial walls comparing with untreated control. However, in the functioning mature syncytia, content of heavily methyl-HG remained abundant with only small fluctuations. The overall changing trend did not differ from previous results: the amount of non-methyl HG decreases along with syncytium maturing while the methyl-HG increases and stays at high levels.

The cause for the change of non-methyl HG levels remain largely unknown. One possibility is that moderate water deficit would stimulate primary root elongation as well as the rate of cell production in Arabidopsis (van der Weele, Spollen *et al.* 2000), and the general higher amounts of non-methyl HG was due to the not fully degraded host cell wall pectic HG. Another possible explanation is the imposed water stress could decelerate the syncytium development process, resulting in the decline of non-methyl HG in a slower rate. This change of development might also account for the fluctuated methyl-HG observed.

In conclusion, via local quantification of antibody binding, we confirmed the alterations of the heavily methyl-HG and non-methyl HG content during parasitism. Based on the above analysis, we propose that the HG content might be affected by host cell growth conditions and the major role in syncytium is more likely related to, such as water and nutrients flow,

rather than providing mechanical support.

The syncytial walls maintain stable chemical structures meanwhile reflect host cell wall characteristics

The proposed function of the two major cell wall components observed in syncytial walls, XyG and pectic arabinans, raise the possibility to use related Arabidopsis mutants to evaluate their importance during nematode parasitism. As depicted in results, no visually significant alternation of antibody binding observed in syncytial walls comparing with wildtype syncytia, apart from the eliminated XyG in syncytial regions along with other host root cell walls in the mutant.

Pectic arabinans are the general common sidechains of pectin in plants and they were shown to be abundant in the syncytial cell walls. Previous researches presumed that the function of arabinans are correlated mostly to cell wall flexibility in various cell types (Jones, Milne *et al.* 2003, Moore, Farrant *et al.* 2008, Cankar, Kortstee *et al.* 2014). The arabinan deficiency mutants used in this study were shown to possess reduction in arabinan content (Harholt, Jensen *et al.* 2006) and displayed altered inflorescence stem heights against mechanical stress (Harholt, Jensen *et al.* 2012, Verhertbruggen, Marcus *et al.* 2013). However, these mutants did not affect successful syncytia forming and the syncytial walls still possess pectic arabinans with different patterns, indicated by anti-arabinan antibodies LM13, LM16 and LM6. It is clear that the presence of arabinans is essential for functioning syncytia, although if the syncytial wall arabinans content has changed along with their hosts are still unknown.

As the most abundant hemicellulose in primary cell walls, XyGs are found in almost every land plant (Park and Cosgrove 2015). Its function was depicted as forming tethered network with cellulose and providing the cell wall extensibility during cell growth as those cross-links were modified by enzymes. However, based on recent discoveries, this model was updated with the 'biomechanical hotspot' hypothesis, the mechanically importance of XyG in primary cell wall is restricted to those limited sites where XyGs are closely intertwined with cellulose (Park and Cosgrove 2015). In the *xxt1/xxt2* mutant, there was no detectable levels of XyG but only minor altered phenotype (Park and Cosgrove 2012). However, this did not prevent syncytia initiation and development, even the same chemical structure feature was reserved in syncytial walls. The immunolabelling results demonstrated that XyG could not be the one component to provide major mechanical properties needed in syncytia though it is widely discovered in syncytial walls. Based on the successful development of cyst nematodes, we believe that the syncytium in this mutant should still maintain its ways of functioning, including proper cell wall structure to cope with the high turgor pressure within, possibly some novel mechanisms adapted from the host cell walls as compensating the presumed role of XyG.

Considering the largely unknown connections among cell wall polymers, the use of mutants provided new insights to understand cyst nematode adaptations to hosts of various conditions. Those revealed syncytial cell wall components are more likely to form a dynamic complex together in order to be functioning during parasitism.

Chapter 5 Investigating the use of a root-cap specific promotor in transgenic wheat

5.1 Introduction

During the cyst nematode life cycle, the successful initiation and formation of a functional syncytium is a crucial step. In the past few decades, fine structural observations of several cyst nematode induced syncytia as well as related nematode effectors have been studied, providing valuable information in this plant-nematode interaction process (as reviewed in Chapter 1). In this study, the cell wall chemical structures of the unique feeding sites induced in some of the most economically important crops were analysed extensively, using a set of plant cell wall antibodies. Further investigations should be made in order to extend our understanding of this complex forming process, as well as other related aspects in the cyst nematode parasitism.

In the study of the plant parasitic cyst nematode interactions, the use of *H. schachtii* infested Arabidopsis as a model system has yielded great outcomes in many aspects (Sijmons, Grundler *et al.* 1991). This is due to the established efficient transformation protocols (An, Watson *et al.* 1986, Lloyd, Barnason *et al.* 1986, Feldmann and David Marks 1987, Clough and Bent 1998) of this model plant (Meinke, Cherry *et al.* 1998) with other easily accessible resources, such as the large collection of insertion mutants (Alonso, Stepanova *et al.* 2003), well functionally annotated full-length cDNA (Seki, Narusaka *et al.* 2002) and informative databases (Rhee, Beavis *et al.* 2003). Meanwhile, Arabidopsis is also used as a model system in pure plant cell wall research (Liepman, Wightman *et al.* 2010), and therefore this system was again included in this syncytial cell wall study. However, Arabidopsis is not a host of economic importance. Meanwhile, cyst nematodes infected hosts in agriculture including almost all the major crops, such as the cereals infected by cereal cyst nematodes (CCNs). Therefore, research implemented in these natural hosts should be able to gain more direct use in the field.

Among the nematode constraints on global production of cereals, the CCNs play a crucial part. The CCNs (*Heterodera avenae* complex, avenae group) are a group of 12 closely related species which have been recorded to adversely affect rain-fed wheat production areas of the world. The most commonly reported species include *H. avenae*, *H. filipjevi* and *H. latipons* (Nicol, Elekcioglu *et al.* 2007). CCN infection can cause wheat roots to become bushy, knotted and shallow, therefore reducing the ability of roots to absorb water and nutrients and resulting in yield loss. Besides, once CCNs have been introduced into a field, eradication is nearly impossible. One known example was that the cyst retained potato cyst nematodes were able to stay dormant for more than 20 years in the field (Turner 1996). Meanwhile, as the most important food staple in many aspects, using 17% of the global cultivable land and accounting for 20% of the calories consumed by humans (FAO 2009, Brenchley, Spannagl *et al.* 2012), wheat (*Triticum aestivum* L.) production is seriously hampered by the CCNs, not to mention simultaneously facing other environmental stress

including climate change. Therefore, comprehensive researches is needed to further elucidate the parasitism process of CCNs during wheat production to aid future nematode control.

As the key step for successful CCN infestation, the complex forming process of the feeding sites is yet largely unknown. In the previous sections, the feeding structures induced in wheat by two of the most important CCN species, *H. avenae* and *H. filipjevi*, have been analysed. Continuous efforts should be made to reveal the mechanism of this crucial transformation process. Therefore, taking both the narrow host range of CCNs and the importance of wheat production into consideration, the use of recombinant DNA based biotechnology to generate transgenic wheat lines holds the potential to provide a platform for further CCN parasitism research, including the mechanism of the formation of the feeding site. Such efforts have been made in a range of plants as well as the most widely used model plant Arabidopsis. Among all these reported transgenic plants, the use of root specific promoters (Lilley, Urwin *et al.* 2004, Lilley, Wang *et al.* 2011, Green, Wang *et al.* 2012, Onyango, Roderick *et al.* 2016), rather than constitutive promoters (Urwin, Troth *et al.* 2001, Urwin, Green *et al.* 2003, Liu, Hibbard *et al.* 2005), were reported to be able to limit the transgene expression to the cyst nematode targeted root systems (Lilley, Urwin *et al.* 2004). Such a strategy should also be applicable in generating transgenic wheat lines for CCNs research.

Although considered as the world's most important crop, wheat is far behind other major cereals in terms of biotechnology application. The first successful transformation was achieved using microprojectile bombardment (Vasil, Castillo *et al.* 1992), and later *Agrobacterium*-mediated transformation was also reported (Cheng, Fry *et al.* 1997). However, despite these successful first reports, the applications of wheat genetic transformation is still largely restrained due to its low efficiency and feasibility, mostly less than 5%. Recently, two studies reported highly efficient *Agrobacterium*-mediated transformation using wheat immature embryos, with reported efficiency up to 90% (Richardson, Thistleton *et al.* 2014, Ishida, Tsunashima *et al.* 2015). Among all the reported cases, most of the studies used immature embryos as explants, as they have the highest regeneration efficiency in tissue culture; and biolistics and *Agrobacterium*-mediated transformation were given priority when choosing transformation methods as both with sufficient successful events reported (Li, Ye *et al.* 2012).

In this section, a root cap-specific protein promoter (RCP1), shown to be capable of driving gene expression specifically in tip (Matsuyama, Yasumura *et al.* 1999, Onyango, Roderick *et al.* 2016), was used to generate transgenic wheat, in hoping to use this spatial expression system for further investigation of the complex wheat-CCN interactions, for instance, the initiation and formation the feeding sites. Immature embryos of wheat cultivar Bobwhite were chosen as explants and both the *Agrobacterium*-mediated transformation and microprojectile bombardment were implemented.

5.2 Materials and methods

5.2.1 Media preparation

Tissue culture media were made fresh before use. The base media was Murashige and Skoog medium (MS) with modifications or added supplements to fulfil specific purposes. Media used in this study were as follows:

MS: made from pre-formulated powder (Murashige & Skoog medium including vitamins, Duchefa Biochemie B.V.) with 20 g/L sucrose and 1% plant agar (Duchefa Biochemie B.V.)

MS+: MS (sucrose 20 g/L, agar 1%) plus 2,4-Dichlorophenoxyacetic acid (2,4-D) 2mg/L, glutamine 500 mg/L, casein hydrolysate 100 mg/L

MSM: MS+ with sucrose replaced by 150 g/L maltose for freshly disserted embryos and 0.2M D-sorbitol (36.43 g/L) + 0.2M D-mannitol (36.43 g/L) for cultured calli (2,4-D is not necessary)

MSR: MS with 0.3 mg/L Indoleacetic acid (IAA) and 1 mg/L Kinetin, add 25 mg/L Hygromycin for selection.

MSRT: ½ MS (½ MS basal salts with full-strength vitamins) plus 25 mg/L Hygromycin and 0.3 mg/L IAA

MSI: MS+ without agar, plus 200 µM Acetosyringone

All media were autoclaved after adjusting pH to 5.8. Thermally unstable substances were filter sterilised and added before the autoclaved media set. For *Agrobacterium* mediated transformation, all media used after the inoculation step had an extra 160 mg/L Timentin added.

5.2.2 Explant preparation

As shown in Figure 5.1, the spring wheat cultivar Bobwhite was grown in the greenhouse as described in 2.1.5. Spikes together with flag leaves were collected 12-14 days post anthesis and were kept, away from light at 4 °C, for up to a week before use. Immature seeds were collected into a sterile glass container and surface sterilised in the following steps in the flow hoods: 75% EtOH for 1 minute, followed by 1% NaClO for 20 minutes with gentle shaking in the dark (alternatively use 25% Bleach for 20 minutes), and finally rinse with sterile water for at least 5 times.

Embryos with a diameter around 1.1 mm were dissected using a sterile sharp scalpel blade (#11). The embryonic axis was cut off and the embryos were placed immediately onto freshly made callus induction media with scutellum side up. The ideal stage of embryos was half translucent and water-like; too young or large creamy too old ones were discarded. As shown in Figure 5.1 B, the large old embryos developed shoots right away and the young

ones will not develop calli efficiently. About 50 embryos were collected on each plate and the induction of embryogenic calli was carried out by keeping the plates at 25 °C in dark for 3-7 days.

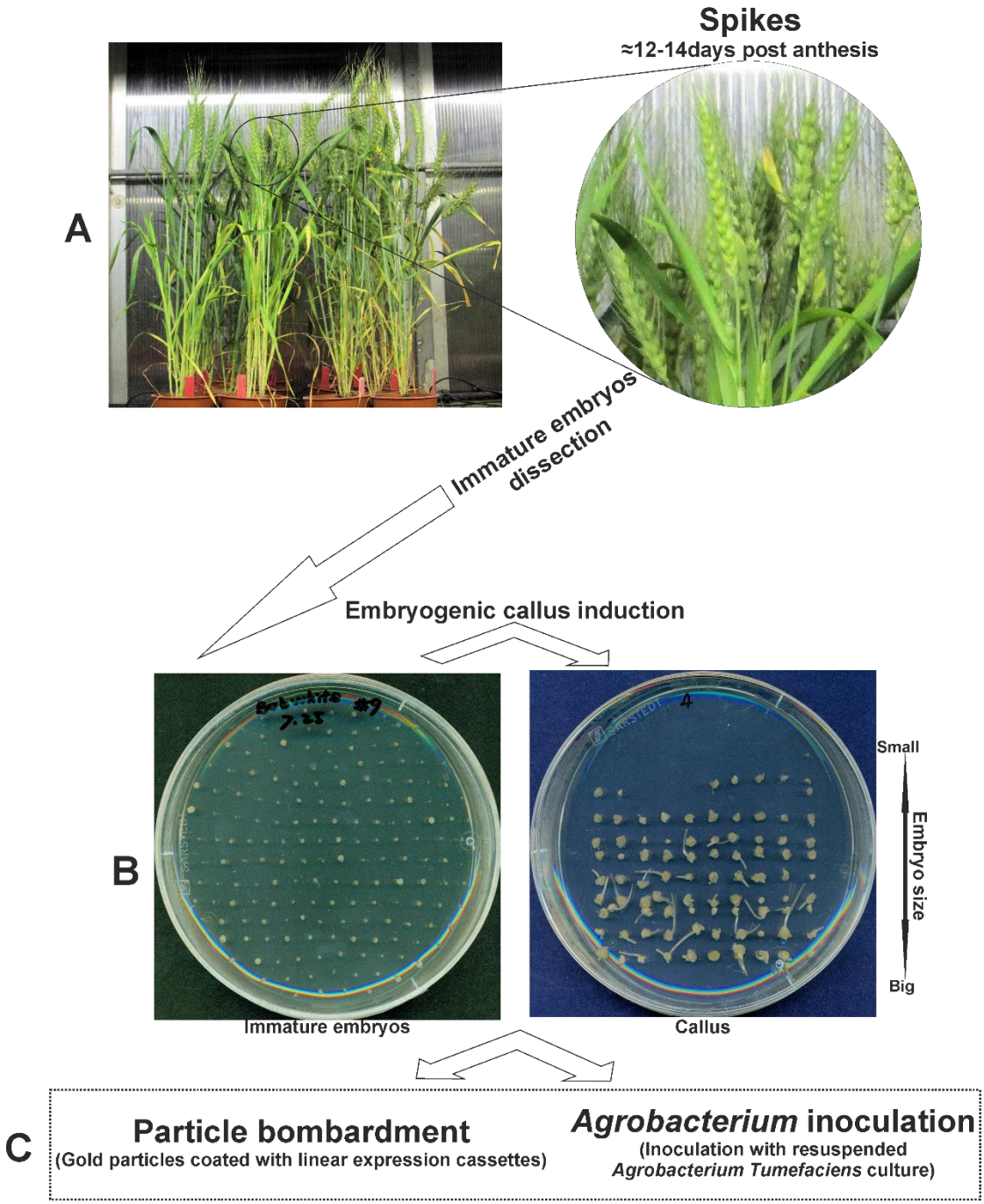

Figure 5.1 Explant preparation for wheat genetic transformation. A. Immature seeds were collected from wheat spikes around 12-14 days post anthesis. **B**. Dissected embryos were cultured to induce embryogenic calli. The callus induction efficiency was correlated with embryo size. **C**. Explants were proceeded to transformation steps, in this study, microprojectile bombardment and *Agrobacterium* inoculation.

5.2.2 Transformation procedure

Two widely used transformation methods, *Agrobacterium*-mediated transformation and particle bombardment, were carried out in this study.

5.2.2.1 *Agrobacterium* mediated transformation

Agrobacterium transformed with recombinant plasmid was cultured in freshly made LB medium with antibiotics at 28 °C. OD_{600} of the cell culture was monitored until it reached around 0.6. Cell culture was then centrifuged at 4500g for 10 minutes and the pellet was resuspend in inoculation medium MSI. Silwet L-77 was later added to a final concentration of 0.015%. The whole medium was then poured into the plates with embryogenic calli and left in dark for 0.5-1 hour. Before starting, some calli were kept as control.

Inoculated calli were transferred to a new MS+ plate or a blank plate with a piece of sterilised filter paper for co-culture for 2 or 3 days in the dark. Calli were then transferred to a new plate of MS+ medium with added Timentin for 1 week. Any possible over-growth of *Agrobacterium* was continuously monitored.

5.2.2.2 Particle bombardment

Pre-cultured embryos were placed in a 3 cm diameter circle on a smaller sized Petri dish poured with MSM medium. On average, embryos to be bombarded were kept after 1.5 to 2 hours on MSM in the dark. They were left on MSM overnight after the bombardment.

For particle bombardment, DNA was coated onto gold particles in the following steps:

1. Preparation of the 0.6 µm gold particles (Bio-Rad) was carried out based on the Bio-Rad instructions.
2. On a sterilised bench, the macrocarriers holders, stopping screens and the rupture disks were soaked in 75% EtOH. The macrocarriers were soaked in 100% EtOH for 20 minutes and air dried before use.
3. 5 µg insert DNA were quickly mixed with 20 µL prepared gold on ice by pipetting. The gold particles were then mixed with 50 µL 2.5 M $CaCl_2$ and 20 µL 0.1 M spermidine. The mixture was vortexed immediately for 15 minutes with intervals of 10 seconds every minute.
4. The mixture was centrifuged for 5 seconds at <4000 rpm. The supernatant was removed and the pellets were resuspended in 250 µL 100% EtOH. After centrifuging for 7 seconds at <6500 rpm, the supernatant was carefully removed. The gold particles were then resuspended in 100 µL pure EtOH.
5. The macrocarriers were assembled in the holders and 10 µL of the gold particles were carefully pipetted to the centre of the disk. This was left to air dry and was used as soon as possible.
6. The rupture disks (900psi, Bio-Rad) and stopping screens were assembled in place and the following bombardment steps were executed according to the instruction manual for PDS-1000 / He system (Bio-Rad).

Calli were then transferred to a new plate with MS+ medium the next day and cultured for 1-2 weeks at 25 °C. Lower light was given in the first several days and later they were kept in light. The growth of calli was checked and any possible contamination was removed immediately.

5.2.3 Regeneration and characterisation

The whole screening and regeneration steps were illustrated in Figure 5.2. After the above transformation procedures, all calli were transferred to new plates with MSR medium (add Timentin for *Agrobacterium* inoculated calli) with proper selection on for 10-14 days in light. Medium was changed every 10-14 days. Regenerated plantlets were transferred to test tubes with soft MS or MSRT media (10 g/L plant agar) for root system regeneration. Naphthaleneacetic Acid (NAA) was used for root development when needed.

Regenerated plants were carefully picked up from the culture media without damaging the roots. Extra medium was washed off and they were transplanted into pots filled with damp compost. Keeping them away from strong light until new leaves started to grow. Further maintenance was carried out as described in 2.1.5. DNA was extracted from newly generated leaves for PCR assay and all negative plants were then eliminated. Downstream characterisation was performed accordingly.

Primers used for adding restriction enzyme digestion sites:

RCP_promoF_HindIII: ACGCCAAGCTTCCTATGTCAATTAAG

RCP_promoR_NcoI: ACACCATGGAGCTCATACTGCTTCTG

Primers used for transgenic plants PCR assay:

gusA specific primers with targeted amplicon of 578bp:

F: AAGTCTTTATACCGAAAGGTTGGGCAGG; R: GATATCACACTCTGTCTGGCTTTTGGCT.

RCP1 promoter specific primers with targeted amplicon of 573bp:

F: TGATCAGATCCTAGATTCGCCCCTGATT; R: TTACTAGCTCGAAAGGAAAGAAGGCGTG.

GUS histochemical staining was performed by adding roots to a working solution and incubate at 37 °C and then rinse thoroughly in water. The X-gluc (5-Bromo-4-chloro-3-indolyl-β-D-glucuronic acid) working solutions was made up with 50 µL X-gluc 0.1M stock to 950 µL X-gluc buffer. The X-gluc buffer was made with 100 mM phosphate buffer (pH 7.0), 10 Mm EDTA and 0.1% Triton X-100. 10 µL of the 50 mM potassium ferricyanide and potassium ferrocyanide were also added to the working solution.

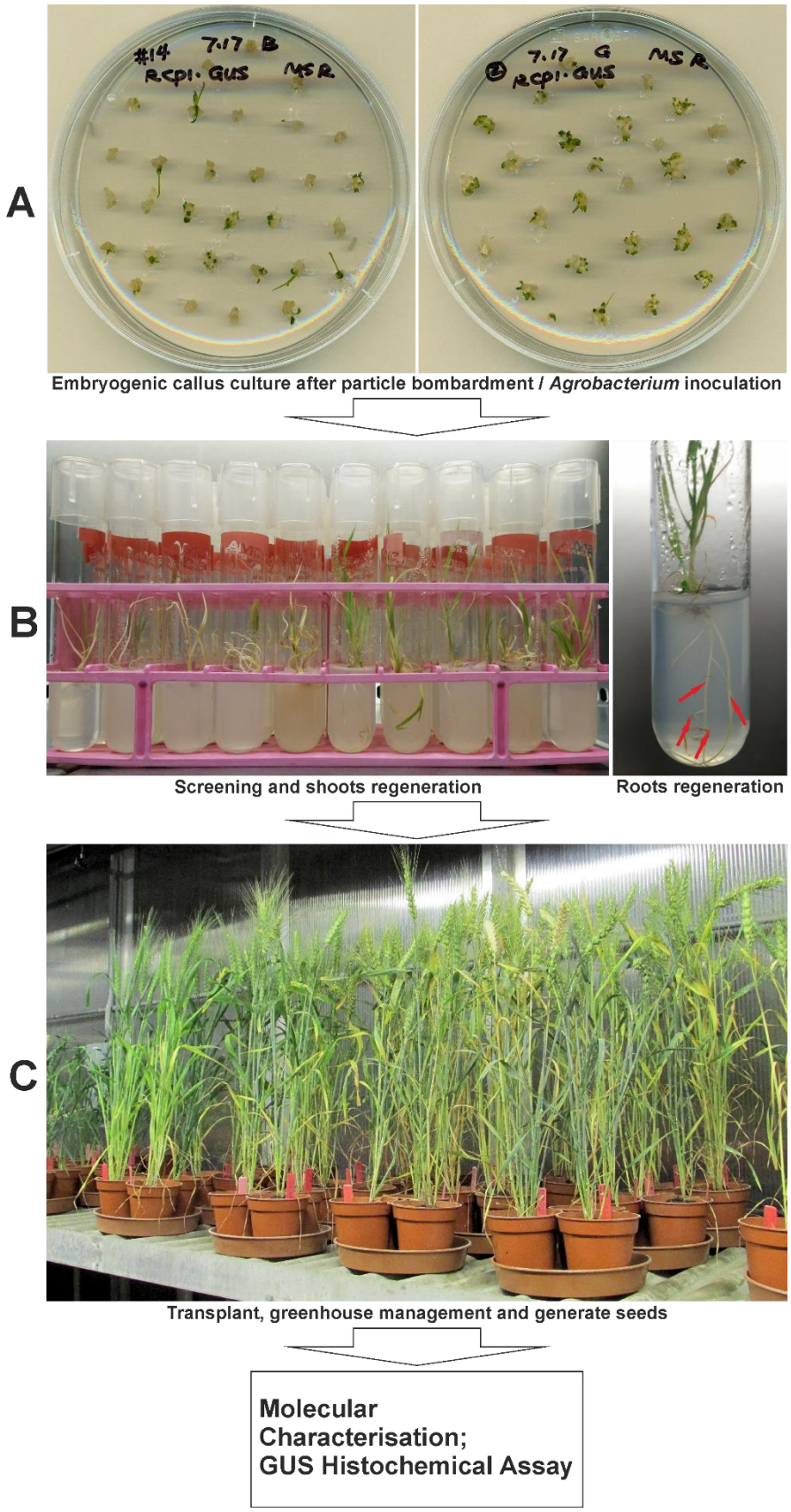

Figure 5.2 Selection and regeneration of transgenic wheat lines. A. Callus culture, selection and regeneration after transgenic procedures. **B**. Shoots regeneration and roots induction (arrow indicated) were carried out in test tubes. **C**. Seedlings were transplanted to soil in greenhouse. Molecular characterisation and GUS histochemical assay were carried out afterwards.

5.3 Results

The wheat immature embryos transformation was implemented first using *Agrobacterium* mediated procedure. In the post-inoculation steps, the use of cefotaxime failed to abolish the *Agrobacterium* growth, resulting in limited numbers of regenerated plants. After PCR assay, no positive plants were identified and the next round of the transformation was then implemented via biolistics. Instead of constructing a new vector, linear expression cassettes from the constructed *Agrobacterium* plasmid were digested and used. The results listed below cover the major steps throughout this transgenic study.

5.3.1 Gene cloning and vector construction

The gene of interest, the root cap specific promoter RCP1, was amplified via high fidelity PCR using specific primers, adding the restriction enzyme digestion sites needed for vector construction. As shown in Figure 5.3.1.1 A, the CaMV35S promoter was replaced with the amplified RCP1 promoter using the two enzyme digestion sites HindII and NcoI. After ligation and transformation of *E. coil* competent cells, double digestion was carried out using plasmid extracted from PCR verified positive clones. They gave a band of the RCP1 promoter with the designated size around 2.1kb in the gel electrophoresis (Figure 5.3.1.1 B). Sequencing was then implemented with the final validation of successful vector construction without mutagenesis.

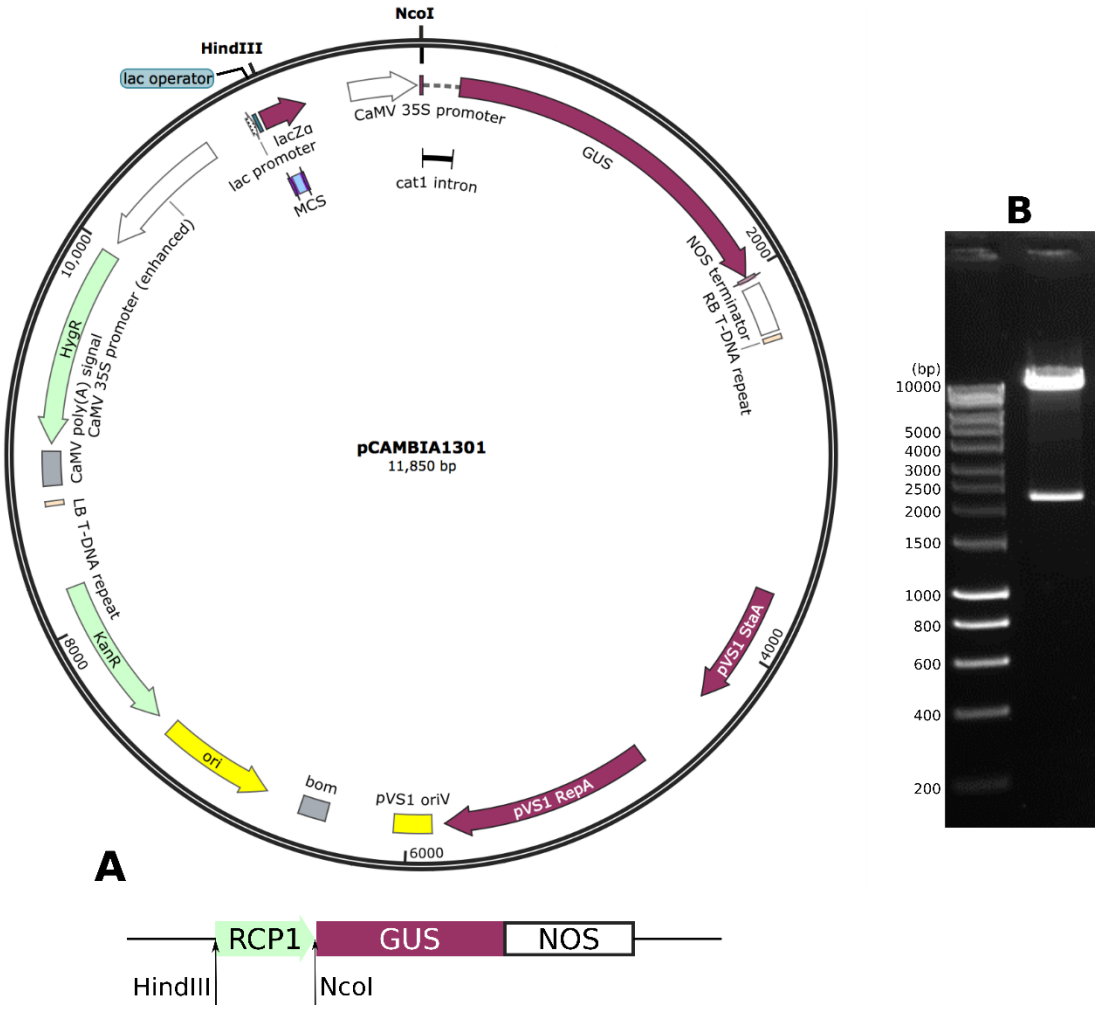

Figure 5.3.1.1 Plasmid vector for transformation and double digestion verification. **A**. Plasmid vector pCAMBIA1301 structure and the construction procedure. The CaMV 35S promoter in the vector was replaced with RCP1 promoter, using the two digestion sites HindIII and NcoI. **B**. Double digestion using HindIII and NcoI was carried out over the plasmid of PCR positive clones for validating the successful insertion.

Agrobacterium mediated transformation was completed using 7day-old embryogenic calli, following the procedure described. Due to the contamination of *Agrobacterium* over-growth, only a limited number of plants successfully regenerated. A PCR assay was carried out and no positive plants were identified.

Another transformation was then implemented via microprojectile bombardment. 3 day-old pre-cultured immature embryos were used as explants and linear expression cassettes digested from the *Agrobacterium* Ti plasmid were used for the transformation. As shown in Figure 5.3.1.2, the constructed plasmid was digested with BglI and SacII, and the band with the size around 8kb in the gel electrophoresis, containing the expression cassettes, was recovered for biolistics.

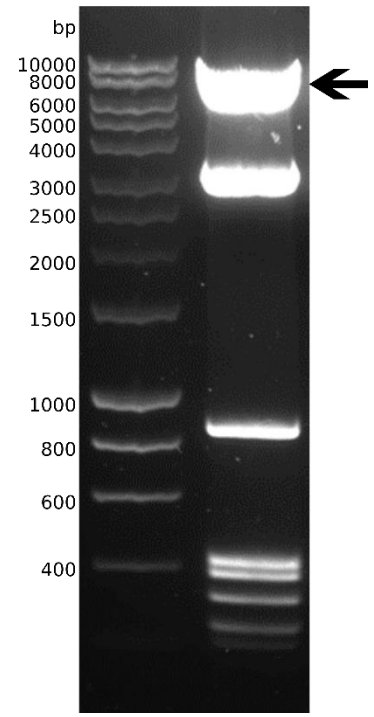

Figure 5.3.1.2 Double digestion of the constructed vector for the linear expression cassettes used in biolistics. BglI and SacII double digestion was carried out over the constructed vector. The arrowed band with a size around 8kb was with genes of interest and later recovered for particle bombardment.

5.3.2 Regeneration and validation of transgenic plants

After particle bombardment of 532 pieces of embryogenic calli, further antibiotic selection was carried out using Hygromycin B. Successfully regenerated seedlings with robust root systems were transplanted to soil in pots and a total of 89 plants were successfully transplanted to a greenhouse. DNA extraction was done on the newly developed leaves and a PCR assay was performed to confirm the successful transformants. In all, 5 independent lines were confirmed as PCR positive for both *RCP1* promoter and *gusA* gene, 2 of them shown in Figure 5.3.2.1, and the overall transformation frequency was 1%. There were no phenotype alterations observed during the growth of the transgenic lines in greenhouse and they generated seeds normally.

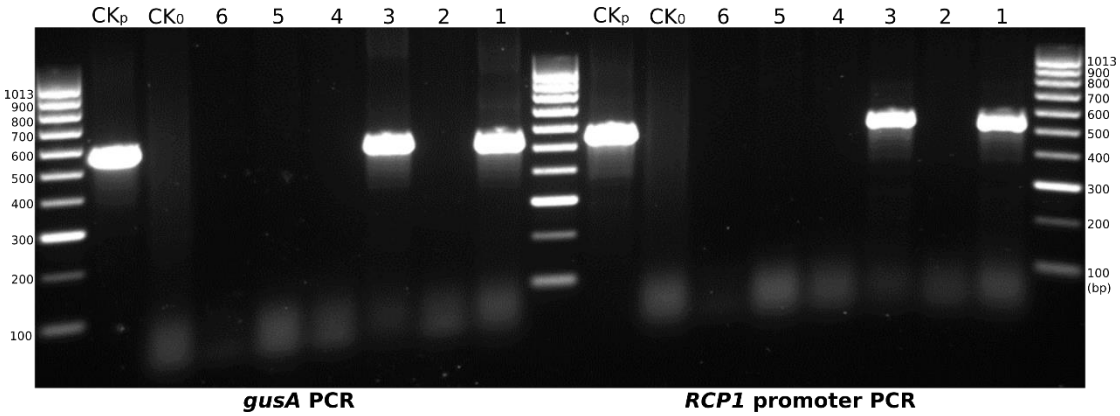

Figure 5.3.2.1 PCR assay of regenerated T_0 plants. PCR assay was carried out over regenerated T_0 plants using specific primers. CK_0, wheat wildtype negative control. CK_p, plasmid positive control. T_0 plants #1 and #3 successfully amplified amplicons of size 573bp and 578bp for *RCP1* promoter and *gusA* respectively.

Tillers of T_0 were labelled individually and a PCR assay was carried out for all the tillers. As shown in Figure 5.3.2.2, the tillers marked as PCR negative were discarded and the seeds from PCR positive ones were collected separately. Seedlings of T_1 were then tested for PCR assay using *RCP1* and *gusA* specific primers and 202 out of 269.T_1 plants were verified as PCR positive for both primers.

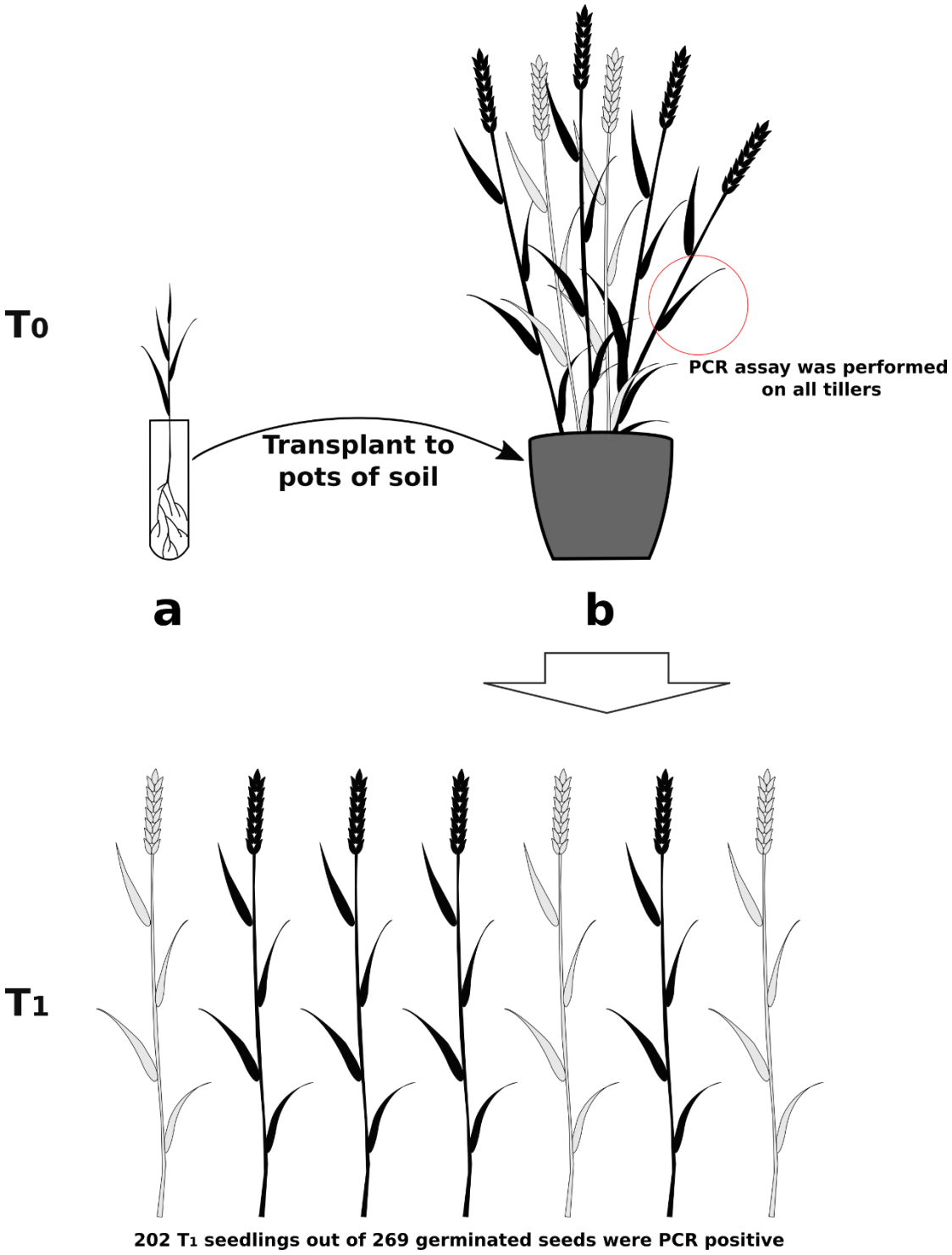

Figure 5.3.2.2 PCR assay for regenerated T_0 and T_1 seedlings. a. Regenerated seedlings were transplanted to soil in pots. **b**. PCR assay was implemented for all tillers. Seeds of positive tillers (black) were kept whilst negative tillers (grey) were discarded. PCR assay was then carried out for all T_1 seedlings, with 202 PCR positive ones (black) out of 269 plants. Negative plants marked grey.

Segregation was observed among seeds generated from the same single spike. As shown in Figure 5.3.2.3, T_1 seedlings generated from a single T_0 spike with verified transformation show different results in the performed PCR assay for both *RCP1* and *gusA* primers. All PCR positive T_1 seedlings were then used for further expression analysis.

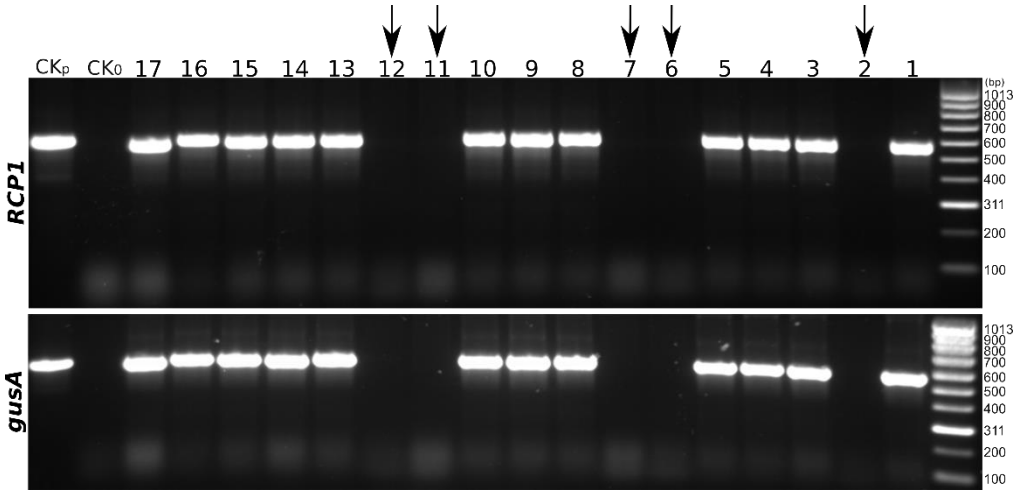

Figure 5.3.2.3 Segregation of PCR assay among T_1 plants. All individuals were from a single T_0 spike with positive PCR verifications. CK_0, wildtype wheat negative control; CK_p, plasmid positive control. Gene specific primers with amplicons of size 573bp for *RCP1* promoter and 578bp for *gusA* were used. Most T_1 individuals were verified as PCR positive with successfully amplified amplicons of designated size and the arrowed ones were noted as PCR negative.

5.3.3 Expression assay of transgenic plants

A GUS histochemical assay was performed over all PCR positive transgenic seedlings, with roots and shoots analysed separately. Samples were soaked in a working solution (as described in 5.2.3) and incubated at 37 °C for 24 hours. For removing the chlorophyll of leaves, samples were transferred to an ethanol series starting from 50% to 100%, with 1 hour incubation at 37 °C each. As shown in Figure 5.3.3.1 A, the GUS activity was not observed in transgenic wheat roots in the expected specific expression pattern (Onyango, Roderick *et al.* 2016), nor in the shoots (images not shown).

Further reverse transcriptase PCR (RT-PCR) analysis was performed over pooled samples, in searching for the possible reasons for the transgenic silencing. cDNA synthesis was done using pooled RNA samples as template via a kit based method (SuperScript, Thermo Fisher) following the manufacture instructions. RNA samples were also used directly as templates to test DNA contamination. As shown in Figure 5.3.3.1 B, no amplicons with designated size were amplified, indicating a possible gene silencing at transcription level. (Due to the lack of applicable positive transformants, genomic DNA was used as the positive control instead of cDNA.)

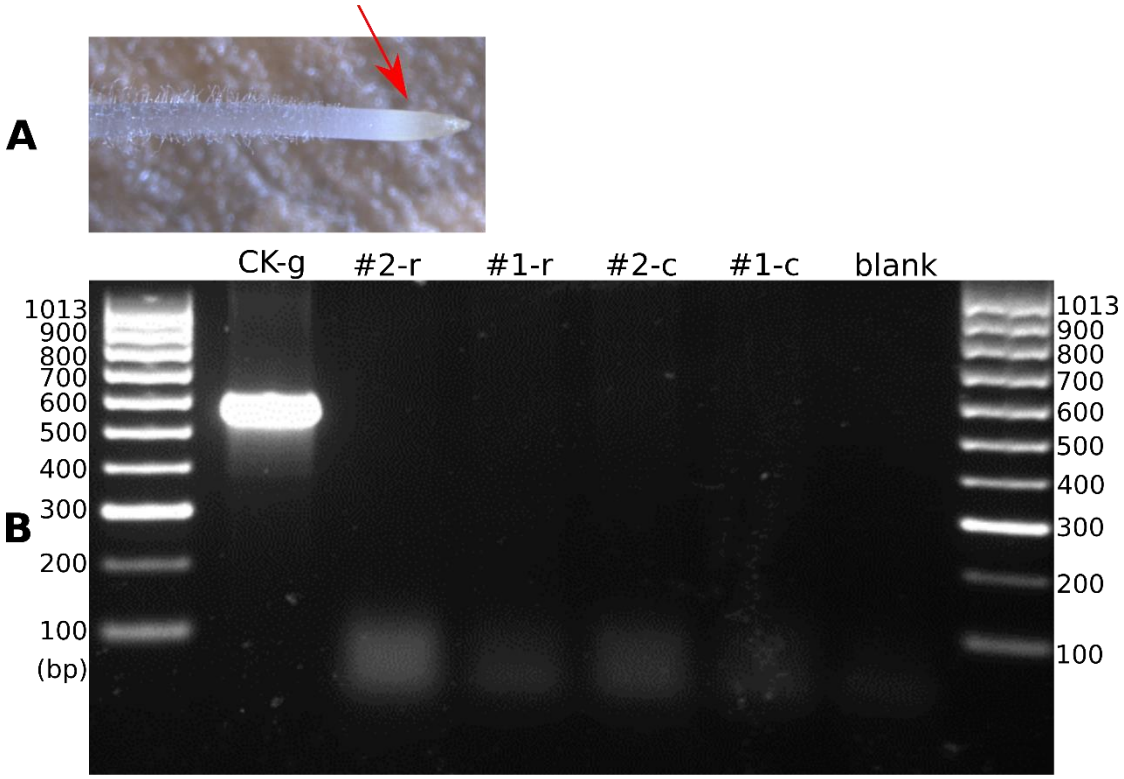

Figure 5.3.3.1 GUS histochemical assay and RT-PCR test of *gusA* in T_1 generation. A. GUS staining assay, wheat root gave no GUS activity. The arrow indicated the root tip. **B**. Pooled samples (#1 and #2) from T_1 positive seedlings were used in RT-PCR assay. Blank, water control; c, cDNA as template; r, RNA as template to check any possible DNA contamination; CK-g, DNA was used as positive control due to the lack of intron in the *gusA* gene. No amplicons of designated size (578bp) were amplified in cDNA samples, indicating transcriptional gene siliencing.

5.4 Discussion

In order to generate transgenic wheat lines with the capability of expressing genes specifically in the root tip against CCNs, a root cap specific promoter RCP1 was used. Wheat immature embryos were chosen as explants and transformation was implemented successfully via biolistics. The regenerated transgenic lines were validated by PCR assay, though the expected expression was not obtained in GUS histochemical assay. Eventually, RT-PCR tests revealed possible gene silencing at transcriptional level.

In plants, transgenes can be silenced at both the transcriptional and post-transcriptional levels (Morel, Mourrain *et al.* 2000). Moreover, the large and complex wheat genome (about 17Gb) (The, Mayer *et al.* 2014) is also expected to be prone to silencing introduced transgenes, and this phenomenon is a common issue in wheat transgenic research, reported mainly in biolistic-mediated transformation (Anand, Zhou *et al.* 2003, Li, Ye *et al.* 2012). DNA methylation is considered to play a significant role in the observed transgenic silencing events. For instance, crossing with the Arabidopsis *ddm1* mutant, which has decreased DNA methylation levels can reduce transcriptional gene silencing (Morel, Mourrain *et al.* 2000). However, the reasons for the gene silencing seen in this study still need further investigations. Previous reports have advocated that the gene silencing problem can be minimised by optimising methods to obtain simple integration patterns (Meyer 1995) or by using flanking matrix attachment regions or spacer control sequence to protect the plants against silencing (Abranches, Shultz *et al.* 2005). Such solutions should be taken into consideration in future experiments.

Another issue encountered in this study is the low transformation frequency, around 1%. This is similar to some of the previous studies using similar transformation procedures (Li, Ye *et al.* 2012). Together with gene silencing, it all added to difficulties in obtaining successful transformants. Recently, a highly efficient *Agrobacterium*-mediated transformation method has been described (Richardson, Thistleton *et al.* 2014, Ishida, Tsunashima *et al.* 2015), possibly paving the way for future transgenic wheat research. In this reported method, the wheat cultivar Fielder was found to have higher transformation frequency than Bobwhite, and they implemented a centrifuging step before *Agrobacterium* inoculation as a critical part for effective transformation (Ishida, Tsunashima *et al.* 2015). Using this method, a recent study has successfully generated transgenic wheat lines expressing several promoters from rice root-predominant genes and they were shown to be able to induce the expression of the reporter gene *GFP* specifically in wheat root system (Xue, Rae *et al.* 2016). Similar experimental procedures can also be adopted in this study to generate transgenic wheat lines with root-cap specific gene expression as a potential research platform for CCNs.

With the recent wheat transformation development that has overcome some of the major barriers for wheat transgenic applications, including the low transformation frequency over decades, the generation of transgenic wheat lines with the capability of inducing gene expression spatially in the CCNs-targeted root system can provide an ideal research tool for extensive investigations over wheat-CCNs interactions in the near future.

Chapter 6 General discussion

The aim of this study to evaluate the cell wall chemical structures of the syncytia induced by cyst nematodes. As the sole nutrient supply for nematode survival and reproduction, the microstructures of this unique feeding site should fulfil the functional requirements imposed by the nematode feeding.

6.1 The cell walls of cyst nematode induced syncytium

The formation and structures of the syncytia have been described extensively for some of the most economically important cyst nematode species over the past years (Gipson, Kim *et al.* 1971, Jones and Northcote 1972, Riggs, Kim *et al.* 1973, Golinowski, Grundler *et al.* 1996, Sobczak, Golinowski *et al.* 1997, Sobczak and Golinowski 2009, Bohlmann and Sobczak 2014). It was depicted as a multicellular feeding site with thickened outer syncytial walls and pronounced cell wall ingrowths, originated from local cell wall dissolutions and protoplasts fusion of host root cells (Bohlmann and Sobczak 2014). This structure can withstand much higher turgor pressure than neighbouring cells, on average more than 2 times in the *H. schachtii* induced syncytium than the neighbouring parenchyma cells (Böckenhoff and Grundler 1994), meanwhile coping with the volume change caused by the large amount of food consumed daily by the nematodes (Muller, Rehbock *et al.* 1981). Therefore, the cell wall chemical compositions, should be directly responsible for such mechanical requirements of the syncytia during nematode feeding and development.

As shown in Chapter 3 and 4, the functional syncytia possess generally stable wall chemical structures during parasitism, and even share high similarities in the syncytial walls among species induced in their different natural hosts. According to the host primary cell wall types, the induced syncytium can be roughly divided into two types based on the major cell wall polymers contained (apart from the common cellulose microfibrils in the walls): the Type I primary wall syncytium, composed with large amount of hemicellulose XyGs, pectic methyl-HG and RG-I related arabinans; the Type II primary wall syncytium, composed with highly substituted hemicellulose xylans and variable MLG, various low levels of RG-I galactan and abundant arabinans. These polymers, all together forming a complex network, can provide both mechanical strength and wall flexibility.

The syncytium is different from transfer cells

Being suggested as a type of multinucleate transfer cells (Jones and Northcote 1972, Jones and Northcote 1972), cyst nematode induced syncytia did share transfer cell-like structural similarities, including the typical cell wall ingrowth to facilitate high rates of apoplasmic/symplasmic solute exchange (Gunning and Pate 1969, Offler, McCurdy *et al.* 2003). However, transfer cells generally develop from various range of differentiated cells, such as phloem cells (Andriunas, Zhang *et al.* 2013), whilst the syncytium was known to be unable to incorporate those types of cells (Bohlmann and Sobczak 2014), showing the difference at the formation processes. Further comparisons of wall chemical compositions also gave distinctive results. For instance, the tapetum, as a typical pollen grain transfer

cell, was revealed to be contain only methyl-HG but completely lack of pectic arabinans throughout the microsporogenesis stages (Majewska-Sawka, Münster *et al.* 2004). Other analysed transfer cells also displayed distinct cell wall microstructures (Vaughn, Talbot *et al.* 2007, Boughanmi, Thibault *et al.* 2010), suggesting that it might not applicable to directly compare the nematode induced syncytium to other transfer cells.

Syncytia formed in different types of hosts

As the sole nutrient supply for cyst nematode feeding, the successfully induced syncytium was proven to be possessing high turgor pressure, raised by the osmotic stress, probably due to the highly elevated sucrose levels during syncytium formation (Hofmann, Wieczorek *et al.* 2007) then accumulated as starch as carbohydrate storage (Hofmann, Szakasits *et al.* 2008), many amino acids and phosphorylated metabolites and some other specific sugars (Hofmann, El Ashry Ael *et al.* 2010) as well. In order to cope with the increased turgor pressure, the outer syncytial walls are generally largely thickened (Bohlmann and Sobczak 2014), although it was shown to be less significant in the syncytia formed in wheat as in Chapter 3.

In the Type I primary wall syncytia, the walls were mainly composed with abundant XyGs, methyl-HG and pectic arabinans. As compared with the classic primary cell wall model, it could be described as a cellulose microfibrils tethered with cross-linking XyGs forming the load-bearing network, further embedded into a pectic gel matrix (Cosgrove 2014). The XyGs-cellulose network is responsible for the mechanical strength required by the syncytium functioning. However, the discovery of a XyG deficiency mutant (Cavalier, Lerouxel *et al.* 2008), showing only minor phenotype changes (Park and Cosgrove 2012), has seriously challenged the validity of this primary cell wall model. Besides, as shown in Chapter 4, the syncytium was induced successfully and functioning normally in the XyG deficiency mutant, with no detectable XyGs along with the host. Moreover, the pectic HG in the Type I primary wall syncytia was mainly the methyl esterified form, therefore no Ca^{2+} cross linking could be formed and not capable of providing mechanical support either. New proposal has been attempted (Peaucelle, Braybrook *et al.* 2012, Cosgrove 2014), resulting the possibility that, in the mature syncytial walls, the cellulose microfibrils were able to form links with both XyGs and the pectic arabinans (Zykwinska, Ralet *et al.* 2005), providing the mechanical support required in facing the much higher inner turgor pressure.

Meanwhile, in the Type II primary wall syncytia, the walls were mainly composed with abundant highly substituted xylans and arabinans. Therefore, the cellulose heteroxylan cross linking should attribute to the major mechanical properties, probably together with the detected variable cross-linking galactan and MLG, even the small amount of XyG as well.

Syncytial wall chemical characteristics

The commonly discovered arabinans in all the syncytial walls might be responsible for the wall flexibility needed during the nematode feeding, as it was shown to be essential in guard cell wall flexibility (Jones, Milne *et al.* 2003) and in maintaining the cell wall flexibility during water deficit stress (Moore, Farrant *et al.* 2008, Moore, Nguema-Ona *et al.* 2013).

Another key character of the syncytial wall chemical structure is that the pectic HGs were predominantly methyl esterified, even the trace level of pectic HG observed in wheat syncytia was also methyl-HG. The methyl esterification of pectic HG has been linked to plant development status (Wolf, Mouille *et al.* 2009). As it was synthesised in the Golgi apparatus and secreted in a fully methylesterified form, the removal of methyl groups, mediated by the PMEs, could cause the formation of intermolecular linkages with Ca^{2+} and Mg^{2+}, therefore leading to harden the pectic gel (Wolf, Mouille *et al.* 2009). Based on related studies, the large amount of syncytial wall methyl-HGs might account for various roles in a functional syncytium. Firstly, the syncytium forming process requires cell wall dissolutions mediated by various cell wall modifying/degrading enzymes. Among which, pectate lyases were postulated to be more important for the degradation of the cell walls in syncytia than polygalacturonases, due to the analysis of gene expression patterns inside the syncytium (Bohlmann and Sobczak 2014). Meanwhile, pectate lyases were known to be able to degrade non-methyl HG, therefore leading the syncytial wall pectic HGs stay intact. Another possible role was the methyl-esterification status of HG was shown to be linked to cell wall porosity, stiffening and cell adhesion (Willats, Orfila *et al.* 2001). Reduction of non-methyl HG in Arabidopsis through transgenic expression of a PMEI or a fungal polygalacturonase was shown to increase the exposure of cellulose to enzymatic saccharification (Lionetti, Francocci *et al.* 2010), suggesting that the non-methyl HG-mediated cross links can act as a glue for other cell wall polysaccharides. In the meantime, the nematode feeding requires the use of water and nutrients flow via both symplasmic and apoplasmic pathways (Böckenhoff, Prior *et al.* 1996, Hofmann and Grundler 2006, Hofmann, Wieczorek *et al.* 2007) and the largely thickened syncytial walls composed with methyl-HG might facilitate the transport of water and solutes during this process.

Upon the abundant methyl-esterified HG in the mature syncytial walls, the syncytial HG methyl esterification in Arabidopsis was noted to be changing along with developmental stages, under abiotic drought stress as well as and in some of the selected pectic HG related mutant lines. The reduction of non-methyl HG in the early stage of the syncytium formation, together with the drought stress related HG fluctuations, might all due to the different nematode developments. A previous study revealed that a cellulose binding protein from *H. schachtii* was expressed in the early phases of feeding cell formation and not during the migratory phase, and it was interacting with Arabidopsis PME3 specifically (Hewezi, Howe *et al.* 2008). This suggested that the increased PME3 facilitated the cell wall degradation at the early syncytium expanding phase, agreeing with the decline of non-methyl HG in the young developing syncytium. However, the concern of the syncytial wall integrity, in regarding to the finding that the transgenic plants overexpressing *AtPme3* was positively correlated with the nematode susceptibility rather than causing impair to the abundant syncytial wall methyl-HG, was also raised (Bohlmann and Sobczak 2014). One possible explanation would be that the activity of PME3 was restrained or restricted, as the PMEs can be selectively and temporally secreted into the cell wall to remove methyl groups, or the activity of PMEs can be regulated/inhibited by the spatially secreted PMEIs (Lionetti, Cervone *et al.* 2012). For instance, the Arabidopsis PMEI4 was co-expressed with PME17 and regulated its activity (Senechal, Mareck *et al.* 2015), and similarly the PMEI7

was able to inhibit the activity of PME3 (Senechal, L'Enfant *et al.* 2015). Both PMEs and PMEIs are from large multigene families and only a few of them were demonstrated with clear functions. The gene expression profile in Chapter 4 as well as in previous microarray data (Szakasits, Heinen *et al.* 2009) reflected the various functions they might play and putative complex interactions between them.

The differentiations of syncytial wall chemical structures

Analysing the antibody binding patterns from high definition results, the mAb epitopes were not shown to be distributing evenly among the 'thickened syncytial walls'. Most of the identified cell wall polymers, represented by these mAbs binding, were located in the relatively thin layer with direct contact to the syncytial cytoplasm. This phenomenon was observed clearly among the much thickened potato, soybean and Arabidopsis syncytia, even for certain mAbs in wheat syncytia as well. Those depicted 'outer cell walls of the syncytia' (Bohlmann and Sobczak 2014) basically only contained pectic HGs, in a position much like the middle lamella layer deposited between cells. As the general primary cell wall is around 0.1-1 µm thick (Cosgrove 2005), the labelled thinner inner layer of the syncytium was named as syncytial primary wall, containing most of the detected wall polymers. The thickened outer layer should still be part of the whole syncytial primary structure rather than taken as secondary walls, as secondary walls were generally deposited within the primary walls when cells ceased growth and they normally were lack of pectin and abundant of different hemicelluloses (such as xylans and mannans) and lignin (Kumar, Campbell *et al.* 2016).

However, this might draw the concern that whether the thin primary wall could withstand and counteract the high osmotic pressure insider the syncytium (Böckenhoff and Grundler 1994). In fact, this concern should be addressed when the pectic HGs in the syncytial walls were found to be predominantly the methyl-esterified form, as no cation cross-links could be induced. Though the fine details remained to be elucidated, one clue was that the guard cells in epidermal peels of broad bean were shown to withstand turgor pressure change ranging from 0.3 MPa to 5.0 MPa with a wall around 2 µm thick (Franks, Buckley *et al.* 2001), generally about 10 times greater than the pressure found in most of other plant cells (Fricke, Jarvis *et al.* 2000, Jones, Milne *et al.* 2003). In the meantime, the turgor pressure reported in syncytial cells were around 9-10 MPa comparing with the vascular parenchyma cells of 4 MPa and cortex cells of 2 MPa. Adding the much thickened surrounding middle lamella layer, rich in pectic methyl-HGs, it was possible that the syncytial primary wall complex was capable of generating such high turgor pressure.

In regard to the overall mAbs binding, the cyst nematodes induced syncytial walls show great similarities to their host primary wall types. The type I primary wall syncytia possess abundant XyGs and pectic HGs and lack of xylans, whilst the wheat syncytial walls contain abundant heteroxylans and marginal pectic HGs, both similar to its host cell wall types (Vogel 2008). Concurrently, comparing with the rest of the host root cells, the syncytial walls possess uniqueness at a chemical composition level. This together indicates that the formation process involves both the wall degradations and the biosynthesis machinery of the hosts for the deposited new wall materials. As a polysaccharides tangled complex, this

sophisticated and responsive feeding structure is capable of using its microstructure to fulfil the normal functional requirements as well as coping with stress.

6.2 The cell wall formation in the syncytium

The syncytium formation is a plant-pathogen interaction process, involving cooperative changes in both the nematode and nematode-induced host cells.

Among the nematode effectors related in this process, plant cell wall modifying/degrading enzymes are most studied and mainly involved in degradation of the host cell wall during the migration stage (Haegeman, Mantelin *et al.* 2011). For instance, the genes encoding β-1,4-endoglucanase were first identified in cyst nematodes, with the cellulose degrading activity (Smant, Stokkermans *et al.* 1998). Then, a functional expansin, being able to loosen cell walls while invading, was produced in *G. rostochiensis* (Qin, Kudla *et al.* 2004). These plant pathogenesis associated enzymes, such as cellulase and pectinase, were also shown to be conserved among various nematode species (Rai, Balasubramanian *et al.* 2015), indicating common roles during the parasitism. In comparison, many host cell originated genes were also entangled in this transformation, such as Arabidopsis expansins (Wieczorek, Golecki *et al.* 2006), β-1,4-endoglucanases (Wieczorek, Hofmann *et al.* 2008) and a ATPase gene (Ali, Plattner *et al.* 2013). One great example of the interaction between nematode effector and host targeted genes was the nematode CBM activating the Arabidopsis PME3 during nematode parasitism (Hewezi, Howe *et al.* 2008). Such collaboration was also found in a recent study, showing that *H. schachtii* was able to produce and release cytokinin in the infection site to activate the cell cycle in the cells adjacent to the feeding site therefore promote syncytium expansion. Meanwhile, it was shown that, during the expansion of the nematode feeding site, the host plants produced cytokinin was also partially involved (Siddique, Radakovic *et al.* 2015).

Although the syncytial wall chemical structures induced in several cell wall mutant lines were analysed in order to find clues of syncytial wall formation (in Chapter 4), meanwhile the attempting to create transgenic wheat lines with root specific gene expression ability was also related to such investigation, not too much is yet known in regarding to the biosynthesis of the syncytial walls. The cooperative effects of both the nematode and the host should also apply in this transformation process. One example was that the Arabidopsis *UGD2* and *UGD3*, related to several cell wall polysaccharides synthesis, were demonstrated to be responsible for the cell wall ingrowth in nematode induce syncytia and the syncytial wall ingrowth was shown to be missing in the double mutant (Siddique, Sobczak *et al.* 2012).

6.3 The syncytium throughout nematode feeding

Apart from providing extra mechanical support besides the syncytial primary walls, the thickened outer layer, with abundant highly methyl-esterified pectic HG, could act as a gel with considerable water holding capacity. One clue was that the pectin gels with higher degree of methyl esterification intend to have smaller volumes of water expelled from the gels during compression, meanwhile the low-methyl-esterification gels were shown to

collapse under compression with little expansion (Willats, Orfila *et al.* 2001). The syncytium formed in eudicot hosts intend to form such thickened outer layers full of highly-methyl-esterified pectin, which could also possess similar water holding capability meanwhile not easily to collapse by expansion when facing compression caused by the higher turgor pressure within. Therefore, the thickened outer layer of syncytia might act as a protection layer attributing to the syncytium integrity and a buffering wrap against host fluid/pressure fluctuation, either caused by host plant development or the ever-changing environment.

Moving from feeding the nematode as a nutrient sink, when the syncytial walls keep high level of methyl-HG throughout the feeding phase, to the eventually disintegrating and collapsing after nematode mature, the syncytium was shown to become translucent and filled with vesicles in the cytoplasm and eventually degenerated. Taking the thickness of the overall syncytial walls and the epitope distribution analysis into consideration, the methyl group needs to be removed during degradation of syncytial wall pectins might account for a considerable amount. In ripening fruit, such reaction was an important source of accumulated methanol, and this was correlated with PME activities (Frenkel, Peters *et al.* 1998). Such phenomenon was extensively studied on the methanol emission from wounded leaves, showing that methanol could act as a signal that facilitates viral spread in neighbouring plant by triggering plasmodesmata dilation (Dorokhov, Komarova *et al.* 2012). More research even suggested that methanol could function in plant-animal signalling, a cross-kingdom role (Dorokhov, Komarova *et al.* 2012). Although, there is no evidence yet proving the existence of methanol accumulation during the syncytial wall degeneration, it is still reasonable to postulate that the abundant methyl esters in the much thickened syncytial walls can act as a potential methanol pool. If this was proven to be true, such signal compound would probably play a role in those nematode related pathogen attacks in the host plants.

References

Abad, P., J. Gouzy, J. M. Aury, P. Castagnone-Sereno, E. G. Danchin, E. Deleury, L. Perfus-Barbeoch, V. Anthouard, F. Artiguenave, V. C. Blok, M. C. Caillaud, P. M. Coutinho, C. Dasilva, F. De Luca, F. Deau, M. Esquibet, T. Flutre, J. V. Goldstone, N. Hamamouch, T. Hewezi, O. Jaillon, C. Jubin, P. Leonetti, M. Magliano, T. R. Maier, G. V. Markov, P. McVeigh, G. Pesole, J. Poulain, M. Robinson-Rechavi, E. Sallet, B. Segurens, D. Steinbach, T. Tytgat, E. Ugarte, C. van Ghelder, P. Veronico, T. J. Baum, M. Blaxter, T. Bleve-Zacheo, E. L. Davis, J. J. Ewbank, B. Favery, E. Grenier, B. Henrissat, J. T. Jones, V. Laudet, A. G. Maule, H. Quesneville, M. N. Rosso, T. Schiex, G. Smant, J. Weissenbach and P. Wincker (2008). "Genome sequence of the metazoan plant-parasitic nematode *Meloidogyne incognita*." Nature Biotechnology **26**(8): 909-915.

Abranches, R., R. W. Shultz, W. F. Thompson and G. C. Allen (2005). "Matrix attachment regions and regulated transcription increase and stabilize transgene expression." Plant Biotechnology Journal **3**(5): 535-543.

Aditya, J., J. Lewis, N. J. Shirley, H. T. Tan, M. Henderson, G. B. Fincher, R. A. Burton, D. E. Mather and M. R. Tucker (2015). "The dynamics of cereal cyst nematode infection differ between susceptible and resistant barley cultivars and lead to changes in (1,3;1,4)-beta-glucan levels and HvCslF gene transcript abundance." New Phytologist **207**(1): 135-147.

Albersheim, P., A. Darvill, K. Roberts and R. Sederoff (2010). Plant cell walls, Garland Science.

Ali, M. A., S. Plattner, Z. Radakovic, K. Wieczorek, A. Elashry, F. M. Grundler, M. Ammelburg, S. Siddique and H. Bohlmann (2013). "An Arabidopsis ATPase gene involved in nematode-induced syncytium development and abiotic stress responses." The Plant Journal **74**(5): 852-866.

Alonso, J. M., A. N. Stepanova, T. J. Leisse, C. J. Kim, H. Chen, P. Shinn, D. K. Stevenson, J. Zimmerman, P. Barajas, R. Cheuk, C. Gadrinab, C. Heller, A. Jeske, E. Koesema, C. C. Meyers, H. Parker, L. Prednis, Y. Ansari, N. Choy, H. Deen, M. Geralt, N. Hazari, E. Hom, M. Karnes, C. Mulholland, R. Ndubaku, I. Schmidt, P. Guzman, L. Aguilar-Henonin, M. Schmid, D. Weigel, D. E. Carter, T. Marchand, E. Risseeuw, D. Brogden, A. Zeko, W. L. Crosby, C. C. Berry and J. R. Ecker (2003). "Genome-wide insertional mutagenesis of *Arabidopsis thaliana*." Science **301**(5633): 653-657.

Altschul, S. F., W. Gish, W. Miller, E. W. Myers and D. J. Lipman (1990). "Basic local alignment search tool." Journal of Molecular Biology **215**(3): 403-410.

An, G., B. D. Watson and C. C. Chiang (1986). "Transformation of tobacco, tomato, potato, and *Arabidopsis thaliana* using a binary Ti vector system." Plant Physiology **81**(1): 301-305.

Anand, A., T. Zhou, H. N. Trick, B. S. Gill, W. W. Bockus and S. Muthukrishnan (2003). "Greenhouse and field testing of transgenic wheat plants stably expressing genes for thaumatin ‐ like protein, chitinase and glucanase against *Fusarium graminearum*." Journal of Experimental Botany **54**(384): 1101-1111.

Anders, N., M. D. Wilkinson, A. Lovegrove, J. Freeman, T. Tryfona, T. K. Pellny, T. Weimar, J. C. Mortimer, K. Stott, J. M. Baker, M. Defoin-Platel, P. R. Shewry, P. Dupree and R. A. Mitchell (2012). "Glycosyl transferases in family 61 mediate arabinofuranosyl transfer onto xylan in grasses." PNAS **109**(3): 989-993.

Andrews, S. "FastQC A quality control tool for high throughput sequence data." from http://www.bioinformatics.babraham.ac.uk/projects/fastqc/.

Andriunas, F., H.-m. Zhang, X. Xia, J. Patrick and C. Offler (2013). "Intersection of transfer cells with phloem biology—broad evolutionary trends, function, and induction." Frontiers in Plant Science **4**(221).

Arioli, T., L. Peng, A. S. Betzner, J. Burn, W. Wittke, W. Herth, C. Camilleri, H. Hofte, J. Plazinski, R. Birch, A. Cork, J. Glover, J. Redmond and R. E. Williamson (1998). "Molecular analysis of cellulose biosynthesis in Arabidopsis." Science **279**(5351): 717-720.

Atmodjo, M. A., Z. Y. Hao and D. Mohnen (2013). "Evolving views of pectin biosynthesis." Annual Review of Plant Biology **64**: 747-779.

Badhan, A., L. Jin, Y. Wang, S. Han, K. Kowalczys, D. C. Brown, C. J. Ayala, M. Latoszek-Green, B. Miki, A. Tsang and T. McAllister (2014). "Expression of a fungal ferulic acid esterase in alfalfa modifies cell wall digestibility." Biotechnology for Biofuels **7**(1): 39.

Baldwin, J. G., S. A. Nadler and B. J. Adams (2004). "Evolution of plant parasitism among nematodes." Annual Review of Phytopathology **42**: 83-105.

Bar-Peled, M., B. R. Urbanowicz and M. A. O'Neill (2012). "The synthesis and origin of the pectic

polysaccharide rhamnogalacturonan II - insights from nucleotide sugar formation and diversity." Frontiers in Plant Science **3**(92): 92.

Basu, S., O. Omadjela, D. Gaddes, S. Tadigadapa, J. Zimmer and J. M. Catchmark (2016). "Cellulose microfibril formation by surface-tethered cellulose synthase enzymes." ACS Nano **10**(2): 1896-1907.

Bethke, G., R. E. Grundman, S. Sreekanta, W. Truman, F. Katagiri and J. Glazebrook (2014). "Arabidopsis PECTIN METHYLESTERASEs contribute to immunity against Pseudomonas syringae." Plant Physiology **164**(2): 1093-1107.

Betsuyaku, S., S. Sawa and M. Yamada (2011). "The function of the CLE peptides in plant development and plant-microbe interactions." The Arabidopsis book **9**: e0149.

Bird, D. M., V. M. Williamson, P. Abad, J. McCarter, E. G. Danchin, P. Castagnone-Sereno and C. H. Opperman (2009). "The genomes of root-knot nematodes." Annual Review of Phytopathology **47**: 333-351.

Blake, A. W., L. McCartney, J. E. Flint, D. N. Bolam, A. B. Boraston, H. J. Gilbert and J. P. Knox (2006). "Understanding the biological rationale for the diversity of cellulose-directed carbohydrate-binding modules in prokaryotic enzymes." The Journal of Biological Chemistry **281**(39): 29321-29329.

Blaxter, M. (2011). "Nematodes: the worm and its relatives." PLoS Biology **9**(4): e1001050.

Blaxter, M., S. Kumar, G. Kaur, G. Koutsovoulos and B. Elsworth (2012). "Genomics and transcriptomics across the diversity of the Nematoda." Parasite Immunology **34**(2-3): 108-120.

Blaxter, M. L., P. De Ley, J. R. Garey, L. X. Liu, P. Scheldeman, A. Vierstraete, J. R. Vanfleteren, L. Y. Mackey, M. Dorris, L. M. Frisse, J. T. Vida and W. K. Thomas (1998). "A molecular evolutionary framework for the phylum Nematoda." Nature **392**(6671): 71-75.

Bleve-Zacheo, T. and G. Zacheo (1987). "Cytological studies of the susceptible reaction of sugarbeet roots to *Heterodera schachtii*." Physiological and Molecular Plant Pathology **30**(1): 13-25.

Böckenhoff, A. and F. M. W. Grundler (1994). "Studies on the nutrient uptake by the beet cyst nematode *Heterodera schachtii* by in situ microinjection of fluorescent probes into the feeding structures in *Arabidopsis thaliana*." Parasitology **109**(02): 249-255.

Böckenhoff, A., D. A. Prior, F. M. Grundler and K. J. Oparka (1996). "Induction of phloem unloading in *Arabidopsis thaliana* roots by the parasitic nematode *Heterodera schachtii*." Plant Physiology **112**(4): 1421-1427.

Bohlmann, H. and M. Sobczak (2014). "The plant cell wall in the feeding sites of cyst nematodes." Frontiers in Plant Science **5**: 89.

Bolger, A. M., M. Lohse and B. Usadel (2014). "Trimmomatic: a flexible trimmer for Illumina sequence data." Bioinformatics **30**(15): 2114-2120.

Bosch, M. and P. K. Hepler (2005). "Pectin methylesterases and pectin dynamics in pollen tubes." The Plant Cell **17**(12): 3219-3226.

Boughanmi, N., F. Thibault, R. Decou, P. Fleurat-Lessard, E. Béré, G. Costa and S. Lhernould (2010). "NaCl effect on the distribution of wall ingrowth polymers and arabinogalactan proteins in type A transfer cells of *Medicago sativa* Gabès leaves." Protoplasma **242**(1-4): 69-80.

Bray, N. L., H. Pimentel, P. Melsted and L. Pachter (2016). "Near-optimal probabilistic RNA-seq quantification." Nature Biotechnology **34**(5): 525-527.

Brenchley, R., M. Spannagl, M. Pfeifer, G. L. Barker, R. D'Amore, A. M. Allen, N. McKenzie, M. Kramer, A. Kerhornou, D. Bolser, S. Kay, D. Waite, M. Trick, I. Bancroft, Y. Gu, N. Huo, M. C. Luo, S. Sehgal, B. Gill, S. Kianian, O. Anderson, P. Kersey, J. Dvorak, W. R. McCombie, A. Hall, K. F. Mayer, K. J. Edwards, M. W. Bevan and N. Hall (2012). "Analysis of the bread wheat genome using whole-genome shotgun sequencing." Nature **491**(7426): 705-710.

Breton, C., L. Snajdrová, C. Jeanneau, J. Koca and A. Imberty (2006). "Structures and mechanisms of glycosyltransferases." Glycobiology **16**(2): 29R-37R.

Brown, D. M., F. Goubet, V. W. Wong, R. Goodacre, E. Stephens, P. Dupree and S. R. Turner (2007). "Comparison of five xylan synthesis mutants reveals new insight into the mechanisms of xylan synthesis." The Plant Journal **52**(6): 1154-1168.

Brown, D. M., Z. Zhang, E. Stephens, P. Dupree and S. R. Turner (2009). "Characterization of IRX10 and IRX10-like reveals an essential role in glucuronoxylan biosynthesis in Arabidopsis." The Plant Journal **57**(4): 732-746.

Buanafina, M. M. D. (2009). "Feruloylation in grasses: current and future perspectives." Molecular Plant **2**(5): 861-872.

Burton, R. A., M. J. Gidley and G. B. Fincher (2010). "Heterogeneity in the chemistry, structure and function of plant cell walls." Nature Chemical Biology **6**(10): 724-732.

Burton, R. A., S. M. Wilson, M. Hrmova, A. J. Harvey, N. J. Shirley, A. Medhurst, B. A. Stone, E. J. Newbigin, A. Bacic and G. B. Fincher (2006). "Cellulose synthase-like CslF genes mediate the synthesis of cell wall (1,3;1,4)-beta-D-glucans." Science **311**(5769): 1940-1942.

Cabrera, J., R. Bustos, B. Favery, C. Fenoll and C. Escobar (2014). "NEMATIC: a simple and versatile tool for the in silico analysis of plant-nematode interactions." Molecular Plant Pathology **15**(6): 627-636.

Caffall, K. H. and D. Mohnen (2009). "The structure, function, and biosynthesis of plant cell wall pectic polysaccharides." Carbohydrate Research **344**(14): 1879-1900.

Cankar, K., A. Kortstee, M. A. J. Toonen, M. Wolters-Arts, R. Houbein, C. Mariani, P. Ulvskov, B. Jorgensen, H. A. Schols, R. G. F. Visser and L. M. Trindade (2014). "Pectic arabinan side chains are essential for pollen cell wall integrity during pollen development." Plant Biotechnology Journal **12**(4): 492-502.

Carpita, N. C. (1996). "Structure and biogenesis of the cell walls of grasses." Annual Review of Plant Physiology and Plant Molecular Biology **47**: 445-476.

Carpita, N. C. and D. M. Gibeaut (1993). "Structural models of primary cell walls in flowering plants: consistency of molecular structure with the physical properties of the walls during growth." The Plant Journal **3**(1): 1-30.

Cassab, G. I. (1998). "Plant cell wall proteins." Annual Review of Plant Biology **49**: 281-309.

Castagnone-Sereno, P., E. G. Danchin, L. Perfus-Barbeoch and P. Abad (2013). "Diversity and evolution of root-knot nematodes, genus Meloidogyne: new insights from the genomic era." Annual Review of Phytopathology **51**: 203-220.

Cavalier, D. M., O. Lerouxel, L. Neumetzler, K. Yamauchi, A. Reinecke, G. Freshour, O. A. Zabotina, M. G. Hahn, I. Burgert, M. Pauly, N. V. Raikhel and K. Keegstra (2008). "Disrupting two *Arabidopsis thaliana* xylosyltransferase genes results in plants deficient in xyloglucan, a major primary cell wall component." The Plant Cell **20**(6): 1519-1537.

Cheng, M., J. E. Fry, S. Pang, H. Zhou, C. M. Hironaka, D. R. Duncan, T. W. Conner and Y. Wan (1997). "Genetic transformation of wheat mediated by *Agrobacterium tumefaciens*." Plant Physiology **115**(3): 971-980.

Chou, Y. H., G. Pogorelko and O. A. Zabotina (2012). "Xyloglucan xylosyltransferases XXT1, XXT2, and XXT5 and the glucan synthase CSLC4 form Golgi-localized multiprotein complexes." Plant Physiology **159**(4): 1355-1366.

Clausen, M. H., W. G. T. Willats and J. P. Knox (2003). "Synthetic methyl hexagalacturonate hapten inhibitors of anti-homogalacturonan monoclonal antibodies LM7, JIM5 and JIM7." Carbohydrate Research **338**(17): 1797-1800.

Clough, S. J. and A. F. Bent (1998). "Floral dip: a simplified method forAgrobacterium ‐ mediated transformation of*Arabidopsis thaliana*." The Plant Journal **16**(6): 735-743.

Cocuron, J.-C., O. Lerouxel, G. Drakakaki, A. P. Alonso, A. H. Liepman, K. Keegstra, N. Raikhel and C. G. Wilkerson (2007). "A gene from the cellulose synthase-like C family encodes a -1, 4 glucan synthase." PNAS **104**(20): 8550-8555.

Cornuault, V., F. Buffetto, M. Rydahl, S. Marcus, T. Torode, J. Xue, M.-J. Crépeau, N. Faria-Blanc, W. T. Willats, P. Dupree, M.-C. Ralet and J. P. Knox (2015). "Monoclonal antibodies indicate low-abundance links between heteroxylan and other glycans of plant cell walls." Planta **242**(6): 1321-1334.

Cornuault, V., I. W. Manfield, M.-C. C. Ralet and J. P. Knox (2014). "Epitope detection chromatography: a method to dissect the structural heterogeneity and inter-connections of plant cell-wall matrix glycans." The Plant Journal **78**(4): 715-722.

Cosgrove, D. J. (2000). "Loosening of plant cell walls by expansins." Nature **407**(6802): 321-326.

Cosgrove, D. J. (2005). "Growth of the plant cell wall." Nature Reviews Molecular Cell Biology **6**(11): 850-861.

Cosgrove, D. J. (2014). "Plant cell growth and elongation." eLS.

Cosgrove, D. J. (2014). "Re-constructing our models of cellulose and primary cell wall assembly." Current Opinion in Plant Biology **22**: 122-131.

Cosgrove, D. J. (2015). "Plant expansins: diversity and interactions with plant cell walls." Current Opinion in Plant Biology **25**: 162-172.

Cotton, J. A., C. J. Lilley, L. M. Jones, T. Kikuchi, A. J. Reid, P. Thorpe, I. J. Tsai, H. Beasley, V. C. Blok, P. J. A. Cock, S. Eves-van den Akker, N. Holroyd, M. Hunt, S. Mantelin, H. Naghra, A. Pain, J. E. Palomares-Rius, M. Zarowiecki, M. Berriman, J. T. Jones and P. E. Urwin (2014). "The genome and life-stage specific transcriptomes of *Globodera pallida* elucidate key aspects of plant parasitism by a cyst nematode." Genome Biology **15**(3): R43.

Culbertson, A., Y.-H. H. Chou, A. L. Smith, Z. T. Young, A. A. Tietze, S. Cottaz, R. Fauré and O. A. Zabotina (2016). "Enzymatic activity of Arabidopsis xyloglucan xylosyltransferase 5." Plant Physiology **171**(3): 1893-1904.

Daher, F. B. and S. A. Braybrook (2015). "How to let go: pectin and plant cell adhesion." Frontiers in Plant Science **6**: 523.

Danchin, E. G. J., M. N. Rosso and P. Vieira (2010). "Multiple lateral gene transfers and duplications have promoted plant parasitism ability in nematodes." PNAS.

Davies, L. J., C. J. Lilley, J. Paul Knox and P. E. Urwin (2012). "Syncytia formed by adult female *Heterodera schachtii* in *Arabidopsis thaliana* roots have a distinct cell wall molecular architecture." New Phytologist **196**(1): 238-246.

Davis, E. L. (2009). "A parasitism gene from a plant‐parasitic nematode with function similar to CLAVATA3/ESR (CLE) of *Arabidopsis thaliana*." Molecular Plant Pathology **10**(1): 151-151.

Davis, J., F. Brandizzi, A. H. Liepman and K. Keegstra (2010). "Arabidopsis mannan synthase CSLA9 and glucan synthase CSLC4 have opposite orientations in the Golgi membrane." The Plant Journal **64**(6): 1028-1037.

de Almeida Engler, J., V. De Vleesschauwer, S. Burssens, J. L. Celenza, D. Inzé, M. Van Montagu, G. Engler and G. Gheysen (1999). "Molecular markers and cell cycle inhibitors show the importance of cell cycle progression in nematode-induced galls and syncytia." The Plant Cell **11**(5): 793-808.

de Almeida Engler, J., T. Kyndt, P. Vieira, E. Van Cappelle, V. Boudolf, V. Sanchez, C. Escobar, L. De Veylder, G. Engler, P. Abad and G. Gheysen (2012). "CCS52 and DEL1 genes are key components of the endocycle in nematode-induced feeding sites." The Plant Journal **72**(2): 185-198.

de Engler, A. J. (2013). "Nematode-induced endoreduplication in plant host cells: why and how?" Molecular Plant-Microbe Interactions.

den Akker, S., C. J. Lilley, A. Reid, J. Pickup, E. Anderson, P. Cock, M. Blaxter, P. E. Urwin, J. T. Jones and V. C. Blok (2015). "A metagenetic approach to determine the diversity and distribution of cyst nematodes at the level of the country, the field and the individual." Molecular Ecology **24**(23): 5842-5851.

Derbyshire, P., M. C. McCann and K. Roberts (2007). "Restricted cell elongation in Arabidopsis hypocotyls is associated with a reduced average pectin esterification level." BMC Plant Biology **7**: 31.

Dhugga, K. S., R. Barreiro, B. Whitten, K. Stecca, J. Hazebroek, G. S. Randhawa, M. Dolan, A. J. Kinney, D. Tomes, S. Nichols and P. Anderson (2004). "Guar seed ß-mannan synthase is a member of the cellulose synthase super gene family." Science **303**(5656): 363-366.

Dick-Pérez, M., Y. Zhang, J. Hayes and A. Salazar (2011). "Structure and interactions of plant cell-wall polysaccharides by two-and three-dimensional magic-angle-spinning solid-state NMR." Biochemistry **50**(6): 989-1000.

Dick‐Perez, M., T. Wang and A. Salazar (2012). "Multidimensional solid‐state NMR studies of the structure and dynamics of pectic polysaccharides in uniformly 13C‐labeled Arabidopsis primary cell walls." Magnetic Resonance in Chemistry **50**(8): 539-550.

Ding, S.-Y., Y.-S. Liu, Y. Zeng, M. E. Himmel, J. O. Baker and E. A. Bayer (2012). "How does plant cell wall nanoscale architecture correlate with enzymatic digestibility?" Science **338**(6110): 1055-1060.

Ding, S. Y., S. Zhao and Y. Zeng (2014). "Size, shape, and arrangement of native cellulose fibrils in maize cell walls." Cellulose.

Doblin, M. S., F. A. Pettolino, S. M. Wilson, R. Campbell, R. A. Burton, G. B. Fincher, E. Newbigin and A. Bacic (2009). "A barley cellulose synthase-like CSLH gene mediates (1, 3; 1, 4)- -D-glucan synthesis in transgenic Arabidopsis." PNAS **106**(14): 5996-6001.

Dolan, L., K. Janmaat, V. Willemsen, P. Linstead, S. Poethig, K. Roberts and B. Scheres (1993). "Cellular organisation of the *Arabidopsis thaliana* root." Development **119**(1): 71-84.

Dorokhov, Y. L., T. V. Komarova, I. V. Petrunia, O. Y. Frolova, D. V. Pozdyshev and Y. Y. Gleba (2012). "Airborne signals from a wounded leaf facilitate viral spreading and induce antibacterial resistance in neighboring plants." PLoS Pathogens **8**(4): e1002640.

Dorokhov, Y. L., T. V. Komarova, I. V. Petrunia, V. S. Kosorukov, R. A. Zinovkin, A. V. Shindyapina, O. Y. Frolova and Y. Y. Gleba (2012). "Methanol May Function as a Cross-Kingdom Signal." PLoS ONE **7**(4): e36122.

Dwivany, F. M., D. Yulia, R. A. Burton, N. J. Shirley, S. M. Wilson, G. B. Fincher, A. Bacic, E. Newbigin and M. S. Doblin (2009). "The CELLULOSE-SYNTHASE LIKE C (CSLC) family of barley includes members that are integral membrane proteins targeted to the plasma membrane." Molecular Plant **2**(5): 1025-1039.

Endler, A. and S. Persson (2011). "Cellulose synthases and synthesis in Arabidopsis." Molecular Plant **4**(2): 199-211.
Endo, B. Y. (1978). "Feeding plug formation in soybean roots infected with the soybean cyst nematode." Phytopathology.
Eves-van den Akker, S., C. J. Lilley, J. R. Ault, A. E. Ashcroft, J. T. Jones and P. E. Urwin (2014). "The feeding tube of cyst nematodes: characterisation of protein exclusion." PLoS ONE **9**(1): e87289.
Eves-van den Akker, S., C. J. Lilley, J. T. Jones and P. E. Urwin (2014). "Identification and characterisation of a hyper-variable apoplastic effector gene family of the potato cyst nematodes." PLoS Pathogens **10**(9): e1004391.
Fangel, J. U., P. Ulvskov, J. P. Knox, M. D. Mikkelsen, J. Harholt, Z. A. Popper and W. G. Willats (2012). "Cell wall evolution and diversity." Frontiers in Plant Science **3**: 152.
FAO. (2009). "How to Feed the World in 2050." Retrieved 12 Sep, 2016, from http://www.fao.org/wsfs/forum2050/wsfs-forum/en/.
Feldmann, K. A. and M. David Marks (1987). "Agrobacterium-mediated transformation of germinating seeds of *Arabidopsis thaliana*: a non-tissue culture approach." Molecular and General Genetics MGG **208**(1): 1-9.
Fernandes, A. N., L. H. Thomas, C. M. Altaner, P. Callow, V. T. Forsyth, D. C. Apperley, C. J. Kennedy and M. C. Jarvis (2011). "Nanostructure of cellulose microfibrils in spruce wood." PNAS **108**(47): E1195-1203.
Fosu-Nyarko, J., P. Nicol, F. Naz, R. Gill and M. G. Jones (2016). "Analysis of the transcriptome of the infective stage of the beet cyst nematode, H. schachtii." PLoS ONE **11**(1): e0147511.
Franks, P. J., T. N. Buckley, J. C. Shope and K. A. Mott (2001). "Guard cell volume and pressure measured concurrently by confocal microscopy and the cell pressure probe." Plant Physiology **125**(4): 1577-1584.
Frenkel, C., J. S. Peters, D. M. Tieman, M. E. Tiznado and A. K. Handa (1998). "Pectin Methylesterase Regulates Methanol and Ethanol Accumulation in Ripening Tomato (Lycopersicon esculentum) Fruit." Journal of Biological Chemistry **273**(8): 4293-4295.
Fricke, W., M. C. Jarvis and C. T. Brett (2000). "Turgor pressure, membrane tension and the control of exocytosis in higher plants." Plant, Cell & Environment **23**(9): 999-1003.
Fry, S. C. (2004). "Primary cell wall metabolism: tracking the careers of wall polymers in living plant cells." New Phytologist **161**(3): 641-675.
Fry, S. C., B. H. W. A. Nesselrode, J. G. Miller and B. R. Mewburn (2008). "Mixed‐linkage (1→3,1→4)‐β‐d‐glucan is a major hemicellulose of Equisetum (horsetail) cell walls." New Phytologist **179**(1): 104-115.
Fry, S. C., W. S. York, P. Albersheim, A. Darvill, T. Hayashi, J. P. Joseleau, Y. Kato, E. Lorences, G. A. Maclachlan, M. McNeil, A. J. Mort, G. J. S. Reid, H. Seitz, R. R. Selvendran, A. G. J. Voragen and A. R. White (1993). "An unambiguous nomenclature for xyloglucan‐derived oligosaccharides." Physiologia Plantarum **89**(1): 1-3.
Fu, L., B. Niu, Z. Zhu, S. Wu and W. Li (2012). "CD-HIT: accelerated for clustering the next-generation sequencing data." Bioinformatics **28**(23): 3150-3152.
Gao, B., R. Allen, T. Maier, E. L. Davis, T. J. Baum and R. S. Hussey (2001). "Molecular characterisation and expression of two venom allergen-like protein genes in *Heterodera glycines*." International Journal for Parasitology **31**(14): 1617-1625.
García, L. E. and M. V. Sánchez-Puerta (2015). "Comparative and evolutionary analyses of *Meloidogyne* spp. based on mitochondrial genome sequences." PLoS ONE **10**(3): e0121142.
Gibeaut, D. M., M. Pauly, A. Bacic and G. B. Fincher (2005). "Changes in cell wall polysaccharides in developing barley (*Hordeum vulgare*) coleoptiles." Planta **221**(5): 729-738.
Gipson, I., K. S. Kim and R. D. Riggs (1971). "An ultrastructural study of syncytium development in soybean roots infected with *Heterodera glycines*." Phytopathology.
Golinowski, W., F. M. W. Grundler and M. Sobczak (1996). "Changes in the structure of*Arabidopsis thaliana* during female development of the plant-parasitic nematode *Heterodera schachtii*." Protoplasma **194**(1-2): 103-116.
Gorham, J., J. Bridges, J. Dubcovsky, J. Dvorak, P. A. Hollington, M. C. Luo and J. A. Khan (1997). "Genetic analysis and physiology of a trait for enhanced K+/Na+ discrimination in wheat." New Phytologist **137**(1): 109-116.
Goubet, F., C. J. Barton, J. C. Mortimer, X. Yu, Z. Zhang, G. P. Miles, J. Richens, A. H. Liepman, K. Seffen and P. Dupree (2009). "Cell wall glucomannan in Arabidopsis is synthesised by CSLA

glycosyltransferases, and influences the progression of embryogenesis." The Plant Journal **60**(3): 527-538.
Goverse, A., J. A. de Engler, J. Verhees, S. van der Krol, J. H. Helder and G. Gheysen (2000). "Cell cycle activation by plant parasitic nematodes." Plant Molecular Biology **43**(5-6): 747-761.
Goverse, A., H. Overmars, J. Engelbertink, A. Schots, J. Bakker and J. Helder (2000). "Both induction and morphogenesis of cyst nematode feeding cells are mediated by auxin." Molecular Plant-Microbe Interactions **13**(10): 1121-1129.
Green, J., D. Wang, C. J. Lilley, P. E. Urwin and H. J. Atkinson (2012). "Transgenic potatoes for potato cyst nematode control can replace pesticide use without impact on soil quality." PLoS ONE **7**(2): e30973.
Griffiths, J. S., K. Šola, R. Kushwaha, P. Lam, M. Tateno, R. Young, C. Voiniciuc, G. Dean, S. D. Mansfield, S. DeBolt and G. W. Haughn (2015). "Unidirectional movement of cellulose synthase complexes in Arabidopsis seed coat epidermal cells deposit cellulose involved in mucilage extrusion, adherence, and ray formation." Plant Physiology **168**(2): 502-520.
Grundler, F., W. Golinowski and M. Sobczak (1999). "Ultrastructure of feeding plugs and feeding tubes formed by *Heterodera schachtii*." Nematology **1**(4): 363-374.
Grundler, F., M. Sobczak and W. Golinowski (1998). "Formation of wall openings in root cells of *Arabidopsis thaliana* following infection by the plant-parasitic nematode *Heterodera schachtii*." European Journal of Plant Pathology **104**(6): 545-551.
Grunewald, W., B. Cannoot, J. Friml and G. Gheysen (2009). "Parasitic nematodes modulate PIN-mediated auxin transport to facilitate infection." PLoS Pathogens **5**(1): e1000266.
Grunewald, W., M. Karimi, K. Wieczorek, E. Van de Cappelle, E. Wischnitzki, F. Grundler, D. Inzé, T. Beeckman and G. Gheysen (2008). "A role for AtWRKY23 in feeding site establishment of plant-parasitic nematodes." Plant Physiology **148**(1): 358-368.
Grunewald, W., G. van Noorden, G. Van Isterdael, T. Beeckman, G. Gheysen and U. Mathesius (2009). "Manipulation of auxin transport in plant roots during Rhizobium symbiosis and nematode parasitism." The Plant Cell **21**(9): 2553-2562.
Grymaszewska, G. and a. W. Golinowski (1987). "Changes in the structure of wheat (*Triticum aestivum* L.) roots in varieties susceptible and resistant to infestation by *Heterodera avenae* Woll." Acta Societatis Botanicorum Poloniae **56**(3): 381-389.
Grymaszewska, G. and W. Golinowski (1991). "Structure of syncytia induced by *Heterodera avenae* Woll. in roots of susceptible and resistant wheat (*Triticum aestivum* L.)." Journal of phytopathology **133**(4): 307-319.
Gunning, B. E. S. and J. S. Pate (1969). ""Transfer cells" Plant cells with wall ingrowths, specialized in relation to short distance transport of solutes? Their occurrence, structure, and development." Protoplasma **68**(1-2): 107-133.
Gutierrez, O. A., M. J. Wubben, M. Howard, B. Roberts, E. Hanlon and J. R. Wilkinson (2009). "The role of phytohormones ethylene and auxin in plant-nematode interactions." Russian Journal of Plant Physiology **56**(1): 1-5.
Haas, B. J., A. Papanicolaou, M. Yassour, M. Grabherr, P. D. Blood, J. Bowden, M. B. Couger, D. Eccles, B. Li, M. Lieber, M. D. MacManes, M. Ott, J. Orvis, N. Pochet, F. Strozzzi, N. Weeks, R. Westerman, T. William, C. N. Dewey, R. Henschel, R. D. Leduc, N. Freidman and A. Regev (2013). "De novo transcript sequence reconstruction from RNA-seq using the Trinity platform for reference generation and analysis." Nature Protocols **8**(8): 1494-1512.
Haegeman, A., S. Mantelin, J. T. Jones and G. Gheysen (2011). "Functional roles of effectors of plant-parasitic nematodes." Gene **492**(1): 19-31.
Harholt, J., J. Jensen, Y. Verhertbruggen, C. Søgaard, S. Bernard, M. Nafisi, C. Poulsen, N. Geshi, Y. Sakuragi, A. Driouich, P. J. Knox and H. Scheller (2012). "ARAD proteins associated with pectic Arabinan biosynthesis form complexes when transiently overexpressed in planta." Planta **236**(1): 115-128.
Harholt, J., J. K. Jensen, S. O. Sørensen, C. Orfila, M. Pauly and H. V. Scheller (2006). "ARABINAN DEFICIENT 1 is a putative arabinosyltransferase involved in biosynthesis of pectic arabinan in Arabidopsis." Plant Physiology **140**(1): 49-58.
Hayashi, T. and R. Kaida (2011). "Functions of xyloglucan in plant cells." Molecular Plant **4**(1): 17-24.
Herth, W. (1983). "Arrays of plasma-membrane "rosettes" involved in cellulose microfibril formation of Spirogyra." Planta **159**(4): 347-356.
Hewezi, T. (2015). "Cellular signaling pathways and posttranslational modifications mediated by nematode effector proteins." Plant Physiology **169**(2): 1018-1026.

Hewezi, T., P. Howe, T. R. Maier, R. S. Hussey, M. G. Mitchum, E. L. Davis and T. J. Baum (2008). "Cellulose binding protein from the parasitic nematode *Heterodera schachtii* interacts with Arabidopsis pectin methylesterase: cooperative cell wall modification during parasitism." The Plant Cell **20**(11): 3080-3093.

Hewezi, T., S. Piya, G. Richard and J. H. Rice (2014). "Spatial and temporal expression patterns of auxin response transcription factors in the syncytium induced by the beet cyst nematode *Heterodera schachtii* in Arabidopsis." Molecular Plant Pathology **15**(7): 730-736.

Hofmann, J., N. El Ashry Ael, S. Anwar, A. Erban, J. Kopka and F. Grundler (2010). "Metabolic profiling reveals local and systemic responses of host plants to nematode parasitism." The Plant Journal **62**(6): 1058-1071.

Hofmann, J. and F. M. Grundler (2006). "Females and males of root-parasitic cyst nematodes induce different symplasmic connections between their syncytial feeding cells and the phloem in *Arabidopsis thaliana*." Plant Physiology and Biochemistry **44**(5-6): 430-433.

Hofmann, J., D. Szakasits, A. Blöchl, M. Sobczak, S. Daxböck-Horvath, W. Golinowski, H. Bohlmann and F. M. W. Grundler (2008). "Starch serves as carbohydrate storage in nematode-induced syncytia." Plant Physiology **146**(1): 228-235.

Hofmann, J., K. Wieczorek, A. Blöchl and F. M. W. Grundler (2007). "Sucrose supply to nematode-induced syncytia depends on the apoplasmic and symplasmic pathways." Journal of Experimental Botany **58**(7): 1591-1601.

Hofmann, J., M. Youssef-Banora, J. de Almeida-Engler and F. M. Grundler (2010). "The role of callose deposition along plasmodesmata in nematode feeding sites." Molecular Plant-Microbe Interactions **23**(5): 549-557.

Hogenhout, S. A., R. A. Van der Hoorn, R. Terauchi and S. Kamoun (2009). "Emerging concepts in effector biology of plant-associated organisms." Molecular Plant-Microbe Interactions **22**(2): 115-122.

Holterman, M., A. van der Wurff, S. Elsen, H. Megen, T. Bongers, O. Holovachov, J. Bakker and J. Helder (2006). "Phylum-wide analysis of SSU rDNA reveals deep phylogenetic relationships among nematodes and accelerated evolution toward crown clades." Molecular Biology and Evolution **23**(9): 1792-1800.

Hoolahan, A. H., V. C. Blok, T. Gibson and M. Dowton (2011). "Paternal leakage of mitochondrial DNA in experimental crosses of populations of the potato cyst nematode *Globodera pallida*." Genetica **139**(11-12): 1509-1519.

Hoth, S., A. Schneidereit, C. Lauterbach, J. Scholz-Starke and N. Sauer (2005). "Nematode infection triggers the de novo formation of unloading phloem that allows macromolecular trafficking of green fluorescent protein into syncytia." Plant Physiology **138**(1): 383-392.

Hu, R., J. Li, X. Wang, X. Zhao, X. Yang, Q. Tang, G. He, G. Zhou and Y. Kong (2016). "Xylan synthesized by Irregular Xylem 14 (IRX14) maintains the structure of seed coat mucilage in Arabidopsis." Journal of Experimental Botany **67**(5): 1243-1257.

Hussey, R. S. (1989). "Disease-inducing secretions of plant-parasitic nematodes." Annual Review of Phytopathology **27**(1): 123-141.

Inoue, H., H. Nojima and H. Okayama (1990). "High efficiency transformation of *Escherichia coli* with plasmids." Gene **96**(1): 23-28.

Inzé, D. and L. De Veylder (2006). "Cell cycle regulation in plant development." Annual Review of Genetics **40**: 77-105.

Ishida, Y., M. Tsunashima, Y. Hiei and T. Komari (2015). Wheat (*Triticum aestivum* L.) transformation using immature embryos. Agrobacterium Protocols: Volume 1. K. Wang. New York, NY, Springer New York**:** 189-198.

Ishii, T. (1997). "Structure and functions of feruloylated polysaccharides." Plant Science **127**(2): 111-127.

Ithal, N., J. Recknor, D. Nettleton, L. Hearne, T. Maier, T. J. Baum and M. G. Mitchum (2007). "Parallel genome-wide expression profiling of host and pathogen during soybean cyst nematode infection of soybean." Molecular Plant-Microbe Interactions **20**(3): 293-305.

Jamet, E., H. Canut, G. Boudart and R. F. Pont-Lezica (2006). "Cell wall proteins: a new insight through proteomics." Trends In Plant Science.

Jiang, N., R. E. Wiemels, A. Soya, R. Whitley, M. Held and A. Faik (2016). "Composition, assembly, and trafficking of a wheat xylan synthase complex (XSC)." Plant Physiology **170**(4): 1999-2023.

Jobling, S. A. (2015). "Membrane pore architecture of the CslF6 protein controls (1-3,1-4)-β-glucan structure." Science Advances **1**(5): e1500069.

Jolie, R. P., T. Duvetter, A. M. Van Loey and M. E. Hendrickx (2010). "Pectin methylesterase and its

proteinaceous inhibitor: a review." Carbohydrate Research **345**(18): 2583-2595.
Jones, J. D. G. and J. L. Dangl (2006). "The plant immune system." Nature **444**(7117): 323-329.
Jones, J. T., A. Haegeman, E. G. Danchin, H. S. Gaur, J. Helder, M. G. Jones, T. Kikuchi, R. Manzanilla-Lopez, J. E. Palomares-Rius, W. M. Wesemael and R. N. Perry (2013). "Top 10 plant-parasitic nematodes in molecular plant pathology." Molecular Plant Pathology **14**(9): 946-961.
Jones, J. T., A. Kumar, L. A. Pylypenko, A. Thirugnanasambandam, L. Castelli, S. Chapman, P. J. Cock, E. Grenier, C. J. Lilley, M. S. Phillips and V. C. Blok (2009). "Identification and functional characterization of effectors in expressed sequence tags from various life cycle stages of the potato cyst nematode *Globodera pallida*." Molecular Plant Pathology **10**(6): 815-828.
Jones, L., J. L. Milne, D. Ashford and S. J. McQueen-Mason (2003). "Cell wall arabinan is essential for guard cell function." PNAS **100**(20): 11783-11788.
Jones, L., G. B. Seymour and J. P. Knox (1997). "Localization of pectic galactan in tomato cell walls using a monoclonal antibody specific to (1->4)-beta-D-galactan." Plant Physiology **113**(4): 1405-1412.
Jones, M. G. K. and D. H. Northcote (1972). "Multinucleate transfer cells induced in coleus roots by the root-knot nematode,*Meloidogyne arenaria*." Protoplasma **75**(4): 381-395.
Jones, M. G. K. and D. H. Northcote (1972). "Nematode-induced syncytium-a multinucleate transfer cell." Journal of Cell Science.
Juergensen, K., J. Scholz-Starke, N. Sauer, P. Hess, A. J. E. van Bel and F. M. W. Grundler (2003). "The companion cell-specific Arabidopsis disaccharide carrier AtSUC2 is expressed in nematode-induced syncytia." Plant Physiology **131**(1): 61-69.
Kazan, K. and J. M. Manners (2009). "Linking development to defense: auxin in plant–pathogen interactions." Trends in Plant Science **14**(7): 373-382.
Kido, N., R. Yokoyama, T. Yamamoto, J. Furukawa, H. Iwai, S. Satoh and K. Nishitani (2015). "The matrix polysaccharide (1;3,1;4)-β-D-glucan is involved in silicon-dependent strengthening of rice cell wall." Plant and Cell Physiology **56**(2): 268-276.
Kiemle, S. N., X. Zhang, A. R. Esker, G. Toriz, P. Gatenholm and D. J. Cosgrove (2014). "Role of (1,3)(1,4)-beta-glucan in cell walls: interaction with cellulose." Biomacromolecules **15**(5): 1727-1736.
Kim, S.-J. J., M. A. Held, S. Zemelis, C. Wilkerson and F. Brandizzi (2015). "CGR2 and CGR3 have critical overlapping roles in pectin methylesterification and plant growth in *Arabidopsis thaliana*." The Plant Journal **82**(2): 208-220.
Kim, Y. H., R. D. Riggs and K. S. Kim (1987). "Structural changes associated with resistance of soybean to *Heterodera glycines*." Journal of Nematology **19**(2): 177-187.
Kimura, Laosinchai, Itoh, Cui, C. R. Linder and R. M. Brown (1999). "Immunogold labeling of rosette terminal cellulose-synthesizing complexes in the vascular plant vigna angularis." The Plant Cell **11**(11): 2075-2086.
Klink, V. P., P. Hosseini, P. D. Matsye, N. W. Alkharouf and B. F. Matthews (2010). "Syncytium gene expression in Glycine max([PI 88788]) roots undergoing a resistant reaction to the parasitic nematode *Heterodera glycines*." Plant Physiology and Biochemistry **48**(2-3): 176-193.
Knoch, E., A. Dilokpimol and N. Geshi (2014). "Arabinogalactan proteins: focus on carbohydrate active enzymes." Frontiers In Plant Science **5**: 198.
Knox, J. P. (2008). "Revealing the structural and functional diversity of plant cell walls." Current Opinion in Plant Biology **11**(3): 308-313.
Knox, J. P., J. Peart and S. J. Neill (1995). "Identification of novel cell, surface epitopes using a leaf epidermal-strip assay system." Planta **196**(2): 266-270.
Koenning, S. R. and J. A. Wrather (2010). "Suppression of soybean yield potential in the continental United States by plant diseases from 2006 to 2009." Plant Health Progress.
Kudla, U., A. L. Milac, L. Qin, H. Overmars, E. Roze, M. Holterman, A. J. Petrescu, A. Goverse, J. Kker, J. Helder and G. Ant (2007). "Structural and functional characterization of a novel, host penetration‐related pectate lyase from the potato cyst nematode *Globodera rostochiensis*." Molecular Plant Pathology **8**(3): 293-305.
Kumar, M., L. Campbell and S. Turner (2016). "Secondary cell walls: biosynthesis and manipulation." Journal of Experimental Botany **67**(2): 515-531.
Kumar, M., N. P. Gantasala, T. Roychowdhury and P. K. Thakur (2014). "De novo transcriptome sequencing and analysis of the cereal cyst nematode, *Heterodera avenae*." PLoS ONE **9**(5): e96311.
Kumar, M. and S. Turner (2015). "Cell wall biosynthesis." eLS: 1-11.
Lamport, D., M. J. Kieliszewski, Y. Chen and M. C. Cannon (2011). "Role of the extensin superfamily in primary cell wall architecture." Plant Physiology **156**(1): 11-19.

Lee, C., D. Chronis, C. Kenning, B. Peret, T. Hewezi, E. L. Davis, T. J. Baum, R. S. Hussey, M. Bennet and M. G. Mitchum (2011). "The novel cyst nematode effector protein 19C07 interacts with the Arabidoipsis auxin influx transporter LAX3 to control feeding site development." Plant Physiology **155**(2): 866-880.

Lee, C., M. A. O'Neill, Y. Tsumuraya, A. G. Darvill and Z. H. Ye (2007). "The irregular xylem9 mutant is deficient in xylan xylosyltransferase activity." Plant and Cell Physiology **48**(11): 1624-1634.

Lee, J.-Y. Y. (2015). "Plasmodesmata: a signaling hub at the cellular boundary." Current Opinion in Plant Biology **27**: 133-140.

Lee, K., S. E. Marcus and P. J. Knox (2011). "Cell wall biology: perspectives from cell wall imaging." Molecular Plant **4**(2): 212-219.

Lee, K. J., V. Cornuault, I. W. Manfield, M.-C. C. Ralet and J. P. Knox (2013). "Multi-scale spatial heterogeneity of pectic rhamnogalacturonan I (RG-I) structural features in tobacco seed endosperm cell walls." The Plant Journal **75**(6): 1018-1027.

Li, J., X. Ye, B. An, L. Du and H. Xu (2012). "Genetic transformation of wheat: current status and future prospects." Plant Biotechnology Reports **6**(3): 183-193.

Liepman, A. H., R. Wightman, N. Geshi, S. R. Turner and H. V. Scheller (2010). "Arabidopsis - a powerful model system for plant cell wall research." The Plant Journal **61**(6): 1107-1121.

Liepman, A. H., C. G. Wilkerson and K. Keegstra (2005). "Expression of cellulose synthase-like (Csl) genes in insect cells reveals that CslA family members encode mannan synthases." PNAS **102**(6): 2221-2226.

Lilley, C. J., H. J. Atkinson and P. E. Urwin (2005). "Molecular aspects of cyst nematodes." Molecular Plant Pathology **6**(6): 577-588.

Lilley, C. J., P. E. Urwin, K. A. Johnston and H. J. Atkinson (2004). "Preferential expression of a plant cystatin at nematode feeding sites confers resistance to *Meloidogyne incognita* and *Globodera pallida*." Plant Biotechnology Journal **2**(1): 3-12.

Lilley, C. J., D. Wang and H. J. Atkinson (2011). "Effective delivery of a nematode ‐ repellent peptide using a root ‐ cap ‐ specific promoter." Plant Biotechnology Journal **9**(2): 151-161.

Liners, F., J. J. Letesson and C. Didembourg (1989). "Monoclonal antibodies against pectin recognition of a conformation induced by calcium." Plant Physiology **91**(4): 1419-1424.

Lionetti, V., F. Cervone and D. Bellincampi (2012). "Methyl esterification of pectin plays a role during plant–pathogen interactions and affects plant resistance to diseases." Journal of Plant Physiology **169**(16): 1623-1630.

Lionetti, V., F. Francocci, S. Ferrari, C. Volpi, D. Bellincampi, R. Galletti, R. D'Ovidio, G. De Lorenzo and F. Cervone (2010). "Engineering the cell wall by reducing de-methyl-esterified homogalacturonan improves saccharification of plant tissues for bioconversion." PNAS **107**(2): 616-621.

Liu, B., J. K. Hibbard and P. E. Urwin (2005). "The production of synthetic chemodisruptive peptides in planta disrupts the establishment of cyst nematodes." Plant Biotechnology Journal **3**(5): 487-496.

Lloyd, A. M., A. R. Barnason, S. G. Rogers, M. C. Byrne, R. T. Fraley and R. B. Horsch (1986). "Transformation of *Arabidopsis thaliana* with Agrobacterium tumefaciens." Science **234**(4775): 464-466.

Lombard, V., H. Golaconda Ramulu, E. Drula, P. M. Coutinho and B. Henrissat (2014). "The carbohydrate-active enzymes database (CAZy) in 2013." Nucleic Acids Research **42**(D1): D490-D495.

Lozano-Torres, J. L., R. H. Wilbers, P. Gawronski, J. C. Boshoven, A. Finkers-Tomczak, J. H. Cordewener, A. H. America, H. A. Overmars, J. W. Van 't Klooster, L. Baranowski, M. Sobczak, M. Ilyas, R. A. van der Hoorn, A. Schots, P. J. de Wit, J. Bakker, A. Goverse and G. Smant (2012). "Dual disease resistance mediated by the immune receptor Cf-2 in tomato requires a common virulence target of a fungus and a nematode." PNAS **109**(25): 10119-10124.

Lozano-Torres, J. L., R. H. Wilbers, S. Warmerdam, A. Finkers-Tomczak, A. Diaz-Granados, C. C. van Schaik, J. Helder, J. Bakker, A. Goverse, A. Schots and G. Smant (2014). "Apoplastic venom allergen-like proteins of cyst nematodes modulate the activation of basal plant innate immunity by cell surface receptors." PLoS Pathogens **10**(12): e1004569.

Lu, S.-W. W., S. Chen, J. Wang, H. Yu, D. Chronis, M. G. Mitchum and X. Wang (2009). "Structural and functional diversity of CLAVATA3/ESR (CLE)-like genes from the potato cyst nematode *Globodera rostochiensis*." Molecular Plant-Microbe Interactions **22**(9): 1128-1142.

Magnusson, C. and a. W. Golinowski (1991). "Ultrastructural relationships of the developing syncytium induced by *Heterodera schachtii* (Nematoda) in root tissues of rape." Canadian Journal of Botany **69**(1): 44-52.

Majewska-Sawka, A., A. Münster and E. Wisniewska (2004). "Temporal and spatial distribution of pectin epitopes in differentiating anthers and microspores of fertile and sterile sugar beet." Plant and Cell Physiology **45**(5): 560-572.

Mangeon, A., R. Junqueira, G. Sachetto-Martins and R. Junqueira (2010). "Functional diversity of the plant glycine-rich proteins superfamily." Plant Signaling & Behavior **5**(2): 99-104.

Marcus, S. E., A. W. Blake, T. A. S. Benians, K. J. D. Lee, C. Poyser, L. Donaldson, O. Leroux, A. Rogowski, H. L. Petersen, A. Boraston, H. J. Gilbert, W. G. T. Willats and J. Paul Knox (2010). "Restricted access of proteins to mannan polysaccharides in intact plant cell walls." The Plant Journal **64**(2): 191-203.

Marcus, S. E., Y. Verhertbruggen, C. Herve, J. J. Ordaz-Ortiz, V. Farkas, H. L. Pedersen, W. G. Willats and J. P. Knox (2008). "Pectic homogalacturonan masks abundant sets of xyloglucan epitopes in plant cell walls." BMC Plant Biology **8**(1): 60.

Marowa, P., A. Ding and Y. Kong (2016). "Expansins: roles in plant growth and potential applications in crop improvement." Plant Cell Reports **35**(5): 949-965.

Matsuyama, T., N. Yasumura, M. Funakoshi, Y. Yamada and T. Hashimoto (1999). "Maize genes specifically expressed in the outermost cells of root cap." Plant and Cell Physiology **40**(5): 469-476.

Mazarei, M., W. Liu, H. Al-Ahmad, P. R. Arelli, V. R. Pantalone and C. N. Stewart, Jr. (2011). "Gene expression profiling of resistant and susceptible soybean lines infected with soybean cyst nematode." Theoretical and Applied Genetics **123**(7): 1193-1206.

McCann, M. C., B. Wells and K. Roberts (1990). "Direct visualization of cross-links in the primary plant cell wall." Journal of Cell Science.

McCartney, L., S. E. Marcus and J. P. Knox (2005). "Monoclonal antibodies to plant cell wall xylans and arabinoxylans." Journal of Histochemistry & Cytochemistry **53**(4): 543-546.

McCartney, L., A. P. Ormerod, M. J. Gidley and J. P. Knox (2000). "Temporal and spatial regulation of pectic (1-->4)-beta-D-galactan in cell walls of developing pea cotyledons: implications for mechanical properties." The Plant Journal **22**(2): 105-113.

McFarlane, H. E., A. Doring and S. Persson (2014). "The cell biology of cellulose synthesis." Annual Review of Plant Biology **65**: 69-94.

McQueen-Mason, S. and D. J. Cosgrove (1994). "Disruption of hydrogen bonding between plant cell wall polymers by proteins that induce wall extension." PNAS **91**(14): 6574-6578.

Meikle, P. J., N. J. Hoogenraad, I. Bonig, A. E. Clarke and B. A. Stone (1994). "A (1→ 3, 1→ 4) - β - glucan - specific monoclonal antibody and its use in the quantitation and immunocytochemical location of (1→ 3, 1→ 4) - β - glucans." The Plant Journal **5**(1): 1-9.

Meinke, D. W., J. M. Cherry, C. Dean, S. D. Rounsley and M. Koornneef (1998). "*Arabidopsis thaliana*: A Model Plant for Genome Analysis." Science **282**(5389): 662-682.

Melillo, M., T. Bleve-Zacheo and G. Zacheo (1990). "Ultrastructural response of potato roots susceptible to cyst nematode *Globodera pallida* pathotype Pa 3." Revue de Nématologie **13**: 17-28.

Meutter, J., T. Tytgat, E. Witters, G. Gheysen, H. Onckelen and G. Gheysen (2003). "Identification of cytokinins produced by the plant parasitic nematodes *Heterodera schachtii* and *Meloidogyne incognita*." Molecular Plant Pathology **4**(4): 271-277.

Meyer, P. (1995). "Understanding and controlling transgene expression." Trends in Biotechnology **13**(9): 332-337.

Micheli, F. (2001). "Pectin methylesterases: cell wall enzymes with important roles in plant physiology." Trends In Plant Science **6**(9): 414-419.

Mitchum, M. G., R. S. Hussey, T. J. Baum, X. Wang, A. A. Elling, M. Wubben and E. L. Davis (2013). "Nematode effector proteins: an emerging paradigm of parasitism." New Phytologist **199**(4): 879-894.

Mitchum, M. G., X. Wang and E. L. Davis (2008). "Diverse and conserved roles of CLE peptides." Current Opinion in Plant Biology **11**(1): 75-81.

Mitsumasu, K., Y. Seto and S. Yoshida (2015). "Apoplastic interactions between plants and plant root intruders." Frontiers in Plant Science **6**: 617.

Moller, I., S. Marcus, A. Haeger, Y. Verhertbruggen, R. Verhoef, H. Schols, P. Ulvskov, J. Mikkelsen, J. P. Knox and W. Willats (2008). "High-throughput screening of monoclonal antibodies against plant cell wall glycans by hierarchical clustering of their carbohydrate microarray binding profiles." Glycoconjugate Journal **25**(1): 37-48.

Moore, J. P., J. M. Farrant and A. Driouich (2008). "A role for pectin-associated arabinans in maintaining the flexibility of the plant cell wall during water deficit stress." Plant Signaling & Behavior **3**(2): 102-104.

Moore, J. P., E. Nguema-Ona, L. Chevalier, G. G. Lindsey, W. F. Brandt, P. Lerouge, J. M. Farrant and A. Driouich (2006). "Response of the leaf cell wall to desiccation in the resurrection plant *Myrothamnus flabellifolius*." Plant Physiology **141**(2): 651-662.

Moore, J. P., E. E. Nguema-Ona, M. Vicré-Gibouin, I. Sørensen, W. G. Willats, A. Driouich and J. M. Farrant (2013). "Arabinose-rich polymers as an evolutionary strategy to plasticize resurrection plant cell walls against desiccation." Planta **237**(3): 739-754.

Moore, J. P., M. Vicré - Gibouin and J. M. Farrant (2008). "Adaptations of higher plant cell walls to water loss: drought vs desiccation." Physiologia Plantarum **134**(2): 237-245.

Morel, J.-B., P. Mourrain, C. Béclin and H. Vaucheret (2000). "DNA methylation and chromatin structure affect transcriptional and post-transcriptional transgene silencing in Arabidopsis." Current Biology **10**(24): 1591-1594.

Morgan, J. L., J. T. McNamara, M. Fischer, J. Rich, H.-M. M. Chen, S. G. Withers and J. Zimmer (2016). "Observing cellulose biosynthesis and membrane translocation in crystallo." Nature **531**(7594): 329-334.

Morgan, J. L. W., J. Strumillo and J. Zimmer (2013). "Crystallographic snapshot of cellulose synthesis and membrane translocation." Nature **493**(7431): 181-186.

Mortazavi, A., B. A. Williams, K. McCue, L. Schaeffer and B. Wold (2008). "Mapping and quantifying mammalian transcriptomes by RNA-Seq." Nature Methods **5**(7): 621-628.

Mortimer, J. C., N. Faria-Blanc, X. Yu, T. Tryfona, M. Sorieul, Y. Z. Ng, Z. Zhang, K. Stott, N. Anders and P. Dupree (2015). "An unusual xylan in Arabidopsis primary cell walls is synthesised by GUX3, IRX9L, IRX10L and IRX14." The Plant Journal **83**(3): 413-426.

Mortimer, J. C., G. P. Miles, D. M. Brown, Z. Zhang, M. P. Segura, T. Weimar, X. Yu, K. A. Seffen, E. Stephens, S. R. Turner and P. Dupree (2010). "Absence of branches from xylan in Arabidopsis gux mutants reveals potential for simplification of lignocellulosic biomass." PNAS **107**(40): 17409-17414.

Mueller, S. C. and R. M. Brown (1980). "Evidence for an intramembrane component associated with a cellulose microfibril-synthesizing complex in higher plants." The Journal of Cell Biology **84**(2): 315-326.

Mukhopadhyay, T. and J. A. Roth (1993). "Silicone lubricant enhances recovery of nucleic acids after phenol-chloroform extraction." Nucleic Acids Research **21**(3): 781-782.

Muller, J., K. Rehbock and U. Wyss (1981). "Growth of *Heterodera schachtii* with remarks on amounts of food consumed." Revue de Nématologie **4**(2): 227-234.

Newman, R. H., S. J. Hill and P. J. Harris (2013). "Wide-angle X-ray scattering and solid-state nuclear magnetic resonance data combined to test models for cellulose microfibrils in mung bean cell walls." Plant Physiology **163**(4): 1558-1567.

Nicol, J. M., I. H. Elekcioglu, N. Bolat and R. Rivoal (2007). "The global importance of the cereal cyst nematode (*Heterodera* spp.) on wheat and international approaches to its control." Communications in Agricultural and Applied Biological Sciences **72**(3): 677-686.

Nicol, J. M., S. J. Turner, D. L. Coyne, L. den Nijs, S. Hockland and Z. T. Maafi (2011). Current nematode threats to world agriculture. Genomics and Molecular Genetics of Plant-Nematode Interactions. J. T. Jones, G. Gheysen and C. Fenoll. Dordrecht, Springer.

Nishitani, K. and R. Tominaga (1992). "Endo-xyloglucan transferase, a novel class of glycosyltransferase that catalyzes transfer of a segment of xyloglucan molecule to another xyloglucan molecule." The Journal of Biological Chemistry **267**(29): 21058-21064.

Offler, C. E., D. W. McCurdy, J. W. Patrick and M. J. Talbot (2003). "Transfer cells: cells specialized for a special purpose." Annual Review of Plant Biology **54**(1): 431-454.

Onyango, S. O., H. Roderick, J. N. Tripathi, R. Collins, H. J. Atkinson, R. O. Oduor and L. Tripathi (2016). "The ZmRCP-1 promoter of maize provides root tip specific expression of transgenes in plantain." Journal of Biological Research **23**: 4.

Palin, R. and A. Geitmann (2012). "The role of pectin in plant morphogenesis." Biosystems **109**(3): 397-402.

Paredez, A. R., C. R. Somerville and D. W. Ehrhardt (2006). "Visualization of cellulose synthase demonstrates functional association with microtubules." Science **312**(5779): 1491-1495.

Park, Y. B. and D. J. Cosgrove (2012). "Changes in cell wall biomechanical properties in the xyloglucan-deficient xxt1/xxt2 mutant of Arabidopsis." Plant Physiology **158**(1): 465-475.

Park, Y. B. and D. J. Cosgrove (2015). "Xyloglucan and its interactions with other components of the growing cell wall." Plant and Cell Physiology **56**(2): 180-194.

Patel, N., N. Hamamouch, C. Li, T. Hewezi, R. S. Hussey, T. J. Baum, M. G. Mitchum and E. L. Davis (2010).

"A nematode effector protein similar to annexins in host plants." Journal of Experimental Botany **61**(1): 235-248.

Pattathil, S., U. Avci, D. Baldwin, A. G. Swennes, J. A. McGill, Z. Popper, T. Bootten, A. Albert, R. H. Davis, C. Chennareddy, R. Dong, B. O'Shea, R. Rossi, C. Leoff, G. Freshour, R. Narra, M. O'Neil, W. S. York and M. G. Hahn (2010). "A comprehensive toolkit of plant cell wall glycan-directed monoclonal antibodies." Plant Physiology **153**(2): 514-525.

Pauly, M., S. Gille, L. F. Liu, N. Mansoori, A. de Souza, A. Schultink and G. Y. Xiong (2013). "Hemicellulose biosynthesis." Planta **238**(4): 627-642.

Pauly, M. and K. Keegstra (2016). "Biosynthesis of the plant cell wall matrix polysaccharide xyloglucan." Annual Review of Plant Biology **67**: 235-259.

Pear, J. R., Y. Kawagoe, W. E. Schreckengost, D. P. Delmer and D. M. Stalker (1996). "Higher plants contain homologs of the bacterial celA genes encoding the catalytic subunit of cellulose synthase." PNAS **93**(22): 12637-12642.

Peaucelle, A., S. Braybrook and H. Hofte (2012). "Cell wall mechanics and growth control in plants: the role of pectins revisited." Frontiers In Plant Science **3**: 6.

Peaucelle, A., S. A. Braybrook, L. Le Guillou, E. Bron, C. Kuhlemeier and H. Hofte (2011). "Pectin-induced changes in cell wall mechanics underlie organ initiation in Arabidopsis." Current Biology **21**(20): 1720-1726.

Peaucelle, A., R. Louvet, J. N. Johansen, H. Höfte, P. Laufs, J. Pelloux and G. Mouille (2008). "Arabidopsis phyllotaxis is controlled by the methyl-esterification status of cell-wall pectins." Current Biology **18**(24): 1943-1948.

Pedersen, H. L., J. U. Fangel, B. McCleary, C. Ruzanski, M. G. Rydahl, M. C. Ralet, V. Farkas, L. von Schantz, S. E. Marcus, M. C. Andersen, R. Field, M. Ohlin, J. P. Knox, M. H. Clausen and W. G. Willats (2012). "Versatile high resolution oligosaccharide microarrays for plant glycobiology and cell wall research." The Journal of Biological Chemistry **287**(47): 39429-39438.

Pelloux, J., C. Rustérucci and E. J. Mellerowicz (2007). "New insights into pectin methylesterase structure and function." Trends in Plant Science **12**(6): 267-277.

Peng, H., J. Cui, H. Long, W. Huang, L. Kong, S. Liu, W. He, X. Hu and D. Peng (2016). "Novel pectate lyase genes of *Heterodera glycines* play key roles in the early stage of parasitism." PLoS ONE **11**(3).

Peng, L., Y. Kawagoe, P. Hogan and D. Delmer (2002). "Sitosterol-beta-glucoside as primer for cellulose synthesis in plants." Science **295**(5552): 147-150.

Perry, R. N. and M. Moens (2013). Plant nematology, CABI.

Popeijus, H., H. Overmars, J. Jones, V. Blok, A. Goverse, J. Helder, A. Schots, J. Bakker and G. Smant (2000). "Degradation of plant cell walls by a nematode." Nature **406**(6791): 36-37.

Popper, Z. A. and S. C. Fry (2004). "Primary cell wall composition of pteridophytes and spermatophytes." New Phytologist **164**(1): 165-174.

Popper, Z. A. A. and S. C. Fry (2003). "Primary cell wall composition of bryophytes and charophytes." Annals of Botany **91**(1): 1-12.

Popper, Z. A. A., G. Michel, C. Hervé, D. S. Domozych, W. G. Willats, M. G. Tuohy, B. Kloareg and D. B. Stengel (2011). "Evolution and diversity of plant cell walls: from algae to flowering plants." Annual Review of Plant Biology **62**: 567-590.

Pryer, K. M., H. Schneider, A. R. Smith, R. Cranfill, P. G. Wolf, J. S. Hunt and S. D. Sipes (2001). "Horsetails and ferns are a monophyletic group and the closest living relatives to seed plants." Nature **409**(6820): 618-622.

Puthoff, D. P., D. Nettleton, S. R. Rodermel and T. J. Baum (2003). "Arabidopsis gene expression changes during cyst nematode parasitism revealed by statistical analyses of microarray expression profiles." The Plant Journal **33**(5): 911-921.

Qin, L., U. Kudla, E. H. Roze, A. Goverse, H. Popeijus, J. Nieuwland, H. Overmars, J. T. Jones, A. Schots, G. Smant, J. Bakker and J. Helder (2004). "Plant degradation: a nematode expansin acting on plants." Nature **427**(6969): 30.

Qin, L., B. Overmars, J. Helder, H. Popeijus, J. R. van der Voort, W. Groenink, P. van Koert, A. Schots, J. Bakker and G. Smant (2000). "An efficient cDNA-AFLP-based strategy for the identification of putative pathogenicity factors from the potato cyst nematode *Globodera rostochiensis*." Molecular Plant-Microbe Interactions **13**(8): 830-836.

Quist, C. W., G. Smant and J. Helder (2015). "Evolution of plant parasitism in the phylum Nematoda." Annual Review of Phytopathology **53**: 289-310.

Rai, K. M., V. K. Balasubramanian, C. M. Welker, M. Pang, M. M. Hii and V. Mendu (2015). "Genome wide

comprehensive analysis and web resource development on cell wall degrading enzymes from phyto-parasitic nematodes." BMC Plant Biology **15**(1): 187.

Reem, N. T., G. Pogorelko, V. Lionetti, L. Chambers, M. A. Held, D. Bellincampi and O. A. Zabotina (2016). "Decreased polysaccharide feruloylation compromises plant cell wall integrity and increases susceptibility to necrotrophic fungal pathogens." Frontiers in Plant Science **7**: 630.

Rehman, S., P. Butterbach, H. Popeijus, H. Overmars, E. L. Davis, J. T. Jones, A. Goverse, J. Bakker and G. Smant (2009). "Identification and characterization of the most abundant cellulases in stylet secretions from *Globodera rostochiensis*." Phytopathology **99**(2): 194-202.

Rehman, S., V. K. Gupta and A. K. Goyal (2016). "Identification and functional analysis of secreted effectors from phytoparasitic nematodes." BMC Microbiology **16**(1): 48.

Rehman, S., W. Postma, T. Tytgat, P. Prins, L. Qin, H. Overmars, J. Vossen, L.-N. N. Spiridon, A.-J. J. Petrescu, A. Goverse, J. Bakker and G. Smant (2009). "A secreted SPRY domain-containing protein (SPRYSEC) from the plant-parasitic nematode *Globodera rostochiensis* interacts with a CC-NB-LRR protein from a susceptible tomato." Molecular Plant-Microbe Interactions **22**(3): 330-340.

Rennie, E. A., S. F. Hansen, E. E. K. Baidoo, M. Z. Hadi, J. D. Keasling and H. V. Scheller (2012). "Three members of the Arabidopsis glycosyltransferase family 8 are xylan glucuronosyltransferases." Plant Physiology **159**(4): 1408-1417.

Rennie, E. A. and H. V. Scheller (2014). "Xylan biosynthesis." Current Opinion in Biotechnology **26**: 100-107.

Rhee, S. Y., W. Beavis, T. Z. Berardini, G. Chen, D. Dixon, A. Doyle, M. Garcia-Hernandez, E. Huala, G. Lander, M. Montoya, N. Miller, L. A. Mueller, S. Mundodi, L. Reiser, J. Tacklind, D. C. Weems, Y. Wu, I. Xu, D. Yoo, J. Yoon and P. Zhang (2003). "The Arabidopsis Information Resource (TAIR): a model organism database providing a centralized, curated gateway to Arabidopsis biology, research materials and community." Nucleic Acids Research **31**(1): 224-228.

Richardson, T., J. Thistleton, T. J. Higgins, C. Howitt and M. Ayliffe (2014). "Efficient Agrobacterium transformation of elite wheat germplasm without selection." Plant Cell, Tissue and Organ Culture (PCTOC) **119**(3): 647-659.

Richmond, T. A. and C. R. Somerville (2000). "The cellulose synthase superfamily." Plant Physiology **124**(2): 495-498.

Riggs, R. D., K. S. Kim and I. Gipson (1973). "Ultrastructural changes in Peking soybeans infected with *Heterodera glycines*." Phytopathology.

Rumpenhorst, H. J. (1984). "Intracellular feeding tubes associated with sedentary plant parasitic nematodes." Nematologica.

Saez-Aguayo, S., M.-C. Ralet, A. Berger, L. Botran, D. Ropartz, A. Marion-Poll and H. M. North (2013). "PECTIN METHYLESTERASE INHIBITOR6 promotes Arabidopsis mucilage release by limiting methylesterification of homogalacturonan in seed coat epidermal cells." The Plant Cell **25**(1): 308-323.

Scheller, H. V. and P. Ulvskov (2010). "Hemicelluloses." Annual Review of Plant Biology **61**: 263-289.

Seki, M., M. Narusaka, A. Kamiya, J. Ishida, M. Satou, T. Sakurai, M. Nakajima, A. Enju, K. Akiyama, Y. Oono, M. Muramatsu, Y. Hayashizaki, J. Kawai, P. Carninci, M. Itoh, Y. Ishii, T. Arakawa, K. Shibata, A. Shinagawa and K. Shinozaki (2002). "Functional annotation of a full-length Arabidopsis cDNA collection." Science **296**(5565): 141-145.

Senechal, F., M. L'Enfant, J. M. Domon, E. Rosiau, M. J. Crepeau, O. Surcouf, J. Esquivel-Rodriguez, P. Marcelo, A. Mareck, F. Guerineau, H. R. Kim, J. Mravec, E. Bonnin, E. Jamet, D. Kihara, P. Lerouge, M. C. Ralet, J. Pelloux and C. Rayon (2015). "Tuning of pectin methylesterification: pectin methylesterase inhibitor 7 modulates the processive activity of co-expressed pectin methylesterases 3 in a pH-dependent manner." The Journal of Biological Chemistry **290**(38): 23320-23335.

Senechal, F., A. Mareck, P. Marcelo, P. Lerouge and J. Pelloux (2015). "Arabidopsis PME17 activity can be controlled by pectin methylesterase inhibitor 4." Plant Signaling & Behavior **10**(2): e983351.

Sethaphong, L., C. H. Haigler, J. D. Kubicki, J. Zimmer, D. Bonetta, S. DeBolt and Y. G. Yingling (2013). "Tertiary model of a plant cellulose synthase." PNAS **110**(18): 7512-7517.

Shanks, C. M., J. H. Rice, Y. Zubo, G. E. Schaller, T. Hewezi and J. J. Kieber (2015). "The role of cytokinin during infection of *Arabidopsis thaliana* by the cyst nematode *Heterodera schachtii*." Molecular Plant-Microbe Interactions **29**(1): 57-68.

Showalter, A. M., B. Keppler, J. Lichtenberg, D. Gu and L. R. Welch (2010). "A bioinformatics approach to the identification, classification, and analysis of hydroxyproline-rich glycoproteins." Plant

Physiology **153**(2): 485-513.
Siddique, S., Z. S. Radakovic, C. M. De La Torre, D. Chronis, O. Novák, E. Ramireddy, J. Holbein, C. Matera, M. Hütten, P. Gutbrod, M. S. Anjam, E. Rozanska, S. Habash, A. Elashry, M. Sobczak, T. Kakimoto, M. Strnad, T. Schmülling, M. G. Mitchum and F. M. Grundler (2015). "A parasitic nematode releases cytokinin that controls cell division and orchestrates feeding site formation in host plants." PNAS **112**(41): 12669-12674.
Siddique, S., M. Sobczak, R. Tenhaken, F. M. Grundler and H. Bohlmann (2012). "Cell wall ingrowths in nematode induced syncytia require UGD2 and UGD3." PLoS ONE **7**(7): e41515.
Sijmons, P. C., F. M. W. Grundler, N. von Mende, P. R. Burrows and U. Wyss (1991). "*Arabidopsis thaliana* as a new model host for plant-parasitic nematodes." The Plant Journal **1**(2): 245-254.
Silva, G. B., M. Ionashiro, T. B. Carrara, A. C. Crivellari, M. A. Tiné, J. Prado, N. C. Carpita and M. S. Buckeridge (2011). "Cell wall polysaccharides from fern leaves: evidence for a mannan-rich Type III cell wall in Adiantum raddianum." Phytochemistry **72**(18): 2352-2360.
Slabaugh, E., J. K. Davis, C. H. Haigler and Y. G. Yingling (2014). "Cellulose synthases: new insights from crystallography and modeling." Trends in Plant Science **19**(2): 99-106.
Smallwood, M., A. Beven, N. Donovan, S. J. Neill, J. Peart, K. Roberts and J. P. Knox (1994). "Localization of cell-wall proteins in relation to the developmental anatomy of the carrot root apex." The Plant Journal **5**(2): 237-246.
Smallwood, M., H. Martin and J. P. Knox (1995). "An epitope of rice threonine- and hydroxyproline-rich glycoprotein is common to cell wall and hydrophobic plasma-membrane glycoproteins." Planta **196**(3): 510-522.
Smant, G., J. P. Stokkermans, Y. Yan, J. M. de Boer, T. J. Baum, X. Wang, R. S. Hussey, F. J. Gommers, B. Henrissat, E. L. Davis, J. Helder, A. Schots and J. Bakker (1998). "Endogenous cellulases in animals: isolation of beta-1, 4-endoglucanase genes from two species of plant-parasitic cyst nematodes." PNAS **95**(9): 4906-4911.
Smith, B. G. and P. J. Harris (1999). "The polysaccharide composition of Poales cell walls: Poaceae cell walls are not unique." Biochemical Systematics and Ecology **27**(1): 33-53.
Smith, R. C. and S. C. Fry (1991). "Endotransglycosylation of xyloglucans in plant cell suspension cultures." Biochemical Journal **279 (Pt 2)**: 529-535.
Sobczak, M. and W. Golinowski Structure of cyst nematode feeding sites. Berlin, Heidelberg, Springer Berlin Heidelberg**:** 1-35.
Sobczak, M. and W. Golinowski (2009). Structure of cyst nematode feeding sites. Cell Biology of Plant Nematode Parasitism. R. H. Berg and C. Taylor, Springer Berlin Heidelberg. **15:** 153-187.
Sobczak, M., W. Golinowski and F. M. W. Grundler (1997). "Changes in the structure of *Arabidopsis thaliana* roots induced during development of males of the plant parasitic nematode *Heterodera schachtii*." European Journal of Plant Pathology **103**(2): 113-124.
Soneson, C., M. Love and M. Robinson (2015). Differential analyses for RNA-seq: transcript-level estimates improve gene-level inferences.
Sørensen, I., F. A. Pettolino, S. M. Wilson, M. S. Doblin, B. Johansen, A. Bacic and W. G. T. Willats (2008). "Mixed‐linkage (1→3),(1→4)‐β‐d‐glucan is not unique to the Poales and is an abundant component of *Equisetum arvense* cell walls." The Plant Journal **54**(3): 510-521.
Stals, H. and D. Inzé (2001). "When plant cells decide to divide." Trends In Plant Science.
Strabala, T. J. and C. P. Macmillan (2013). "The Arabidopsis wood model-the case for the inflorescence stem." Plant Science **210**: 193-205.
Swiecicka, M., M. Filipecki, D. Lont, J. Van Vliet, L. Qin, A. Goverse, J. Bakker and J. Helder (2009). "Dynamics in the tomato root transcriptome on infection with the potato cyst nematode *Globodera rostochiensis*." Molecular Plant Pathology **10**(4): 487-500.
Szakasits, D., P. Heinen, K. Wieczorek, J. Hofmann, F. Wagner, D. P. Kreil, P. Sykacek, F. M. W. Grundler and H. Bohlmann (2009). "The transcriptome of syncytia induced by the cyst nematode *Heterodera schachtii* in Arabidopsis roots." The Plant Journal **57**(5): 771-784.
The, K. F. X. Mayer, J. Rogers, J. Dole el, C. Pozniak, K. Eversole, C. Feuillet, B. Gill, B. Friebe, A. J. Lukaszewski, P. Sourdille, T. R. Endo, M. Kubalakova, J. ihalikova, Z. Dubska, J. Vrana, R. perkova, H. imkova, M. Febrer, L. Clissold, K. McLay, K. Singh, P. Chhuneja, N. K. Singh, J. Khurana, E. Akhunov, F. Choulet, A. Alberti, V. Barbe, P. Wincker, H. Kanamori, F. Kobayashi, T. Itoh, T. Matsumoto, H. Sakai, T. Tanaka, J. Wu, Y. Ogihara, H. Handa, P. R. Maclachlan, A. Sharpe, D. Klassen, D. Edwards, J. Batley, A. O. Olsen, S. R. Sandve, S. Lien, B. Steuernagel, B. Wulff, M. Caccamo, S. Ayling, R. H. Ramirez-Gonzalez, B. J. Clavijo, J. Wright, M. Pfeifer, M. Spannagl, M. M. Martis, M. Mascher, J. Chapman, J.

A. Poland, U. Scholz, K. Barry, R. Waugh, D. S. Rokhsar, G. J. Muehlbauer, N. Stein, H. Gundlach, M. Zytnicki, V. Jamilloux, H. Quesneville, T. Wicker, P. Faccioli, M. Colaiacovo, A. M. Stanca, H. Budak, L. Cattivelli, N. Glover, L. Pingault, E. Paux, S. Sharma, R. Appels, M. Bellgard, B. Chapman, T. Nussbaumer, K. C. Bader, H. Rimbert, S. Wang, R. Knox, A. Kilian, M. Alaux, F. Alfama, L. Couderc, N. Guilhot, C. Viseux, M. Loaec, B. Keller and S. Praud (2014). "A chromosome-based draft sequence of the hexaploid bread wheat (*Triticum aestivum*) genome." Science **345**(6194): 1251788-1251788.

Thomas, L. H., V. T. Forsyth, A. Sturcova, C. J. Kennedy, R. P. May, C. M. Altaner, D. C. Apperley, T. J. Wess and M. C. Jarvis (2013). "Structure of cellulose microfibrils in primary cell walls from collenchyma." Plant Physiology **161**(1): 465-476.

Thorpe, P., S. Mantelin, P. J. Cock, V. C. Blok, M. C. Coke, S. Eves-van den Akker, E. Guzeeva, C. J. Lilley, G. Smant, A. J. Reid, K. M. Wright, P. E. Urwin and J. T. Jones (2014). "Genomic characterisation of the effector complement of the potato cyst nematode *Globodera pallida*." BMC Genomics **15**(1): 1-15.

Triantaphyllou, A. C. and P. R. Esbenshade (1990). "Demonstration of multiple mating in *Heterodera glycines* with biochemical markers." Journal of Nematology **22**(4): 452-456.

Tuomivaara, S. T., K. Yaoi, M. A. O'Neill and W. S. York (2015). "Generation and structural validation of a library of diverse xyloglucan-derived oligosaccharides, including an update on xyloglucan nomenclature." Carbohydrate Research **402**: 56-66.

Turner, S. J. (1996). "Population decline of potato cyst nematodes (*Globodera rostochiensis*, G-pallida) in field soils in Northern Ireland." Annals of Applied Biology **129**(2): 315-322.

Ulvskov, P., H. Wium, D. Bruce, B. Jørgensen, K. B. Qvist, M. Skjøt, D. Hepworth, B. Borkhardt and S. O. Sørensen (2005). "Biophysical consequences of remodeling the neutral side chains of rhamnogalacturonan I in tubers of transgenic potatoes." Planta **220**(4): 609-620.

Urbanowicz, B. R., M. J. Peña, S. Ratnaparkhe, U. Avci, J. Backe, H. F. Steet, M. Foston, H. Li, M. A. O'Neill, A. J. Ragauskas, A. G. Darvill, C. Wyman, H. J. Gilbert and W. S. York (2012). "4-O-methylation of glucuronic acid in Arabidopsis glucuronoxylan is catalyzed by a domain of unknown function family 579 protein." PNAS **109**(35): 14253-14258.

Urwin, P. E., J. Green and H. J. Atkinson (2003). "Expression of a plant cystatin confers partial resistance to Globodera, full resistance is achieved by pyramiding a cystatin with natural resistance." Molecular Breeding **12**(3): 263-269.

Urwin, P. E., K. M. Troth, E. I. Zubko and H. J. Atkinson (2001). "Effective transgenic resistance to *Globodera pallida* in potato field trials." Molecular Breeding **8**(1): 95-101.

Valent, B. S. and P. Albersheim (1974). "The structure of plant cell walls: v. On the binding of xyloglucan to cellulose fibers." Plant Physiology **54**(1): 105-108.

van der Weele, C. M., W. G. Spollen, R. E. Sharp and T. I. Baskin (2000). "Growth of *Arabidopsis thaliana* seedlings under water deficit studied by control of water potential in nutrient ‐ agar media." Journal of Experimental Botany **51**(350): 1555-1562.

van Megen, H., S. van den Elsen, M. Holterman, G. Karssen, P. Mooyman, T. Bongers, O. Holovachov, J. Bakker and J. Helder (2009). "A phylogenetic tree of nematodes based on about 1200 full-length small subunit ribosomal DNA sequences." Nematology **11**(6): 927-S927.

Vanholme, R., B. Demedts, K. Morreel, J. Ralph and W. Boerjan (2010). "Lignin biosynthesis and structure." Plant Physiology **153**(3): 895-905.

Vanneste, S. and J. Friml (2009). "Auxin: a trigger for change in plant development." Cell **136**(6): 1005-1016.

Vasil, V., A. M. Castillo, M. E. Fromm and I. K. Vasil (1992). "Herbicide resistant fertile transgenic wheat plants obtained by microprojectile bombardment of regenerable embryogenic callus." Nature Biotechnology **10**(6): 667-674.

Vaughn, K. C., M. J. Talbot, C. E. Offler and D. W. McCurdy (2007). "Wall ingrowths in epidermal transfer cells of Vicia faba cotyledons are modified primary walls marked by localized accumulations of arabinogalactan proteins." Plant and Cell Physiology **48**(1): 159-168.

Vega-Sánchez, M. E., Y. Verhertbruggen, H. V. Scheller and P. C. Ronald (2013). "Abundance of mixed linkage glucan in mature tissues and secondary cell walls of grasses." Plant Signaling & Behavior **8**(2): e23143.

Verhertbruggen, Y., S. E. Marcus, J. Chen and P. J. Knox (2013). "Cell wall pectic arabinans influence the mechanical properties of *Arabidopsis thaliana* inflorescence stems and their response to mechanical stress." Plant and Cell Physiology **54**(8): 1278-1288.

Verhertbruggen, Y., S. E. Marcus, A. Haeger, J. J. Ordaz-Ortiz and J. P. Knox (2009). "An extended set of monoclonal antibodies to pectic homogalacturonan." Carbohydrate Research **344**(14): 1858-1862.

Verhertbruggen, Y., S. E. Marcus, A. Haeger, R. Verhoef, H. A. Schols, B. V. McCleary, L. McKee, H. J. Gilbert and J. Paul Knox (2009). "Developmental complexity of arabinan polysaccharides and their processing in plant cell walls." The Plant Journal **59**(3): 413-425.

Verhertbruggen, Y., L. Yin, A. Oikawa and H. Scheller (2014). "Mannan synthase activity in the CSLD family." Plant Signaling & Behavior **6**(10): 1620-1623.

Vogel, J. (2008). "Unique aspects of the grass cell wall." Current Opinion in Plant Biology **11**(3): 301-307.

Wan, J., T. Vuong, Y. Jiao, T. Joshi, H. Zhang, D. Xu and H. T. Nguyen (2015). "Whole-genome gene expression profiling revealed genes and pathways potentially involved in regulating interactions of soybean with cyst nematode (*Heterodera glycines* Ichinohe)." BMC Genomics **16**: 148.

Wang, J., C. Lee, A. Replogle, S. Joshi, D. Korkin, R. Hussey, T. J. Baum, E. L. Davis, X. Wang and M. G. Mitchum (2010). "Dual roles for the variable domain in protein trafficking and host-specific recognition of *Heterodera glycines* CLE effector proteins." New Phytologist **187**(4): 1003-1017.

Wang, M., S. Heimovaara-Dijkstra, R. Van der Meulen, J. P. Knox and S. Neill (1995). "The monoclonal antibody JIM19 modulates abscisic acid action in barley aleurone protoplasts." Planta **196**(2): 271-276.

Wang, T., Y. B. Park, J. C. Daniel and M. Hong (2015). "Cellulose-pectin spatial contacts are inherent to never-dried *Arabidopsis thaliana* primary cell walls: evidence from solid-state NMR." Plant Physiology **168**(3): 871-884.

Wang, T., O. Zabotina and M. Hong (2012). "Pectin–cellulose interactions in the Arabidopsis primary cell wall from two-dimensional magic-angle-spinning solid-state nuclear magnetic resonance." Biochemistry **51**(49): 9846-9856.

Wang, X., M. G. Mitchum, B. Gao, C. Li, H. Diab, T. J. Baum, R. S. Hussey and E. L. Davis (2005). "A parasitism gene from a plant-parasitic nematode with function similar to CLAVATA3/ESR (CLE) of *Arabidopsis thaliana*." Molecular Plant Pathology **6**(2): 187-191.

Wang, Z., M. Gerstein and M. Snyder (2009). "RNA-Seq: a revolutionary tool for transcriptomics." Nature Review Genetics **10**(1): 57-63.

Weining, S., L. Ko and R. J. Henry (1994). "Polymorphisms in the alpha-amy1 gene of wild and cultivated barley revealed by the polymerase chain reaction." Theoretical and Applied Genetics **89**(4): 509-513.

Weining, S. and P. Langridge (1991). "Identification and mapping of polymorphisms in cereals based on the polymerase chain reaction." Theoretical and Applied Genetics **82**(2): 209-216.

Wieczorek, K., A. Elashry, M. Quentin, F. M. Grundler, B. Favery, G. J. Seifert and H. Bohlmann (2014). "A distinct role of pectate lyases in the formation of feeding structures induced by cyst and root-knot nematodes." Molecular Plant-Microbe Interactions **27**(9): 901-912.

Wieczorek, K., B. Golecki, L. Gerdes, P. Heinen, D. Szakasits, D. M. Durachko, D. J. Cosgrove, D. P. Kreil, P. S. Puzio, H. Bohlmann and F. M. Grundler (2006). "Expansins are involved in the formation of nematode-induced syncytia in roots of *Arabidopsis thaliana*." The Plant Journal **48**(1): 98-112.

Wieczorek, K., J. Hofmann, A. Blöchl, D. Szakasits, H. Bohlmann and F. M. W. Grundler (2008). "Arabidopsis endo-1,4-beta-glucanases are involved in the formation of root syncytia induced by *Heterodera schachtii*." The Plant Journal **53**(2): 336-351.

Wightman, R. and S. R. Turner (2008). "The roles of the cytoskeleton during cellulose deposition at the secondary cell wall." The Plant Journal **54**(5): 794-805.

Wildermuth, M. C. (2010). "Modulation of host nuclear ploidy: a common plant biotroph mechanism." Current Opinion in Plant Biology **13**(4): 449-458.

Willats, W. G., S. E. Marcus and J. P. Knox (1998). "Generation of monoclonal antibody specific to (1-->5)-alpha-L-arabinan." Carbohydrate Research **308**(1-2): 149-152.

Willats, W. G., C. Orfila, G. Limberg, H. C. Buchholt, G. J. van Alebeek, A. G. Voragen, S. E. Marcus, T. M. Christensen, J. D. Mikkelsen, B. S. Murray and J. P. Knox (2001). "Modulation of the degree and pattern of methyl-esterification of pectic homogalacturonan in plant cell walls - Implications for pectin methyl esterase action, matrix properties, and cell adhesion." The Journal of Biological Chemistry **276**(22): 19404-19413.

Willats, W. T., L. McCartney, C. Steele-King, S. Marcus, A. Mort, M. Huisman, G.-J. van Alebeek, H. Schols, A. J. Voragen, A. Le Goff, E. Bonnin, J.-F. Thibault and J. P. Knox (2004). "A xylogalacturonan epitope is specifically associated with plant cell detachment." Planta **218**(4): 673-681.

Wilson, S. M., Y. Y. Ho, E. R. Lampugnani, A. M. Van de Meene, M. P. Bain, A. Bacic and M. S. Doblin (2015). "Determining the subcellular location of synthesis and assembly of the cell wall polysaccharide (1,3; 1,4)-β-D-glucan in grasses." The Plant Cell **27**(3): 754-771.

Winter, S. M. J., I. Rajcan and B. J. Shelp (2006). "Soybean cyst nematode: challenges and opportunities." Canadian Journal of Plant Science.

Wolf, S. and S. Greiner (2012). "Growth control by cell wall pectins." Protoplasma **249 Suppl 2**: S169-175.

Wolf, S., G. Mouille and J. Pelloux (2009). "Homogalacturonan methyl-esterification and plant development." Molecular Plant **2**(5): 851-860.

Wyss, U. (1992). "Observations on the feeding behaviour of *Heterodera schachtii* throughout development, including events during moulting." Fundamental and Applied Nematology.

Wyss, U., C. Stender and H. Lehmann (1984). "Ultrastructure of feeding sites of the cyst nematode *Heterodera schachtii* Schmidt in roots of susceptible and resistant Raphanus sativus L. var. oleiformis Pers. …." Physiological Plant Pathology.

Wyss, U. and U. Zunke (1986). "Observations on the behaviour of second stage juveniles of *Heterodera schachtii* inside host roots." Revue de Nématologie **9**(2): 153-165.

Xu, D.-L., H. Long, J.-J. Liang, J. Zhang, X. Chen, J.-L. Li, Z.-F. Pan, G.-B. Deng and M.-Q. Yu (2012). "De novo assembly and characterization of the root transcriptome of *Aegilops variabilis* during an interaction with the cereal cyst nematode." BMC Genomics **13**(1): 1-9.

Xue, G.-P., A. L. Rae, R. G. White, J. Drenth, T. Richardson and C. L. McIntyre (2016). "A strong root-specific expression system for stable transgene expression in bread wheat." Plant Cell Reports **35**(2): 469-481.

Yapo, B. M. (2011). "Pectic substances: From simple pectic polysaccharides to complex pectins A new hypothetical model." Carbohydrate Polymers **86**(2): 373-385.

Yates, E. A., J. F. Valdor, S. M. Haslam, H. R. Morris, A. Dell, W. Mackie and J. P. Knox (1996). "Characterization of carbohydrate structural features recognized by anti-arabinogalactan-protein monoclonal antibodies." Glycobiology **6**(2): 131-139.

Yin, Y., J. Huang and Y. Xu (2009). "The cellulose synthase superfamily in fully sequenced plants and algae." BMC Plant Biology **9**: 99.

York, W. S. and M. A. O'Neill (2008). "Biochemical control of xylan biosynthesis—which end is up?" Current Opinion in Plant Biology.

Yuan, Y., Q. Teng, R. Zhong and Z.-H. H. Ye (2016). "Roles of Arabidopsis TBL34 and TBL35 in xylan acetylation and plant growth." Plant Science **243**: 120-130.

Yuan, Y., Q. Teng, R. Zhong and Z.-H. H. Ye (2016). "TBL3 and TBL31, two Arabidopsis DUF231 domain proteins, are required for 3-O-monoacetylation of xylan." Plant and Cell Physiology **57**(1): 35-45.

Zabotina, O. A., U. Avci, D. Cavalier, S. Pattathil, Y.-H. H. Chou, S. Eberhard, L. Danhof, K. Keegstra and M. G. Hahn (2012). "Mutations in multiple XXT genes of Arabidopsis reveal the complexity of xyloglucan biosynthesis." Plant Physiology **159**(4): 1367-1384.

Zabotina, O. A., W. T. van de Ven, G. Freshour, G. Drakakaki, D. Cavalier, G. Mouille, M. G. Hahn, K. Keegstra and N. V. Raikhel (2008). "Arabidopsis XXT5 gene encodes a putative alpha-1,6-xylosyltransferase that is involved in xyloglucan biosynthesis." The Plant Journal **56**(1): 101-115.

Zeng, W., N. Jiang, R. Nadella, T. L. Killen, V. Nadella and A. Faik (2010). "A glucurono (arabino) xylan synthase complex from wheat contains members of the GT43, GT47, and GT75 families and functions cooperatively." Plant Physiology **154**(1): 78-97.

Zeng, W., E. R. Lampugnani, K. L. Picard, L. Song, A. Wu, I. M. Farion, J. Zhao, K. Ford, M. Doblin and A. Bacic (2016). "Asparagus IRX9, IRX10 and IRX14A are essential for xylan biosynthesis in the Golgi apparatus of Asparagus." Plant Physiology **171**(1): 93-109.

Zhang, T., S. Mahgsoudy-Louyeh, B. Tittmann and D. J. Cosgrove (2014). "Visualization of the nanoscale pattern of recently-deposited cellulose microfibrils and matrix materials in never-dried primary walls of the onion epidermis." Cellulose **21**(2): 853-862.

Zhong, R. and Z.-H. Ye (2009). Secondary cell walls. eLS, John Wiley & Sons, Ltd.

Zhong, R. and Z.-H. H. Ye (2015). "Secondary cell walls: biosynthesis, patterned deposition and transcriptional regulation." Plant and Cell Physiology **56**(2): 195-214.

Zykwinska, A. W., M.-C. J. C. Ralet, C. D. Garnier and J.-F. J. F. Thibault (2005). "Evidence for in vitro binding of pectin side chains to cellulose." Plant Physiology **139**(1): 397-407.